




ADVERTIMENT. L'accés als continguts d'aquesta tesi queda condicionat a l'acceptació de les condicions d'ús establertes per la següent llicència Creative Commons:  http://cat.creativecommons.org/?page_id=184

ADVERTENCIA. El acceso a los contenidos de esta tesis queda condicionado a la aceptación de las condiciones de uso establecidas por la siguiente licencia Creative Commons:  <http://es.creativecommons.org/blog/licencias/>

WARNING. The access to the contents of this doctoral thesis it is limited to the acceptance of the use conditions set by the following Creative Commons license:  <https://creativecommons.org/licenses/?lang=en>



**Universitat Autònoma
de Barcelona**

Doctoral Program in Neuroscience-Institut de Neurociències

Universitat Autònoma de Barcelona

Vall d'Hebrón Institut de Recerca

DOCTORAL THESIS

**Brain, lung and plasma alterations induced
by diesel exhaust particle exposure in the
context of ischemic stroke**

Mercedes Arrúe Gonzalo

Thesis Director:

Anna Rosell Novel, PhD

Thesis Tutor:

Joan Montaner Villalonga, MD, PhD

Barcelona, 2021

This doctoral thesis has been conducted in the neurovascular research laboratory of the Vall d'Hebron research institute (VHIR), with the support of a biomedicine research project (201731) funded by "La Marató de TV3".



*“Lo que nos hace humanos
es la habilidad de hacer preguntas”*

Jane Goodall

ABSTRACT

Air pollution in cities is composed of particulate matter (PM), gases, organic compounds and metals. However, it is considered that the particulate matter fraction from the artificial combustion of fossil fuels, namely Diesel Exhaust Particles (DEP), is the most harmful for human health. As the particle becomes smaller in size, the more it can penetrate the organs and the more damaging actions it can inflict.

Additionally, air pollution is ranked as an important risk factor for mortality and recent data indicates that global mortality and morbidity of cardiovascular disease are strongly influenced by PM damaging actions. Among cardiovascular diseases, stroke is the second leading cause of death globally and 85% of strokes are caused by the occlusion of blood vessels supplying the brain. In this context, PM is thought to contribute to the ischemic stroke pathology through mechanisms of inflammation, pro-thrombosis and/or impaired recovery.

This thesis aims to investigate the possible interaction of DEP with the pathophysiological mechanisms of cerebral ischemia before and during the acute phase of the disease, by means of experimental models including an *in vivo* mouse model of cerebral ischemia, by *in vitro* Neural Stem Cells (NSC) cultures and by an *ex vivo* turbidimetric assay of clot formation and tPA-induced lysis with plasma samples from humans and mice.

Matrix metalloproteinases (MMPs) are key enzymes related to injury and inflammation in acute stroke but are also essential in post-stroke tissue remodeling. In the lungs of healthy mice exposed to DEP for 3 days (acute) or 3 weeks (chronic), MMPs' levels were not altered. However, in the brain they decreased after DEP acute exposure but raised after chronic exposure. Chronic exposure reduced the amounts of cortical neurons while both exposures showed fewer NSC in the rostral migratory stream matching with *in vitro* data where NSC viability was compromised.

After acute or chronic DEP exposure, mice underwent permanent Middle Cerebral Artery occlusion (ischemia). In the lungs of the chronically exposed

group, an altered MMP response was observed along with reduced alveolar macrophages and increased interstitial macrophages and monocytes. However, brain injury produced by brain ischemia was not exacerbated by the pre-exposure to DEP, and no changes in brain MMPs' levels nor in the cell counts of different CNS cells were observed.

The potential systemic effects of DEP exposure related to stroke were studied analyzing thrombogenic/thrombolytic plasmatic characteristics through turbidimetry. After ischemia, mouse and human plasma presented pro-thrombogenic features in the presence of DEP, while thrombolysis slowed in the ischemic chronic group returning to basal levels after DEP exposure. Additionally, humans living in high polluted areas presented accelerated thrombolysis compared to individuals living in less polluted areas.

In conclusion, this thesis shows that diesel exhaust particulate matter can regulate the expression of brain proteases in healthy animals while reducing the progenitor and mature neuronal pools, compromising the CNS physiological balance. The expected detrimental role of DEP exposure in the context of cerebral ischemia by exacerbating the infarct lesion has not been observed in the tested conditions although the influence in post-stroke repair needs to be elucidated. Systemically, DEP exposure influenced the recruitment of inflammatory leukocyte populations in the lungs after ischemia and induced pro-thrombotic characteristics in plasma which could influence the brain clots in stroke disease and the outcome of thrombolytic therapies which nowadays are the only treatment for ischemic stroke in the acute phase of the disease.

RESUMEN

La contaminación del aire en las ciudades está compuesta por material particulado (PM), gases, compuestos orgánicos y metales. Sin embargo, se considera que la fracción de material particulado proveniente de la combustión artificial de combustibles fósiles, las llamadas partículas de escape de diésel (DEP), es la más dañina para la salud humana: cuanto más pequeña es la partícula mayor capacidad de penetración tiene y más daño puede infligir.

Datos recientes indican que la mortalidad y la morbilidad global de las enfermedades cardiovasculares están fuertemente influenciadas por las acciones perjudiciales de la PM. De las enfermedades cardiovasculares, el ictus es la segunda causa de muerte a nivel mundial y el 85 % son causados por la oclusión de vasos sanguíneos que irrigan el cerebro. Actualmente se cree que la PM contribuye a la patología del ictus isquémico a través de mecanismos de inflamación, pro-trombosis y/o impidiendo procesos de recuperación.

Esta tesis tiene como objetivo investigar la posible interacción de las DEP con los mecanismos fisiopatológicos de la isquemia cerebral antes y durante la fase aguda de la enfermedad empleando modelos experimentales que incluyen un modelo murino de isquemia cerebral *in vivo*, cultivos de células madre neurales (NSC) *in vitro* y un ensayo turbidimétrico *ex vivo* de formación de coágulos y lisis inducida por tPA con muestras plasmáticas humanas y murinas.

Las metaloproteinasas de matriz (MMPs) son enzimas clave relacionadas con las lesiones y la inflamación aguda por ictus, pero también son esenciales en la fase de reparación. En los pulmones de ratones sanos expuestos a DEP durante 3 días (exposición aguda) o 3 semanas (crónica), los niveles de MMPs no se alteraron. Sin embargo, en el cerebro disminuyeron tras la exposición aguda y aumentaron tras la crónica. Además, la exposición crónica redujo las neuronas corticales, mientras que ambas exposiciones mostraron menos NSC en la vía migratoria rostral coincidiendo con resultados *in vitro* que mostraron menor viabilidad de las NSC en presencia de DEP.

Tras la exposición a DEP (aguda/crónica), los ratones fueron sometidos a una oclusión permanente de la arteria cerebral media (isquemia). Sólo en los pulmones del grupo expuesto crónicamente, las MMPs se vieron alteradas junto con una reducción de los macrófagos alveolares y un aumento de los macrófagos intersticiales y monocitos. Sin embargo, la lesión cerebral producida por la isquemia no se vio agravada por la pre-exposición a DEP ni tampoco se alteraron los niveles de MMPs ni el recuento de diferentes células del sistema nervioso central (SNC).

Los posibles efectos sistémicos de la exposición a DEP se estudiaron analizando las características trombogénicas/trombolíticas del plasma mediante turbidimetría. En el plasma de ratón y humano se produjeron cambios pro-trombogénicos tras la isquemia, que se exacerbaban en presencia de DEP. La trombólisis se ralentizó en el grupo crónico-isquémico que retornó a parámetros basales en presencia de DEP y se vio acelerada en los plasmas de personas residentes en zonas altamente contaminadas.

Sintetizando, las DEP pueden regular la expresión de proteasas cerebrales en animales sanos, así como reducir las poblaciones de progenitores neurales y de neuronas maduras, comprometiendo el balance fisiológico del SNC. Sin embargo, no se ha observado una exacerbación de la lesión isquémica cerebral tras la exposición a DEP, aunque es necesario dilucidar su influencia en fases posteriores de reparación. A nivel sistémico, la exposición a DEP sí influyó en el reclutamiento de leucocitos en los pulmones tras la isquemia e indujo características pro-trombóticas en el plasma, lo que podría influir en el desarrollo de coágulos cerebrales y en la eficacia de las terapias trombolíticas con tPA (único fármaco disponible para tratar el ictus isquémico en fase aguda).

RESUM

La contaminació de l'aire a les ciutats està formada per material particulat (PM), gasos, compostos orgànics i metalls. No obstant, es considera que la fracció de material particulat provinent de la combustió artificial de combustibles fòssils, anomenada partícules d'escapament de dièsel (DEP), és la més perjudicial per a la salut humana: com més petita és la partícula més capacitat de penetració té i més mal pot infligir.

Dades recents indiquen que la mortalitat i la morbiditat global de les malalties cardiovasculars estan fortament influenciades per les accions perjudicials de la PM. De les malalties cardiovasculars, l'ictus és la segona causa de mort a nivell mundial sent el 85% causats per l'oclusió de vasos sanguinis que irriguen el cervell. Actualment es creu que la PM contribueix a la patologia de l'ictus isquèmic a través de mecanismes d'inflamació, pro-trombosi i/o impeding processos de recuperació.

L'objectiu d'aquesta tesi és investigar la possible interacció de les DEP amb els mecanismes fisiopatològics de la isquèmia cerebral abans i durant la fase aguda de la malaltia emprant models experimentals que inclouen un model murí d'isquèmia cerebral *in vivo*, cultius de cèl·lules mare neurals *in vitro* (NSC) i un assaig turbidimètric *ex vivo* de formació de coàguls i lisi induïda per tPA amb mostres plasmàtiques humanes i murines.

Les metal·loproteïnases de matriu (MMPs) són enzims clau relacionats amb les lesions i la inflamació aguda per ictus, però també són essencials en la fase de reparació. Als pulmons de ratolins sans exposats a DEP durant 3 dies (exposició aguda) o 3 setmanes (crònica), els nivells de MMPs no es van alterar. No obstant, al cervell van disminuir després de l'exposició aguda i van augmentar després de la crònica. A més, l'exposició crònica va reduir les neurones corticals, mentre que les dues exposicions van disminuir les NSC a la via migratòria rostral coincidint amb resultats *in vitro* que van mostrar menor viabilitat de les NSC en presència de DEP.

Després de l'exposició a DEP (aguda/crònica), els ratolins van ser sotmesos a una oclusió permanent de l'artèria cerebral mitjana (isquèmia). Només als pulmons del grup exposat crònicament, les MMPs es van veure alterades juntament amb una reducció dels macròfags alveolars i un augment dels macròfags intersticials i monòcits. Tot i això, la lesió cerebral produïda per la isquèmia no es va veure agreujada per la preexposició a DEP ni tampoc es van alterar els nivells de MMPs ni el recompte de diferents cèl·lules del sistema nerviós central (SNC).

Els possibles efectes sistèmics de l'exposició a DEP es van estudiar analitzant les característiques trombogèniques/trombolítiques del plasma mitjançant turbidimetria. Al plasma de ratolí i humà es van produir canvis pro-trombogènics després de la isquèmia, que es van exacerbar en presència de DEP. La trombòlisi es va alentir en el grup crònic-isquèmic que va retornar als paràmetres basals en presència de DEP i es va veure accelerada als plasmes de persones residents en zones altament contaminades.

Sintetitzant, les DEP poden regular l'expressió de proteases cerebrals en animals sans, així com reduir les poblacions de progenitors neurals i neurones madures, comprometent el balanç fisiològic del SNC. Tot i això, no s'ha observat una exacerbació de la lesió isquèmica cerebral després de l'exposició a DEP, encara que cal dilucidar la seva influència en la fase de reparació. A nivell sistèmic, l'exposició a DEP sí que va influir en el reclutament de leucòcits als pulmons després de la isquèmia i va induir característiques pro-trombòtiques al plasma, cosa que podria influir en el desenvolupament de coàguls cerebrals i en l'eficàcia de les teràpies trombolítiques amb tPA (únic fàrmac disponible per tractar l'ictus isquèmic en fase aguda).

INDEX

List of abbreviations	19
Introduction.....	23
1.1. Air pollution and disease	25
Particulate Matter and Diesel Exhaust Particles	25
Routes of entry to the Central Nervous System	27
Diesel exhaust particles, CNS and cardiovascular diseases.....	29
Diesel exhaust particles and mechanisms of injury related to cardiovascular diseases	32
1.2. Stroke.....	34
Stroke description and epidemiology	34
Stroke etiology.....	37
Ischemic cascade	39
Inflammation	42
Post-stroke Neurorepair	43
Peripheral response	47
Current stroke treatment and future perspectives.....	48
Animal models	50
1.3. Matrix metalloproteinases	52
Matrix metalloproteinases and acute ischemic stroke	53
Matrix metalloproteinases and neurorepair mechanisms	55
1.4. Thesis hypothesis:	56
Objectives.....	59
Materials and Methods.....	63
3.1. Diesel exhaust particles	65
3.2. Determination of particle size distribution	65
Laser Diffraction	65
Dynamic Light Scattering (DLS).....	66
Scanning Electron Microscopy (SEM)	67
Cryo-Transmission Electron Microscopy (Cryo-TEM)	67

3.3. Neurosphere and Neural Stem Cells Yields	67
3.4. <i>In vivo</i> exposure to diesel exhaust particles and experimental mouse model of cerebral ischemia	69
Preparation of DEP	69
Animals.....	69
DEP exposure.....	69
Grip strength-meter test.....	72
Permanent focal cerebral ischemia model.....	72
Euthanasia and sample processing.....	73
3.5. Infarct volume assessment and brain structural analyses.....	75
TTC staining	75
<i>In vivo</i> Magnetic Resonance Imaging (MRI).....	75
Diffusion Tensor Imaging (DTI)	76
3.6. Tissue homogenates	77
3.7. Multiplex immunoassay	77
3.8. Bradford assay	78
3.9. Immunofluorescence	78
3.10. Flow cytometry	79
3.11. Turbidimetric clot assay	83
3.12. Data processing and Statistical Analyses	86
Results	87
4.1. Characterization of diesel exhaust particles	89
Sonication of suspended DEP in PBS for 10 minutes increases the percentage of smaller-sized particles.....	89
Freezing the DEP suspensions did not affect the smaller-sized particle fraction.	92
4.2. Effect of DEP on Neural stem cells <i>in vitro</i>	94
DEP reduced the viability of neurosphere-forming NSC.	94
4.3. Effects of DEP exposure in naïve mice	97
General mice condition after DEP exposure	97
PBS instillations altered the MMP content in the brain.....	98

The exposure time and composition of the diesel exhaust particles altered the levels of MMPs in the brains of naïve mice.....	99
Chronic exposure to DEP reduced the neural progenitor cells in the rostral migratory stream.	104
Summary: Lung and brain alterations after DEP exposure in naïve mice.....	107
4.4. Effects of DEP exposure in cerebral ischemia	107
General mice condition after DEP exposure followed by pMCAo.....	108
Chronic exposure to DEP did not exacerbate infarct lesion.	109
Acute exposure to DEP did not significantly alter MMPs neither in the lungs nor in the brain whereas chronic DEP exposure significantly decreased MMP levels in the lungs after ischemia.	113
Exposure to SRM1650b material in ischemic mice did not alter CNS cell populations.....	119
Study of leukocytes' population in the lungs of chronically exposed ischemic mice.....	119
Summary: Lung and brain alterations in ischemic mice previously exposed to DEP	122
4.5. Alterations of thrombogenic and thrombolytic plasma characteristics under DEP exposure	122
Pro-thrombogenic changes in mouse plasma after ischemia can be boosted depending on the DEP exposure time.	122
DEP exacerbate the thrombogenic characteristics of plasma samples from ischemic patients.	126
Prolonged inhalation of PM _{2.5} in hypertense subjects alters the t-PA mediated thrombolysis profile, ex-vivo.....	129
Summary: alterations in plasma thrombogenesis and thrombolysis	131
Discussion.....	133
5.1. The selected dose does not directly affect the animal's wellbeing	135
5.2. PBS instillation does not alter MMPs in the lungs, but it decreases MMP levels in the brain.	136
5.3. In brains of naïve mice, chronic exposure to SRM1650b/DEP increases the MMP inflammatory response.	137
5.4. DEP exposure impairs neurogenesis.	141
5.5. Pre-exposure to DEP does not modify the infarct lesion and has no impact on the ischemia-induced MMP increase in the ischemic hemisphere.	143

5.6. Chronic exposure to diesel exhaust particles can have detrimental consequences in lung inflammatory response after cerebral ischemia.....	145
5.7. Acute and chronic particulate matter exposure alters the pro-thrombogenic plasma characteristics developed after ischemia, whereas chronic exposure could accelerate tPA-mediated thrombolysis.....	149
5.8. Limitations of the study and future perspectives	153
Conclusions.....	155
Bibliography	159
Annex I.....	195
SCIENTIFIC CARREER OF THE DOCTORAL STUDENT	197
Annex II – Certificate of Analysis SRM2975	199
Annex III – Certificate of Analysis SRM1650b	213
Annex IV	227
Supplementary Immunofluorescence in naïve mice	229
Supplementary Immunofluorescence in ischemic mice.....	231
Notes	233

List of abbreviations

ACA	Anterior Cerebral Artery
AHT	Arterial Hypertension
AMPA	α -Amino-3-Hydroxy-5-Methyl-4-Isoxazolepropionic Acid Receptor
ATP	Adenosine Triphosphate
BALF	Bronchoalveolar Lavage Fluid
BBB	Blood-Brain Barrier
Ca ²⁺	Calcium
CL	Contralateral
CNS	Central Nervous System
COPD	Chronic Obstructive Pulmonary Disorder
COX-2	Cyclooxygenase-2
CRc	Clot formation rate
Cryo-TEM	Cryo-Transmission Electron Microscopy
CSF	Cerebrospinal Fluid
CT	Computed Tomography
CX	Cortex
DAMP	Damage-Associated Molecular Patterns
DCX	Doublecortin
DEP	Diesel Exhaust Particles
DLS	Dynamic Light Scattering

DTI	Diffusion Tension Imaging
EEA	European Environmental Agency
EPA	Environmental Protection Agency
EPC	Endothelial Progenitor Cells
FA	Fractional Anisotropy
FBS	Fetal Bovine Serum
FDA	Food and Drug Administration
FMOs	Fluorescence Minus One
GDF10	Growth and Differentiation Factor 10
HBSS	Hank's Balanced Salt Solution
HC	Hippocampus
HEPES	4-(2-hydroxyethyl)-1-piperazineethanesulfonic acid
HR	Hazard Ratio
Iba-1	Allograft Inflammatory Factor
IL-	Interleukin
IL	Ipsilateral
iNOS	inducible Nitric Oxide Synthase
IQR	Interquartile Range
KO	Knock-Out
LR	Lysis Rate
MaxAbs	Maximum Absorbance
MCA	Middle Cerebral Artery
MCAo	Middle Cerebral Artery occlusion

MHC II	Major histocompatibility complex II
MMP	Matrix metalloproteinase
MRI	Magnetic Resonance Imaging
mRNA	Messenger Ribonucleic Acid
NeuN	Neuronal Nuclei
NF- κ B	Nuclear factor kappa B
NK	Natural Killer cells
NMDA	N-Methyl-D-Aspartate Receptor
NSC	Neural Stem Cells
OB	Olfactory Bulb
OD	Optical Densities
PAH	Polycyclic Aromatic Hydrocarbons
PAI	Plasminogen Activator Inhibitor
PBS	Phosphate Buffered Saline
PCA	Posterior Cerebral Artery
PM	Particulate Matter
pMCAo	permanent MCA occlusion
PMN	Polymorphonuclear Cells
RI	Refractive Index
RMS	Rostral Migratory Stream
ROIs	Regions of Interest
ROS	Reactive Oxygen Species
rtPA	Recombinant tissue Plasminogen Activator

SD	Standard Deviation
SEM	Scanning Electron Microscopy
SGZ	Subgranular Zone
SIID	Stroke-Induced Immunodepression
SNS	Sympathetic Nervous System
SRM	Standard Reference Material
ST	Striatum
SVZ	Subventricular Zone
T2WI	T2-Weighed Image
TAFI	Thrombin activatable fibrinolysis inhibitor
Th	T-helper cell
TIMP	Tissue Inhibitors of Metalloproteinases
tMCAo	Transient Middle Cerebral Artery occlusion
TNF α	Tumoral Necrosis Factor α
tPA	Tissue Plasminogen Activator
TTC	2,3,5-Triphenyl-2H-Tetrazolium Chloride
UFPM	Ultra-Fine Particulate Matter
CV	Coefficient of Variation
VEGF	Vascular Endothelial Growth Factor
vWF	Von-Willebrand Factor
WHO	World Health Organization
WT	Wild Type

Introduction

1.1. Air pollution and disease

The effects of air pollution on health started to wreak havoc in the twentieth century. Several incidents were critical, such as in 1930 in Belgium, when thousands of people suffered from acute pulmonary symptoms and 60 people died after sulfur dioxide emissions from a factory mixed with fog. Or in 1952 when a dense smog, containing sulfur dioxide and smoke particles, covered London and resulted in excess mortality for several months. From then on, the lethal effects of air pollution were tangible and led to the first scientific proof of the detrimental effects of air pollution on human health (Anderson *et al.*, 2012; Nemery *et al.*, 2001).

According to the United Nations report, over 4,300 million people worldwide live in urban areas where indoor and outdoor air pollution has become a major health problem to address (Mannucci *et al.*, 2019; United Nations Department of Economic and Social Affairs Population, 2018). In this regard, air pollution in cities is a mixture of Particulate Matter (PM), gases, organic compounds and metals. Among all these components, particulate matter and ozone are the ones most associated with human diseases (Block and Calderon-Garcidueñas, 2009). Of increasing interest is the PM fraction since it is believed to affect human health more than any other pollutant (Maynard *et al.*, 2017).

Particulate Matter and Diesel Exhaust Particles

Particulate matter is a generic term to describe mixtures of solid and liquid particles of different sizes and compositions. PM can originate from natural or human activities, being the main anthropogenic source of PM the combustion of solid fossil fuels, largely used in transport vehicles and named Diesel Exhaust Particles (DEP), which are considered the most toxic component in urban air. They consist of a core of solid carbon, that tends to aggregate, plus heavy carbohydrates adsorbed, hydrated sulfate species, Polycyclic Aromatic Hydrocarbons (PAH) and traces of heavy metals (**Fig.1**) (Tobwala *et al.*, 2013).

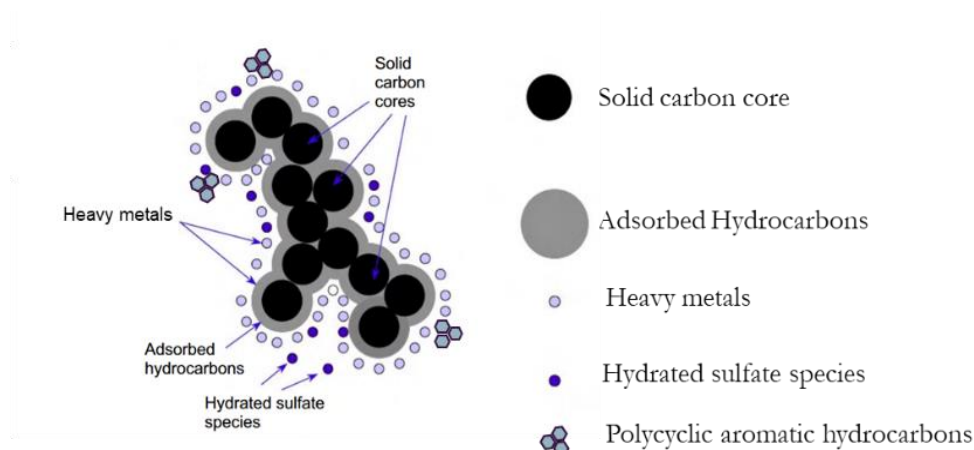


Figure 1: Schematic representation of the composition of Diesel Exhaust Particles (DEP). Solid carbon particles tend to agglomerate and adsorb species of hydrocarbons, hydrate sulfates, polycyclic aromatic hydrocarbons and heavy metals. Modified from Twigg *et al.*, 2009 and Tobwala *et al.*, 2013

PM is often classified by their size in (Calderón-Garcidueñas *et al.*, 2014):

- PM₁₀: Coarse particles, of 10 μm diameter and below.
- PM_{2.5}: Fine particles, of 2.5 μm diameter and below.
- Ultra-Fine Particulate Matter (UFP): Particle diameter below 0.1 μm (equivalent to 100 nm).

In view of the health risks that the exposure to these particulate fractions entailed (estimating over 7 million premature deaths worldwide), the World Health Organization (WHO) published in 2005 the Air Quality Guidelines (World Health Organization, 2005) when the annual mean values of exposure were set to 10 $\mu\text{g}/\text{m}^3$ for PM_{2.5} and 20 $\mu\text{g}/\text{m}^3$ for PM₁₀. But in September 2021 these values were reviewed and were modified becoming more strict: the annual mean limit is now set to 5 $\mu\text{g}/\text{m}^3$ for PM_{2.5} and 15 $\mu\text{g}/\text{m}^3$ for PM₁₀ (World Health Organization, 2021). However, the air pollution safety standards established by the European Environmental Agency (EEA) are more permissive (annual mean for PM_{2.5}: 25 $\mu\text{g}/\text{m}^3$ and for PM₁₀: 40 $\mu\text{g}/\text{m}^3$). With this, very few European countries are

registering PM₁₀ levels below the WHO air quality guidelines though most of them fulfill European air quality standards (González Ortiz and Soares, 2020) (**Fig. 2**).

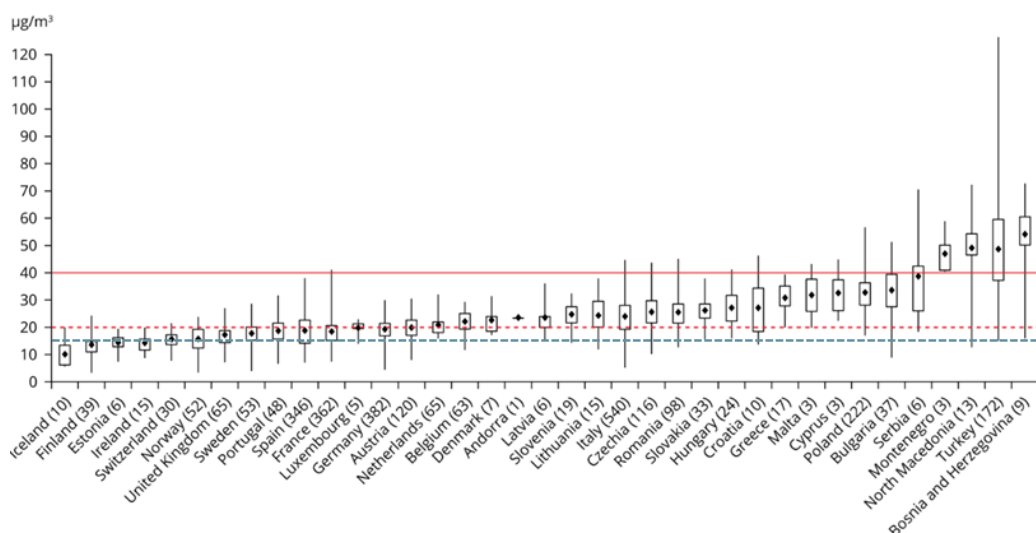


Figure 2: PM₁₀ annual mean concentrations and number of stations considered (in brackets) for each European country in 2018. The red line marks the European PM₁₀ limit and the dashed lines the WHO limits **before** (red) and **after** (blue) the revision. It can be observed that the new annual mean value set by the WHO was exceeded by the majority of the countries. Extracted from González Ortiz and Soares, 2020.

Routes of entry to the Central Nervous System

Different routes of entry into the organism have been demonstrated such as the skin (Fiorito *et al.*, 2011), the gastrointestinal tract (Bosch *et al.*, 2018) or the respiratory system (de Homdedeu *et al.*, 2020; Geiser *et al.*, 2005; Oberdörster *et al.*, 2004). And it is accepted that the smaller the particle, the deeper it can penetrate the body organs.

Once in the organism, particles can enter the circulation (Miller *et al.*, 2017) and distribute through the body where they can exert their damaging actions, even reaching the Central Nervous System (CNS) (González-Maciel *et al.*, 2017; Maher *et al.*, 2016) by different routes of entry:

- **Nose-to-brain translocation:** Ultrafine particles tend to accumulate in the nasopharyngeal tract. Considering that this region directly communicates with the CNS it has been studied their presence in the brain after nasal administrations. In this regard, Oberdörster and colleagues placed rats in whole-body chambers where they inhaled ultrafine C¹³ for 6h, and 1, 3, 5 and 7 days after exposure they observed an increase of this component in the Olfactory Bulb (OB) comparing with the OB of non-exposed animals (Oberdörster *et al.*, 2004). Also, in mice instilled with 2D graphene-sheets (10- 550 nm) combined with a tracer and after one single instillation of 30 µg, researchers found increasing amounts of the tracer signal in the OB in a size-dependent manner 24 hours after instillation (the smaller the particle, the stronger the signal) (Newman *et al.*, 2020).

Another group of researchers administered nano-sized DEP to mice through inhalative body chambers for 4 weeks and tracked them to the olfactory epithelium. They also found metal components of DEP in the OB glomerular layer (where the olfactory nerve synapses with the mitral cells) (Matsui *et al.*, 2009). Likewise Calderón-Garcidueñas and colleagues found PM in OB neurons of young human adults brains (Calderón-Garcidueñas *et al.*, 2008b). Consequently, it is accepted that after breathing polluted air, fine and ultrafine particles can reach the brain by **passive diffusion** through the nasal olfactory mucosa, olfactory nerve and finally reach the OB in the brain.

Another proposed entrance are the peripheral neuron afferents such as the trigeminus or vagal nerves, but less documented (Chung *et al.*, 2020).

- Crossing alveolar and intestinal epitheliums from breathed and swallowed particles, reaching **systemic circulation** and finally the brain. In another study, Oberdörster and colleagues exposed rats to inhalation of ultra-fine particles of C¹³ for 6h. Twenty-four hours later, they unexpectedly found high amounts of C¹³ in the liver pointing to a joint burden of the liver deposits from respiratory and gastrointestinal tracts (Oberdörster *et al.*, 2002). Furthermore, nanosized particles were found in erythrocytes of rats

that had inhaled TiO₂ (Geiser *et al.*, 2005). However, in an *in vitro* setting exposing rat, mouse and human erythrocytes to DEP, the authors found significant amounts of particles in the first two species but not in humans (Nemmar *et al.*, 2012). Whereas other authors have reported, in young human adults, PM smaller than 100 nm inside erythrocytes from lung and trigeminal ganglia capillaries (Calderón-Garcidueñas *et al.*, 2008b).

Diesel exhaust particles, CNS and cardiovascular diseases

Although several studies have reported consistent associations between exposure to diesel particles and respiratory diseases such as asthma (de Homdedeu *et al.*, 2020; Kim *et al.*, 2011; Manners *et al.*, 2014), lung cancer (Song *et al.*, 2017) or Chronic Obstructive Pulmonary Disorder (COPD) (Burnett *et al.*, 2014; Song *et al.*, 2017), the interest of this thesis is focused in the effects of DEP in the cardiovascular system and the CNS.

Nowadays, there is solid scientific background supporting the presence of traffic-related particles in the **CNS**. For instance, Calderón-Garcidueñas and colleagues have published several articles pointing to diesel exhaust particles as harmful for the CNS. They showed, in a study comparing MRI findings in healthy children living in high vs. low polluted areas, that the former exhibited significant deficits in cognitive tasks that could be explained because 56% of the cohort presented white matter hyperintense lesions that were also observed in dogs that underwent similar exposures thus linking high pollution levels with structural brain alterations and cognitive deficits (Calderón-Garcidueñas *et al.*, 2008a). The same group studied whether to live in cities with high pollutant levels was associated with neuroinflammation in healthy children and young adults that died suddenly, observing an upregulation in COX-2, IL-1 β in OB, frontal cortex, substantia nigrae and vagus nerves (Calderón-Garcidueñas *et al.*, 2008b). They also investigated the olfactory functions of individuals living in high- vs. low- polluted cities describing more olfaction deficit in the polluted group and OB endothelial hyperplasia. Furthermore, they found traffic-related UFP in the endothelial cytoplasm and basement membranes of the OB (Calderón-garcidueñas *et al.*, 2010). More recently, in 2017 the same authors reported the presence of

combustion-derived nanoparticles in brains of young adults living in a highly polluted city particularly in neurons, glia, choroid plexus, endothelium, nasal and olfactory epithelium and Cerebrospinal Fluid (CSF) (González-Maciel *et al.*, 2017).

Regarding **cerebrovascular diseases**, it was in 1993 when Dockery and colleagues demonstrated that, among other air pollutants, particulate matter was positively associated with deaths from *cardiopulmonary* diseases in a prospective cohort study in the USA including 8,111 subjects (Dockery *et al.*, 1993) and studying specific causes of death related to the cardiovascular system.

Later, the hospital admissions for **cardiac causes** were studied in 8 European cities and associated with the levels of airborne particles that same day and the day before. After performing a meta-analysis it was found that a 10 $\mu\text{g}/\text{m}^3$ increase in black smoke was associated with a 1.1 increased risk percentage for cardiac admissions of all ages even after controlling for other pollutants (CO or NO₂), suggesting that the effects on cardiac admissions were associated with diesel exhaust in the air (Le Tertre *et al.*, 2002). And two years later, long-term PM exposures were associated with 8-18% increased risk of cardiovascular causes of death (Pope *et al.*, 2004). More recent studies have shown positive associations between increases in 10 $\mu\text{g}/\text{m}^3$ PM and hospital admissions related to heart attacks in Barcelona (Bañeras *et al.*, 2018), to a 0.34% daily increase in hospital admissions for ischemic stroke in China (Tian *et al.*, 2018) or to admissions due to deep vein thrombosis in a highly polluted city of Iran (Borsi *et al.*, 2020).

In this line, a meta-analysis study linked long- and short-term exposures of outdoor PM_{2.5} and the incidence of nonfatal **strokes**, and found that for every 10 $\mu\text{g}/\text{m}^3$ increase in PM_{2.5} the risk ratio was 1.06 for long-term exposures which was higher than for short-term ones: 1.007 (Shin *et al.*, 2014). In another analysis including 20 studies to quantify the association between stroke incidence and mortality with PM exposure, for each 10 $\mu\text{g}/\text{m}^3$ increase in PM₁₀, they found a Hazard Ratio (HR) of 1.06 for having a stroke event and 1.08 for stroke mortality. Considering an increment of 5 $\mu\text{g}/\text{m}^3$ in PM_{2.5}, the HR was also 1.06 and 1.12 for stroke events and mortality, respectively (Scheers *et al.*, 2015). Regarding ischemic stroke onset, no association was detected between PM_{2.5} or black carbon from previous 72 hours

exposures in a study in Barcelona, but it did associate with the presence of large-artery atherosclerotic occlusions subtype (Vivanco-Hidalgo *et al.*, 2018).

Regarding stroke mortality, a first study related previous-day levels of PM_{2.5} and UFP with deaths from stroke (Kettunen *et al.*, 2007). Later, in patients presenting an ischemic stroke whose place of residence was known, it was reported higher post-stroke mortality among people living near high-traffic roadways, up to 20% higher rate, than patients living more distant to the roadway (Wilker *et al.*, 2013). In the same line, another group performed a meta-analysis including 45 studies and found that PM_{2.5} and PM₁₀ were associated with 1.4 and 0.5 risk ratios respectively with cerebrovascular disease mortality for every 10 µg/m³ increase in both PM, with no relevant associations between ischemic or hemorrhagic subtypes (Wang *et al.*, 2014). In China, a study conducted between 2014 and 2016 suggested that PM_{2.5} contributed to 40.3% of total stroke deaths (Song *et al.*, 2017), and another one conducted between 2008 and 2014 in a total of 63,997 ischemic stroke cases, showed that the relative risk of ischemic stroke onset increased with high levels of PM₁₀ (Wang *et al.*, 2020).

Within the ESCAPE project, a European collaboration of more than 30 European cohort studies, an increase in 5 µg/m³ in annual PM_{2.5} was associated with a 19% increased risk of stroke events even at the lower concentrations set by the air quality standards (Stafoggia *et al.*, 2014).

Altogether, these findings associate particulate matter from air pollution with cardiovascular events onset, hospital admissions and mortality, yet their relationship with the different subtypes of stroke remains unclear. All this evidence is further supported by the latest Global Burden of Disease report showing that among all worldwide deaths (59 million annually) 38% are due to cerebrovascular diseases, and ranking air pollution as the 5th risk factor (among a list of 79, above cancer or COPD) and stroke as the 2nd leading cause of death (Johnson *et al.*, 2019; Mannucci *et al.*, 2019).

Finally, supporting the idea that exposures to air pollution below the current EEA and Environmental Protection Agency (EPA, USA) standards might be too loose, an article published in September 2021 within the ELAPSE project, that

investigated the relationship between mortality and exposures to particulate matter in six European countries in a total of 325,367 participants and followed for an average of 19.5 years, pointed that an increase of 5 $\mu\text{g}/\text{m}^3$ in $\text{PM}_{2.5}$ was associated with 13% increase in natural deaths (Strak *et al.*, 2021). In line with these findings the WHO has recently presented more restricted guidelines with lower exposure limits for cities (pag.26).

Diesel exhaust particles and mechanisms of injury related to cardiovascular diseases

Despite these pieces of clinical evidence, the **mechanisms** through which particulate matter pollutants exert their actions and influence the development of stroke are still being under study.

Accordingly, there is some evidence associating the exposure to PM with brain alterations such as a) inflammation, b) altered repair mechanisms and c) increased pro-coagulating molecules (Brook *et al.*, 2010).

a) In humans, Calderón-Garcidueñas and colleagues observed increased expression of COX-2 and IL-1 β mRNA in brain regions (OB, frontal cortex and substantia nigra) of young adults residents of highly polluted areas, as well as disruption of the Blood Brain Barrier (BBB) (specifically, with an abnormal ZO-1 expression) (Calderón-Garcidueñas *et al.*, 2008b).

In healthy animals, several types of particles and different brain regions have been studied to identify different susceptibilities. For example, in analyzed OB, hippocampus (HC), thalamus, hypothalamus and entorhinal cortex of canines living in a highly polluted city vs. a low polluted one they showed a higher expression of nuclear factor-KB (NF- KB) and iNOS in cortical and endothelial cells, as well as degeneration of cortical neurons and apoptotic glial white matter cells in the first group (Calderón-Garcidueñas *et al.*, 2002). Other authors have reported that after the instillation of ultrafine carbon black (125 μg) in mice, 1 day/week, during 4 weeks, four hours after the last dose there was an induction of pro-inflammatory cytokines' (IL-1 β , TNFa) and chemokines' (CCL-2, CCL-3)

mRNA expression in the OB but not in the HC with the smallest-sized particles used (14 nm vs. 95 nm) (Win-Shwe *et al.*, 2006).

However, mice exposed to PM_{2.5} for 10 months, displayed elevated mRNA pro-inflammatory cytokine expression (IL-1 β , TNF α) and unaltered IL-6 in the hippocampus compared to animals exposed to filtered air (Fonken *et al.*, 2011).

Other studies exposing rats to different concentrations of diesel exhaust for 6 months (0, 35, 100, 311 and 992 $\mu\text{g}/\text{m}^3$), resulted in elevated levels of TNF α in the OB, frontal lobe, temporal lobe, midbrain and cerebellum, mainly with the highest tested dose (992 $\mu\text{g}/\text{m}^3$). Regarding Interleukines, no increase in IL-6 expression was observed, and only IL-1 β was increased in the midbrain with the highest concentration tested (Levesque *et al.*, 2011). In a different study, the same group exposed rats to inhale DEP for 4 weeks describing elevated levels of IL-6 and Iba-1 in the whole brain, as well as region-specific increases of TNF α , IL-1 β , IL-6, MIP1 α and Iba-1 in the OB, midbrain and cortex (Levesque *et al.*, 2011).

These previous investigations support the hypothesis that the smallest PM fractions can develop a higher inflammatory response and that it can change depending on the exposure time and the brain region studied.

b) Apart from the inflammatory responses, studies in rodents have reported reduced neurogenesis after DEP exposure. In rats that were born from mothers exposed during gestation to UFPM traffic-related air pollution had reduced adult neurogenesis, showing fewer new neurons in the Subgranular Zone (SGZ) of the HC (Woodward *et al.*, 2018). In mice, it was also observed a reduction in neurogenesis in the SGZ, Subventricular Zone (SVZ) and OB in males exposed to diesel exhaust only for 6 hours while in females the reduction was only observed in the OB (Coburn *et al.*, 2018).

In another study testing the effect on the olfactory function and proteolytic-Matrix Metalloproteinase (MMP) activation in BALB/c mice that inhaled DEP (100 $\mu\text{g}/\text{m}^3$) for 4 weeks or 8 weeks, the results showed that the short-time exposure group exhibited less olfactory sensitivity, which was recovered later as was seen in the 8-week group where no alteration was observed. The authors claimed that

the animals got adapted to the initial deleterious effect of the particles changing their response to the same stimulus after longer exposures (Kim *et al.*, 2019). Related to relevant components in neurovascular remodeling, such as the matrix metalloproteinases, the same study reported that after 8-weeks exposure, MMP-9 and MMP-14 were elevated in the temporal cortex compared with the control group. Indicating possible remodeling activation after long-term DEP exposure (Kim *et al.*, 2019).

c) Regarding the pro-thrombogenic changes, it has been described that in men with previous myocardial infarction, the exposure to DEP reduced the acute release of endogenous Tissue Plasminogen Activator (tPA), affecting their fibrinolytic capacity (Mills *et al.*, 2007). Also, increases in ambient PM_{2.5} were associated with shortened prothrombin time and more sCD40L (present in platelets), relating PM with enhanced clot formation factors (Xu *et al.*, 2019). Additionally, in pre-clinical models investigating the pro-thrombotic effects of DEP, mice that were exposed to DEP also showed reduced pro-thrombin time (Budinger *et al.*, 2011) and increased plasma fibrinogen (Emmrechts *et al.*, 2010) while in humans plasmatic fibrinogen did not associate to DEP exposure (Thompson *et al.*, 2010).

Overall, it has been described a consistent pro-inflammatory response in the brain after different DEP exposures in humans and in rodent models together with detrimental effects in neural cell populations. In addition, in the circulatory system, studies support the role of DEP unbalancing the coagulation system.

1.2. Stroke

Stroke description and epidemiology

Stroke is a cerebrovascular disease resulting from a pathological process of blood vessels (e.g., thrombosis, rupture, embolism...) that affects the brain parenchyma causing severe tissue damage and the loss of neurological functions. More specifically, stroke occurs after a sudden reduction in the blood flow of a brain blood vessel which in time leads to an area of complete cell death (infarction or hemorrhage) which might be surrounded by hypoperfused tissue at risk (ischemic

penumbra) or hematoma expansion, but also by reorganizing tissue (Carmichael, 2016).

Whereas ischemic stroke represents around 85% of all strokes, the mortality rate after a hemorrhagic stroke is higher (67.9%) than after an ischemic stroke (57.4%) (Virani *et al.*, 2021), thus the present thesis will focus on the ischemic stroke subtype by developing pre-clinical models of cerebral ischemia and an ex-vivo turbidimetric assay of clot formation and lysis.

Although stroke's incidence and mortality differ between countries, geographical regions, ethnic groups and sex, its incidence is expected to continue growing as the population ages and middle and low-income countries shift from an epidemiological communicable disease pattern to a non-communicable disease one (Johnson *et al.*, 2019; Katan and Luft, 2018; Manwani and McCullough, 2011). Related to mortality, stroke is the second leading cause of death globally: 5.5 million people deceased in 2016 (Johnson *et al.*, 2019). Moreover, one-third of stroke patients survive with neurological deficits, which would make them dependent on day-life activities. Particularly in Spain, stroke was the second cause of global death in 2017 (26,937 deaths), third in men and first in women and had a prevalence of 1.7% (661,512 people) measured that same year (Weber, 2019).

As explained above, and according to the Global Burden of Disease Study (Johnson *et al.*, 2019), among the total number of prevalent strokes worldwide in 2016 (80.1 million), 84.4% were ischemic (ischemic stroke), while 15.6% were the result of cerebral hemorrhages (hemorrhagic stroke).

Depending on the affected vessel and the site of the occlusion, different clinical features could be observed, corresponding to the absence of proper functionality of the non-irrigated brain area (**Fig. 3**). The Middle Cerebral Artery (MCA) is the most common artery involved in ischemic stroke, for example in a large study made with 2,213 ischemic patients, 50.8% had an MCA occlusion followed by 12.8% of small-vessel occlusions (12.8%) (Ng *et al.*, 2007). The MCA is one of the three major paired arteries supplying the brain, it irrigates parts of the frontal, temporal and parietal cortex (**Fig. 3**) and part of the basal ganglia and

the internal capsule, for this reason, its occlusion can result in many different neurological symptoms. For example, complete proximal occlusion of the MCA can cause contralateral hemiparesis, facial weakness, dysphagia or aphasia (Dusenbury and Alexandrov, 2020).

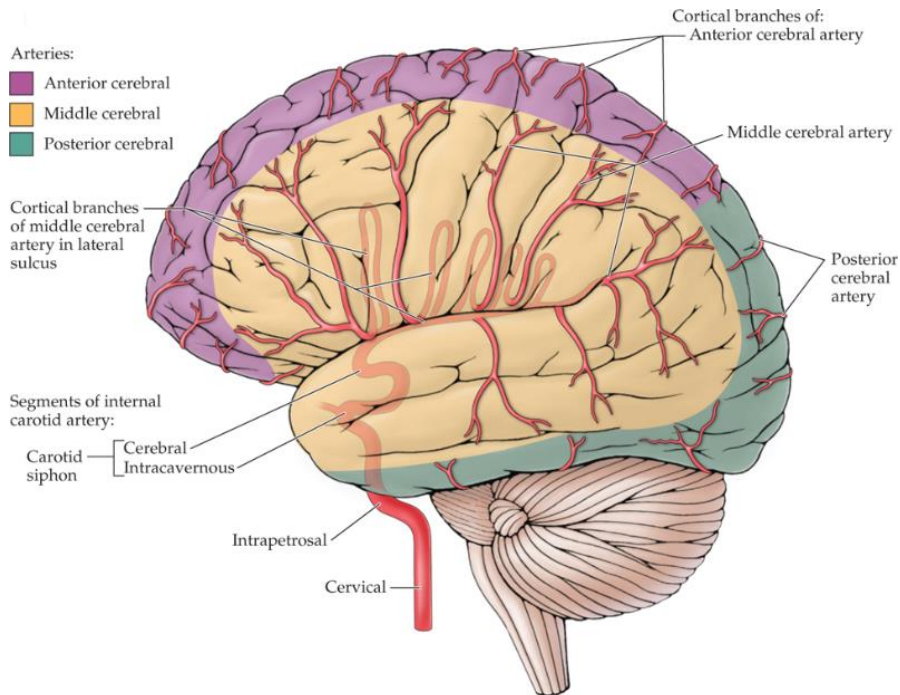


Figure 3: Vascular territories of the human brain: Cortical areas and blood vessel supply from the 3 main pairs of arteries: Anterior Cerebral Artery (ACA, pink shade), Middle Cerebral Artery (MCA, yellow shade) and Posterior Cerebral Artery (PCA, green shade). Extracted from Martin, JH. (2021). Neuroanatomy, text and atlas. McGraw Hill.

Further on, ischemic stroke can be subdivided into categories that represent its etiology: cardioembolic, atherosclerotic, lacunar, other specific causes or other unknown causes (Adams *et al.*, 1993). On the other hand, hemorrhagic stroke occurs when a blood vessel breaks giving place to intraparenchymal or subarachnoid hemorrhages (Murphy and Werring, 2020) (**Fig. 4**), a stroke presentation not covered in this thesis.

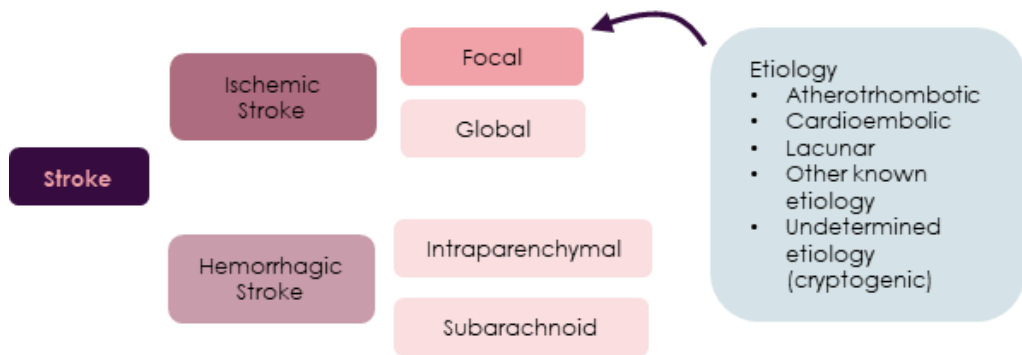


Figure 4: Classification of stroke subtypes and etiologies of focal ischemic stroke.

Associated with stroke, there are non-modifiable and modifiable risk factors. Non-modifiable risk factors are sex, ethnicity or age, whereas the modifiable ones are smoking, alcohol consumption, obesity, diet or hypertension, among others. Recently, air pollution exposure is being considered a modifiable risk factor for stroke disease, which has been discussed in more detail in previous pages (Boehme *et al.*, 2017; Dockery *et al.*, 1993; Kettunen *et al.*, 2007).

Importantly, the incidence of stroke could be reduced by changing lifestyle to reduce the incidence of the modifiable risk factors. The INTERSTROKE study found that 10 modifiable risk factors, including diet, physical activity or Arterial Hypertension (AHT), accounted for 90% of the risk for having a stroke (O'Donnell *et al.*, 2016). Whereas another study found that highly active individuals presented a 26% risk reduction of having an ischemic stroke when compared to insufficiently active individuals (Kyu *et al.*, 2016), highlighting the importance of first-stroke prevention.

Stroke etiology

Atherosclerosis and cardioembolisms are the two major causes of ischemic stroke. Atherosclerotic strokes are caused by the rupture of an atherosclerotic plaque that develops in the arteries supplying the brain, normally related to high cholesterol, atherosclerosis or diabetes. In the second case, the thrombus forms elsewhere and reaches the brain through the bloodstream, normally related to cardiac atrial fibrillation (Badimon and Vilahur, 2014).

The main difference among the formed clots is that cardioembolic specimens are mainly composed of red blood cells while the atherosclerotic ones have high proportions of platelets (Lee, 2020). However, in both situations, the activation of the coagulation cascade is involved and the presence of the fibrin component is relevant in both cases (see **Fig. 5**).

In the case of atherosclerosis, the atherosclerotic plaque which is a necrotic core surrounded by a lipid-rich cover makes the adjacent endothelial cells more fragile. At the end, after disruption of the endothelial cells or the atherosclerotic plaque, the necrotic core components are exposed in the circulation activating the intrinsic pathway of the coagulation cascade (**Fig. 5**).

In the cardioembolic etiology, a core of red blood cells is formed in the heart (usually) which can also activate the coagulation cascade.

This cascade triggers the formation of a blood thrombus which may compromise the arterial lumen leading to the presentation of acute ischemic syndromes. In the final steps of the cascade, fibrinogen, in the presence of thrombin, is turned into fibrin which covers the clot and at the same time the endothelium releases the Plasminogen Activator Inhibitor (PAI) switching the hemostatic system into a pro-coagulant situation (Badimon and Vilahur, 2014).

Under physiological conditions, the clot can be degraded in a process known as fibrinolysis. Here, endogenous cleavage of the fibrin takes place when tissue plasminogen activator promotes the conversion of plasminogen to plasmin that will finally degrade the fibrin. The synthesis of tPA by endothelial cells and secreted locally is stimulated by thrombin, hypoxia or adrenalin (Badimon and Vilahur, 2014).

In the end, the interplay between the described risk factors and these two pathways might be determinant for the occurrence of vessel occlusion. At this point and as a remark, the only approved pharmacological treatment to treat ischemic stroke consists in the Recombinant tPA (rtPA) which is a protease produced by recombinant cDNA technology capable of inducing thrombolysis in the occluded vessel (Gonzalez *et al.*, 2006) as shown in **Figure 5**.

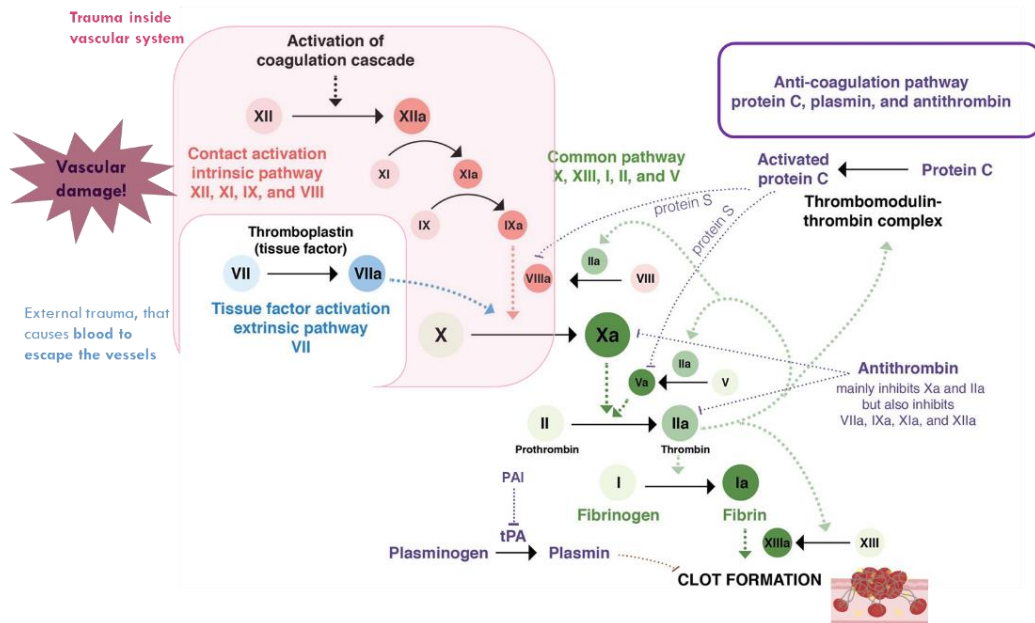


Figure 5: Coagulation cascade leading to clot formation and fibrinolytic pathways:

After vascular damage, hemostasis mechanisms are triggered. The intrinsic pathway (in pink) is activated after vascular damage inside the vessels, whereas the extrinsic pathway (in blue) activates if the damage occurs outside the blood vessels. Both pathways converge in the common pathway (in green), leading to clot formation. In purple appear the endogenous mechanisms of clot lysis. PAI: plasminogen activator inhibitor. tPA: tissue plasminogen activator.

Adapted from <https://step1.medbullets.com/hematology/111020/factor-v-leiden>

Ischemic cascade

If ischemic stroke finally occurs, there are several pathophysiological consequences underlying, described in the so-called *ischemic cascade*. This process leads to the formation of an infarct "core" where irreversible cell death starts within a few minutes after stroke onset, along with a surrounding tissue named "penumbra", which is a hypo-perfused area that still has the potential to recover within the first hours as long as the blood flow is properly restored (Astrup *et al.*, 1981; Hossmann, 1994; Kaufmann *et al.*, 1999).

It is worth understanding that both the core and penumbra, are dynamic units that can change in size depending on the collateral's supply, the occlusion site and duration. If penumbra is not rescued it will progressively become infarcted and the core will expand (Donnan *et al.*, 2009).

As mentioned, if there is a blood flow impairment it will lead to a series of neurochemical processes in the tissue known as the ischemic cascade (Dirnagl *et al.*, 1999) (**Fig.6**).

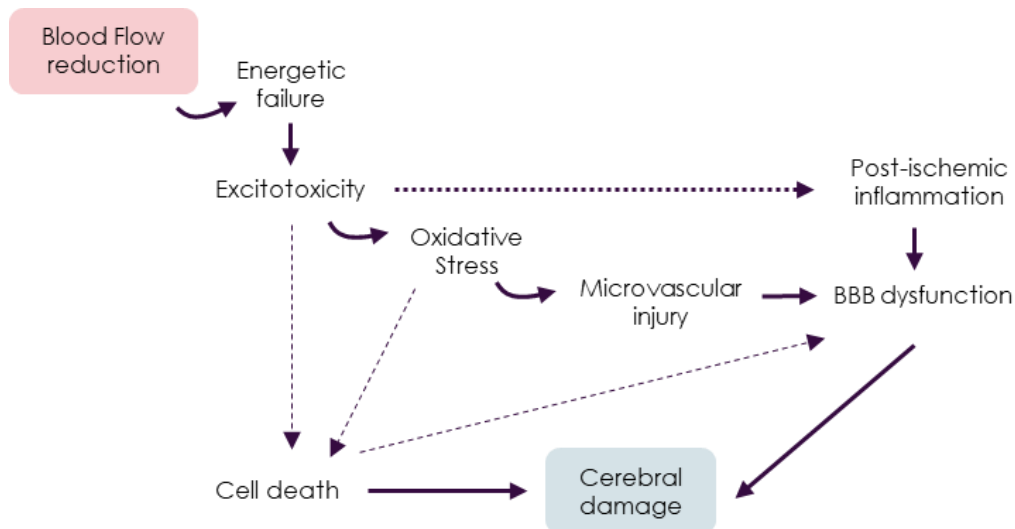


Figure 6: Diagram representing the main pathological mechanisms underlying acute ischemic stroke.

The brain is highly dependent on energy and oxygen; hence, neurons and glia will consume all available Adenosine Triphosphate (ATP) and glucose, resulting in loss of energy storage and causing a dysfunction in the energy-dependent ion transport pumps. Glutamate, the main excitotoxic neurotransmitter, will accumulate in the extracellular space because the reuptake process is collapsed, thus it will bind to Kainate, α -Amino-3-Hydroxy-5-Methyl-4-Isloxazole Propionic Acid Receptor (AMPA) and N-Methyl-D-Aspartate Receptor (NMDA) promoting massive calcium (Ca^{2+}) influx to the intracellular compartment (McCulloch, 1992). More intracellular calcium generates more glutamate release which amplifies again the initial ischemic injury.

Following the high ionic concentrations, water diffuses passively, resulting in cell swelling, cytotoxic edema and shrinking of extracellular space, which are the first markers studied with Magnetic Resonance Imaging (MRI) and Computed Tomography (CT) within the first hours after stroke. The excessive ionic load will

stimulate mitochondrial oxygen radical production in ischemic cells. These Reactive Oxygen Species (ROS) together with Ca^{2+} , a universal second messenger, will also activate proteolytic enzymes that will degrade cytoskeletal as well as extracellular proteins. As a result of excessive ROS, mitochondria function will be impaired, the inner membrane disrupted and the cytochrome C will be released (Fujimura *et al.*, 1998). At the end, these cascades will result in neuronal and glial death comprising necrosis, apoptosis and autophagy mechanisms (Qin *et al.*, 2008).

Besides cerebral cellular damage, oxidative stress also leads to matrix degradation and degeneration of endothelial cells by activation of matrix metalloproteinases causing vasculature injury and increasing blood-brain barrier permeability. At this point, the cerebrovascular system cannot auto-regulate anymore, and more inflammatory mediators and water will enter the injured site by increasing cerebral damage and infarct expansion into the ischemic penumbra (Brouns and De Deyn, 2009; Dirnagl *et al.*, 1999; Moskowitz *et al.*, 2010; Xing *et al.*, 2012).

Inflammation

As the ischemic cascade progresses rapidly after the insult, the initial phase of cell death leads to a new phase of inflammation (**Fig.7**).

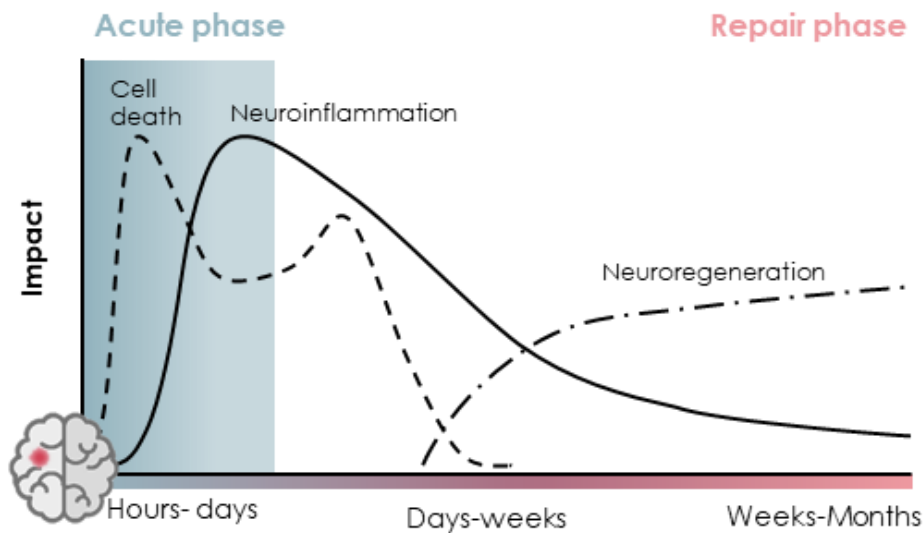


Figure 7: Timelapse of main events after ischemic stroke. Adapted from Roth and Liesz, 2016 and Carmichael, 2016.

There are inflammatory processes initiated in the brain parenchyma by the release of Damage-Associated Molecular Patterns (DAMP) from dying neurons. They will activate receptors on resident microglia and astrocytes that will as well produce inflammatory cytokines and chemokines (Anrather and Iadecola, 2016). These pro-inflammatory mediators such as cytokines (IL-1 β , IL-6, IL-10, IL-17), chemokines (MIP-1 α , IL-8), proteases (MMP-2, MMP-8, MMP-9) and other molecules (free radicals, iNOS, COX-2) released by neurons, astrocytes, glia and endothelial cells will attract circulating leukocytes, neutrophils, macrophages and mast cells, initiating a vascular inflammatory response. These cells will release more pro-inflammatory molecules promoting the infiltration of leukocytes (neutrophils, lymphocytes and monocytes) through the damaged BBB, causing a secondary brain injury (Buscemi *et al.*, 2019; Iadecola and Anrather, 2012; Roth and Liesz, 2016; Vogelgesang *et al.*, 2014).

The inflammatory phase is self-limiting and after some days it will be followed by a phase of tissue remodeling, reorganization and functional recovery.

Post-stroke Neurorepair

Weeks to months after stroke, patients might recover full or partial functional abilities because healthy areas take over functions of the injured regions, but also because the brain is a plastic tissue and it is able to trigger repair mechanisms in an attempt to recover the injured tissue (Pascual-Leone *et al.*, 2005; Patel *et al.*, 2000). Since the imaging of these processes in humans is still challenging (Sztriha *et al.*, 2012), the pre-clinical models in rodents can be useful to demonstrate nervous system plasticity, angiogenesis, neurogenesis and oligodendrogenesis related to functional recovery.

As explained above, cell death might expand through the penumbra and peri-infarct regions, triggering secondary injury cascades like reperfusion injury, due to the release of cytokines, MMPs, ROS, etc. But these same messengers are responsible for initiating neural repair and recovery mechanisms.

Plasticity refers to anatomical and functional changes in the CNS involving axonal sprouting, synaptogenesis and activation of parallel circuits to maintain the affected functions, leading to the formation of new connections (Angels Font *et al.*, 2010). Axonal sprouting involves the formation of new connections in peri-infarct areas and several molecules have been involved in these processes. For example, Growth and Differentiation Factor 10 (GDF10), secreted by neurons has been seen to promote axonal sprouting and enhance functional motor recovery in mice after stroke (Li *et al.*, 2015). Carmichael and colleagues studied the waves of expression of neuronal growth-promoting genes within the peri-infarct cortex during the period of axonal sprouting, being able to determine their sequential activation and inhibition and to identify a growth-promoting peri-infarct zone in contrast with a region of the glial scar (Carmichael *et al.*, 2005).

Synapse plasticity is another mechanism taking place after stroke. A decrease of spine density in surviving pyramidal neurons in the peri-infarct area, compared to control mice was reported by Mostany and colleagues, but after 2 months,

dendrites were slowly recovered depending on the degree of tissue perfusion (Mostany *et al.*, 2010).

Additionally, under normal conditions, adult mammalian brains present two areas of active **neurogenesis**: the SVZ of the lateral ventricles and the SGZ of the hippocampus, which are regions where new Neural Stem Cells (NSC) proliferate (Altman and Das, 1965). The NSC from the SVZ (**Fig.8**) migrate along the Rostral Migratory Stream (RMS) to finally mature into GABAergic interneurons in the granular and glomerular layers of the OB, where they seem to be essential for spatial memory and odor discrimination (Ming and Song, 2011). NSC of the SGZ will differentiate into glutamatergic granule cells in the Dentate Gyrus of the hippocampus (**Fig.9**), contributing to spatial-navigation learning or long-term spatial memory (Ming and Song, 2011).

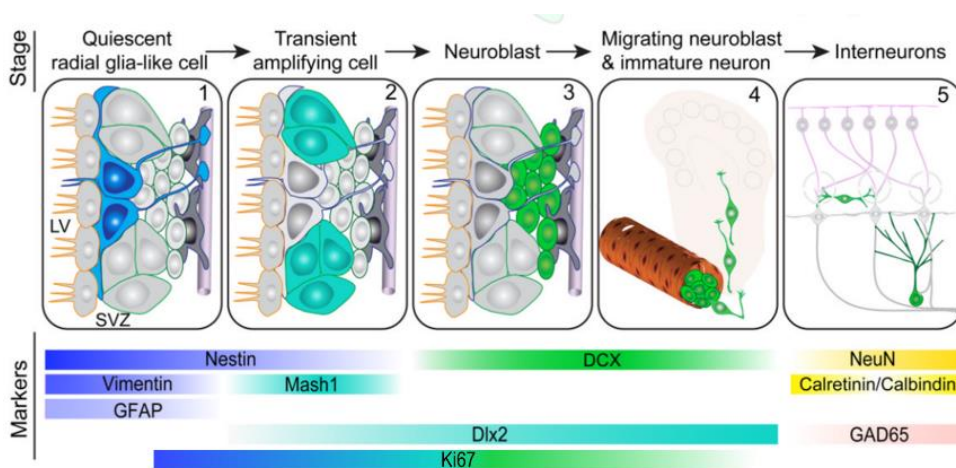


Figure 8: Adult neurogenesis in the subventricular zone. Radial glia-like cells develop with stage-specific markers into mature neurons: 1) Activation of quiescent radial glial cell-like cells; 2) Proliferation of transient amplifying cells; 3) Generation of neuroblasts; 4) Chain migration of neuroblasts along the RMS and radial migration in the olfactory bulb; 5) Synaptic integration and maturation of granule cells in the olfactory bulb. Adapted from Ming and Song, 2011.

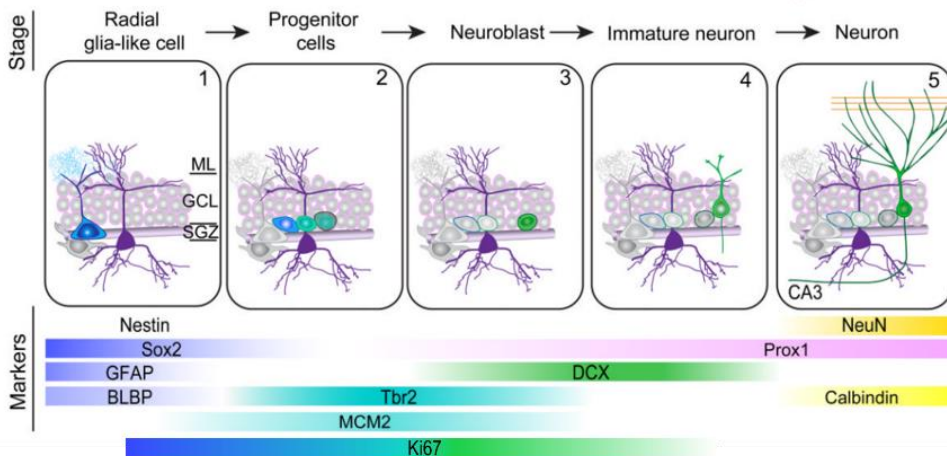


Figure 9: Adult neurogenesis in the subgranular zone with its stage-specific markers: 1) Activation of quiescent radial glial cell-like cells; 2) Proliferation of intermediate precursors; 3) Generation of neuroblasts; 4) Integration of immature neurons; 5) Synaptic integration and maturation of Dentate Gyrus' granule cells. Adapted from Ming and Song, 2011.

Several groups studied the endogenous post-stroke neurogenesis triggered by the ischemic injury, for example, free radicals generated in the infarcted tissue are one of the signals triggering poststroke neurogenesis, while their blockade reduced it (Hu *et al.*, 2014). Other stimulatory signals, that increase neuroblast proliferation in the SVZ, are cytokines like SDF-1 or angiopoietin-2 (Carmichael, 2016). Moreover, after proliferation, some neuroblasts were seen to re-route toward the damaged brain tissue (Arvidsson *et al.*, 2002). If the lesion reaches the striatum or the basal ganglia (structures next to the SVZ), the neuroblasts would migrate to these areas, a small proportion would mature and establish long-distance connections, though most of them would die. If the lesion was more distant to the SVZ (such as in the cortex), fewer neuroblasts migrate and even fewer numbers survive over time (Carmichael, 2016; Ohab and Carmichael, 2008).

For a proper maturation of newly formed neurons and an adequate brain function, cell to cell interactions are essential. In this sense, neurons, vessels and glia are in close association in the healthy brain, in a cellular arrangement called

the *neurovascular niche* where, for example, if the vessel's integrity is at stake it will affect other cells compromising the correct function of the tissue (Ohab and Carmichael, 2008). That gets importance at the SVZ and SGZ where **angiogenesis** is essential for neurogenesis and vice versa. After stroke, endothelial cells can secrete proteases, chemokines and growth factors to support newly formed neurons that are tightly coupled with blood vessels at the peri-infarct region (Ohab and Carmichael, 2008). *In vitro*, the co-culture of ischemic rat endothelial cells, with healthy SVZ neural progenitors increased the neural progenitor cell's proliferation and neural progenitors stimulated angiogenesis measured by capillary tube formation through the Vascular Endothelial Growth Factor (VEGF) secretion (Teng *et al.*, 2007).

In the brains of patients who died from an ischemic stroke, it has been described higher counts of blood vessels and activated endothelial cells in peri-infarct tissue compared to their contralateral hemispheres (Krupinski *et al.*, 1994). A similar pattern was observed in ischemic rats, whose vascular density of the ipsilateral hemisphere increased from day 1 to day 7 and then decreased again until day 14 (Lin *et al.*, 2002).

Several experiments show the **neurovascular coupling** within the repairing mechanisms. For example, rats subjected to striatal infarction (with endothelin-1) and treated 24h later with extracellular vesicles from mesenchymal stem cells, showed increased connectivity vs. control group with more proliferating cells co-localizing with markers of astrocytes or neuroblasts, which are essential components of the neurovascular unit, and displayed better performance in the rotarod or beam walking tests 28 days after the lesion (Otero-Ortega *et al.*, 2020). Also, in an experiment treating ischemic mice with Endothelial Progenitor Cells (EPC) or conditioned media from these EPC, both showed higher capillary density in peri-infarct areas and more axonal tracts only the EPC-treated mice compared to sham animals, which could be the anatomical basis for the forelimb strength improvement observed in both sets of treated animals (Rosell *et al.*, 2013). Another example is a study where in a mouse model of permanent distal MCA occlusion, a hyaluronic acid hydrogel with VEGF (encapsulated in heparin

nanocapsules) was injected into the stroke lesion. Five days after stroke it promoted tissue repair through the activation of endothelial cells, resulting in the formation of new vessels in the stroke cavity and the peri-infarct area, altogether leading to neurogenesis and axonogenesis 10 days after the transplant (Nih *et al.*, 2018).

Peripheral response

Nevertheless, the consequences of ischemia are not restricted to the injured brain. During the first days of stroke (**Fig.7**) once DAMP and cytokines reach the circulation, they induce a systemic immunological response stimulating primary (bone marrow and thymus) and secondary lymphoid organs (spleen and lymph nodes) (Liesz *et al.*, 2015).

In addition, the effect of stroke in systemic inflammation has been observed in patients and animal models: in patients, measurable inflammatory parameters such as body temperature or white blood cells counts correlated with stroke volumes. After successful thrombolysis, both parameters got significantly reduced, relating the systemic inflammatory response to stroke lesion and its attenuation with successful thrombolysis (Audebert *et al.*, 2004). In a study by Offner and colleagues, they observed an acute increase in levels of inflammatory cytokines in spleens, lymph nodes and T cells from ischemic mice, contrary to the suppression of all mediators observed in the spinal cord (Offner *et al.*, 2006). In the same line, Wong and colleagues demonstrated that after stroke, activation of the noradrenergic innervation in the mouse liver accounted for the immune suppression of Natural Killer T cells, while a blockade of the beta-adrenergic receptors boosted the immune response of these cells (Wong *et al.*, 2011). Moreover, the lungs of rats, 24 hours after stroke, evidenced pulmonary edema and presented higher amounts of pro-inflammatory markers (Samarý *et al.*, 2018).

With this background, it is assumed that, approximately 2 days post-stroke, the early inflammatory response gives place to a second phase known as Stroke-Induced Immunodepression (SIID) where lymphopenia and a shift of the T helper (Th) cell response from a Th-1 response to a Th-2 anti-inflammatory response is

observed (Iadecola and Anrather, 2012; Malone *et al.*, 2019; Winklewski *et al.*, 2014). The mechanisms underlying the SIID are thought to be:

- Exhaustion of immune cells in the periphery (Liesz *et al.*, 2015).
- Activation of the Sympathetic Nervous System (SNS) that innervates lymphoid organs: after stroke, the SNS activates and releases norepinephrine that inhibits the stimulation of the lymphoid organs (Liu *et al.*, 2017; Wong *et al.*, 2011).

By downregulating the peripheral immune response (lymphopenia), the CNS can protect itself from autoimmunity, but also be more prone to bacterial infections (Faura *et al.*, 2021; Malone *et al.*, 2019; Winklewski *et al.*, 2014).

In this sense, stroke-associated infections are one of the major complications, occurring in around 30% of patients. Among them, 10% develop pneumonia and urinary tract infections and 16% acute lung injury (Faura *et al.*, 2021; Samary *et al.*, 2018), then suggesting a special vulnerability of the lungs after brain damage.

Studies on how ischemic stroke affects lung immunity and cell populations have shown that 24 hours after transient MCA occlusion, lung's mice presented an increase in alveolar macrophages and neutrophils together with a reduction in T cells, B cells, Natural Killer cells (NK) and eosinophils, in concordance with the described immunodepression (Farris *et al.*, 2019). Others have reported increased IL-1 β mRNA expression in lung tissue of ischemic mice, without histological evidence of lung injury (Austin *et al.*, 2019) as well as increased lung macrophages on day 7 after stroke (Hoyer *et al.*, 2019). All of which points to the lungs as a fairly sensitive organ to the stroke insult.

Current stroke treatment and future perspectives

The only approved pharmacological agent to treat ischemic stroke patients is the recombinant tPA, commercialized as alteplase which acts degrading clot fibrin. The therapeutic window of this agent is 4.5 hours after stroke onset and it is known that a delayed administration is associated with increased intracranial hemorrhages and mortality, which narrows its therapeutic time window (Hacke *et al.*, 1998, 1995).

As described in previous pages, the microvascular environment is destabilized so recanalization can damage the BBB and participate in the development of hemorrhages. Moreover, tPA is a protease that can activate MMPs and increase BBB disruption (Kim, 2019). In consequence, a cautious screening of the patients needs to be done to select candidates for thrombolysis.

Even after thrombolytic therapy with rtPA, clots in large arteries can remain undissolved. In 2015, five randomized clinical trials concluded that mechanical thrombectomy within the first 8 hours improved functional recovery compared to groups only receiving pharmacological treatment (Aver *et al.*, 2015; Berkhemer *et al.*, 2014; Campbell *et al.*, 2015; Goyal *et al.*, 2015; Jovin *et al.*, 2015), all of them supporting the mechanical removal of the clot with endovascular procedures for acute stroke treatment which has become a new therapeutic approach for ischemic stroke.

However, a lot of research is still being conducted to widen the therapeutic possibilities for stroke patients. The main objectives are to find interventions able to reverse the ischemic process or to extend the therapeutic window by protecting the neural tissue (neuroprotection strategies). Additionally, since the efficiency of the endogenous repair mechanisms is low, and still one-third of stroke patients survive with neurological deficits, stroke research is also targeting the recovery phase (neurorepair strategies). In animal models, different approaches have been tested: to reduce neuroinflammation (Dabrowska *et al.*, 2019) by reducing excitotoxicity or ROS (Yang *et al.*, 2019) or by inactivating MMPs (Suofu *et al.*, 2012) or improving neuroangiogenesis mechanisms (Ma *et al.*, 2015; Nih *et al.*, 2018). However, nowadays no repair treatments have been approved beyond the neurorehabilitation programs to recover functional independence (Langhorne *et al.*, 2011). In this field, in August 2021, the Food and Drug Administration (FDA) approved a vagus nerve stimulation micro system to treat severe upper extremity motor deficits in chronic stroke patients (Engineer *et al.*, 2019) (<https://www.fda.gov/news-events/press-announcements/fda-approves-first-its-kind-stroke-rehabilitation-system>).

Animal models

Animal models of cerebral ischemia allow science to understand the pathology of the disease and to test potential therapeutic interventions. As explained above (**Fig.4**), stroke presents a heterogeneous spectrum of etiologies, each of them following different mechanisms of injury and repair.

In general, there are four types of animal models of ischemic stroke: complete global cerebral ischemia, incomplete global ischemia, focal cerebral ischemia and multifocal cerebral ischemia. Since ischemic stroke is the most prevalent type of stroke, the most frequently used models are the ones pursuing focal cerebral ischemia (Liu and Mccullough, 2010). Also, the most frequently involved artery in stroke is the MCA, so the focal ischemia models seek to occlude the MCA or its branches at proximal (large vessel occlusion) or distal levels (Llovera *et al.*, 2014).

The approximations developed can be summarized in:

- Models not requiring craniotomy: embolic model, intraluminal suture MCA occlusion model, photo-thrombosis model.
- **Models requiring craniotomy:** distal MCA occlusion model, endothelin-1 model.
- Posterior cerebral circulation stroke models.
- Venous thrombosis models.

The selected model, for the studies conducted in this thesis, is the distal Middle Cerebral Artery occlusion (MCAo). Traditionally, it can be achieved by ligation of the artery, its transient compression or by permanent electrocoagulation.

The last approach was first set up in 1937 in primates (Peterson *et al.*, 1937) and adapted to rodents by Tamura and colleagues (Tamura *et al.*, 1981). Nowadays this model has been refined and it is mostly performed in rodents requiring only a minor craniotomy to reach the distal part of the MCA, which is later occluded. The electrocoagulation method for the permanent MCA occlusion (pMCAo) was chosen for the present work.

In mice and rats, the ethical issues are more accepted despite the strict rules to Reduce, Refine and Recycle, “the 3Rs” that must be followed in the animal experimental procedures. Also, the tissue processing is simpler and the maintenance costs are reduced. Besides, rodent models allow the use of transgenic mice which is a research tool largely extended nowadays. Further

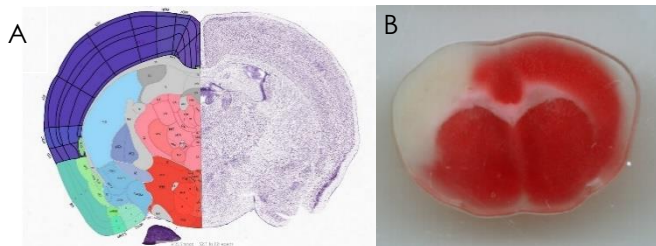


Figure 10: Images showing the infarcted cortex after permanent distal MCAo. A: Reference brain atlas image of a coronal section in the mouse brain. Highlighted in purple, in the left hemisphere, is the neocortex, the affected region after permanent distal occlusion. Image credit: Allen Institute. B: Fresh coronal slice of a mouse brain after permanent distal MCAo and viability staining. The infarcted neocortex, non-viable tissue, appears in white.

advantages of this model are that the obtained infarct is restricted to the neocortex (**Fig.10**) and finally, it is a model with high reproducibility and low mortality (Llovera *et al.*, 2014) allowing long-term follow-up after stroke, reducing costs and animal suffering.

However, it is important to note that all models have limitations and will only recreate part of the human condition. When studying molecular and cellular responses after stroke, which is in the scope of this thesis, differences in brain functional organization and complexity are less important, than in studies analyzing chronic recovery of function. For instance, the amount of white matter in human brains accounts for 60% and its affection clearly complicates cognitive improvement, but in rodents, the amount of white matter stands around 10% (Sommer, 2017). Other factors that affect stroke outcomes in humans are age, sex or the co-existence of cardiovascular risk factors, whereas in models, the species, strain or anesthesia exposure, are also factors to consider before selecting the experimental model (Liu and Mccullough, 2010).

The main disadvantage of the permanent MCAo model is the absence of reperfusion, but a large number of studies are already done in transient MCAo (tMCAo) models (88% in 2016), while short-time reperfusion only occurs in 2.5-11.3% of stroke patients (Carmichael, 2005; McBride and Zhang, 2017).

1.3. Matrix metalloproteinases

In the context of stroke, tPA and MMPs are the most important proteases that contribute to extracellular matrix remodeling. The reasons are the consistent links between MMPs and stroke lesions development and that rtPA is the only approved thrombolytic therapy to treat stroke (Gonzalez *et al.*, 2006).

MMPs are calcium-dependent zinc-endopeptidases that possess a catalytic domain with a Zn^{2+} -binding site preceded by a pro-peptide that maintains them as zymogens. They are classified into 6 families according to their structural domains and substrates (**Fig.11**): collagenases, gelatinases, stromelysins, Matrilysins, membrane-type MMPs and others (Rempe *et al.*, 2016).

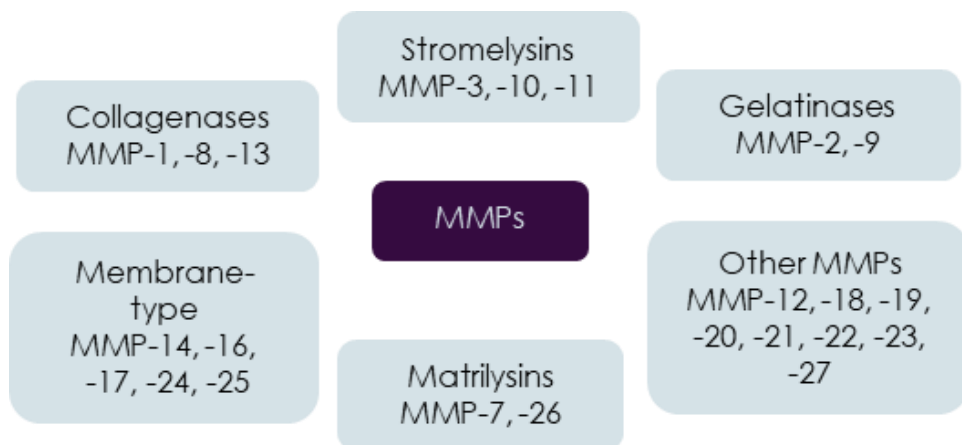


Figure 11: Classification of MMPs according to their substrate and structure.

In the CNS, MMPs are present at low levels in glia, neurons and endothelial cells, that rise when needed, except MMP-2 and membrane-type MMPs that are generally expressed constitutively (Rempe *et al.*, 2016; Yang and Candelario-Jalil, 2017).

Generally, MMPs are secreted outside the cell and activated, by cleavage of the pro-peptide, by other MMPs or proteases and frequently the plasminogen activator is involved. Once they are active, under physiological conditions, they can degrade the basal lamina and extracellular matrix components, playing an important role in regulating neurovascular unit permeability, tissue morphogenesis and brain plasticity and under pathological conditions they can be activated by ROS, nitric oxide, pH variations, etc. (Rempe *et al.*, 2016). Inhibition of their enzymatic activity involves Tissue Inhibitors of Metalloproteinases (TIMP1-4), that prevent excessive tissue degradation (Lakhan *et al.*, 2013; Yang and Rosenberg, 2015).

Matrix metalloproteinases and acute ischemic stroke

In the acute phase of stroke, neurons and glial cells release DAMP that activate astrocytes and microglia which in turn will secrete pro-inflammatory cytokines, chemokines and MMPs that will attract circulating cells to the injured site where they will release more MMPs (Iadecola and Anrather, 2012). Due to the activity of the MMPs, the degradation of the basement membrane will favor the malfunction of the neurovascular unit and will lead to BBB permeability and larger infarct lesions, giving rise to more leukocyte infiltration, cerebral edema and hemorrhagic complications (Yang and Rosenberg, 2015).

In human brain samples from ischemic strokes, levels of several MMPs are found higher than in controls: MMP-9 (Rosell *et al.*, 2006) or MMP-13 (Cuadrado *et al.*, 2009), both associated with larger lesion sizes (Rosell *et al.*, 2005). MMP-2 is also increased in plasma of first-stroke patients and was even higher in recurrent stroke (Li *et al.*, 2021). Additionally, MMP-8 was increased in serum samples of cardioembolic stroke patients and positively correlated with stroke severity (Palm *et al.*, 2018). Moreover, MMPs have been related to the presence of hemorrhagic transformations in humans (Abilleira *et al.*, 2003; Montaner *et al.*, 2003; Rosell *et al.*, 2006).

In a literature search and after Mendelian randomization to evaluate the causality of MMP levels and ischemic stroke risk by Cárcel-Márquez and colleagues, a strong association of MMP-12 plasma levels and all ischemic strokes

was established. Later, subdividing by type, large-artery atherosclerosis was associated with MMP-1 and MMP-12 levels, however, stroke outcome was not related to any MMP (Cárcel-Márquez *et al.*, 2021).

In animal models of ischemic stroke, MMP levels were also increased and the pathological mechanisms have been analyzed. In this regard, MMP-2, -3 and -9 have been deeply studied: for example, MMP-2 and -9 were increased in mice brains 8 hours after transient MCAo (Suofu *et al.*, 2012). In another study mRNA expression was observed at different times points: MMP-3 was increased 1 day after stroke, MMP-10 was increased 2 days after and MMP-2, -8, -9 and -13 were increased on day 3 (Cai *et al.*, 2020). Concerning rat models, 30 mins after ischemia, MMP-13 was already augmented in the ischemic brain compared to controls (Cuadrado *et al.*, 2009). Further on, in rats subjected to a tMCAo, the increased activation of MMP-2 correlated with the degradation of claudin-5 and occludin, essential BBB proteins (Yang *et al.*, 2007). To further characterize changes in MMP content in mice 6h, 24h and 72h after tMCAo and treatment with rtPA, another group studied a larger number of MMPs (MMP-1, -2, -3, -7, -8, -9, -10, -12 and -13) and found that MMP-1, -2, -9, -10 and -13 were increased at 24h post-ischemia and that MMP-1, -2 and -10 were further increased at 72 hours (Lenglet *et al.*, 2014).

All of these studies evidence the acute role of MMPs in ischemic brain injury both in humans and rodents, which has led to other studies on their potential role as stroke biomarkers. For example, MMP-9 was found increased in mice plasma 24h after MCAo (Park *et al.*, 2009) and in CSF and serum of Rhesus monkeys (Zhang *et al.*, 2017). In this last study, MMP-9 levels, in the acute phase, correlated with brain injury at 24 hours post-reperfusion matching with the correlation observed in humans for MMP-8, -9 and -13 (Cuadrado *et al.*, 2009; Palm *et al.*, 2018; Rosell *et al.*, 2006).

As detailed, following the acute phase of ischemic stroke, high amounts of MMPs can aggravate the lesion and drive to complications (larger infarcts or intracranial hemorrhages). For this reason, these molecules have been studied as possible therapeutic targets for stroke, especially after thrombolysis. Studies in

Knock-Out (KO) mice mainly proved reduced infarct volumes, as in MMP-9 KO (Morancho *et al.*, 2015) and MMP-13 KO animals after tMCAo (Ma *et al.*, 2016a). However, others reported no reduction in the infarct lesion in MMP-9 KO mice that underwent a transient MCAo procedure (Suzuki *et al.*, 2007). Also, double KO MMP-2/MMP-9 mice had smaller infarct volumes and were protected against hemorrhages in cortical areas compared to Wild Type (WT) mice and single KO for each MMP (Suofu *et al.*, 2012). In the same line, MMP-3 KO mice that underwent a photo-thrombotic MCAo procedure displayed less intracerebral bleedings induced by tPA than WT animals (Suzuki *et al.*, 2007).

Matrix metalloproteinases and neurorepair mechanisms

Although MMPs participate during the acute phase of stroke (**Fig.7**) degrading the extracellular matrix and increasing the lesion, they are **essential** during the neurorepair phase. Years after studying the detrimental actions of MMPs, it is accepted that treatments inhibiting MMPs have proven beneficial in acute rodent models, but if maintained for days they resulted detrimental regarding recovery outcomes (Yang and Rosenberg, 2015).

In this regard, rats treated with MMP inhibitors (BB-94) from day 7 until day 14 post tMCAo, the neurovascular remodeling was suppressed in peri-infarct areas (related to decreased VEGF) and the infarct volume became larger, impairing functional recovery at 14 days (Zhao *et al.*, 2006). Consequently, these proteinases are essential for repairing mechanisms after stroke but also in the previously mentioned processes of neurogenesis, synaptic plasticity and angiogenesis. Regarding neurogenesis, 2 weeks after tMCAo in mice, neuroblasts from the SVZ co-localized with MMP-9, but after inhibiting MMP-9 the number of migrating neuroblasts was reduced (Lee *et al.*, 2006).

In vitro, the patterns of expression of MMP-1, -2 and -9 were studied in human adult olfactory ectomesenchymal stem cells and correlated with the migration ability of the cells, but after removing MMP-2 and -9 from the media, the previously observed neurite growth and axodendritic differentiation of cortical neurons were abolished (Ould-Yahoui *et al.*, 2013).

Another proof of their implication in neurorepair is that MMPs also favor the formation of peri-neural networks which are formed by large molecules surrounding neurons (like proteoglycans) and are essential for synaptic function and neuroplasticity by participating in their re-organization by cleaving the surrounding molecules (Yang and Candelario-Jalil, 2017). Angiogenesis is another process that depends on the presence of MMPs. After MMP-13 inhibition, pro-angiogenic factors (VEGF-A, angiopoietin-2), as well as vessel density, were reduced in peri-infarct brain vs. WT mice (Ma et al., 2016a), similar to what other authors described in rats after blocking MMPs' activity after ischemia (Zhao et al., 2006).

With this, we have learned that inhibiting MMP activity for a long time might not be the adequate approach in ischemic stroke treatment, a better situation would be to modulate them in order to reduce the detrimental effects during the acute phase and potentiate the beneficial ones required in the repair phase.

1.4. Thesis hypothesis:

Diesel exhaust particles interact with pathophysiological mechanisms of injury and repair in the context of ischemic stroke

As we explained, there are strong associations between traffic-related pollutants with the cardiovascular disease burden. However, the pathophysiological mechanisms of DEP exposure that could influence development, damage or recovery referring to ischemic stroke are poorly understood.

Very recently, Xu and colleagues correlated peaks of PM_{2.5} in China, with increased circulating MMP-1, -2, -3, -7, -8, -9 and decreased TIMP-1 and -2. Together with a shortened pro-thrombin time and increased sCD40L, and IL-1 β in humans (Xu et al., 2019), therefore interconnecting air pollutants with stroke by means of stimulating potential inflammatory and thrombogenic factors closely involved in the disease.

Basic research to understand how outdoor particulate matter is affecting ischemic stroke is needed. Up to date, only one pre-clinical study investigated exposure to particles *before* ischemia in mice receiving nanoPM collected from Los Angeles for 5 hours/day, 3 days/week during 3 weeks through exposure chambers. Twenty-four hours after the last exposure they underwent transient MCAo and 24 hours later they were euthanized. Researchers found an increased infarct volume, higher granulocyte cell counts and more complement C5 in the ischemic core compared to the filtered air animals. Suggesting that inhalation with PM has an impact on the size and severity of the stroke (Liu *et al.*, 2016). Although another study (Zhang *et al.*, 2016) found increased astrocytic activity and reduced locomotion in ischemic rats instilled with PM_{2.5} for 7 days *after* MCAo compared to the ischemic group alone.

The work presented in this thesis aims to further elucidate the plausible association between diesel particles, brain inflammation and its subsequent relation with potential brain lesion exacerbation after stroke, but also their possible interaction with the hemostatic system which could predispose individuals to develop an ischemic stroke. The final goal is to better understand the risks and mechanisms underlying this pathology and provide insights to take action and prevent stroke in the near future.

Objectives

General objective

To study the influence of inhaled diesel exhaust particles in the brain, lungs and blood related to the development of acute ischemic stroke.

Secondary objectives

1. To evaluate the effects of the acute and chronic DEP inhalation in naïve mice that could influence stroke injury and posterior recovery evolution after ischemia.
2. To evaluate brain injury exacerbation, molecular and cellular changes after acute and chronic DEP exposure in a mouse model of cerebral ischemia.
3. To describe changes induced by DEP exposure in mouse and human plasma samples in clot formation and tPA-induced thrombolysis in a turbidimetric clot assay, in the context of stroke.

Materials and Methods

3.1. Diesel exhaust particles

DEP were purchased at the National Institute of Standards and Technology (NIST, Gaithersburg, USA), as Standard Reference Material (SRM). Specifically, SRM2975 is obtained from an industrial diesel-powered forklift and SRM1650b is representative of a heavy-duty exhaust engine, both containing all constituents of the diesel particulate matter. Characteristics of SRM2975 and SRM1650b dust are well characterized and are shown in Annex II and Annex III.

Since DEP contain constituents of known and unknown toxicities and mutagenicities, during their handling extreme caution and security measures were taken: all manipulation took place under a laboratory fume hood, double gloves, a filtering face piece-3 mask (FFP-3, Kimberly-Clark, Jackson safety, India) and safety glasses were used to prevent direct particle contact.

For *in vivo* intranasal mice instillations, DEP were diluted in Phosphate Buffered Saline (PBS, 1x) at 7.5 mg/ml and for *in vitro* experiments the same dilutant was used but different concentrations were tested as described below.

3.2. Determination of particle size distribution

The size distribution of these particles in different conditions after dilution in PBS was studied by laser diffraction, dynamic light scattering and electron microscopy to determine the optimal protocol for the intranasal instillation considering the fractions of PM₁₀ and PM_{2.5} contained in the preparations.

The optical properties of the particles SRM1650b (Refractive Index, RI: 1.5, Absorption Index, AI: 0.1), SRM 2975 (RI: 2.45, AI: 0.5) and the dispersant: PBS (viscosity, cP: 0.8882, RI: 1.33, DC: 79) were set for the Mastersizer and Zetasizer analyzers.

Laser Diffraction

The laser diffraction technique determines the particle size distribution of a suspension by measuring the angular variation in the intensity of scattered light as a laser beam passes through a dispersed particulate sample. Relative to the

laser beam, large particles scatter light at small angles and small particles scatter light at larger angles.

A Mastersizer 2000 (Small Volume Sample Dispersion Unit, Malvern Panalytical, Netherlands and UK) is capable of detecting particle sizes in a broad range (from 0.02 to 2000 μm) using this technology. The equipment, available at the Institute of Material Science in Barcelona (Nanbiosis platform from CIBER-BBN at ICMAB), was used for particle size distribution in suspended preparations of DEP (SRM2975 and SRM1650b) in PBS.

DEP suspensions of 0.5 mg/ml ($n=4$ per SRM2975 and SRM1650b) were freshly prepared 2 hours before measurements, sonicated (Branson 5800 Ultrasonic Cleaner, 2.5-gallon, 40 kHz) for different times (0, 10, 30 and 60 minutes) and then analyzed.

Dynamic Light Scattering (DLS)

The measurements of the suspended particles, in this case, are taken at short time intervals and are based on the Brownian motion of the particles. Theoretically, particles in a liquid move randomly and constantly, if the change in movement is small the samples can be classified as large, on the contrary, if there has been more movement the sample will be identified as small. The Zetasizer system can detect particle sizes in the range of $3 \times 10^{-4} \mu\text{m}$ to $10 \mu\text{m}$ keeping the measurements in the smaller range fraction of particulate matter and up to PM_{10} .

For this reason and to further understand the particle-size distribution under our experimental conditions and particularly the smaller fraction distribution of both SRM2975 and SRM1650b, DEP suspensions of 7.5 mg/ml ($n=3$ per SRM) were analyzed in a Nano Zetasizer (Malvern Panalytical, Netherlands and UK) under the following conditions:

1. Freshly prepared and sonicated 10 minutes.
2. Freshly prepared, sonicated 10 minutes, frozen for 5 days, thawed and sonicated for 10 minutes.

Scanning Electron Microscopy (SEM)

DEP suspensions were further imaged by Field Emission SEM as follows: 3 µl of fresh and frozen SRM2975 and SRM1650b (7.5 mg/ml), sonicated for 10 minutes, were deposited on a silicon chip and let dry overnight. Uncoated samples were observed using a Zeiss Merlin Field Emission Scanning Microscope at 3Kv acceleration voltage and images were obtained with the secondary electron detector.

Cryo-Transmission Electron Microscopy (Cryo-TEM)

The above-mentioned samples for the SEM analysis were also used for Cryo-TEM imaging.

After glow discharge, 3.9 µl of DEP suspensions were deposited onto a 400-mesh copper grid supported by a Holey Carbon film which was mounted on a plunger (Leica EM GP), blotted for 1.9-10 seconds with Whatman no. 1 filter paper and finally vitrified by rapid immersion in liquid ethane (-179°C).

The grid was mounted on a Gatan 626 cryo-transfer system and inserted into the microscope. Images were obtained using a Jeol JEM 2011 cryo-electron microscope operated at 200kV, recorded on a Gatan Ultrascan US1000 CCD camera.

3.3. Neurosphere and Neural Stem Cells Yields

Neurosphere cultures derived from the SVZ of adult mice were conducted to assess the effect of DEP on the viability of NSC, involved in neurogenesis. Frozen NSC were cultured in floating conditions to allow neurosphere formation and growth as described by our group (Gabriel-Salazar *et al.*, 2021).

For DEP testing, single NSC were cultured in uncoated 25 cm² flasks, with 5 ml of growth media containing a 1:1 proportion of high glucose DMEM media (Gibco™, 11965084) with Ham's F12 (Gibco™, 21765-037), supplemented with FGF (Gibco™, PHG0021), EGF (Gibco™, PHG0011-100µg), heparin (Sigma, H-3149-50Ku), L-glutamine, B27 (Gibco™, 12587-010) and Penicillin/Streptomycin. After 5 days in culture at 37 °C with 5% of CO₂, cells formed the neurosphere structures

and were ready for collection when they were first centrifuged at 285 rcf for 5 min, then disaggregated by manual pipetting and finally seeded for experimental testing.

For all experiments, single NSC were cultured in uncoated 12-well plates at a density of 30,000 cells/ml. In the first set of experiments, single cells were treated immediately after seeding (T_0) with different doses of DEP (SRM 2975) ranging from 0.1 to 25 $\mu\text{g/ml}$. In the second set of experiments, DEP were added to the wells in the same concentrations 2 days after seeding (T_2), when neurospheres were already formed. All conditions were tested by duplicate in each experiment plate and replicated 3-7 times.

The effect of the DEP on NSC viability was assessed by two parallel methods: a commercially available kit based on WST-8 tetrazolium salt reduction (Cell Counting Kit-8, Dojindo) and direct cell counting with Trypan blue. Briefly, at day 4 after seeding, WST-8 reagent (10% of final volume) was added to the wells with growing media and after 1-hour incubation, culture media with floating neurospheres was removed and centrifuged at 1,500 rpm for 5 mins to obtain the supernatant where the absorbance at 450 nm was determined. For the direct cell counting, the remaining cell pellet was re-suspended in 200 μl of fresh NSC media by gentle pipetting to disaggregate the neurospheres into single cells. The cell suspension was then diluted with Trypan Blue at 1:1 and cells were counted in a Neubauer chamber under a phase-contrast microscope. With the trypan blue exclusion method, non-viable cells incorporate the blue staining and can be distinguished from the viable cells that remain bright. Cell viability and cell counts were referred to as the percentage of absorbance or number of cells, respectively, and compared to the control vehicle group.

Additionally, just before the WST-8 assay at day 4 after seeding, 2 images per well were acquired with a MicroCopiaDigital XM Full HD Camera connected to a Nikon Eclipse TS100 microscope with the 4x objective. Later, using the Image J software, the number of neurospheres per field of view was counted and the mean diameter of all neurospheres in the image was measured.

3.4. *In vivo* exposure to diesel exhaust particles and experimental mouse model of cerebral ischemia

Preparation of DEP

SRM2975 and SRM1650b of DEP were suspended in PBS at 7.5 mg/ml. Aliquots of suspended DEP or only PBS, which served as vehicle solution for the control group, were sonicated for 10 minutes using an ultrasonic bath (Branson 5800 Ultrasonic Cleaner, 2.5-gallon, 40 kHz) and frozen at -20°C until use. Before administration, the solution was thawed and sonicated 10 minutes again before use.

Animals

Male BALB/cAnNRj mice (6 to 9 weeks old) were purchased from Janvier Labs (Saint Berthevin, France). All animals were housed in groups of 3 to 5 in plastic cages (Innovive, San Diego, USA) where food and water were given *ad libitum*. Prior to the experimental procedure, mice were acclimatized to the housing facility (Temperature: 24°C, relative humidity: 30-70% and 12 hours light-dark cycle) for several days.

All experimental procedures were approved by the Ethics Committee of Animal Experimentation of the Vall d'Hebron Research Institute (CEEa 57/17) with posterior Governmental approval and conducted following Spanish legislation and the Directives of the European Union.

DEP exposure

DEP exposure was conducted by intranasal instillations of PBS, SRM297 or SRM1650b. Instillation was performed using a micropipette, with the mice in supine position and after 3 minutes of 5% inhalative anesthesia (Isoflurane, Abbot Laboratories, Spain) in medicinal air (79%N₂, 21%O₂). Mice received 20 µl of PBS or 150 µg of DEP suspended in 20 µL of PBS (7.5 mg/ml) at small drops in each nostril. Afterward, animals were left to recover in a cage with a heating pad.

Mice were assigned into DEP or Control groups according to the following aims:

Objective 1 (Fig.12): to evaluate the effects of acute and chronic DEP instillation in the inflammatory MMP response in brains and lungs and the CNS cellular affection in **healthy** (naïve) animals.

- A. Acute exposure (**Fig. 12A**): Mice were exposed for 3 consecutive days, 24 hours after the last instillation they were euthanized and brains, lungs and plasmas were collected and stored frozen until use.
- B. Chronic exposure (**Fig. 12B**): Mice were exposed for 3 weeks with 5 consecutive daily instillations per week except for the last week when 24 hours after the 4th instillation they were euthanized and their organs collected.

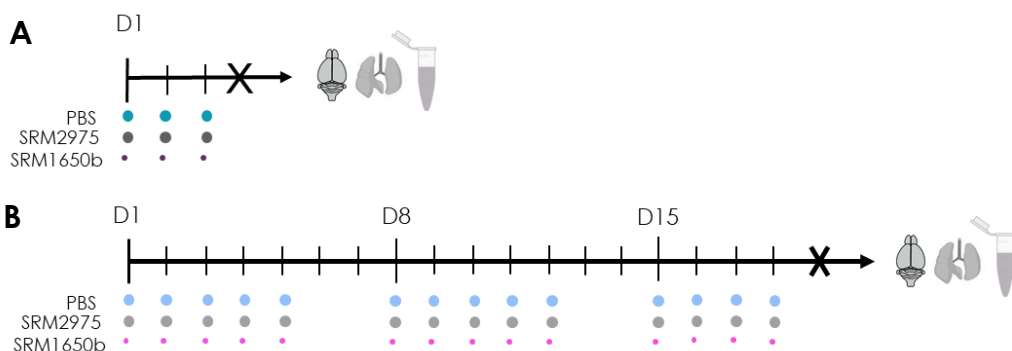


Figure 12: Experimental protocol to study the effects of DEP instillation influencing the physiology of healthy animals. Two exposure times were studied: A: acute (3 days) and B: chronic (3 weeks). D (day), X (euthanasia). After euthanasia brains, lungs and plasma were obtained for future analyses.

Objective 2 (Fig. 13): To evaluate acute brain injury, MMP levels and CNS cell population's alterations together with lung systemic inflammatory response after chronic DEP exposure in a mouse model of cerebral **ischemia**.

- A. Acute exposure before ischemia (**Fig. 13A**): Mice were exposed for 3 consecutive days (PBS, SRM2975, SRM1650b), 24 hours after the last instillation they underwent distal permanent MCAo surgery and 24 hours later they were euthanized. Forepaw strength was evaluated before and after ischemia by the grip strength meter test.

- B. Chronic exposure before ischemia (**Fig. 13B**): Mice were exposed for 3 weeks (PBS, SRM2975, SRM1650b), as previously described, 24 hours after the last instillation they underwent distal permanent MCAo surgery and 24 hours later they were euthanized. The grip test was also conducted.
- C. Acute exposure (PBS or SRM1650b) was followed by ischemia and 48 hours later the animals were euthanized (**Fig. 13C**).
- D. Ischemia was performed 24 hours after the chronic exposure (PBS or SRM1650b) and 48 hours later mice were euthanized (**Fig. 13D**).

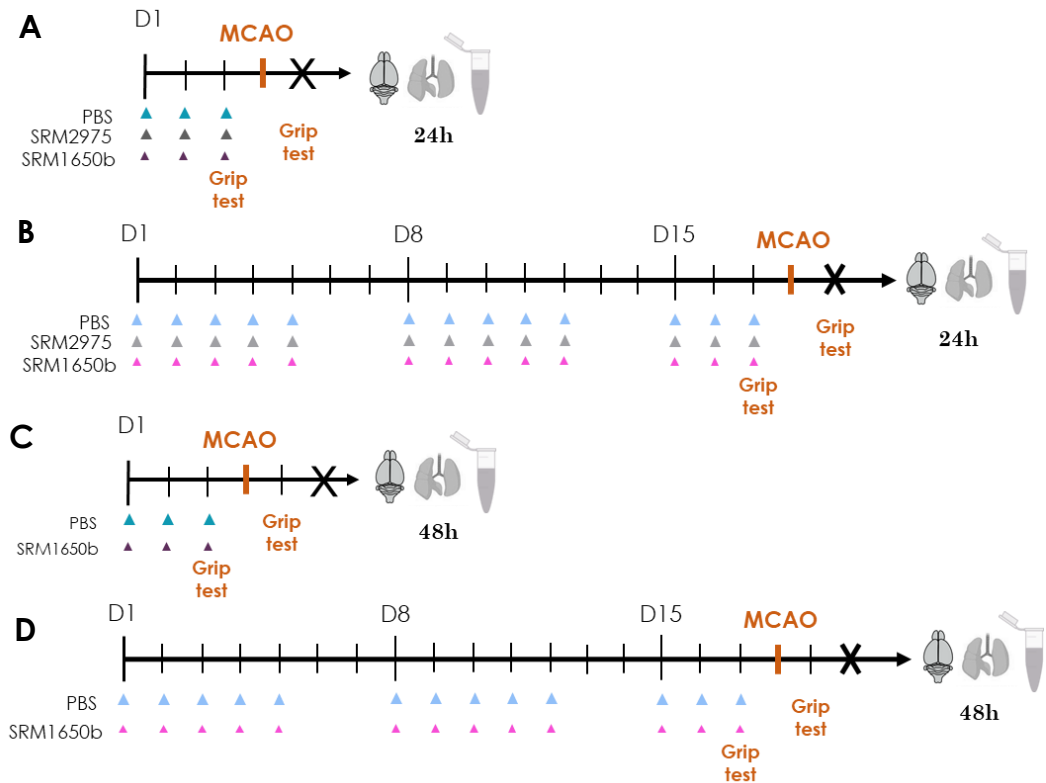


Figure 13: Experimental protocol to study the effects of DEP instillation after ischemic brain injury. Animals were instilled acutely (3 days, A, C) or chronically (3 weeks, B, D) with DEP or vehicle as indicated. Twenty-four hours after the last instillation, animals underwent permanent distal MCAo and they were euthanized 24 or 48 hours after surgery. Grip Tests were performed before and after surgery. D (day), X (euthanasia).

Grip strength-meter test

This test is used to evaluate both stroke severity and functional outcome during ischemia. It measures the forelimb maximal force a mouse can exhibit when grasping a grid. Briefly, a trained researcher blinded to treatment holds the mouse from the base of the tail allowing its forepaws to grab the center of the grid. The animal is then pulled back and the force is recorded in the strength-meter (Bioseb, France). Each animal had 6 attempts and the mean value was used for analyses.

Permanent focal cerebral ischemia model

As detailed in **Figure 13**, 24 hours after the last instillation, animals underwent distal pMCAo which causes cortical ischemic injury (**Fig. 10**) (Rosell *et al.*, 2013).

The procedure, schematically represented in **Figure 14**, started with deep anesthesia induction with 5% isoflurane (Abbot Laboratories, Spain) and was maintained with 2% in medicinal air (79%N₂, 21%O₂). Body temperature was controlled between 36-37 °C by placing the mice on a self-regulating heating pad, also the eyes were protected from drying during surgery with ophthalmic ointment (LipolacTM, Angelini Farmaceutica, Spain). Then, the skin area between the left eye and ear was disinfected and an incision was made to expose the temporal muscle which was cut and retracted with a 6-0 silk suture (TB10, Suturas Aragó, Spain). The MCA was identified through the translucent skull with the use of a microscope (Leica MS5, Leica, Heerburg, Switzerland) and the laser Doppler probe (Moor Instruments, UK) was positioned distally in a thinned spot of the frontal lobe onto the posterior branch of the MCA to monitor transcranial cortical MCA blood flow.

Next, a small craniotomy in the frontotemporal bone was performed using a high-speed microdrill (FST, 19007-05) to expose the cortical MCA portion, which later was compressed by a 30G needle with the help of a micromanipulator (**Fig. 14**).

After ensuring an 80% decrease in the cerebral blood flow (considering 100% the pre-occlusion value) the cortical portion (before the bifurcation of the anterior branch), was finally electrocoagulated indirectly through the needle with the use

of a cauterizer (Change-A-Tip™, Aaron Medical) (Ballesteros *et al.*, 2014; Dorr *et al.*, 2007) (**Fig. 14**).

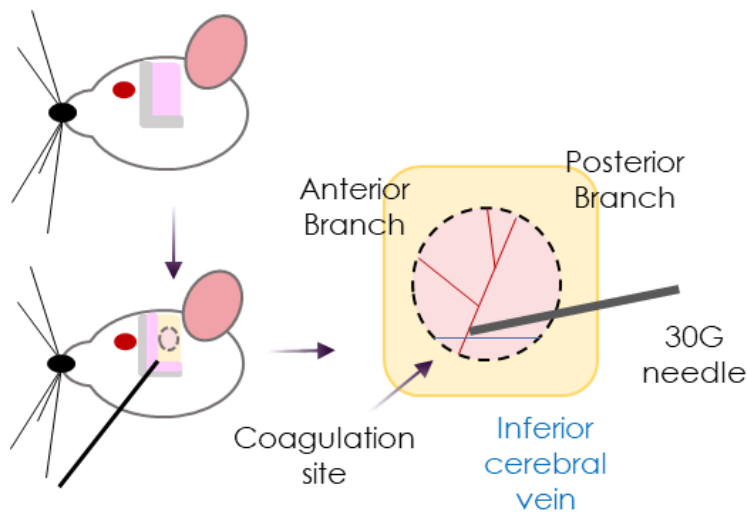


Figure 14: Representation of permanent MCAo distal surgery. After retracting the skin and the temporal muscle, the MCA is identified, a small craniotomy is done in the frontotemporal lobe and then it is coagulated in the trunk below the anterior branch of the MCA. Adapted from Ballesteros *et al.*, 2014.

Muscle and skin were re-placed to their original position, the skin was sutured with a 5-0 silk (TB12, Suturas Aragón, Spain) and disinfected once again. Buprenorphine (0.1 mg/Kg, Divasa Farma-Vic S.A.) was administered subcutaneously to avoid post-surgical pain and discomfort and finally, mice were allowed to recover spontaneously in a nursing cage with a heating pad.

Euthanasia and sample processing

Twenty-four hours after surgery (**Fig. 13**), animals were deeply anesthetized (4% isoflurane), the chest was exposed and a cardiac puncture was done in the left ventricle to obtain arterial blood samples. Blood was transferred into 3.2% citrate microtubes (0.5 ml, Sarstedt, Spain), centrifuged at 1,500 rcf for 10 minutes at 4°C to obtain the plasma fraction and stored at -80°C.

Later, mice were euthanized by transcardial perfusion of 20 ml of ice-cold saline and liver and lungs were obtained, frozen in dry ice and stored at -80°C. Finally,

whole brains were removed and followed different storing protocols depending on their subsequent use.

For immunohistological purposes, 10 minutes before euthanasia mice were injected intravenously (retro-orbitally) with Dylight 594-labeled tomato lectin (35 µg/mouse, DL-1177, Vector Laboratories, USA), to label functional blood vessels. After euthanasia, the complete left hemisphere of naïve mice (n=19, **Fig. 12**) was immersed overnight in 4% formaldehyde (AppliChem), transferred to 30% sucrose until sunk (48h), embedded in OCT (Tissue Tek) and frozen at -80°C until use. Ischemic brains (n=20, **Fig. 13**) were divided into ipsilateral and contralateral hemispheres and followed the same fixation protocol.

For molecular biology, the brain (n=75, **Fig. 12** and **Fig. 13**) was extracted and dissected in the OB, HC, striatum (ST) and cortex (CX) which were snap-frozen in dry ice and kept at -80°C for posterior homogenization and collection of the protein fraction (**Fig.15**).

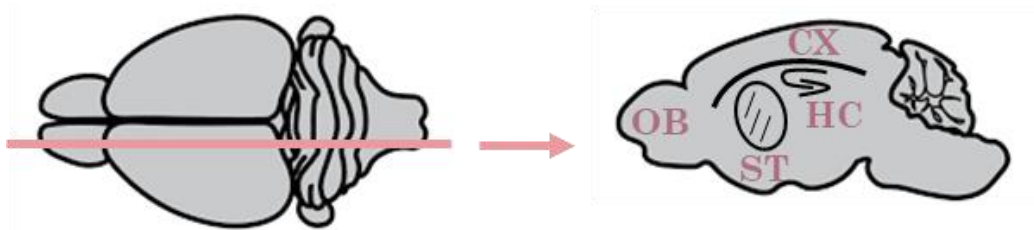


Figure 15: Representation of the dissected brain areas in mice. The left illustration shows a dorsal view of a mouse brain. The pink line marks a theoretical sagittal slice that is then represented at the right part. In this drawing the dissected brain areas are represented: olfactory bulb (OB), striatum (ST), hippocampus (HC) and cortex (CX).

To evaluate the ischemic lesion, freshly obtained brains (n=36, **Fig. 13**) were sliced coronally and stained with TTC as described in the following section.

A total of 208 animals were used but 31 were discarded: 5 died during the instillation period (2 PBS, 2 SRM2975 and 1 SRM1650b), 8 due to complications during surgery and 18 due to mistaken arterial occlusions leading to no infarct (1), only anterior infarct (1) and only posterior infarct (16).

3.5. Infarct volume assessment and brain structural analyses

TTC staining

Brains from ischemic mice were studied at 24h (chronic exposure n=19, **Fig. 13B**) or 48 hours after the ischemia (acute exposure n=9, **Fig. 13C** and chronic exposure n=9, **Fig. 13D**). They were sliced in one-millimeter-thick coronal sections, starting after the olfactory bulb, and incubated for 15 minutes with 2.5% 2,3,5-Triphenyl-2H-Tetrazolium Chloride (TTC, Sigma, St. Louis, USA) diluted in saline at room temperature.

After staining with TTC, infarcted tissue remains unstained (pale area, **Fig. 10**) while the rest becomes strongly stained in red. The first 6 serial stained slices were scanned, digitalized and analyzed later.

The Regions of Interest (ROIs), corresponding to the ischemic tissue, were manually drawn on the images, the obtained areas were added and multiplied by 1 mm (slice thickness) to calculate the lesion volume (mm³). The same volume calculation was conducted to obtain the Ipsilateral (IL) and Contralateral (CL) hemispheres' volumes.

Analyzed parameters were: edema index and infarct percentage (Morancho *et al.*, 2012).

$$\text{Edema index: } \frac{\text{IL volume (mm}^3\text{)}}{\text{CL volume (mm}^3\text{)}}$$

$$\text{Infarct percentage (\%): } \frac{\text{Infarct volume (mm}^3\text{)}}{\text{IL volume (mm}^3\text{)}} \times 100$$

In vivo Magnetic Resonance Imaging (MRI)

A subgroup of ischemic animals (n=7, **Fig. 13B**) underwent an MRI acquisition to evaluate infarct volume 24 hours after MCAo surgery.

To that end, anesthesia was induced by inhalation of 5% isoflurane and maintained at 1.5% in medicinal air and throughout the procedure, respiratory

rate and body temperature were monitored. After the acquisition, the mice did not recover consciousness and were euthanized, following the same protocol previously described.

MRI was performed with a 7-Tesla Bruker BioSpec spectrometer (Bruker BioSpin, Germany). Whole-brain high-resolution T2-Weighted Images (T2WI) were acquired in the axial, sagittal and coronal plane to study infarct volume (30 slices, 19 slices and 16 slices, respectively; thickness: 0.5 mm, gap: 0.05 mm, TR: 4.2 s, effective TE: 60 ms, resolution= 256 x 256, echo train= 8, four repetitions, scanning time: 6 min 43 s per plane).

Infarcts were analyzed in the high-resolution coronal T2-weighted images where the infarct ROIs were manually drawn on each slide, the obtained areas were added and multiplied by 0.5 mm (slice thickness) to calculate the lesion volume (mm³). The same procedure was repeated to obtain the ipsilateral and contralateral hemispheres' volume. To study the ischemic lesion, the same parameters as for TTC staining were analyzed: edema index and infarct percentage.

Diffusion Tension Imaging (DTI)

Fractional Anisotropy (FA) data were acquired with a diffusion segmented Echo Planar Imaging sequence using respiration gating for minimizing the motion artifacts (TR= 3800 ms, TE_{eff}= 24 ms, FOV= 1.92 cm x 1.92 cm, and MTX= 128 x 128). A total of 15 slices of 1 mm of thickness and an interslice distance of 1.1 mm covering the whole brain were acquired. For each slice, 5 non-diffusion weighted ($b = 0$ s/mm²) and diffusion-weighted images in 30 different diffusion gradient directions using 3 b values (200, 600, and 1,000 s/mm²) were acquired with diffusion gradient time = 5 ms, time between diffusion gradients = 10 ms, and non-gated Experimental time= 24 min. Diffusion-weighted images were processed with the Paravision 5.1 software (Bruker BioSpin, Ettlingen, Germany) to obtain the diffusion tensor providing FA values as the mean of the principal diffusivities. Finally, mean FA values were obtained from ROIs selected in the anterior commissure and the corpus callosum of the ipsilateral and contralateral hemispheres, related to the infarcted cortex.

3.6. Tissue homogenates

OB, HC, ST, CX and Lung tissues stored at -80°C were used for protein extraction. For every 0.25 grams of tissue, 1 ml of complete fresh homogenization lysis buffer was used [5mM Tris-HCl, 150mM NaCl, 5mM CaCl₂, 0.05% Brig-35, 0.02% NaN₃, 1% Triton X-100, 1% phenylmethanesulfonyl fluoride (PMSF; Sigma-Aldrich, USA) and 0.5% aprotinin (Sigma-Aldrich, USA)]. After the addition of the lysis buffer, the samples were homogenized with a 5 mm drill (OMNI international, Kennesaw, Georgia), in low protein-binding eppendorfs. Then they were centrifuged at 15,300 rcf, for 12 minutes at 4°C. The supernatant, with the protein fraction, was collected and stored in low protein-binding eppendorfs at -80°C until use.

3.7. Multiplex immunoassay

The content of MMPs was determined in brain samples (OB, HC, ST, CX) and lungs using a MILLIPLEX ® kit (Merck KGaA, Germany):

- MMMP3MAG-79K: simultaneous measurement of MMP-3, -8, -9 in:
 - o **Naïve** acutely exposed mice (**Fig. 12A**, PBS=6, SRM2975=6, SRM1650b=6) and chronically (**Fig. 12B**, PBS=6, SRM2975=7, SRM1650b=6).
 - o **Ischemic** mice previously exposed acutely (**Fig. 13A**, PBS=5, SRM2975=5, SRM1650b=6) and chronically (**Fig. 13B**, PBS=8, SRM2975=8, SRM1650b=6).

Samples were tested in duplicates and the experiment was run as follows:

A 96-well plate was firstly washed with wash buffer, then 25 µl of sample and standard were added into each well together with 25 µl of assay buffer and 25 µl of the pre-mixed magnetic beads. The plate was incubated overnight at 4°C and later the content was removed and the plate was washed two times with the use of a handheld magnet.

Later, 25 µl of the detection antibodies were added and after 1-hour incubation, 25 µl of streptavidin-phycoerythrin were also incorporated. After 30 minutes of incubation, the well content was removed and finally, 150 µl of Drive Fluid were added before the measurement readings on MAGPIX® with xPONENT software.

Analyte concentrations were obtained from the Median Fluorescent Intensity readings by using a 5-parameter logistic method. The mean value of both duplicates was calculated, being valid when the Coefficient of Variation (CV) was below 25%. All plaques had an inter-assay CV <25% obtained from 3 different internal control samples (2 quality controls supplied in the kit and 1 sample of brain homogenate).

3.8. Bradford assay

At the same time as thawing the samples for the Milliplex assay, Bradford assay was conducted to determine the total protein content ($\mu\text{g/ml}$) inferring from a standard albumin curve (0-2mg/ml, 23209, Thermo Scientific™, IL, USA).

In brief, 5 μl of standard, homogenized tissue samples or corresponding blank, were pipetted in duplicates in the appropriate 96-well plate. Then, 250 μl of Pierce™ Coomassie (23200, Thermo Scientific™, IL, USA) were added to each well and after 5 minutes'-incubation, at room temperature, the absorbance was read at 595 nm in a BIO-TEK Elx-808 microplate reader with Gen5 software. The results were expressed based on the total protein content of the sample (pg/mg).

3.9. Immunofluorescence

Brains embedded in OCT and stored at -80°C , as described above (pag. 74), were used for immunohistochemical purposes.

- Acute DEP exposure, naïve mice (**Fig. 12A**, PBS=5, SRM1650b=5)
- Chronic DEP exposure, naïve mice (**Fig. 12B**, PBS=4, SRM1650b=5)
- Acute exposure, ischemic mice (**Fig. 13A**, PBS=4, SRM1650b=6)
- Chronic exposure, ischemic mice (**Fig. 13B**, PBS=4, SRM1650b=6)

With the help of a cryostat, brains were cut into 12 μm -thick sagittal slices, collected in glass slides and frozen at -80°C until use. Later, 3 consecutive slices containing the Rostral Migratory Stream were studied for different immunolabeling markers.

For the immunofluorescence labeling, the slices were placed at room temperature for 10 min, washed 5 min in 0.1% PBS-Tween, 10 min 0.03%-PBS-Triton

X-100 and 5 min 0.1% PBS-Tween. The Sections were encircled with a PAP-pen and then blocked for 1 hour with 0.1% PBS-Tween containing 1% BSA (Sigma-Aldrich, MO, USA) and 5% goat serum (Merck Millipore, MA, USA). Next, samples were incubated overnight at 4°C with the following antibodies: 1:200 anti-DCX (ab207175, Abcam, UK), 1:200 anti- NeuN (ab190565, Abcam), 1:200 anti-ki67 (550609, BD Biosciences), 1:200 anti-Nestin (556309, BD Biosciences) and 1:200 anti-IBA-1 (ab178847, Abcam). As a reminder, all slices were labeled with Lectin (DL-1177, Vector Laboratories, USA) since it was injected during euthanasia, as detailed on page 73.

Slices were then washed 3 times for 5 min at RT with 0.1% PBS-Tween followed by 1-hour incubation at RT with the corresponding secondary antibodies at 1:500 (Alexa fluor 488 goat anti-rabbit IgG, Alexa fluor 488 goat anti-rat IgG, Alexa fluor 647 goat anti-rabbit IgG or Alexa fluor 488 goat anti-mouse). Later, they were washed 3 times for 5 min at RT with 0.1% PBS-Tween, mounted in Vectashield™ with DAPI (Vector Laboratories, USA) and sealed. Whole sagittal section images were obtained from all slides with a Panoramic 250 FLASH (3D HISTECH).

At the time of labeling and to ensure the specific positive signal of each marker, parallel samples were used as negative controls and followed the same process except that no primary antibodies were added.

3.10. Flow cytometry

To study the immune cellular response in lungs after diesel particle exposure and cerebral ischemia, a subgroup of BALB/c male mice received chronic instillations (n=8, **Fig. 13D**), 24 hours after the last instillation they underwent pMCAo (detailed in pag. 72) and 48 hours after surgery they were euthanized and lungs obtained (detailed in the following paragraphs) for the study of leukocytes' subpopulations. Finally, their brains were also extracted to evaluate lesion size by TTC staining as described in page 75.

During euthanasia and under deep anesthesia (4% isoflurane in medicinal air), each mouse was perfused with ice-cold saline through the heart's left ventricle. The lungs were isolated and one lobe was stored for molecular analyses (pag.

74) and the remaining four lobes were minced and digested with 5 ml of Digestion Solution [Collagenase A 1.5 mg/ml, DNase I 0.4 mg/ml, Hank's Balanced Salt Solution (HBSS) 1X, Fetal Bovine Serum (FBS) 5%, HEPES (4-(2-hydroxyethyl)-1-piperazineethanesulfonic acid) 10 mM in H₂O] at 37°C for 30 minutes. After digestion, 25 ml of PBS were added and the mixture was then filtered through a 70 µm cell strainer (Corning, NY, USA). To collect the remaining tissue fractions, 10 ml of HBSS with 5% FBS were passed through the filter, the solution was centrifuged (500 rcf, 5 mins at 4°C) and the supernatant was removed. The pellet was then treated with ACK RBC lysis buffer for 2 minutes (Gibco, Carlsbad, CA, USA), followed by the addition of 10 ml of HBSS-5% FBS. The suspension was centrifuged and washed twice with 5 ml of Dulbecco's Phosphate-Buffered Saline (DPBS). Then, the re-suspended cells in DPBS were counted with the Trypan Blue method (1:1).

Once the cells were counted with an automated cell counter (LUNA II, Logos biosystems), 10⁶ cells were brought to 1 ml DPBS and incubated for 15 minutes with 1:1000 Fixable Viability Stain 510 (FVS510, BD Biosciences), centrifuged and re-suspended twice in 2 ml of blocking solution (DPBS-1%, FBS-0.01%, 0.01% sodium azide). After one last centrifugation, the pellet was re-suspended and incubated for 10 minutes with 100 µl of blocking solution containing 1:2 BD Horizon Brilliant Stain Buffer and 1:200 CD16/CD32 (Mouse BD Fc Block).

After this incubation, 1:100 APC-R700 CD11b (564985, BD Biosciences), 1:100 BV786 CD11c (563735, BD Biosciences), 1:400 APC-Cy7 rat anti-mouse CD45 (561037, BD Biosciences), 1:100 BV605 I-A/I-E (563413, BD Biosciences), 1:400 CD24 (553262, BD Biosciences), 1:100 BV650 Ly-6G (740554, BD Biosciences), 1:100 Brilliant Violet 421 CD64 (139309, Biolegend) and 1:40 PerCP-Cyanine5.5 Ly-6C (48-5932, eBioscience) monoclonal antibodies were added and incubated for 30 minutes. Followed twice by the addition of 2 ml of blocking solution and centrifugation. The obtained pellet was re-suspended in a final volume of 350 µl of blocking solution.

In parallel, the same number of cells (10^6) were brought to the final volume of 350 μ l in blocking solution but did not follow the labeling process and thus were used as a negative control.

Data was acquired by an LSR Fortessa cell analyzer (BD Biosciences, San Jose, CA, USA) using FACSDiva software (BD Biosciences) and analyzed using FlowJo software (TreeStar, Ashland, OR, USA). To set up the panel Compensation and Fluorescence Minus One (FMOs) controls were used. The different cell subtypes (B cells, T cells, NK cells, Macrophages (total, alveolar and interstitial), Dendritic cells (CD11+Ly6C+, CD11-Ly6C+, CD11-Ly6C-, CD11+Ly6C-), monocytes (total, resident and inflammatory), neutrophils, eosinophils, plasmatic cells and CD11c+ Lymphocytes), were obtained after several sequential gatings plus the use of the specified fluorescent markers: B cells (MHCII⁺ CD24⁺), T cells (MHCII⁻ CD24⁻), natural killer cells (MHCII⁻ SSC^{low} CD11b^{int} CD64⁻), macrophages (MHCII⁺ SSC^{hi} CD64⁺ CD24⁻), further subdivided in alveolar (CD64⁺ CD11b⁻ CD11c⁻) and interstitial macrophages (CD64⁺ CD11b⁺ CD11c⁻), dendritic cells (MHCII⁺ SSC^{hi} CD64⁻ CD24⁺), monocytes (MHCII⁻ SSC^{low} CD11b^{hi} CD64^{int}), further subdivided in inflammatory monocytes (Ly6C^{hi} CD11c⁻) and resident monocytes (Ly6C⁻ CD11c⁺), neutrophils (Ly6G⁺), eosinophils (MHCII⁻ CD11b⁺), plasmatic cells (MHCII⁻ CD24⁺) and lymphoid cells (MHCII⁻, SSC low, CD11c⁺, CD11b⁻ CD64⁻) (**Fig. 16**) (Yu *et al.*, 2016)

The final data was analyzed as a percentage referred to the previous cell population (parent) or the total live leukocytes.

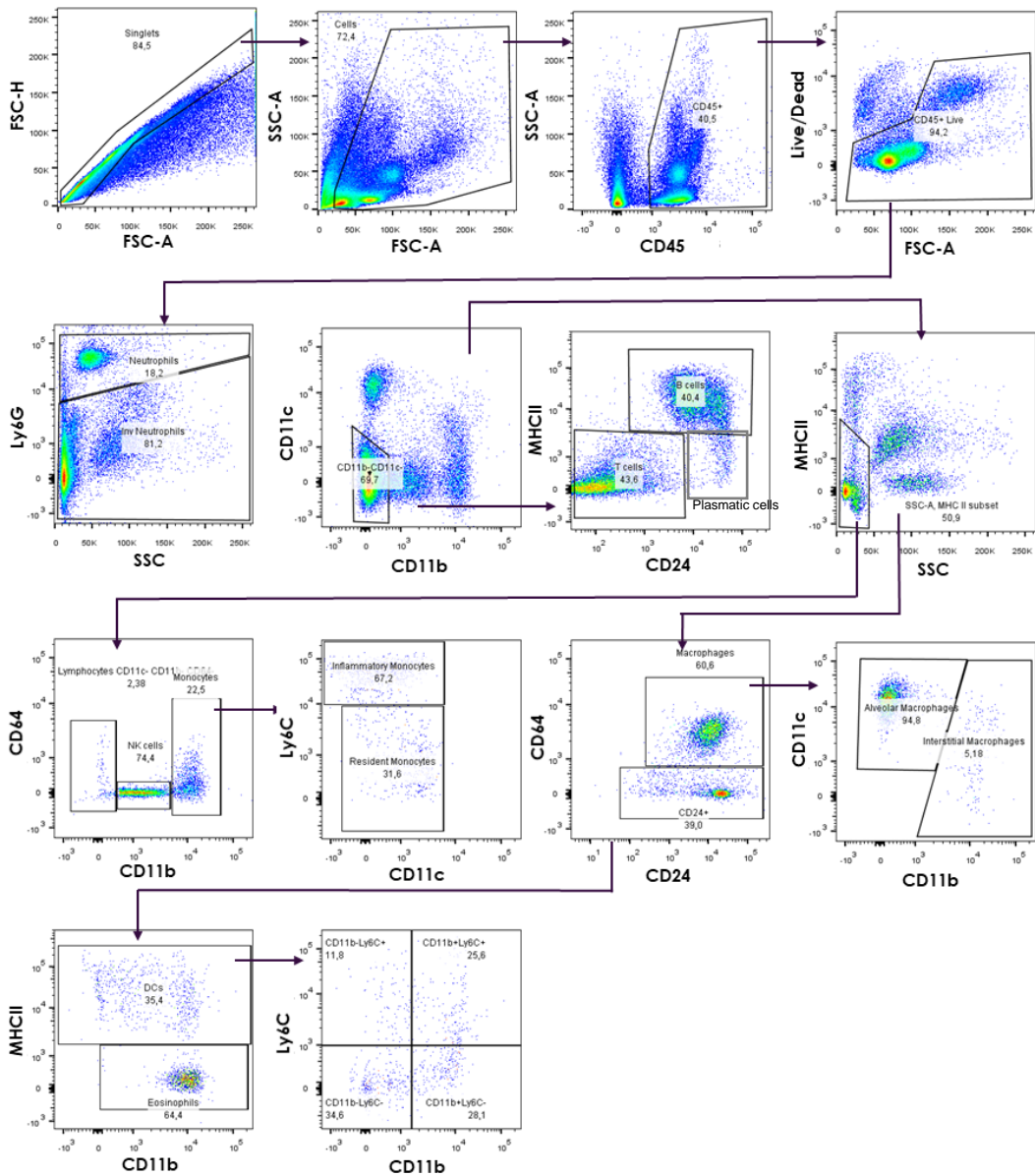


Figure 16: Example of the flow cytometric analysis of the mouse lung. Pseudocolor plots of windows and gating strategy for the identification of immune cells is shown.

3.11. Turbidimetric clot assay

This assay was conducted to evaluate the influence of DEP on clot formation and lysis under thrombolytic conditions with tPA ([Objective 3](#)), based on a turbidimetric assay published by Carter *et al.*, 2007 with some modifications. With this aim, citrate plasma samples from 3 different studies were analyzed (**Fig. 17**):

- A. Mouse plasma samples from acutely and chronically exposed naïve and ischemic mice (**Fig. 17A**).
- B. Human plasma samples from ischemic stroke patients and matching control subjects, obtained from the SMARRTS cohort (Ma *et al.*, 2016b). Plasmas were also tested with the exogenous addition of DEP (SRM2975) that was established at 0.1 µg/ml after a pilot study where increasing concentrations of DEP were added to evaluate their interaction with the formation/lysis experiment and the absorbance readings. The selected concentration did not interfere in the absorbance readings nor the development of the assay (data not shown) (**Fig. 17B**).
- C. Human plasma samples from control subjects living in areas below or above annual European PM_{2.5} standards. Plasmas were obtained from the ISSYS cohort recruited in our Laboratory (Riba-Llena *et al.*, 2013) and in collaboration with Dr. Michelle Turner from ISGlobal. These are hypertensive subjects without dementia or stroke events at baseline whose place of residence was geocoded and thus the estimated residential levels of PM₁₀ and PM_{2.5} were obtained using a land-use-regression model (de Bont *et al.*, 2019). Consequently, we could differentiate two groups based on their annual mean exposure to particulate matter in high (PM_{2.5} ≥ 25 µg/m³) and low (PM_{2.5} < 25 µg/m³) exposures, according to the EEA guidelines (**Fig. 17C**).

All samples were preserved at -80°C and were thawed for the clot/lysis assay. Then, 25 µl of citrate plasma were added to a transparent 96-well microtiter plate. Activation of coagulation in the tested plasma samples was initiated by addition 50 µl of Activation Mix containing 7.5mM CaCl₂ and 0.03U/ml thrombin (Trombina Sigma T6884-100UN).

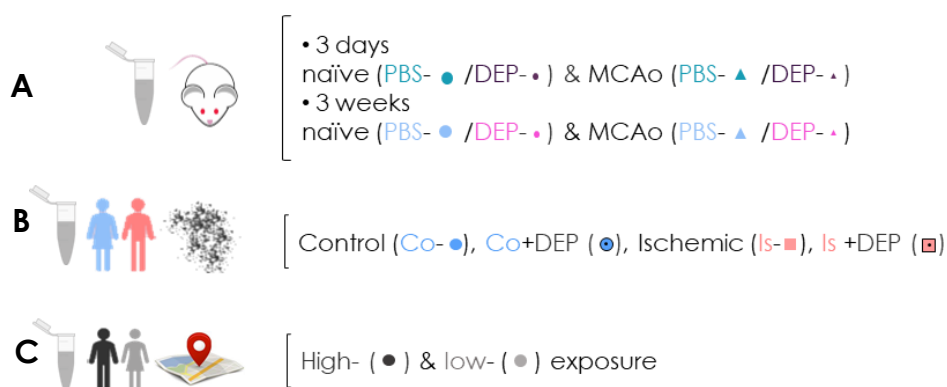


Figure 17: Plasma samples used to study the effects of DEP exposure in human and mice. Co: Control, Is: Ischemic, DEP: Diesel exhaust particles.

To measure fibrinolysis potential, recombinant tissue plasminogen activator (rt-PA Actylise®, Boehringer, 83 ng/mL) was added in 75 µl of Assay Buffer containing 0.05M Tris-HCl (Sigma-Aldrich, USA), 1M NaCl (Sigma-Aldrich) at pH=7.4. Assay Buffer and Activation mix were added consecutively and Optical Densities (OD) were immediately read at 405 nm every 40 seconds for 3 hours at 37°C using a BIO-TEK Elx-808 microplate reader and Gen5 software (**Fig. 18**).

Note that Human SMARRTS stroke and control plasmas (**Fig. 17B**) were exogenously exposed to 0.1 µg/ml of SRM2975 mixed in the 75 µl of Assay Buffer.

All samples were run per triplicate and the accepted CV of the resulting mean curve was <25% to be included in the analysis. Also, each plasma sample had an reference plasma control without rtPA to confirm the correct formation of the clot and each independent experiment was run with inter-assay plasma control samples that showed a CV <30%.

The changes in OD along time correspond to the different phases of clot formation and lysis in the shape of a turbidimetric curve in which 9 parameters related to clot formation (1-3) and lysis (4-9) were analyzed, as previously described (Carter *et al.*, 2007) (**Fig. 18**):

1. **Lagtime**: a sharp rise in OD consistent with the time required for protofibrils to aggregate and ensure clot formation (given in minutes).

2. **Clot formation rate** (CRc): maximum change in clot formation OD, reflects the maximum rate of fibrin fiber assembly (given OD per seconds).
3. **Maximum Absorbance** (MaxAbs): maximum OD minus baseline OD, reflects the structural density of the thrombus (given in OD).
4. **Lysis Rate** (LR): maximum rate of fibrin fibers disassembly (given in OD per seconds).
5. **Lysis time**: Fibrinolysis duration (given in hours or minutes).
6. **Clot area**: area under the curve, the balance between formation and lysis.
7. **Clot time**: clot lifetime (given in hours or minutes).
8. Lysis 50 from time 0 (**Lysis 50 t_0**): time to 50% clot lysis from clot formation initial time (given in hours or minutes).
9. Lysis 50 from time of Maximum Absorbance (**Lysis 50 t_{Max}**): time to 50% clot lysis from clot MaxAbs time point (given in hours or minutes).

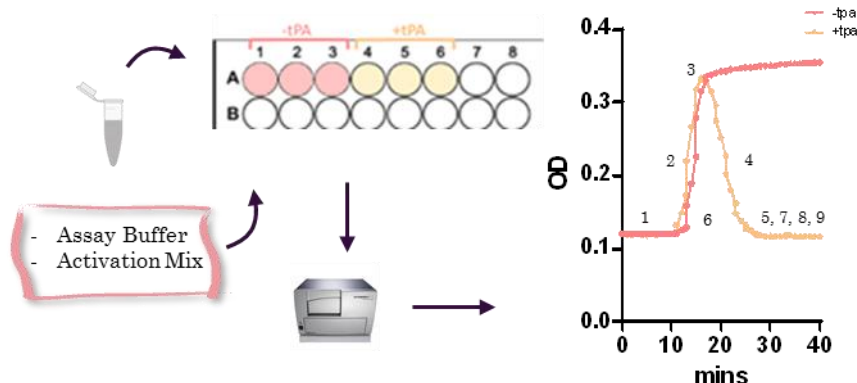


Figure 18: Schematic representation of the turbidimetric clot/lysis assay and the analyzed parameters. Human and mouse citrated plasma samples were added in triplicates in a 96-well plate. Later, the Assay Buffer with/out rtPA was added together with the Activation Mix that contained the Thrombin. Immediately after, the plate is taken to the microplate reader where the Optical Density (OD) measurements gave a curve of the clot formation and lysis. From these curves 9 parameters were analyzed: 1. Lag time, 2. Clot formation rate (CRc), 3. Maximum Absorbance (MaxAbs), 4. Lysis Rate (LR), 5. Lysis time, 6. Clot area, 7. Clot time, 8. Lysis 50 from time 0 (Lys50_{t0}) and 9. Lysis 50 from time of MaxAbs (Lysis 50_{t_{Max}}).

3.12. Data processing and Statistical Analyses

All images obtained from SEM, CryoTEM, neurosphere cultures, TTC, MRI, DTI and immunofluorescence were analyzed blindly with *ImageJ* (free software, NIH). All data was processed blindly and represented as mean \pm Standard Deviation (SD) or median \pm Interquartile Range (IQR) using GraphPad Prism 9.0 according to the normal or non-normal distribution of the variable, respectively. Statistical analyses were performed with SPSS 20.0. The normality of continuous variables was assessed by Shapiro-Wilk test ($n < 30$) or Kolmogorov-Smirnov ($n \geq 30$). Normally distributed variables were analyzed by Student t-tests or ANOVA and Tukey or Dunnett's *post-hoc*. Whereas non-normally distributed variables were analyzed by Mann-Whitney U-test or Kruskal Wallis tests and Dunn's *post-hoc*. For correlation analyses, Pearson (for normal distribution) or Spearman (for non-normal distribution) tests were used. Results with $p < 0.05$ were considered statistically significant (*) and $0.1 < p < 0.05$ were considered strong tendencies and indicated in the graphs.

Results

4.1. Characterization of diesel exhaust particles

DEP were suspended in PBS, a commonly used vehicle for intranasal instillation (Pöss *et al.*, 2013; Robinson *et al.*, 2018; Yang Li *et al.*, 1999). Since PBS might present dispersion problems (Buford *et al.*, 2007), we first studied the effect of different sonication times on particle distribution and size of the prepared DEP suspensions.

Sonication of suspended DEP in PBS for 10 minutes increases the percentage of smaller-sized particles.

DEP suspensions of 0.5 mg/ml were sonicated for 0, 10, 30 and 60 minutes and the volume's relative distribution of the particles was obtained using the light scattering technique.

The results show that the non-sonicated SRM2975 DEP presented 58% of PM₁₀ particles, while SRM1650b only 26.4% (**Table 1**). After 10-minutes sonication there is a clear shift of the size of the particles to the smaller range which can be observed in graphs of **Figure 19A** and **19B**. At this sonication time, 88% of SRM2975 volume corresponds to PM₁₀ and similarly occurs for the SRM1650b that presents a 74% of PM₁₀ (**Table 1**). Looking at the particle distribution of PM_{2.5}, the increase in smaller particles is larger: from 10.9 % to 69.1% for the SRM2975 and from 8.9% to 60.2% for the SRM1650b which implies a 6-fold increase for both particles. Regarding the volume of the UFPM, the 10 minutes sonication increased from 0.1 to 12.5 for the SRM2975 (125-fold) and from 0.2% to 5.9% for the SRM1650b (29-fold).

	SRM2975 (Mean %)				SRM1650b (Mean %)			
	0 mins	10 mins	30 mins	60 mins	0 mins	10 mins	30 mins	60 mins
UFPM	0.1	12.5	13.4	9.3	0.2	5.9	5.1	9.3
PM2.5	10.9	69.1	71.9	67.9	8.9	60.2	46.9	78.3
PM10	58.7	88.1	83.9	94	26.4	74.0	53.3	85.0
TOTAL	100	100	100	100	100	100	100	100

Table 1: Particle size distribution after sonication. Results show the mean percentage of UFPM, PM_{2.5} and PM₁₀ of total DEP suspensions in PBS after different sonication times (n=4 per particle type).

Importantly, significant differences were found in the UFPM, PM_{2.5} and PM₁₀ fractions after 10 minutes of sonication compared to non-sonicated samples in both types of particles (**Fig. 19A, 19B**), strongly supporting the reduction of aggregates and the increase of the finest fraction of particles which is known to have a detrimental impact in health. Importantly, longer sonication times did not significantly modified the particle size distribution as seen in **Table 1**.

When comparing the particle fractions of UFPM, PM_{2.5} and PM₁₀ and total DEP between SRM2975 and SRM1650b preparations after 10 minutes of sonication (**Fig. 19C**), there were no significant differences.

In view of the exposed results, all the DEP suspensions used in the experiments conducted in the present thesis were prepared in PBS with 10 minutes sonication.

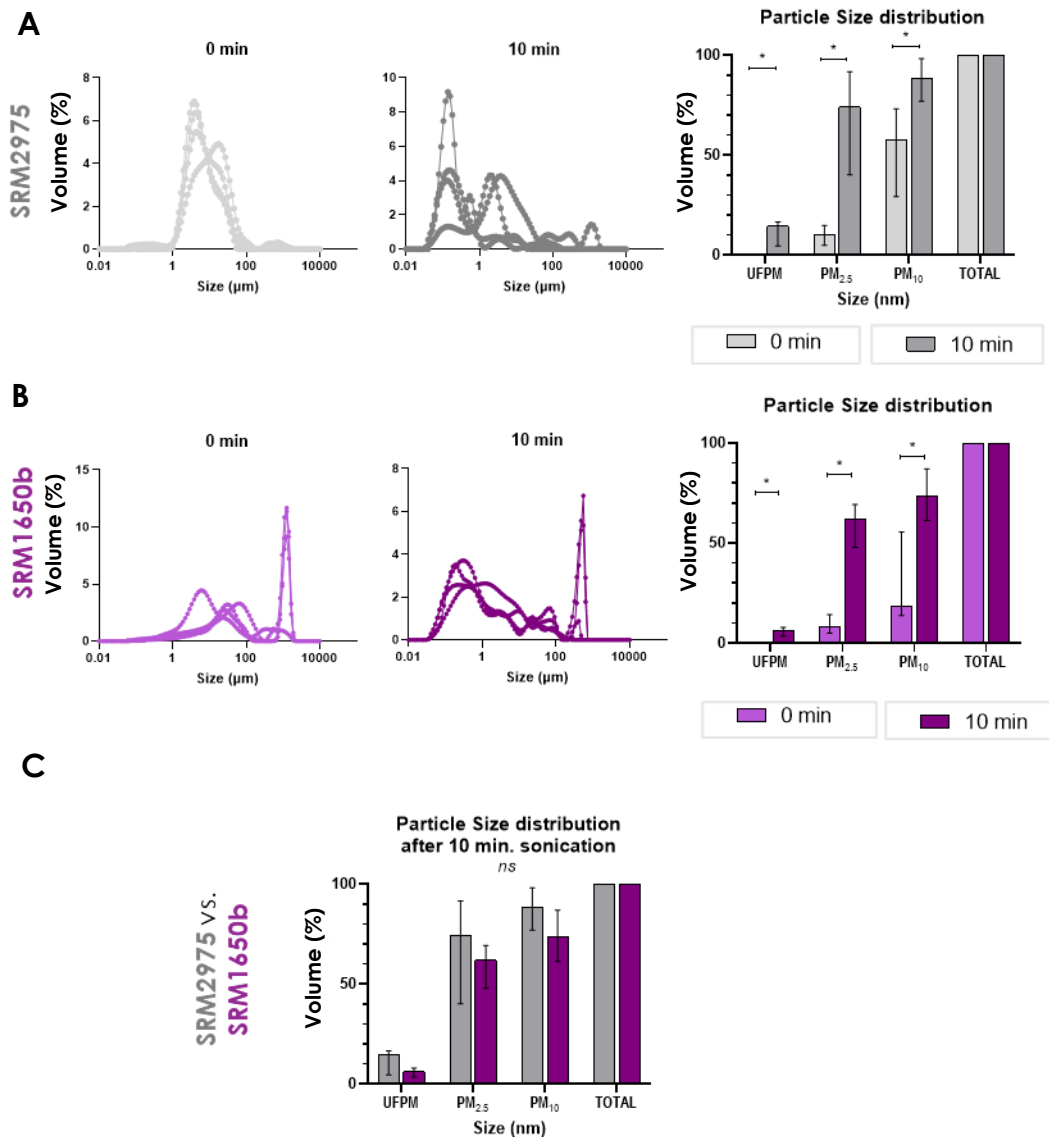


Figure 19: PM fractions distribution in DEP suspensions with or without sonication. Representative curves of volume of particles distribution without (0 min) or with sonication (10 min). Accompanied at the right part with histograms representing significant differences in median PM volumes after sonication. **A:** SRM2975 particle size distribution. **B:** 1650b particle size distribution. **C:** No differences were observed in the percentage of PM fractions of SRM2975 and 1650b once sonicated. Data is represented as median (IQR). ns: not significant * $p < 0.05$. (n=4 per condition).

Freezing the DEP suspensions did not affect the smaller-sized particle fraction.

Further characterization of the particles was done to elucidate if freezing the DEP suspensions could affect the particle fractions.

To that end, three suspensions of both types of particles at 7.5 mg/ml (concentration adjusted for the posterior *in vivo* dose in mice, as explained in **Section 4.3**, pag.97), were analyzed by DLS after being thawed for 5 days, vortexed and sonicated for 10 minutes. Readings were obtained and the results were analyzed as fractions of PM (**Fig.20**).

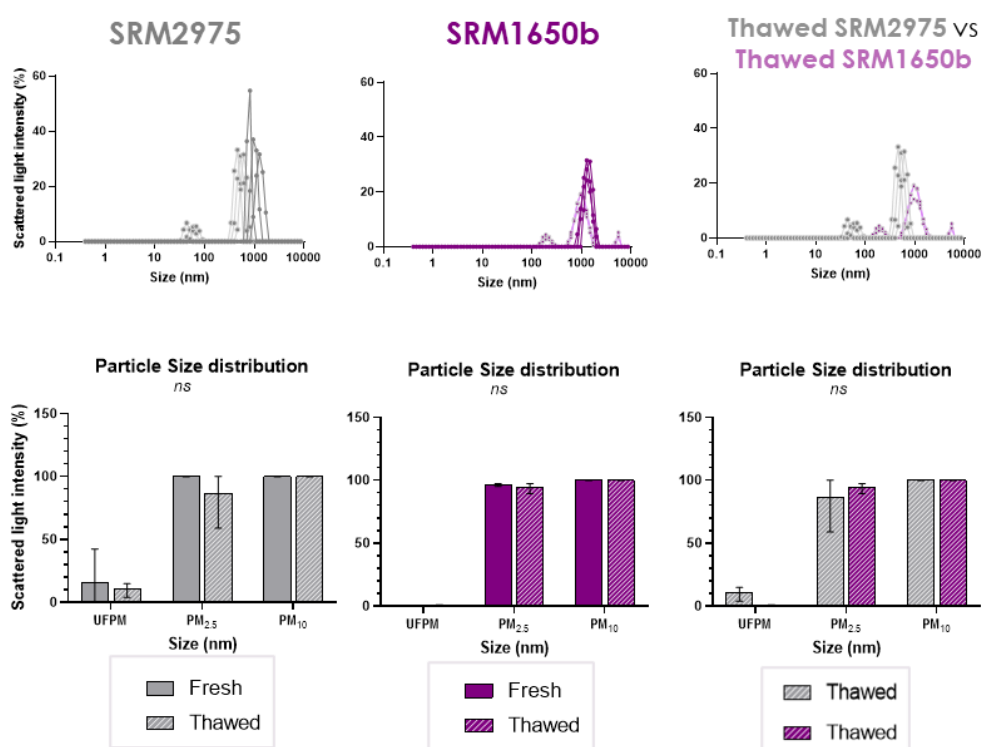


Figure 20: Distribution of PM fractions after freezing the DEP samples.

Representative curves of Scattered light intensity in SRM2975 and SRM1650b giving the UFPM, PM_{2.5} and PM₁₀. Fractions of SRM2975 and SRM1650b were not altered once thawed. Data is represented as mean \pm SD. ns: not significant (n=3 per SRM).

Frozen preservation of the prepared DEP suspensions did not alter the proportion of UFPM, PM_{2.5} or PM₁₀ fractions. Even more, there were no differences regarding particle size distribution between both types of SRM material.

The samples were also imaged by Cryo-TEM and SEM. The median size of single particles analyzed in Cryo-TEM images (**Fig. 21**) was 33.3 nm for the fresh SRM2975 and 44.92 nm for the fresh SRM1650b. After thawing, the particle size in SRM2975 was 38.58 nm and in SRM1650b was 36.26 nm, with no statistical differences found between the type of material (SRM2975/SRM1650b) in any of the conditions studied (fresh/thawed). Besides, our measurements differed from the ones described in the Certificate of analysis where the particles were suspended in distilled water with 0.001% triton and the size was based on Mastersizer measurements (see Annex II: SRM2975= 19.4µm, pag. 199 and Annex III: SRM1650b= 180nm, pag. 213), thus getting different sizes depending on the adequacy and resolution of the technique used.

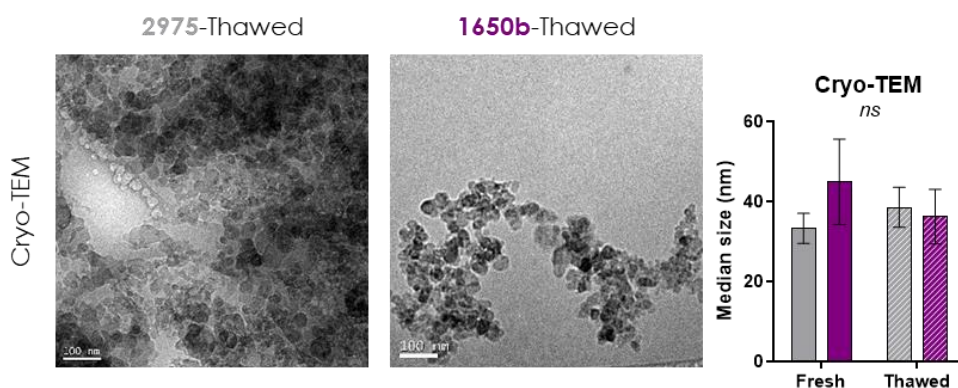


Figure 21: Cryo-TEM particle size imaging and analysis. Images of thawed and sonicated DEP suspensions accompanied by a bar graph of particle measurements ($n=12$ in each condition). Scale: 100 nm. Data is represented as median (IQR). ns: not significant.

SEM was also performed in the same DEP suspensions confirming that particles tended to form aggregates even after sonication (**Fig. 22**).



$\pm 20.6\%$, $p=0.006$) (**Fig. 23 and Fig. 24**). Also, the load of diesel particles within the neurospheres increased with the dose, as can be seen in the images.

Cell viability, assessed by the Cell Counting Kit-8, directly related with the mitochondrial cellular activity, started to decrease at T_0 when compared with the vehicle-treated cells with the $5\text{ }\mu\text{g/ml}$ dose of DEP ($87.1\pm 10.1\%$ $p=0.03$), showing the lowest viability the highest tested dose ($81.5\pm 10.7\%$ $p=0.004$) (**Fig. 23**). However, NSC exposed at T_2 did not show decreased viability at any tested DEP concentration (**Fig. 24**).

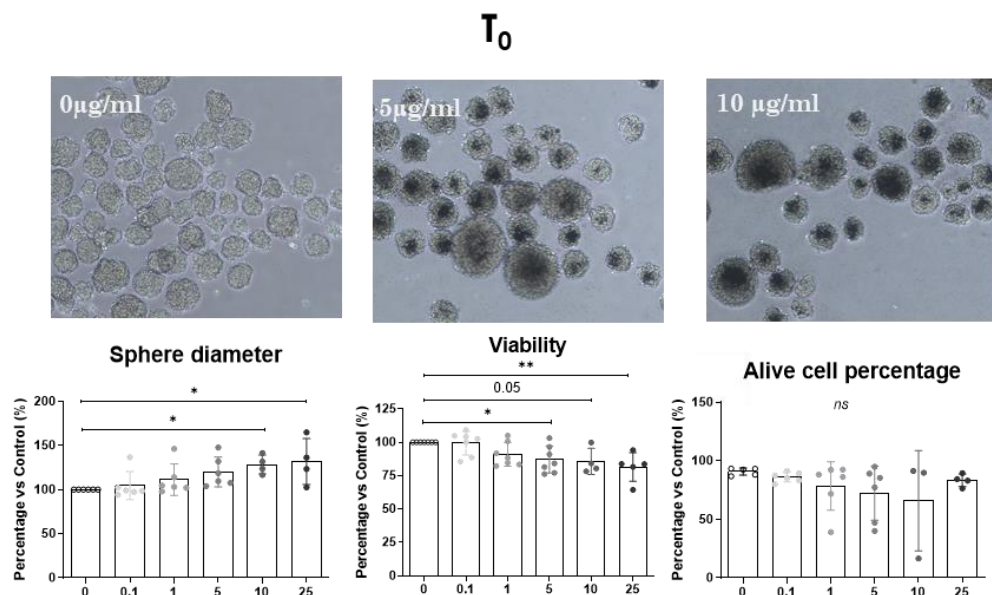


Figure 23: Neurospheres formed by NSC exposed to increasing doses of SRM2975 (T₀). Representative images of neurospheres treated with 3 doses of DEP. Bar graphs show neurosphere diameter, cell viability and alive cell percentage. Data is represented as mean±SD. *ns* not significant * $p<0.05$, ** $p<0.01$ ($n=3-7$).

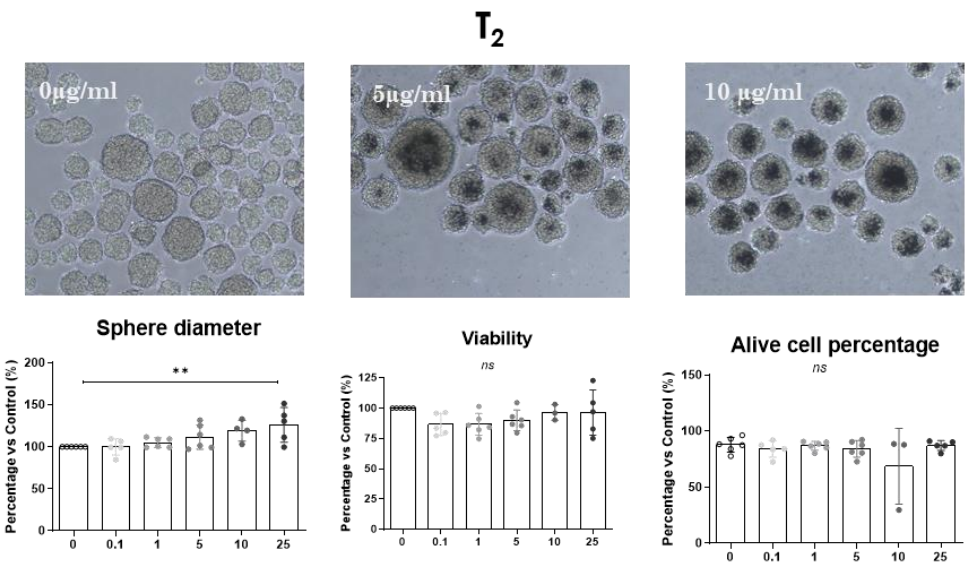


Figure 24: Neurospheres formed by NSC exposed to increasing doses of SRM2975 (T₂). Neurosphere representative images of doses 0, 5 and 10 µg/ml. Bar graphs showing: sphere diameter, cell viability and alive cell percentage. Data is represented as mean±SD. *ns*: not significant * $p<0.05$, ** $p<0.01$. $n=4-7$.

Together with cell viability, the number of alive/dead cells was assessed with the Trypan blue exclusion test assay (which dyes cells that have the cell membrane compromised). The **alive cells** (as a percentage of the total cells counted) were the same regardless of the DEP dose and the time of administration (see **Fig. 23** and **Fig. 24**).

In conclusion, the metabolic activity of NSC was compromised with increasing doses of DEP during neurosphere formation, however, in already formed neurospheres none of the tested DEP doses did compromise significantly their mitochondrial activity.

4.3. Effects of DEP exposure in naïve mice

BALB/c male mice were intranasally instilled with 20 µl of 7.5 mg/ml of DEP or only PBS for 3 days or 3 weeks (**Fig. 25A**). Twenty-four hours after the last instillation, brains, lungs and plasmas were obtained for matrix metalloproteinases content analysis (**Fig. 26, 27** and **28**), for immunofluorescence labeling (**Fig. 29** and **Fig. 30**) and clot formation and lysis analyses (**Section 4.5**). To identify specific anatomical sensitivities to DEP exposure, the brain was divided into the olfactory bulb, hippocampus, striatum and cortex.

General mice condition after DEP exposure

Regarding the weight evolution in the 3-days instillation group, the percentage of variation versus baseline was not significantly different between groups. And similar results were observed for the 3 weeks DEP exposure group except that reduced weight gain was recorded for the SRM1650b exposed mice [**6.2** (7.8-3.3)% for the PBS, **7.01** (11.2-4.5)% for the SRM2975 and **3.6** (5.3-0.8)% for the 1650b group; $p=0.03$], see **Fig. 25**.

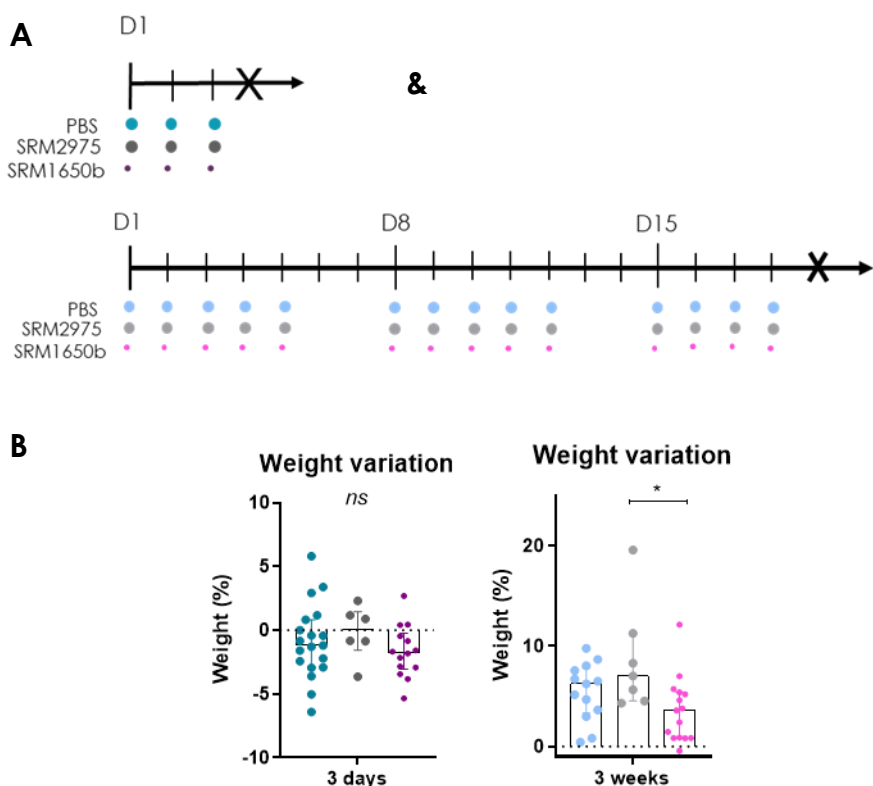


Figure 25: Instillation protocol and weight follow-up. **A:** Time-line protocol description for the 3 days and 3 weeks exposed mice. One day after last dose, mice were euthanized (indicated as X) and their organs obtained for further studies. **B:** body weight was recorded along the instillation protocol and analyzed as percentage vs. baseline. Data is represented as median (IQR). *ns*: not significant, * $p < 0.05$.

PBS instillations altered the MMP content in the brain.

To study if the control instillations were interfering with our design, we analyzed the MMP levels in both brains and lungs, in the PBS-instilled mice (**Fig. 26**). Unexpectedly, as the instillation period increased from 3 days to 3 weeks, the content on MMPs decreased in brains, in particular in the OB area, although not in the lungs.

In this regard, the 3 days- compared to the 3 weeks-instilled group presented higher MMP levels, specifically in the OB: MMP-3 [19.3 (12.8-24) vs. 5.5 (4.2-14.3) pg/mg, $p = 0.03$], MMP-8 (180.2 (105.8-197.7) vs. 43 (13.9-124.9) pg/mg, $p = 0.03$]

and MMP-9 (1,059.8 (642.8-1,222.9) vs. 323.3 (179.1-548.4) pg/mg, $p = 0.01$) and in the hippocampus: MMP-3 [6.2 (3.8-10.9) vs. 2.1 (1.1-2.7) pg/mg, $p = 0.01$] (Fig. 26). By contrast, no differences were observed in the lungs (Fig. 26).

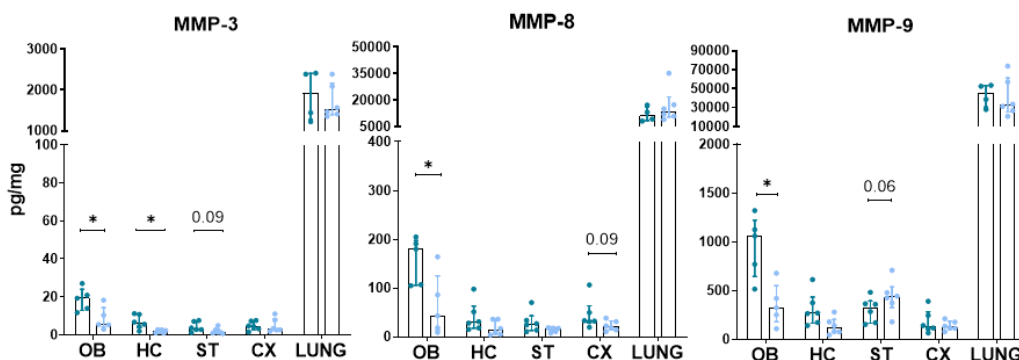


Figure 26: MMPs in naïve control mice. Increased MMPs were found after PBS instillation for 3 days compared to 3 weeks, mainly in OB and HC areas. Data is represented as median (IQR). ns: not significant * $p < 0.05$ ($n = 6$ per group).

With the reported results we can establish a direct connection between the nasal instillation procedure and an alteration of the MMP response in brain structures, suggesting that some regions are more sensitive to this process such as the olfactory bulbs and hippocampus. For this reason, this thesis will not compare the effect of particle exposure between different time points as we consider that the results could be biased as a consequence of the MMP response to the acute instillations.

The exposure time and composition of the diesel exhaust particles altered the levels of MMPs in the brains of naïve mice.

A set of mice were instilled for 3 consecutive days with PBS, SRM2975 or SM1650b (Fig. 27A).

In the lungs, which is the first organ encountered by the inhaled particles, no significant differences in levels of MMP-3, -8 or -9 were found (Fig. 27B). In the brain, it is noticeable that after instillation, the highest levels of MMPs were found in the OB compared to the HC, ST or CX (Fig. 27C), in the same line with the previous observation in PBS instillations, where the OBs responded more than the

other brain regions (**Fig. 26**). However, after the acute instillation (3 days) with SRM1650b, MMPs were reduced in the OB [MMP-3: **20.1** (13.4-34.3) vs. **9.3** (7.4-14.1) pg/mg, $p = 0.01$], the HC [MMP-3: **6.2** (3.8-10.9) vs. **3.1** (2.1-4.3) pg/mg, $p = 0.09$; MMP-8: **29.5** (17.4-62.8) vs. **10.9** (7.6-13.6) pg/mg, $p = 0.004$; and MMP-9: **266.6** (164.6-433.6) vs. **120** (93.6-132.9), $p = 0.01$), the ST [MMP-3: **3.3** (2.4-7.2) vs. **0.9** (0.8-1.7) pg/mg, $p = 0.02$] and the CX [MMP-8: **32.7** (28.2-63.8) vs. **21.8** (12.8-25.4) pg/mg, $p = 0.03$; and MMP-9: **266.5** (164.6-433.6) vs. **120** (93.7-132.9) pg/mg, $p = 0.02$] (**Fig. 27C**). Interestingly, the hippocampus was the only region where the 3 studied MMPs were reduced after SRM1650b instillation. On the contrary, the SRM2975 DEP did not alter the MMPs' amounts in the studied brain areas, neither in the lungs (**Fig. 27B and C**).

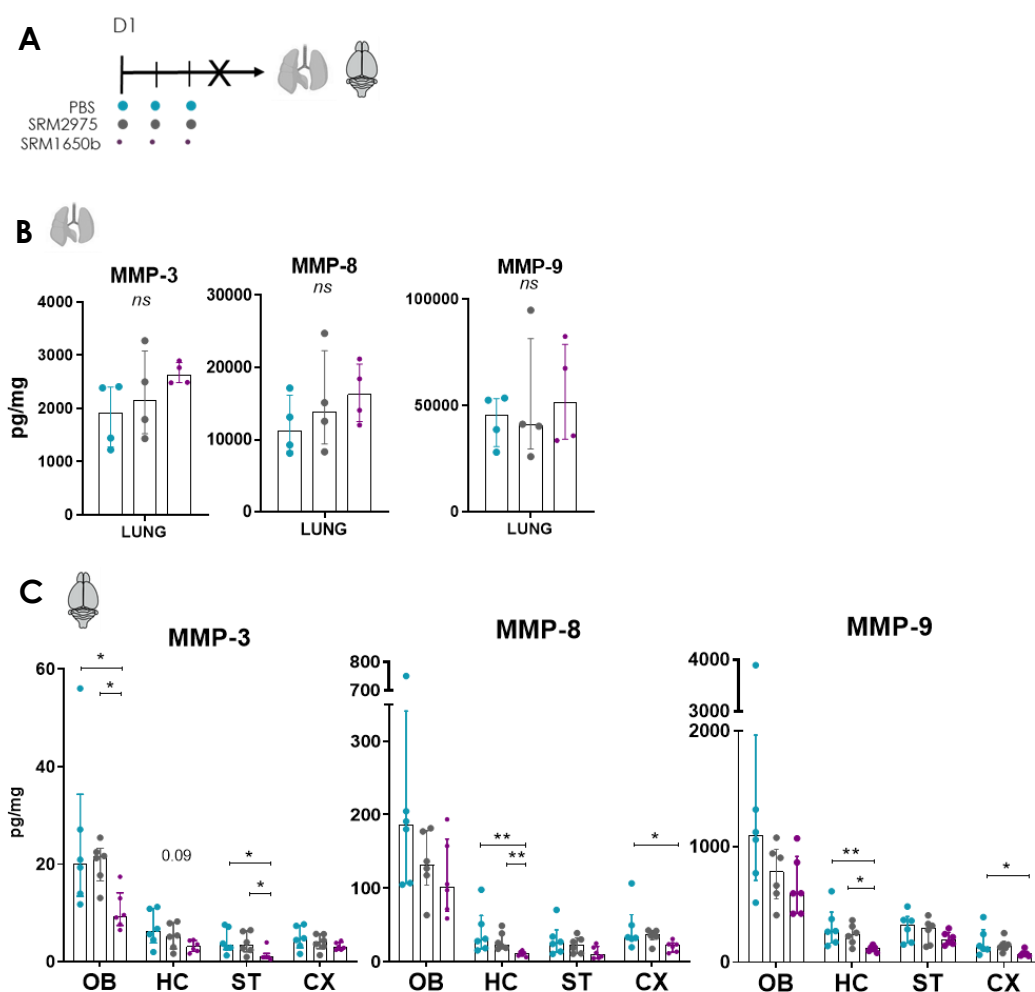


Figure 27: Acute exposure to SRM1650b DEP decreases MMP levels in the brain of naïve mice. **A:** Experimental design: after 3 days exposure, brains and lungs were obtained for MMP analysis. **B:** Levels of MMP-3, -8 and -9 in the lungs. **C:** MMPs were analyzed in different brain regions showing decreased MMP levels in several of these areas. Data is represented as median (IQR). ns: not significant, * $p < 0.05$, ** $p < 0.01$, PBS (n=6), SRM2975 (n=6) or SRM1650b (n=6).

After chronic exposure (3 weeks) (**Fig. 28A**), no differences in the lung MMPs' were observed (**Fig. 28B**). In brains (**Fig. 28C**), again, the highest levels of MMPs were observed in OBs regardless of the instilled suspension. However the chronic administration of SRM1650b caused an increase of MMPs compared to PBS in the HC [MMP-3: 2.1 (1.1-2.7) vs. 4.6 (2.9-10.1) pg/mg, $p = 0.03$] and the CX [MMP-8: 20.3 (13.4-32.8) vs. 51.8 (41-60.3) pg/mg, $p = 0.09$ and MMP-9: 123.7 (103.7-184.6)

vs. 247.6 (180.7-338.7) pg/mg, $p=0.09$], contrary to what was observed with the acute SRM1650b exposure, where MMP levels decreased. Also, chronic exposure to SRM2975 did not affect MMPs in mice's lungs or brains, as was seen with acute instillation.

In conclusion, the MMPs' content after DEP exposure was differentially regulated in lungs and brain, showing larger responses to the SRM1650b DEP material in specific brain areas such as the hippocampus and cortex by decreasing the MMP levels at a short time (3 days) and increasing them after longer exposures (3 weeks), whereas MMPs remained unaltered in the lungs.

Given these results, it could be plausible that the MMP alteration after DEP exposure in naïve mice could influence the inflammatory responses involved in both stroke injury and repair, since MMPs are known to play a key role in these processes.

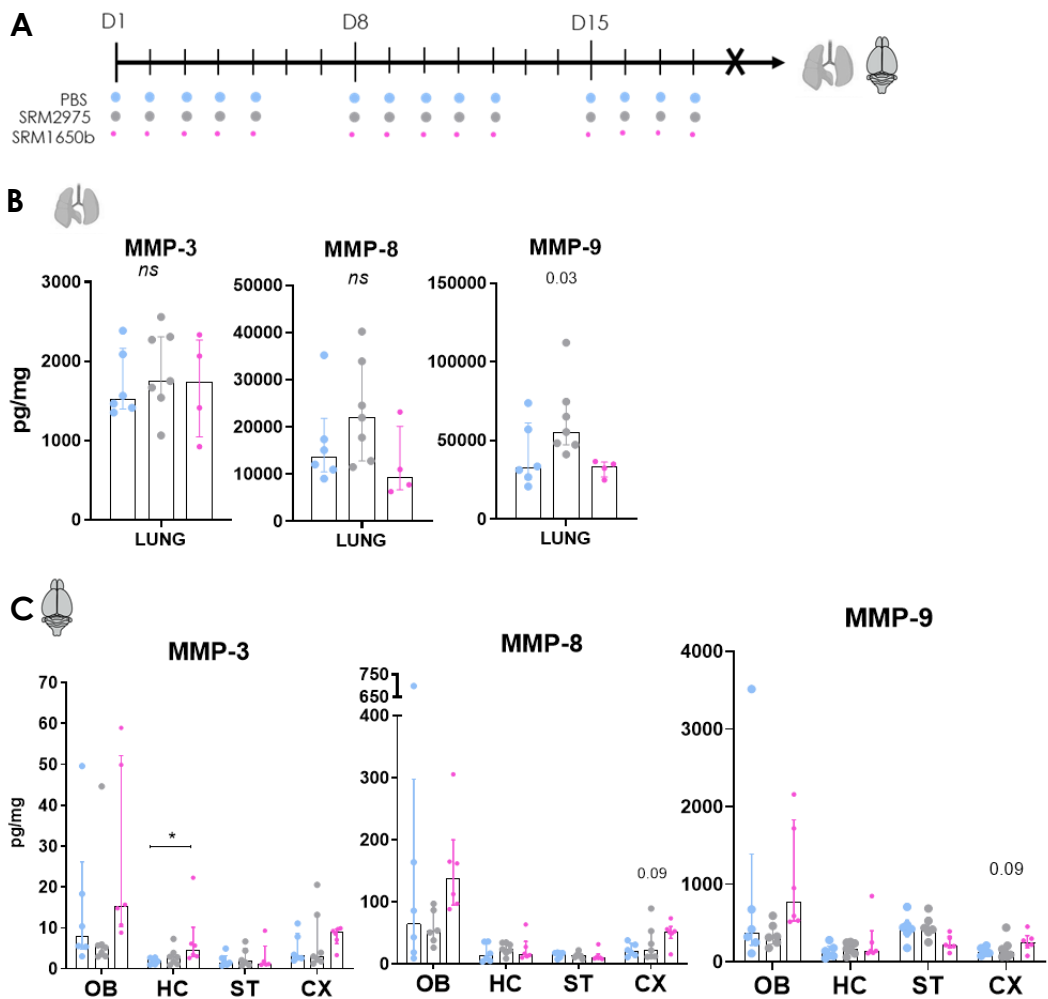


Figure 28: Chronic exposure to SRM1650b DEP increased MMP levels in the hippocampus and the cortex of naïve mice. **A:** Experimental design: MMP analyses were done in lungs and brains of mice instilled for 3 weeks. **B:** Levels of MMP-3, -8 and -9 in mice's lungs. **C:** MMP levels were analyzed in the different brain regions, showing increased MMP content in HC and CX. Data is represented as median (IQR). *ns*: not significant * $p < 0.05$. PBS ($n=6$), SRM2975 ($n=7$) or SRM1650b ($n=6$).

Chronic exposure to DEP reduced the neural progenitor cells in the rostral migratory stream.

Immunofluorescence studies targeting different brain cell populations were conducted to complement the studies in naïve mice focusing on the exposure to SRM1650b material (**Fig. 29**). First, considering our previous observations that DEP reduced cell viability in NSC-derived neurospheres *in vitro* and that they altered MMP content in the HC, we investigated the Rostral Migratory Stream and hippocampus neurogenic areas focusing on proliferative cells, neural progenitor cells and immature neurons. The immunofluorescence study was complemented with immunolabeling targeting CNS inflammatory cells (microglia) and neurovascular unit cellular components (endothelial cells or neurons) known to respond to MMP alterations.

Vessels (labeled with lectin), neurons (labeled with NeuN) and microglia (labeled with Iba-1) were studied in HC, ST and CX. While markers for proliferative cells (Ki-67), neural progenitor cells (Nestin) and migrating neuroblasts (DCX) that are restricted to the proliferative niches of the SVZ (that migrate through the RMS until the OB) and the SGZ of the hippocampus, were also studied (**Fig. 29**).

Two unexpected findings limited a small part of the immunofluorescence study: anecdotic labeling of Ki-67 was found in the hippocampus and the OBs were challenging to preserve through the whole process of brain fixation, tissue slicing and staining. Also, in the thesis main text, only significant results of the extensive immunofluorescence study are shown, however, the complete analyses of the studied markers can be consulted in Annex IV (pag.227).

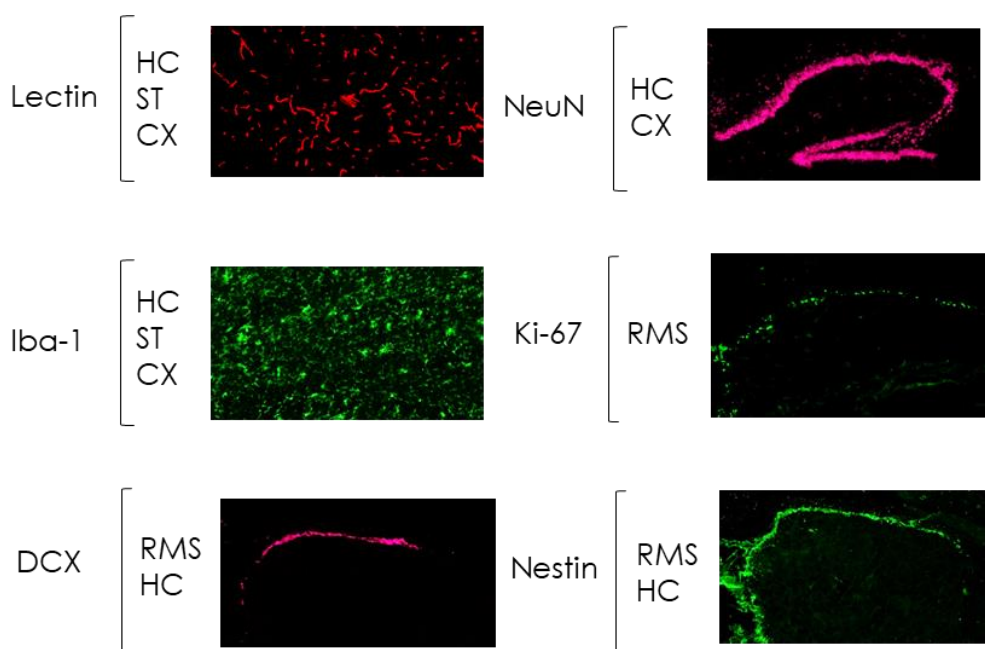


Figure 29: Summary of the brain immunofluorescence study and specific markers analyzed. Vessels (lectin), neurons (NeuN), microglia (Iba-1), proliferation marker (Ki-67), neuroblasts (DCX) and neural progenitor cells (nestin) were studied in HC, ST, CX and RMS.

The immunofluorescence study in naïve mice exposed acutely to DEP (**Fig. 30**), showed a strong tendency to exhibit fewer Ki-67⁺ proliferative cells in the RMS [**13.5** (7.9-23.2) vs. **7.2** (1.5-8) μm^2 , $p=0.05$] (**Fig. 30B**), but it did not result in fewer Nestin⁺ neural progenitors (**Fig. 30C**), DCX⁺ migrating neuroblasts or NeuN⁺ neurons (see Annex IV, pag. 227).

In chronically instilled naïve mice (**Fig. 30A**), though no differences were found in Ki-67⁺ proliferating cells, DEP exposure significantly reduced the amounts of Nestin⁺ neural progenitor cells of the RMS [**24,667.1** (16,368.1-38,781.4) vs. **8,467.1** (4,726.1-10,820.7) μm^2 , $p=0.02$] (**Fig. 30C**). But as in acutely exposed animals, a similar amount of DCX⁺ migrating neuroblasts were observed between control and DEP exposed mice (see Annex IV, pag. 227). Interestingly, less NeuN⁺ cortical neurons were observed after SRM1650b exposure, particularly after 3 weeks exposure [**57,567.4** (29,789.2-109,393) vs. **20,357.1** (12,590.8-45,744.7) μm^2 , $p=0.06$] (**Fig. 30C**).

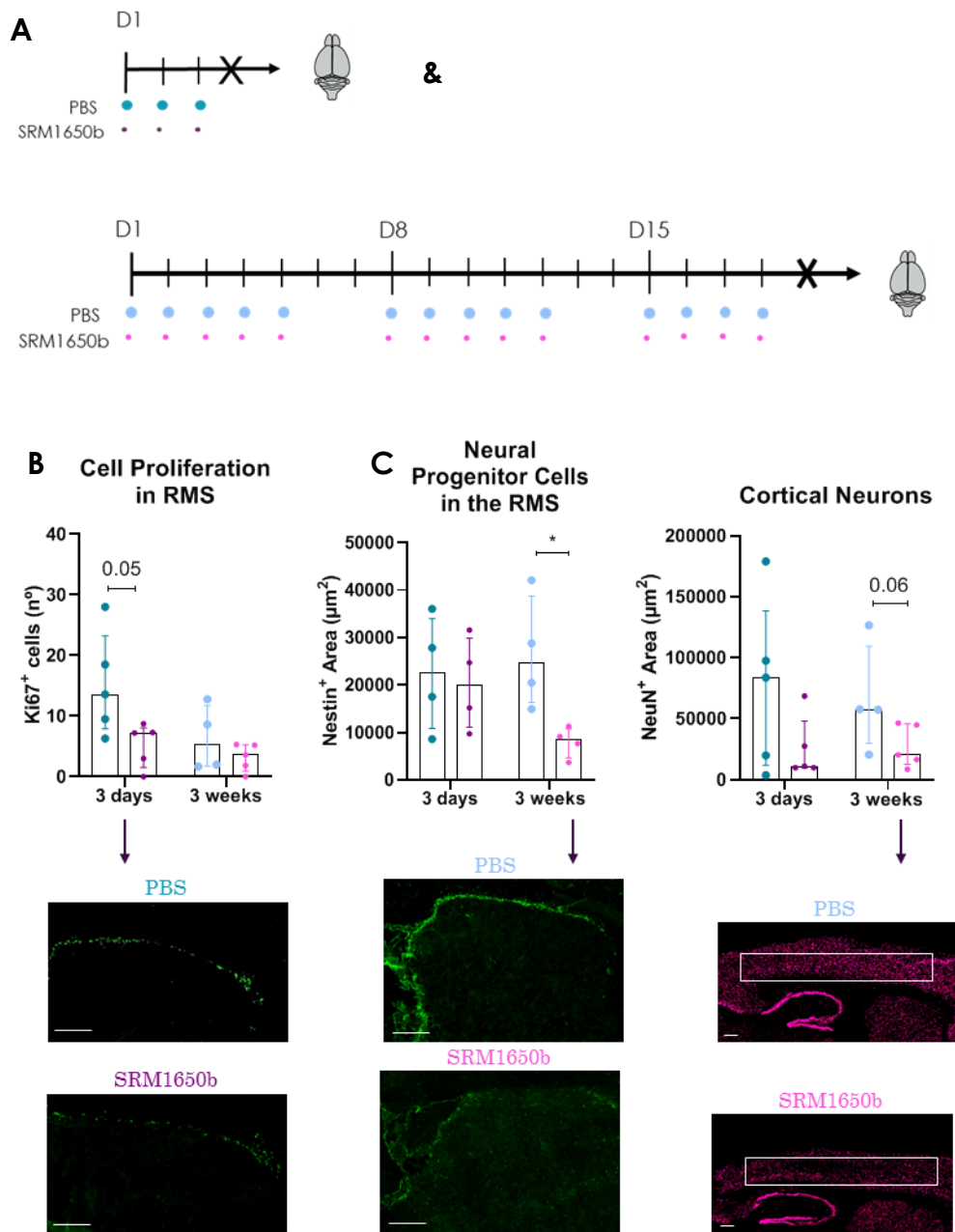


Figure 30: Brain neurogenesis markers were reduced after exposure to SRM1650b in naïve mice. **A:** Experimental design: 3 days and 3 weeks DEP exposure before the immunofluorescence study in brain. **B:** Bar graphs and representative images showing Ki-67⁺ reduction in acutely exposed mice. **C:** Bar graphs and representative immunofluorescence images of the Nestin⁺ and NeuN⁺ study showing reduced positive area in chronically exposed mice. Data is represented as median (IQR). Scale: 200 µm. Comparisons are made between DEP and PBS. ns: not significant, * $p < 0.05$. Acute-PBS (n=5), SRM1650b (n=5) and chronic-PBS (n=4), SRM1650b (n=5).

Summary: Lung and brain alterations after DEP exposure in naïve mice.

Firstly, MMP results can be summarized as shown in **Figure 31**. Considering all the results from naïve animals together, they showed that MMPs in the **lungs** did not change after acute or chronic exposure to DEP (**Figs. 27B, Fig. 28B**) but, in the **brain**, DEP reduced the proliferative cells in the RMS after an **acute** exposure (**Fig. 30B**) which occurred together with reduced MMPs in the OB, HC, ST and CX (**Fig. 27C, Fig. 31**). When DEP exposure was extended up to **3 weeks**, it resulted in fewer neural progenitor cells in the RMS and in reduced number of cortical neurons (**Fig. 30C**) as well as in an increase in MMPs at the same exposure time (**Fig. 28C, Fig. 31**), suggesting an inflammatory response after chronic exposure.

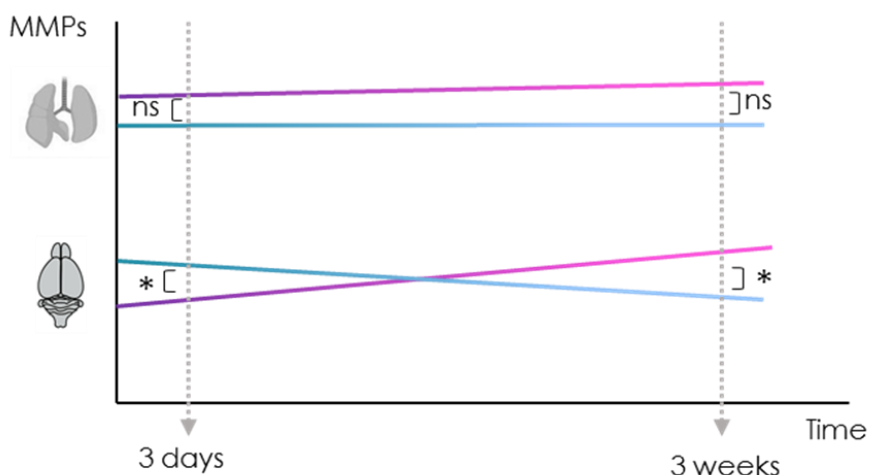


Figure 31: Schematic representation of MMP alterations in lungs and brains of naïve mice.

4.4. Effects of DEP exposure in cerebral ischemia

To continue the study and evaluate if this decrease in neural progenitors or the disbalance of MMPs in the brain after DEP exposure would lead to a worsened brain injury or an altered inflammatory response after cerebral ischemia, another set of animals received instillations for 3 or 13 days (**Fig. 32A**), 24 hours after the last instillation mice underwent proximal permanent MCAo surgery, and 24 hours later they were euthanized to obtain lungs, brains and plasma. Weight was

recorded every day to surveil the animals' general status and the grip test was performed before and after surgery to evaluate neurological outcome.

General mice condition after DEP exposure followed by pMCAo

Before surgery, all animals increased their body weight, being larger in those followed for two weeks. Weight gain was more variable within the first 3 days, however, no differences were observed between exposure groups after acute or chronic exposures. Later, after surgery, all groups presented a slight decrease in their body weight, around 3%, but was similar between groups (**Fig. 32B**).

Interestingly, acute instillation with SRM1650b tended to worsen the grip strength, while the chronic instillation showed an increase of the grip strength in the SRM2975-exposed animals (**Fig. 32C**).

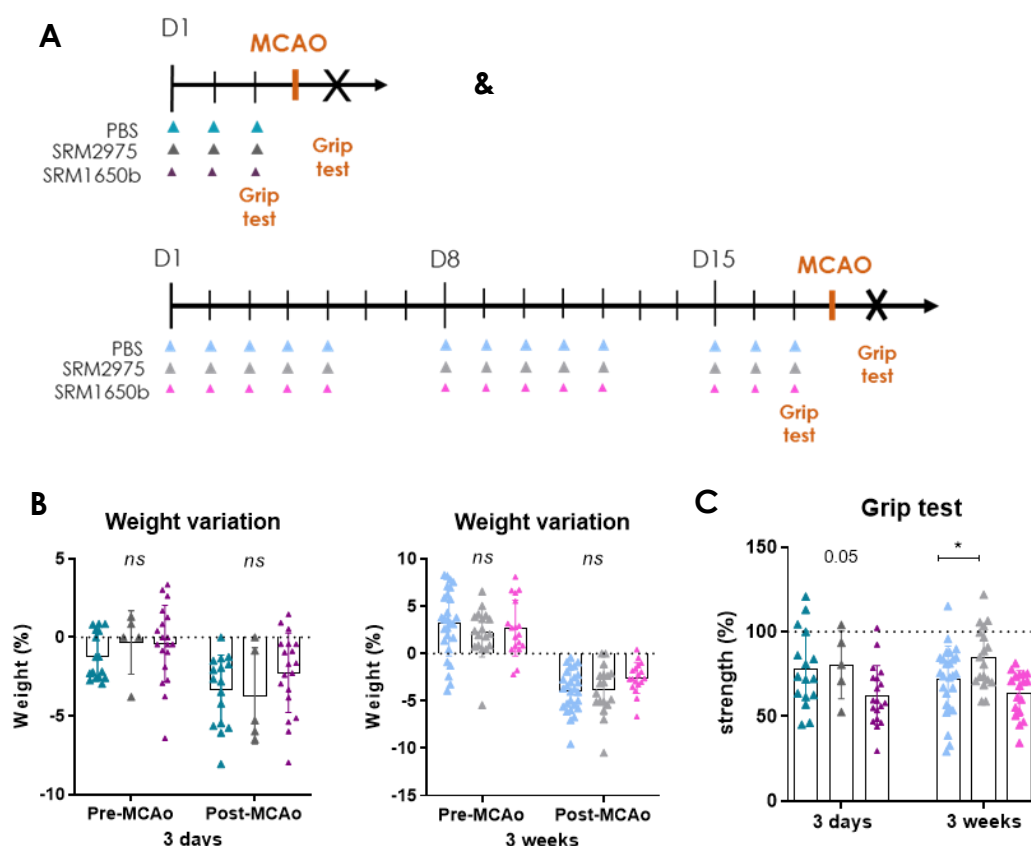


Figure 32: Ischemic mice instillation protocol, weight variation before and after surgery and grip test performance. **A:** Mice received PBS or DEP for 3 days or 3 weeks. One day after last exposure, MCAo surgery was performed and 24 hours later their organs were extracted. **B:** Weight was recorded every day. Data is represented as mean \pm SD. **C:** The grip test was done before and after surgery. Data is represented as median (IQR). *ns*: not significant, * $p < 0.05$.

Chronic exposure to DEP did not exacerbate infarct lesion.

Infarct volume, a primary endpoint for brain injury, was studied at 24 (Fig. 33 and 34) and 48 hours (Fig. 35) after cerebral ischemia.

In the brains of chronically instilled mice with SRM2975 (Fig. 33A), no differences were found in the infarct percentage or the brain edema at 24 hours post-ischemia measured by TTC staining (Fig. 33B).

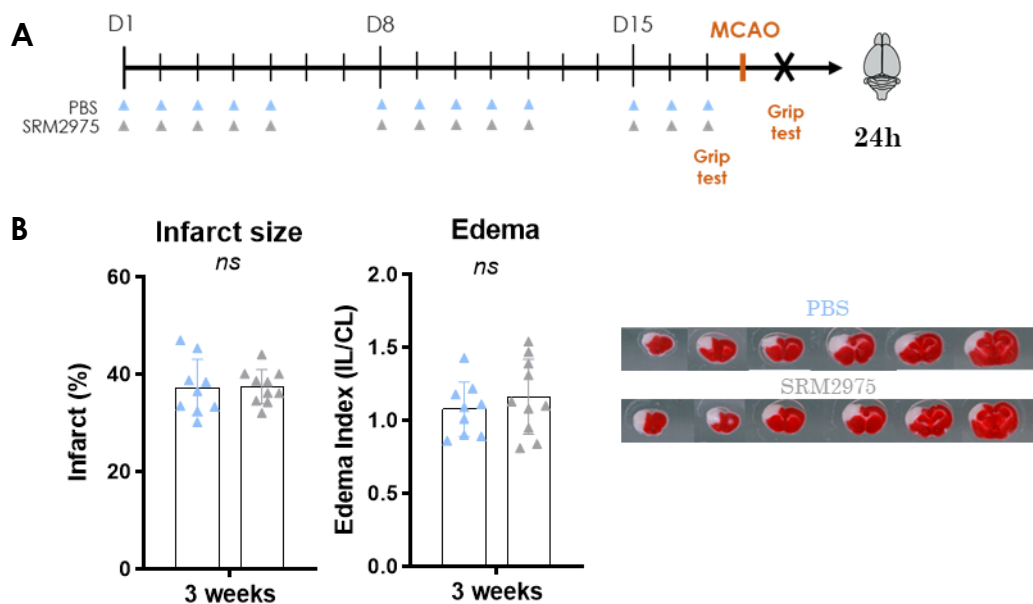


Figure 33: Infarct lesion measurements after chronic DEP exposure at 24 hours of permanent ischemia. A: Experimental design overview. **B:** Bar graphs showing the infarct and edema quantifications and TTC representative images. Data is represented as mean±SD. ns: not significant. PBS (n=9), SRM2975 (n=10).

With these unexpected results and considering that the TTC staining could be considered a rough measurement of non-viable tissue, a small set of animals that underwent chronic SRM2975 instillation and cerebral ischemia (**Fig. 34A**) were taken to an MRI facility and the infarct lesion was quantified in the acquired T2W images (**Fig. 34B**). At the acquisition session, DTIs were also obtained to evaluate the orientation of the myelin fibers in the anterior commissure and the corpus callosum. Despite these efforts, no differences were found after DEP chronic instillation neither in infarct size, not in fractional anisotropy measurements (**Fig. 34C**).

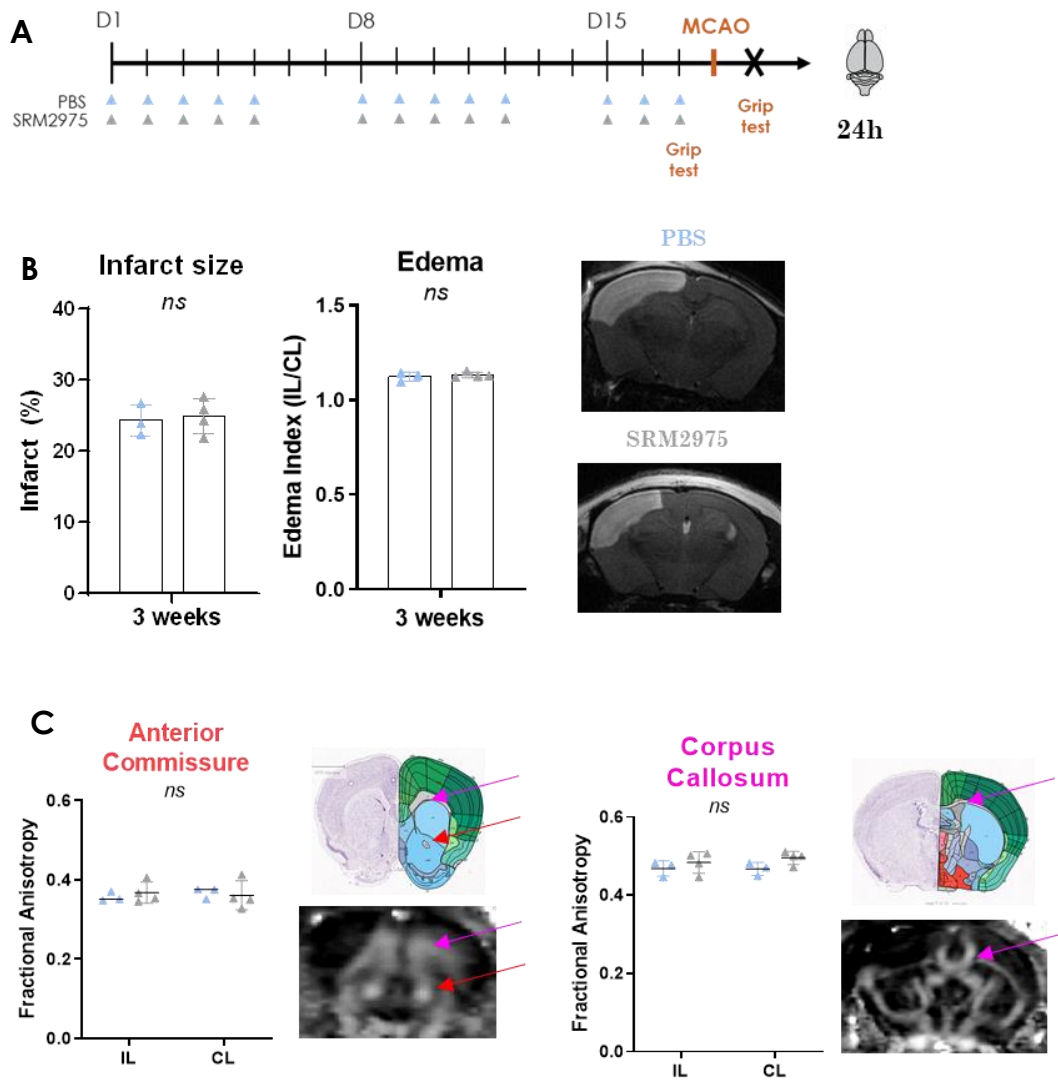


Figure 34: Infarct lesion and axonal fiber tract integrity measurements after chronic DEP exposure at 24 hours of cerebral ischemia. **A:** Experimental design overview. **B:** Lesion size evaluated by MRI in T2WI, bar-graphs show similar lesion between groups. **C:** Fractional anisotropy measurements after DTI acquisition in the selected fiber tracts. At the right side of the graphs, atlas images (up) and corresponding DTI images (down) with pink arrows indicating the corpus callosum and the red arrows indicating the anterior commissure in the ipsilateral (IL) and contralateral hemispheres (CL). Data is represented as mean \pm SD. *ns*: not significant. PBS (n=3), SRM2975 (n=4).

In another group of animals, acutely or chronically instilled with SRM1650b, infarct size was further investigated at 48 hours post-ischemia (**Fig. 35A**) since in naïve mice, this material had shown damaging effects at both molecular and cellular levels. But results remained consistent, and no exacerbation of the lesion was evidenced after exposure to SRM1650b (**Fig. 35B**).

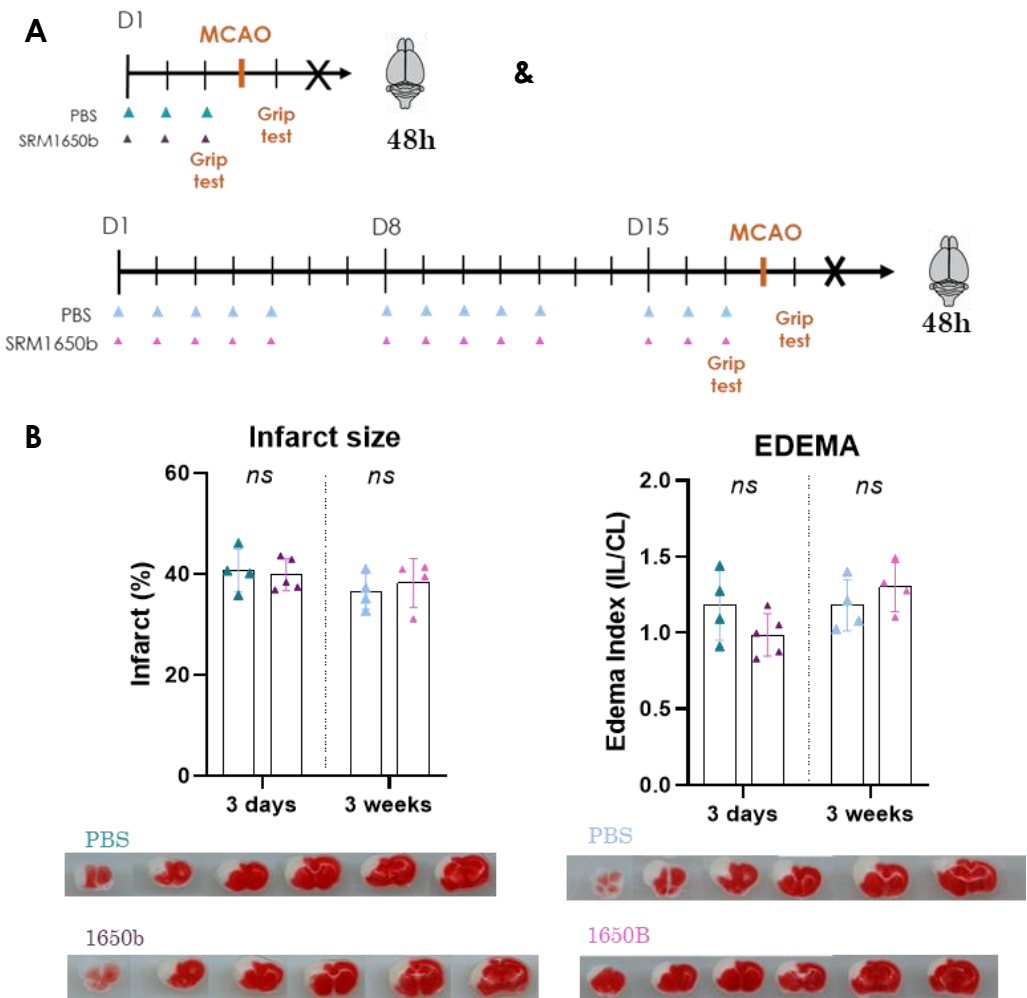


Figure 35: Infarct lesion measurements at 48 hours post ischemia. A: Experimental design overview. **B:** Infarct damage and edema analyses accompanied by TTC representative images of the 4 groups. Data is represented as mean±SD. Comparisons are made between PBS and SRM1650b. ns: not significant. Acute- PBS (n=4), SRM1650b (n=5) and Chronic- PBS (n=4), SRM1650b (n=4).

Though, in chronically exposed naïve animals with SRM1650b we observed a reduced number of cortical neurons (**Fig. 30C**), the cell death induced by ischemia was not different with any of the DEP material, post-ischemia time point or evaluation technique.

Acute exposure to DEP did not significantly alter MMPs neither in the lungs nor in the brain whereas chronic DEP exposure significantly decreased MMP levels in the lungs after ischemia.

In this study, we aimed at investigating if the instillation of DEP could alter the inflammatory response of the lungs and brain tissue after cerebral ischemia. Acute instillation of particles (**Fig. 36A**) before ischemia did not significantly altered MMP levels in the **lungs** compared to PBS-instilled MCAo mice (**Fig. 36B**).

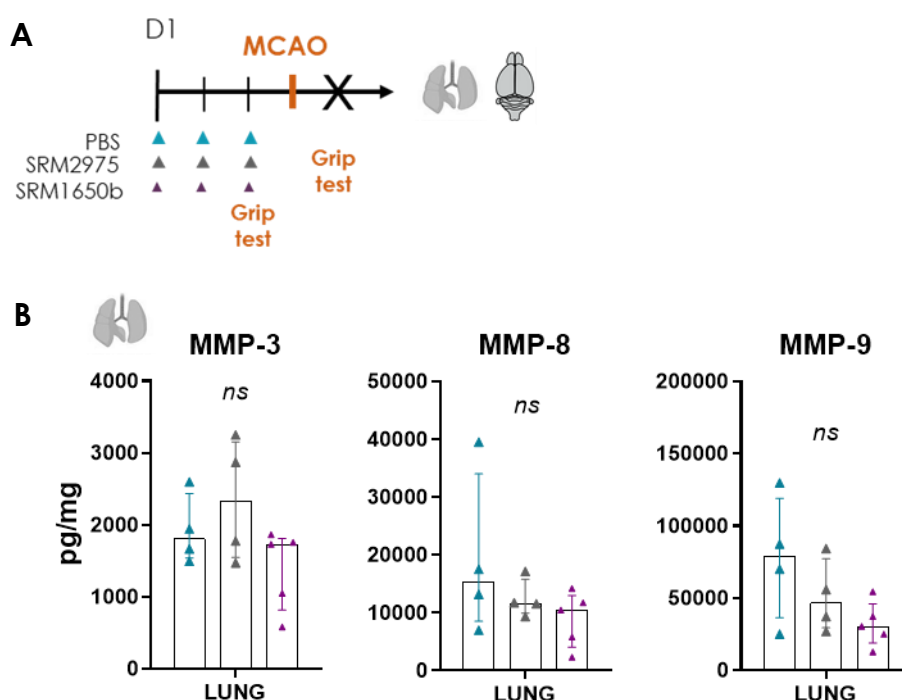


Figure 36: Acute exposure to DEP did not alter MMPs in the lungs. **A:** After 3 days exposure, mice underwent pMCAo surgery and 24 hours later, brains and lungs were obtained for MMP analyses. **B:** Bar graphs showing MMP-3, -8 and -9 measured in lungs. Data is represented as median (IQR). ns: not significant. PBS (n=4), SRM2975 (n=4) or SRM1650b (n=5).

The MMP study in the **brain** of mice acutely exposed to SRM material or PBS, showed a robust increase of all MMPs in the ipsilateral ischemic cortex, as expected corresponding with the lesion area in this model (**Fig. 37**). However, ischemia also induced an increase of MMP-3 and MMP-8 in the periinfarct areas of the striatum and hippocampus of the ipsilateral hemisphere regardless of the received suspension (**Fig. 37**). However, only isolated responses to SRM 1650b instillation were observed for MMP-8 which slightly decreased in the ipsilateral hippocampus [**234.5** (191.1-345.8) vs. **136.9** (106.9-192.3) pg/mg, $p=0.06$] and in the contralateral striatum [**378.8** (209.5-483.9) vs. **243** (161.5-371) pg/mg, $p=0.09$] (**Fig. 37**).

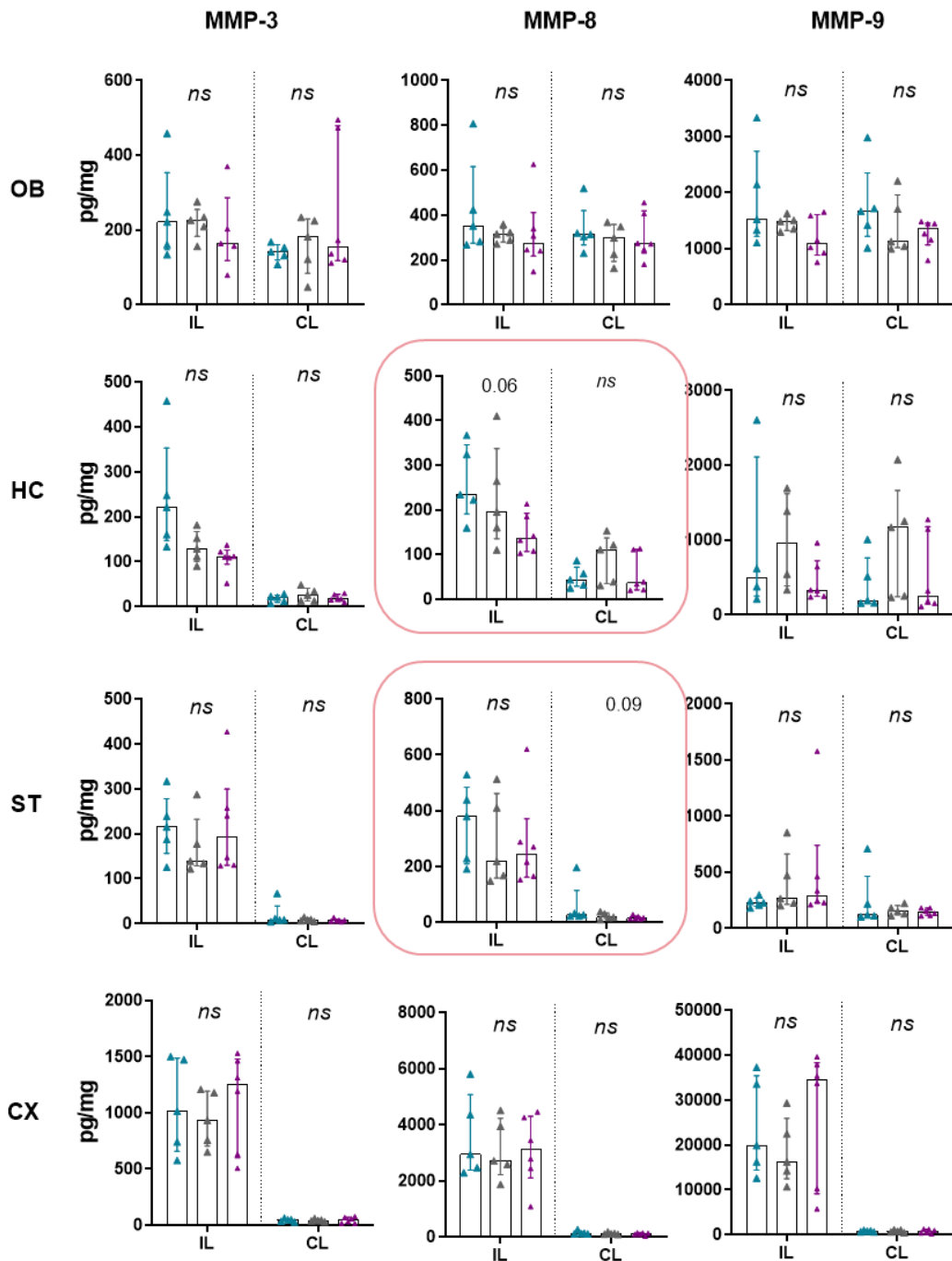


Figure 37: Acute DEP exposure and MMP levels in the ischemic brains. Bar graphs show how MMPs in the ipsilateral (IL) studied areas responded to the ischemia rising MMPs compared to the contralateral (CL) side (HC, ST and CX). MMP-8 showed a decrease in the IL HC and CL ST after SRM1650b exposure vs. PBS. Data represented as median (IQR). ns: not significant, * $p < 0$. PBS (n=5), SRM2975 (n=5) or SRM1650b (n=6).

Chronic exposure to DEP was studied in another set of animals that received PBS, SRM2975 or SRM1650b instillations for 3 weeks and were subjected to cerebral ischemia, as detailed in **Fig. 38A**.

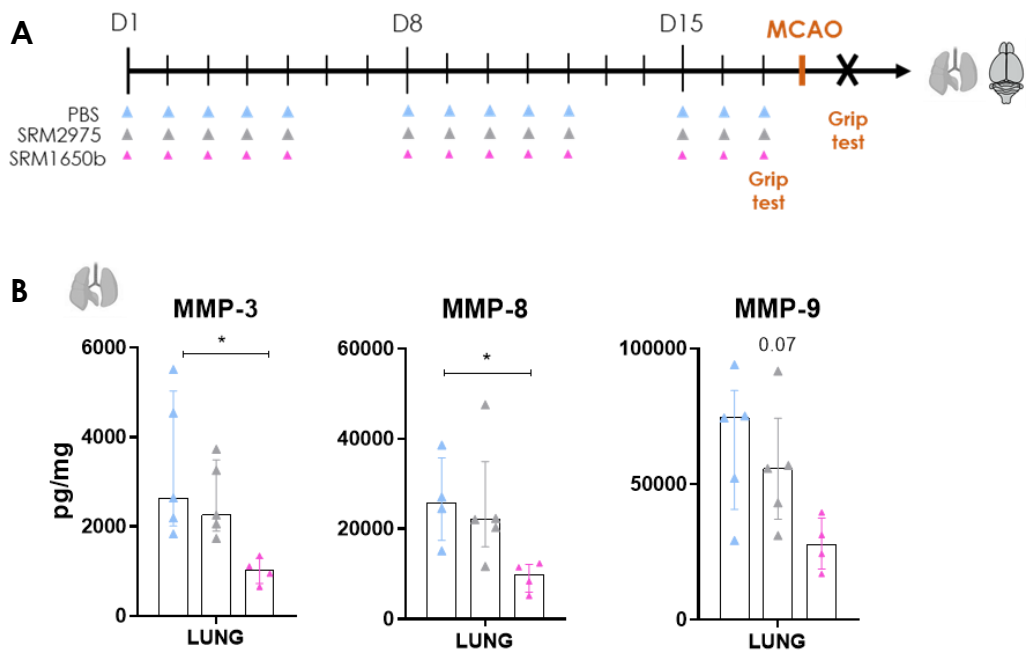


Figure 38: MMP analysis in lungs of chronically exposed MCAo mice. A: Mice received DEP or PBS for 13 days, then they underwent pMCAo surgery and 24 hours later they were euthanized and their brains and lungs obtained for MMP study. **B:** MMPs were reduced in lungs of SRM1650b instilled mice. Data represented as median (IQR). ns: not significant, * $p < 0.05$. PBS (n=5), SRM2975 (n=5) or SRM1650b (n=5).

In the lungs of ischemic mice, instillation with SRM1650b reduced the levels of MMP-3 [2,640.3 (2,014.1-5,031) vs. 1,032.3 (725.7-1,290.8) pg/mg, $p = 0.01$], MMP-8 [25,803.1 (17,478.3-35,736.2) vs. 9,940.8 (5,954.4-12,110.6) pg/mg, $p = 0.02$] and MMP-9 [74,497.6 (40,700.8-84,580.8) vs. 27,747.8 (18,725.24-37,453.6) pg/mg, $p = 0.07$], whereas no variation was observed by SRM2975 (**Fig. 38B**).

Furthermore, in chronically instilled mice with PBS the MMP content increased in lungs after ischemia compared to the naïve group [MMP-3: 1,516.4 (1,398.3-2,163.1) vs. 2,640.3 (2,014.1-5,031) pg/mg, $p = 0.03$; MMP-8: 13,588.1 (10,486.5-21,859.2) vs. 25,803.1 (17,478.3-35,736.1) pg/mg, $p = 0.08$; MMP-9: 32,475.9

(25,347.6-61,225.1) vs. **74,497.6** (40,700.8-84,580.8) pg/mg, $p=0.1$]. However, this increase did not occur in the ischemic mice instilled chronically with SRM1650b. Which suggests that chronic exposure to DEP is suppressing the ischemic inflammatory response in the lungs (**Fig. 39**).

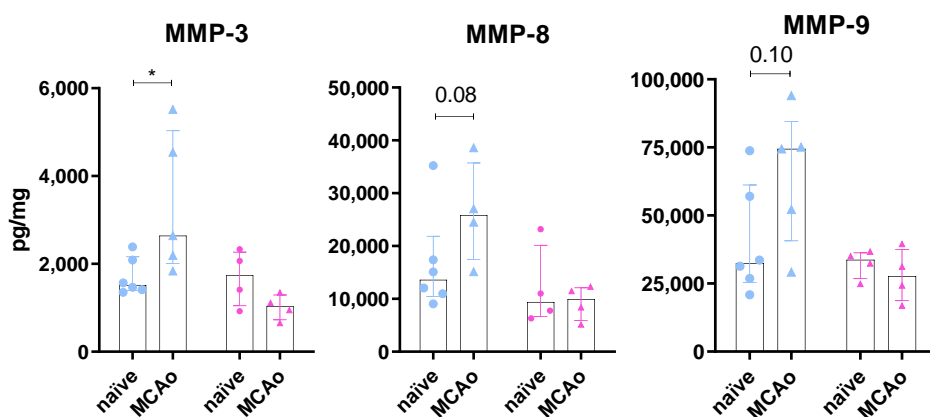


Figure 39: MMP alterations in the lungs after ischemia in chronically exposed mice.

There is an inflammatory MMP response after ischemia in lungs of PBS-ischemic mice, which is not observed after the chronic exposure to SRM1650b. Data represented as median (IQR). ns: not significant, * $p<0.05$. Naïve: PBS (n=6), SRM1650b (n=4) and MCAO- PBS (n=5), SRM1650b (n=5).

In the brains of these animals exposed to chronic PBS or SRM material and subjected to cerebral ischemia (**Fig. 38A**), similar responses to ischemia were observed in the cortex, striatum and hippocampus as in the acutely exposed group, and again, isolated MMP responses were observed for MMP-3 which decreased in the IL hippocampus in DEP exposed mice compared to the vehicle group [**189.8** (170.2-200.1) vs. **106.6** (27.1-153.6) vs. **148.9** (105.8-186.3) pg/mg, $p=0.006$] and for MMP-9 which showed a trend to decrease in the IL striatum [**1,080.3** (593.1-133.2) vs. **432.6** (408.1-785.8) vs. **461.4** (295.7-1021.7) pg/mg, $p=0.07$]. It can also be observed a reduction of MMP-8 in two additional areas, the contralateral olfactory bulb [**480.4** (315.4-684) vs. **289.5** (267.2-348.5) pg/mg, $p=0.08$] and the contralateral cortex [**204.7** (113.1-282.4) vs. **114.9** (136.5-89.5) pg/mg, $p=0.06$] (**Fig. 40**).

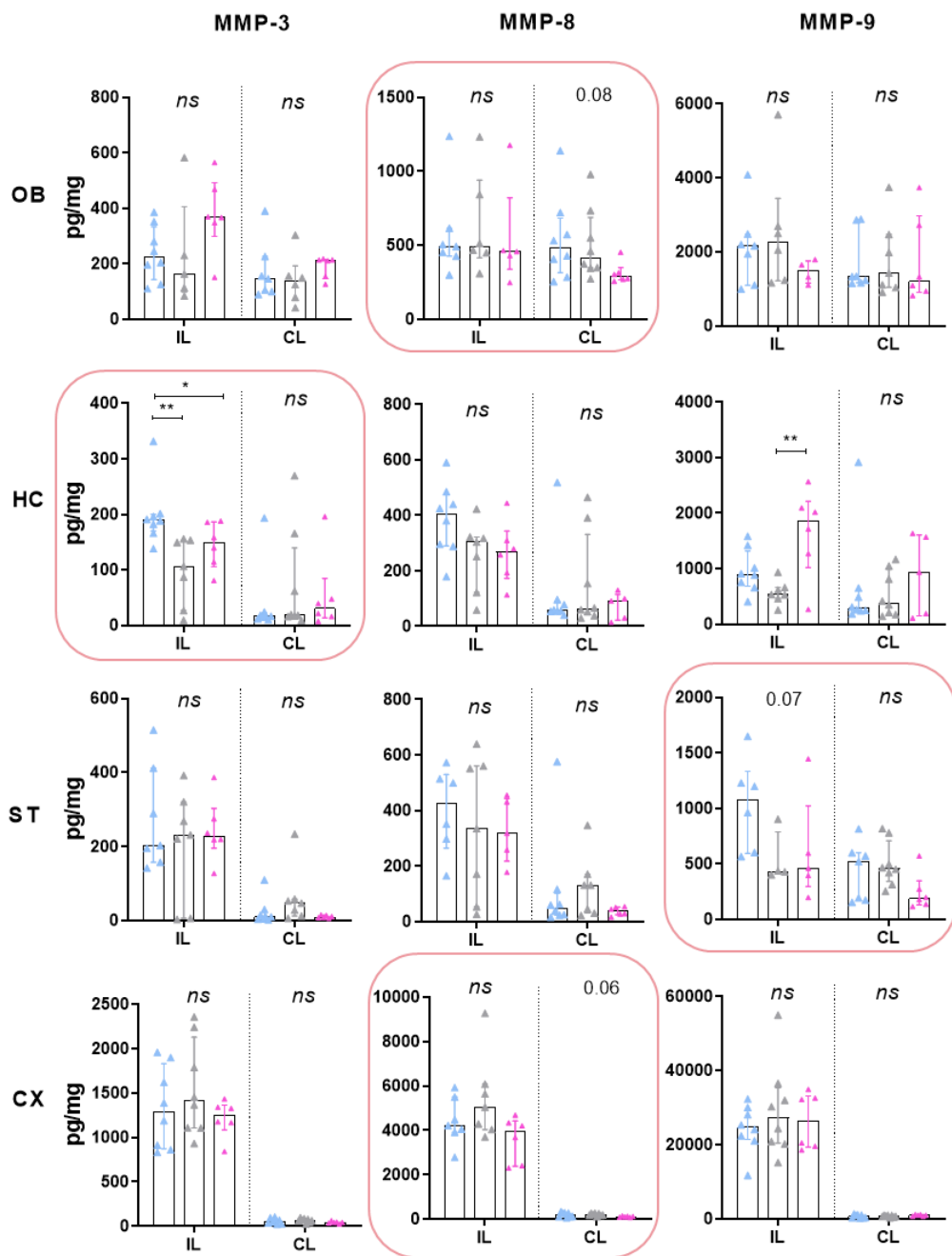


Figure 40: Chronic DEP exposure and MMP levels in brains of MCAo mice. Bar graphs showing increased MMP levels in the ipsilateral (IL) studied areas as a response to the ischemia compared to the contralateral hemisphere (HC, ST and CX). MMP-3 showed a decrease in the IL HC after DEP exposure and MMP-9 in IL ST, compared to PBS. MMP-8 tended to decrease in CL CX and CL OB. Data is represented as median (IQR). ns: not significant, * $p < 0.05$, ** $p < 0.01$. PBS (n=8), SRM2975 (n=8) or SRM1650b (n=6).

Exposure to SRM1650b material in ischemic mice did not alter CNS cell populations.

The same immunofluorescence markers analyzed for naïve mice (**Fig. 29**) were studied in animals exposed to PBS or SRM1650b material and subjected to pMCAo (**Fig. 41**).

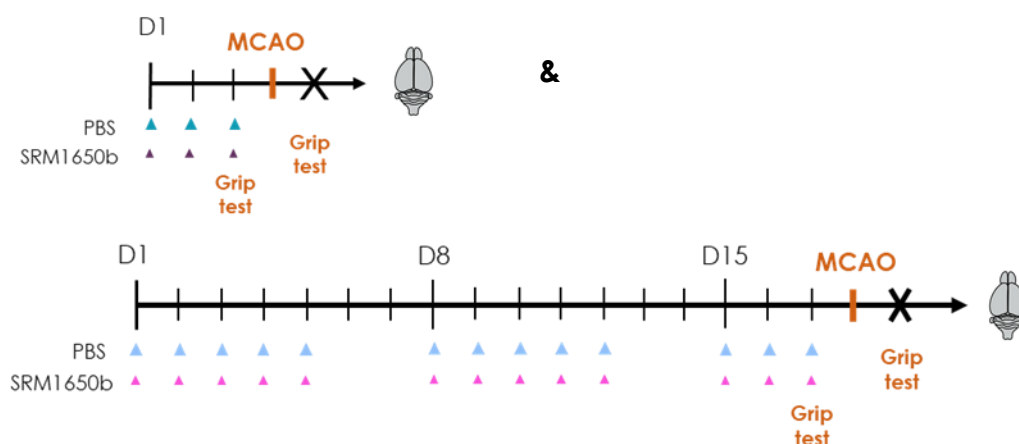


Figure 41: Experimental procedure for immunofluorescence analyses in ischemic mice. Experimental protocol: mice were exposed for 3 days or 3 weeks to PBS or SRM1650b, then underwent MCAo surgery and 24h later brains were obtained for immunofluorescence studies. Acute PBS (n=4) or SRM1650b (n=6) and chronic PBS (n=4) or SRM1650b (n=6).

Lectin, NeuN, Iba-1, Ki-67, Nestin and DCX analysis showed no significant differences in the IL or CL hemispheres of SRM1650b compared to PBS exposed mice (see Annex IV on page 227).

Study of leukocytes' population in the lungs of chronically exposed ischemic mice.

With this background pointing at a plausible alteration of the ischemic inflammatory response in the lungs of chronically exposed mice to DEP, we instilled a new group of mice chronically (**Fig. 42A**), cerebral ischemia was induced as described and, 48 hours later, lungs were obtained for the study of 10 different leukocyte populations by flow cytometry (see pag. 79 and **Fig. 16**).

After the analysis, only some cell populations referred to the major histocompatibility complex II (MHC II) were altered by the instillation of DEP which was the case of the macrophages and monocytes (**Fig. 42B**).

After ischemia, no differences in total macrophages were observed, but the alveolar macrophages subpopulation was significantly reduced in the DEP instilled group compared to PBS (93.6 ± 0.6 vs. 91.2 ± 1.1 %, $p = 0.01$). On the contrary, the interstitial macrophages subpopulation (6.2 ± 0.5 vs. 8.5 ± 1.2 %, $p = 0.01$) and total monocytes (19.3 ± 1.1 vs. 23.5 ± 2.8 %, $p = 0.03$) were significantly increased after chronic DEP exposure compared to PBS (**Fig. 42C**). These results confirm an altered systemic inflammatory response of the diesel exhaust exposed lungs after the ischemia.

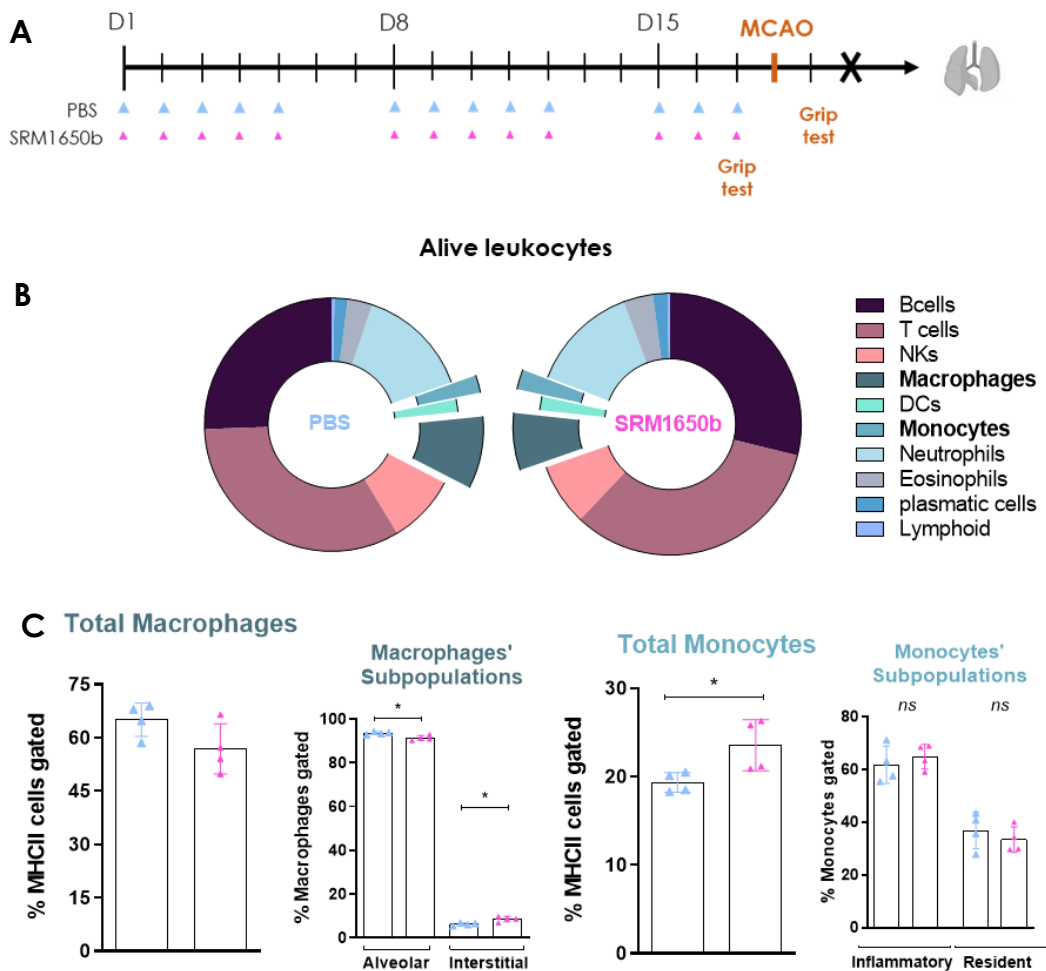


Figure 42: Chronic SRM1650b inhalation reduces alveolar macrophages and increases total monocytes in lungs of ischemic mice. **A:** Mice underwent MCAO after chronic instillation, 48 hours later they were euthanized and their lungs studied by flow cytometry. **B:** Donut chart representing the proportion of alive leukocytes' subpopulations with the monocytes' and macrophages' portion extruded. **C:** Further analyses in total macrophages, macrophages' subpopulations and total monocytes and monocytes' subpopulations. Data is represented as mean \pm SD. ns: not significant. * $p < 0.05$. PBS (n=4) or SRM1650b (n=4).

Summary: Lung and brain alterations in ischemic mice previously exposed to DEP

So far, it is shown that previous instillation with DEP did not worsen the ischemic brain lesion at 24/48 hours post-MCAo surgery. After ischemia, the inflammatory response in the brain is sudden and devastating thus, the inflammatory effect of the diesel particles exposure does not impact in lesion extension in the acute phase of the disease, only observing slight decreases in selected MMPs in structures not directly affected by the infarct. However, lungs of ischemic mice previously exposed to SRM1650b chronically, clearly present lower MMPs and altered proportions of lung leukocyte subpopulations (macrophages and monocytes) indicating an effect of diesel particles inhalation on the lung pathophysiology after stroke.

4.5. Alterations of thrombogenic and thrombolytic plasma characteristics under DEP exposure

Turbidimetric clot assays were conducted to evaluate the influence of DEP on clot formation and lysis in the presence of rtPA in mouse and human plasma samples (consult **Fig.17**).

Pro-thrombogenic changes in mouse plasma after ischemia can be boosted depending on the DEP exposure time.

Plasmas of acutely (**Fig. 43A**) and chronically (**Fig. 44A**) exposed naïve and ischemic mice were first studied.

In acutely exposed mice (**Fig. 43A**), significant differences were observed in parameters of clot formation, but not in those related with the lysis phase. Specifically, a reduction in the clot formation time in plasma of ischemic mice compared to the naïve has been observed [Lagtime: **4.9** (2.6-6.9) vs. **1.3** (0.6-2.2) mins, $p=0.007$] (**Fig. 43B**). Also, ischemic mice presented increased speed clot formation (CRc) and clot density (MaxAbs) compared to naïve mice [CRc: **12.6** (11.3-15.2) vs. **43.1** (28.1-50.7) OD/sec, $p=0.02$; MaxAbs: **0.07** (0.05-0.09) vs. **0.17** (0.13-0.19) OD, $p=0.03$] (**Fig. 43B**). Importantly, the highest values in speed clot

formation and clot density were observed in ischemic mice exposed to SRM1650b material compared to PBS exposure [CRc: **12.6** (11.3-15.2) vs. **55.5** (38.5-60.1) OD/sec, $p = 0.001$; MaxAbs: **0.07** (0.05-0.09) vs. **0.22** (0.21-0.23) OD, $p = 0.002$] (**Fig. 43B**), suggesting that the exposure to DEP could translate into denser clots that were formed faster in the plasma of stroke mice.

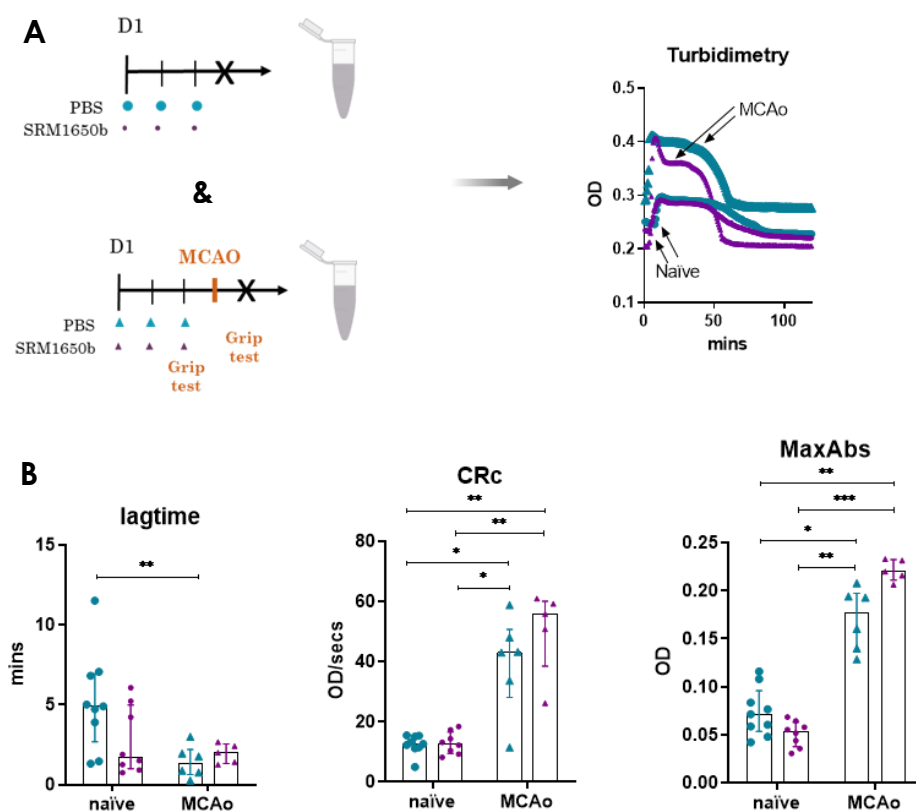


Figure 43: Turbidimetry study of clot formation and lysis in acutely exposed naïve and ischemic mice. **A:** Experimental design overview with representative turbidimetric curves. **B:** After ischemia the lag time shortens, the slope formation accelerates (CRc) and the density of the thrombus (MaxAbs) increases. Data represented as median (IQR). ns: not significant. * $p < 0.05$, ** $p < 0.01$, *** $p < 0.001$. naïve-PBS (n = 9), SRM1650b (n = 8) and MCAO-PBS (n = 6), SRM1650b (n = 5).

Next, plasma of animals that received instillations chronically (**Fig. 44A**) presented similar results as those acutely exposed regarding clot formation parameters: clots formed faster and were denser in ischemic than in naïve mice [CRc: **11.1**

(7.25-17.46) vs. **36.7** (29.8-48.5) OD/sec, $p=0.01$; MaxAbs: **0.06** (0.04-0.07) vs. **0.17** (0.16-0.23) OD, $p=0.02$] peaking when exposed to SRM1650b DEP [CRC: **11.1** (7.25-17.46) vs. **54.6** (43.4-60.9) OD/sec, $p=0.001$; MaxAbs: **0.06** (0.04-0.07) vs. **0.2** (0.18-0.23) OD, $p=0.01$] (**Fig. 44B**). Moreover, the chronic exposure also modified some clot lysis parameters towards a slower lysis time in ischemic mice compared to naïve PBS-exposed cohorts [Clot time: 1.2 ± 0.3 vs. 1.7 ± 0.16 hours, $p=0.02$; Lysis time 1.1 ± 0.3 vs. 1.6 ± 0.1 hours, $p=0.03$; Lys 50 t_0 : 0.6 ± 0.1 vs. 0.9 ± 0.08 hours, $p=0.01$ and Lys 50 t_{MAX} : 0.55 ± 0.1 vs. 0.8 ± 0.08 hours, $p=0.03$] (**Fig. 44B**), but not in ischemic mice exposed to DEP chronically.

In summary, in PBS-exposed mice after ischemia, pro-thrombogenic changes take place in their plasma evidenced by shorter latency times and faster and denser clots being formed, ex vivo, which was exacerbated in mice exposed to DEP before ischemia. On the other hand, plasma from naïve mice exposed to **PBS chronically** lysed the clots faster than ischemic mice, but this was not observed in the chronic DEP exposed mice which presented similar lysis features between naïve and ischemic animals.

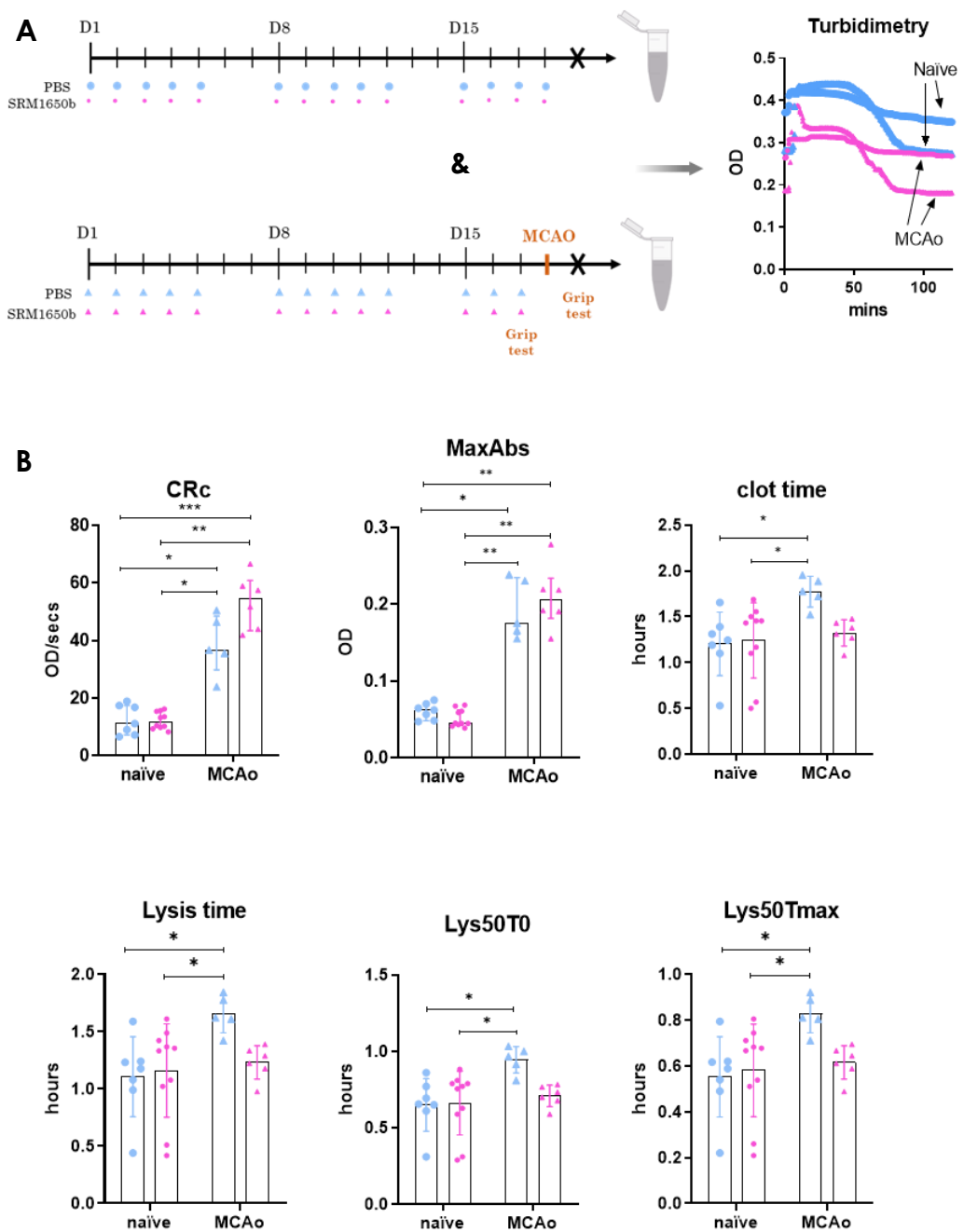


Figure 44: Thrombus formation and lysis in chronically exposed naïve and MCAO animals. **A:** Experimental design overview. **B:** CRc and MaxAbs, formation parameters, are altered in the ischemic group and boosted after DEP exposure, while lysis parameters showed differences only after ischemia in the DEP exposed mice Data represented as mean±SD or median (IQR). ns: not significant. * $p < 0.05$, ** $p < 0.01$, *** $p < 0.001$. naïve-PBS (n= 7), SRM1650b (n= 9) and MCAO- PBS (n= 5), SRM1650b (n= 6).

DEP exacerbate the thrombogenic characteristics of plasma samples from ischemic patients.

To validate whether the observed pro-thrombogenic response in plasma from ischemic mice is exacerbated with the previous exposure to DEP material in human samples, the turbidimetric assay was conducted in human plasma from stroke subjects and matching controls, but exposed exogenously to SRM2975 (0.1 µg/ml) as represented in **Fig. 45A**.

The population consisted of 32 subjects, recruited at Vall d'Hebron Hospital, below 70 years of age and divided into first-ever ischemic stroke cohort who underwent intensive rehabilitation therapy in our hospital (IS, n=15) and a matching healthy-control cohort (Co, n=17). All data regarding demographic characteristics, vascular risk factors and medication in use is shown in **Table 2**. The plasma samples from the IS patients were extracted, on average, the day 12 after the event (**Table 2**) and although efforts were made to have both groups balanced, control subjects were older than strokes (64.1 ± 4.1 vs. 52.6 ± 5.2 years old, $p=0.001$), tended to be more obese (64.7% vs. 28.6% , $p=0.07$) and consume more alcohol (52.9% vs. 20% $p=0.07$) (**Table 2**).



	 Control n=17	 Ischemic n=15	p-value
DEMOGRAPHICS			
Sex (f)	47.1% (8)	20% (3)	0.14
Age (years \pm SD)	64.1 \pm 4.1	52.6 \pm 5.2	0.001
Sample taken (days \pm SD)		12.4 \pm 3	
VASCULAR RISK FACTORS			
Alcohol (yes)	52.9% (9)	20% (3)	0.07
Active smoker (yes)	17.6% (3)	40% (6)	0.24
Physical activ (yes)	82.4% (14)	53.8% (7)	0.12
Obesity (yes)	64.7% (11)	28.6 (4)	0.07
Auricular Fibrillation (yes)	0%	13.3% (2)	0.21
Hypertension (yes)	88.2% (15)	60% (9)	0.10
Dyslipemia (yes)	70.6% (12)	40% (6)	0.15
Diabetes (yes)	23.5% (4)	14.3% (2)	0.66
MEDICATION USE			
Antiaggregant (yes)	29.4% (5)	46.7% (7)	0.46
Anticoagulant (yes)	0%	0%	
Statins (yes)	41.2% (7)	73.3% (11)	0.08
Antihypertensive (yes)	82.4% (14)	60% (9)	0.24
Insulin (yes)	17.6% (3)	20% (3)	0.60

Table 2: Principal characteristics of selected control and ischemic stroke patients.

Values are expressed as mean \pm SD or as percentage (%).

The analysis of the turbidimetric variables concerning the clot formation, showed pro-thrombogenic features in the same sense as previously described in mice plasma (**Fig. 45B, Fig. 44B and 43B**). Here, plasma samples from strokes exposed to DEP presented reduced lagtime than control non-exposed plasmas [10.5 (7.6-12.8) vs. **16.2** (10.2-23.7) mins, $p=0.07$], and increased speed and density compared to control non-exposed plasmas [CRc: **31.7** (23.1-39.5 vs. **40.5** (33.4-59.7)) OD/sec, $p=0.02$; MaxAbs: **0.18** (0.14-0.26) vs. **0.14** (0.1-0.19) OD, $p=0.04$].

Again, involving DEP in exacerbating plasma thrombogenic features in the context of ischemia.

Regarding the lysis parameters, no significant changes were observed in stroke and control plasma exposed to DEP (data not shown).

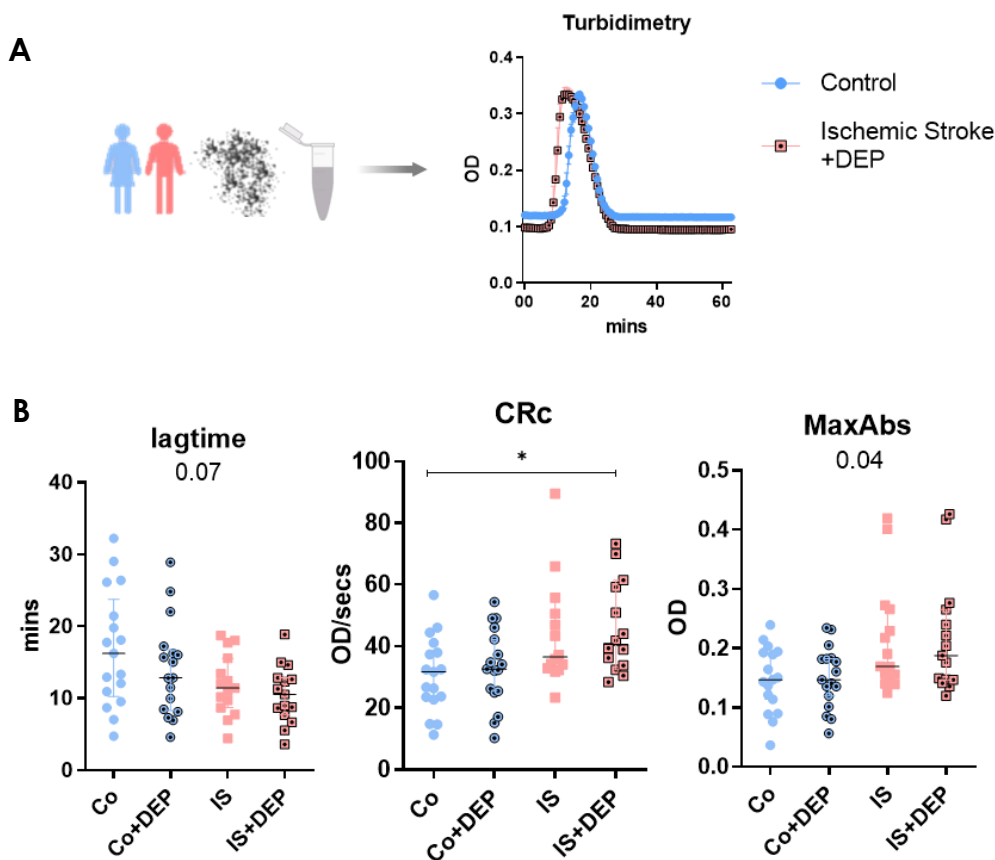


Figure 45: Turbidimetric assay in plasmas of control and ischemic stroke patients.

A: Experimental design overview and representative turbidimetric curves. **B:** Reduced Latency times (lagtime), increased Clot formation rates (CRc) and Maximum Absorbances were observed in clots of IS patients whose plasma was exposed to DEP during the assay. This difference turned significant in Clot formation rate when compared non-exposed plasma from Controls. Data represented as median (IQR). ns: not significant. * $p < 0.05$. Co: Control, IS: ischemic stroke.

Overall, our studies in mice and human plasma both showed that in the context of cerebral ischemia, faster and denser clots might be formed in the presence of DEP suggesting a more pro-thrombogenic profile in highly polluted environments.

Prolonged inhalation of PM_{2.5} in hypertense subjects alters the t-PA mediated thrombolysis profile, ex-vivo.

Finally, we aimed at studying the clot formation & lysis characteristics of humans' plasma exposed to different levels of particulate matter depending on their place of residence, which was geocoded. With this information, we established two study groups: a **low PM-exposure** group in which the annual mean exposure to PM_{2.5} was estimated to be around 11 µg/m³ (below the recommended European guidelines of PM_{2.5} annual exposure of <25 µg/m³) and a **high PM-exposure** group whose mean exposure was around 26 µg/m³ (that exceeded the yearly average European limit of 25 µg/m³), see **Table 3**. Moreover, all individuals were hypertense (Arterial systolic pressure >120 mm Hg) and they did not present a medical history of stroke or dementia. Relevant risk factors and medication are exposed in the table below (**Table 3**) where it can also be seen that low- and high-exposure groups matched in age and sex as well as in cardiovascular risk factors and medication use, but differed significantly in the PM_{2.5} and PM₁₀ mean annual exposure according to the place of residence. Plasmas were obtained between November 2010 and May 2012.



	 Low exposure (n=14)	 High exposure (n= 17)	p-value	
CHARACTERIZATION				
PM _{2.5} Annual mean 2013 (µg/m ³) ± SD	10.9 ± 0.1	25.7 ± 0.9	0.001	
PM ₁₀ Annual mean 2013 (µg/m ³) ± SD	30.1 ± 0.6	37.8 ± 2.7	0.001	
DEMOGRAPHICS				
Age (years ± SD)	60.1 ± 5.8	61.0 ± 4.9	0.66	
Sex (F)	64.3% (9)	47.1% (8)	0.47	
Arterial Systolic Preasure (mean±SD)	142.1±9.2	140.6 ± 7.7	0.79	
Education	No studies	14.3% (2)	0.81	
	Primary uncompleted	21.4% (3)		
	Primary completed	21.4% (3)		
	Secondary completed	22.2% (2)		
	University	7.1 % (1)		
VASCULAR RISK FACTORS				
Dyslipemia	Hypercholesterolemia	64.3% (9)	0.60	
	Hypertriglyceridemia	0% (0)		
	Mixed	7.1% (1)		
	Unknown	7.1% (1)		
Ischemic cardiopathy (yes)		0%	17.64% (3)	0.09
Diabetes type II (yes)		28.6% (4)	41.2% (7)	0.70
Alcohol consumption (yes)		64.32% (9)	47.1% (8)	0.47
Active smoker		21.4% (3)	17.6% (3)	0.13
Obesity (yes)		50% (7)	70.6 (12)	0.24
MEDICATION USE				
Antiaggregant (yes)		0%	17.6% (3)	0.22
Antihypertensive (yes)		100% (14)	88.2% (15)	0.48
Statins (yes)		35.7% (5)	53.3% (8)	0.46
Treatment adherence		50% (7)	58.8% (10)	0.72

Table 3: Principal characteristics of selected individuals living in high and low polluted areas. Values are expressed as mean±SD or as percentage (%).

In this context, the turbidimetric assay was performed (**Fig. 46A**) but no differences in the clot formation variables were observed between high- and low-exposure groups (data not shown). On the contrary, lysis parameters were significantly shortened in the highly exposed compared to the lower exposed group (Clot time: **25.9 ± 6.9** vs. **30.5 ± 4.6**, $p=0.04$; Lysis time: **22.6 ± 4** vs. **18.6 ± 4.9** mins, $p=0.02$; Lys 50t_{Max}: **11.3 ± 2** vs. **9.3 ± 2.4** mins, $p=0.02$) (**Fig. 46B**), indicating

that clots of individuals living in areas of high concentrations of $PM_{2.5}$ were lysed significantly faster than those living in less polluted regions.

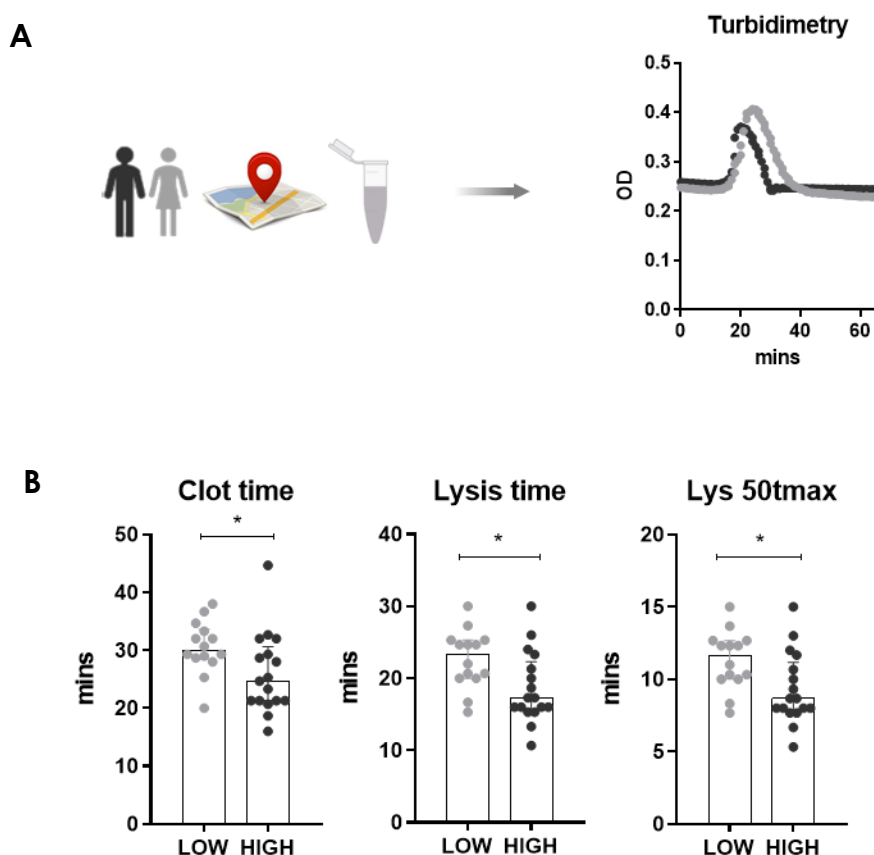


Figure 46: Lysis of the clot is faster in the highly $PM_{2.5}$ exposed group. A: Experimental design overview and representative turbidimetric curves. **B:** Graph bars displaying reduced clot time, lysis time and Lysis 50 t_{max} in the highly exposed group compared to the lower-exposed one. Data represented as median (IQR). ns: not significant. * $p < 0.05$.

Summary: alterations in plasma thrombogenesis and thrombolysis

Subsequently, DEP increase the plasma thrombogenicity in mice and humans (**Fig. 43B**, **Fig. 44B** and **Fig. 45B**). Chronic exposures can enhance clot fibrinolysis in ischemic mice (**Fig. 44B**) and in plasmas from hypertensive subjects exposed to high particulate matter concentrations for long periods of time (**Fig. 46B**).

Discussion

Exposure to **air pollution**, and more specifically the particulate matter fraction, has become a risk factor which should be controlled for preserving human health. In a very recent study, it was demonstrated that even PM-exposures within the established safety limits were associated with a 13% increase in natural deaths (Strak et al., 2021), positioning air pollution in the spotlight and a public health priority. In 2019, around 99% of the Earth's inhabitants were living in areas where the air quality did not meet the safety standards and were consequently exposed to this risk factor which impacts health (United Nations Department of Economic and Social Affairs Population, 2018). Furthermore, since 1993 growing evidence links the inhalation of particulate matter to cardiovascular diseases (Dockery et al., 1993) which nowadays have become the major cause of death globally according to the WHO. Among cardiovascular diseases, **stroke** is the second leading cause of death and both short- and long-term exposures to the outdoor particulate matter have been associated with higher stroke incidence and mortality (Shin et al., 2014; Wilker et al., 2013).

Although increasing evidence supports these associations, the mechanisms underlying the pathological actions induced by the DEP in the context of stroke are currently being investigated. The work of this thesis develops under this framework.

5.1. The selected dose does not directly affect the animal's wellbeing.

The dose of DEP (150 µg) that the mice received in this study, was calculated on the basis that a single dose of 50 µg is a moderate dose comparable to human's particle inhalation in one day (Linderholm et al., 2015; Martins et al., 2015). Additionally, we wanted to determine the detrimental effects of inhaling high concentrations of diesel exhaust mimicking a highly polluted city (60 µg/m³), assuming a mouse's ventilating capacity of 0.06 m³/day accumulated through its life expectancy (around 1.5 years) (Pöss et al., 2013).

Bodyweight was registered during the whole instillation process as an indicator of general wellbeing and no effect of the instillation was observed during the 3

weeks follow-up. After the surgery of cerebral ischemia, all animals lost around 3% of their baseline weight which is considered normal and within accepted welfare guidelines, since only a weight loss over 10% is considered alarming and requires food and liquid supplementation (Percie Du Sert *et al.*, 2017). The grip test was performed pre- and post-surgery to evaluate stroke severity and motor function. In the distal pMCAo model the affected brain region is the primary motor and sensory cortex (Llovera *et al.*, 2014), but since we did not find differences regarding infarct size between exposed and non-exposed animals, we did not expect differences in the grip test results. However, a tendency to perform worse in mice acutely exposed to SRM1650b has been observed, as well as a better performance of the chronically exposed mice to SRM2975 versus control mice. Since the brain infarct was similar among groups and the exposure to the two types of particles showed opposite results in the grip test performance, it is difficult to attribute these observations to the DEP exposure, although more studies increasing the number of animals and modeling stroke with other surgical approaches would be needed to conclude on the infarct size and neurological deficits outcome after DEP exposure, especially in aged mice or in those presenting comorbid conditions such as diabetes, hypertension or dyslipidemia, among others.

5.2. PBS instillation does not alter MMPs in the lungs, but it decreases MMP levels in the brain.

Firstly, in the *in vivo* experiments we observed significant differences in MMP levels between 3 days and 3 weeks in the brains of PBS-instilled naïve mice: as the number of instillation days increased all investigated MMPs decreased in the OB, and in the HC, ST and CX a similar tendency was observed. Moreover, we did not observe any PBS instillation effect in the lungs.

To instill the particles, they were suspended in a vehicle solution. In an article examining the effect of different vehicles in rats' lungs after *intratracheal* instillation, the authors concluded that instillation with saline or PBS elicited a mild response when compared with untreated animals, regarding inflammatory cell counts in Bronchoalveolar Lavage Fluid (BALF) (Numano *et al.*, 2020). In our

setting, PBS solution was **intranasally instilled** in the mice, which has been demonstrated as a successful pathway to distribute particles to both the respiratory system and nervous system (Chung *et al.*, 2020; Erdő *et al.*, 2018; Newman *et al.*, 2020). Moreover, this administration route was selected since it mimics a real-life situation has been reported to distribute around 25% of the instilled preparation into the lungs compared to a 95% in intratracheal instillation (Linderholm *et al.*, 2015; Wu *et al.*, 2020).

In another study, comparing intranasal with intratracheal instillations of PBS the authors did not observe differences in the total cell or neutrophil counts in mice's BALF (Linderholm *et al.*, 2015) arguing that the PBS did not evoke an inflammatory response in lungs along with what we observed regarding the MMP response in this organ and proving that PBS did not develop an inflammatory response in lungs. Other articles have examined the effects of intranasal PM instillation in the expression of inflammatory cytokines (TNF α , IL-1 β or IL-6) in the brain (Campbell *et al.*, 2005; Fonken *et al.*, 2011; Win-Shwe *et al.*, 2012, 2006), but none has reported an effect in the brain of the control animals not even when instilling MiliQ water for different time periods (Wang *et al.*, 2008), which can cause a stronger inflammatory response than PBS or saline in lung cells (Numano *et al.*, 2020).

Our results are in line with these previous observations in the lungs' response to PBS instillations but indicate that at the brain level there might be some inflammatory acute and transient response caused by the administration procedure especially in the olfactory bulb which is in close contact with the nasal cavity (Newman *et al.*, 2020; Oberdörster *et al.*, 2004).

5.3. In brains of naïve mice, chronic exposure to SRM1650b/DEP increases the MMP inflammatory response.

The effects of particles' inhalation in the brain has been studied under different conditions by different authors: with different types of particulate matter, exposure times, species and targeting different inflammatory markers (Fonken *et al.*, 2011; Gerlofs-Nijland *et al.*, 2010; Suwannasual *et al.*, 2018; Win-Shwe *et al.*, 2006). In general, the main molecules that have been studied are well-known

inflammatory cytokines such as TNF α , IL-1 β , IL-6 or molecules related to the oxidative stress such as the superoxide dismutase (SOD-2). To my knowledge this is the first time that matrix metalloproteinases have been studied in the lungs and brain after DEP instillation in the context of cerebral ischemia. These MMPs are key proteases involved in the progression of ischemic stroke (Palm *et al.*, 2018; Rosell *et al.*, 2006; Yang and Rosenberg, 2015), both in injury and repair, becoming interesting molecules to monitor after DEP exposure in naïve brains (before the cerebral ischemia).

Briefly, the described results showed that after acute exposure (3 days) to SRM1650b, there were lower levels of the 3 examined MMPs in all studied brain areas (OB, HC, ST and CX) but after a longer exposure (3 weeks) their levels increased in both the HC and CX and no changes were observed in the lungs at any time point.

In the **acute phase**, the presence of the SRM1650b-particles could be enhancing the effect of the instillation, as we have seen that instillation only, can cause a decrease in brain MMP levels.

Other authors have shown that after a single instillation of DEP (50 μ g), no difference in the mRNA expression of TNF α and IL-1 β was found in the OB or the HC of BALB/c mice compared to control animals at 24 hours after the exposure (Win-Shwe *et al.*, 2012). Suggesting that short exposures might not trigger an inflammatory response in the brain. However, if the exposure increased for several days, (once a week for 4 consecutive weeks) in another setting instilling BALB/c mice with 14 and 95 nm carbon black particles (125 μ g), the authors reported higher mRNA expression levels in the OB compared to HC, in line to our results for the MMPs. But no differences of IL-1 β , TNF α and some chemokines (CCL-2, CCL-3) compared with the vehicle-treated group neither in the OB nor in the HC were observed (Win-Shwe *et al.*, 2006). Moreover, Bos and colleagues placed mice in a roadside tunnel for 5 days and observed a downregulation of the IL-1 α , COX-2 and IL-6 genes in the OB while in HC COX-2 was increased compared to the control groups (Bos *et al.*, 2012).

From all these studies, we can conclude that i) the brain region that expressed more inflammatory markers was the OB and ii) that after acute exposures the presence of particles might not trigger a cytokine-inflammatory response or could alter it differently depending on the targeted brain area, the composition of the particles or the period of exposure. Particularly in our study, after 3 days of exposure, the MMPs were decreased in all studied brain regions, although the **HC appeared more sensitive** as the 3 MMPs were decreased. This hypothesis is supported by other studies showing that a prolonged exposure to PM_{2.5} for 28 consecutive days inhibited the maturation process of immature neurons and diminished their dendritic complexity in the subgranular zone without an impact on the number of neural stem cells or the rates of differentiation between the two exposed groups (Cheng *et al.*, 2017). Also, another study associated long-term exposures (114 µg/m³, 5 h/day, 5 days/week for 3 months) to diesel exhaust secondary organic aerosols with worse memory function, also based in an altered expression of the NMDA receptor subunits, essential in processes of learning and memory function in the hippocampus (Win-Shwe *et al.*, 2014).

Curiously, only the intranasal instillations with the SRM1650b induced some MMP responses in the brain, but the physical analyses (light scattering, DLS, Cryo-TEM) of both types of particles SRM2975 and SRM1650b, did not show significant differences regarding the PM fractions nor in the size of the particle, so we cannot assume that the variations in brain MMP content were due to the size of the particles in each suspension, however, the components may be different since they were originated from different engines (Annex II, pag. 199 and Annex III, pag. 213).

Our observations that brain MMP-3 increased in the HC and MMP-8 and -9 in the CX after **longer exposure** times to DEP (3 weeks), matches with the inflammatory brain response described by other authors. In this regard, brains of rats that inhaled diesel engine exhaust chronically (6 hours/day, 5 days/week for 4 weeks) showed reduced protein levels of TNFα in the OB but increased TNFα and IL-1α in ST compared to control animals. However, in this study, the mRNA levels or transcription factors were not affected (Gerlofs-Nijland *et al.*, 2010). After chronic

exposure, the same study continues to see a differential response regarding the studied brain area, and they suggested that the increase in brain pro-inflammatory cytokines was mediated by a systemic response since the preceding processes (mRNA expression) were not altered in the brain tissue. Another study in BALB/c mice that inhaled DEP chronically (5 hours/day, 5 days/week) for 4 weeks or 8 weeks, did not observe a response in the OB, but TNF α was increased after 4 weeks in the ST and CX compared to control mice and after 8 weeks it increased in the ST, CX and cerebellum together with SOD-2 in ST and CX (Kim *et al.*, 2018). These articles, both point to a consistent activation of antioxidant and pro-inflammatory mechanisms in several brain regions after several weeks of DEP exposure.

Other studies investigated the effect of months of DEP exposure. In this regard, in rats that inhaled DEP for 6 months (35, 100 or 992 $\mu\text{g}/\text{m}^3$ daily) it was found that TNF α was already increased in the midbrain in the 100 $\mu\text{g}/\text{m}^3$ vs. control. In the OB, frontal and temporal lobes only the highest dose of 992 $\mu\text{g}/\text{m}^3$ showed increased TNF α . This differential sensitivity of the midbrain was not extended to other tested cytokines such as IL-1 β , IL-6 or MIP-1 α (Levesque *et al.*, 2011). Also, in mice that received concentrated PM_{2.5} for 11 months, (94.38 $\mu\text{g}/\text{m}^3$ / 6 hours/day, 5 days/week), the hippocampal pro-inflammatory cytokine expression of TNF α and IL-1 β was increased (Fonken *et al.*, 2011). Therefore, the pro-inflammatory activity in the brain is maintained if the exposure extends for months.

Regarding MMPs, two recent articles explored the effects of DEP on brain MMPs. The first one aimed to elucidate whether a high-fat diet could exacerbate brain damage generated by traffic pollutants. Accordingly, the authors exposed C57BL/6 mice to mixed vehicle emissions (6 h/day, 7 d/w) for 30 days and found no differences in the cerebral microvessels' MMP-9 expression between low-fat + filtered air vs. low-fat + mixed vehicle emissions (similar conditions to our experiment), but the MMP-9 protein activity was increased in the exposed group compared to the low-fat + filtered air (Suwannasual *et al.*, 2018). This study also reported that the high-fat diet + the mixed exposure resulted in altered microvascular integrity. The other study that exposed BALB/c mice (100 $\mu\text{g}/\text{m}^3$, 5

h/d, 5 d/w) for 4 weeks or 8 weeks, found that MMP-9 was increased in the CX and OB vs. control group at both time points and MMP-14 only in the OB and the CX after 8 weeks (Kim *et al.*, 2019).

It appears that after chronic exposure to particulate matter pollutants there is an activation of the antioxidant mechanisms in the brain (Kim *et al.*, 2018), an increase in the pro-inflammatory cytokines (Fonken *et al.*, 2011; Gerlofs-Nijland *et al.*, 2010; Kim *et al.*, 2019) as well as increased matrix metalloproteinases levels.

5.4. DEP exposure impairs neurogenesis.

As mentioned in the thesis, MMPs are essential for tissue architecture and homeostasis. They participate in repair mechanisms after stroke: neurogenesis, cell migration or angiogenesis (Nih *et al.*, 2018; Stamenkovic, 2003). Since we have seen they were altered by the DEP exposure, we further we investigated the proliferative neurogenic brain niches (the SVZ and the SGZ).

Following **acute** exposure to DEP, we found a significant decrease in proliferating cells of the rostral migratory stream. In this line, in an experiment where mice were exposed only to 6h of diesel exhaust and proliferation was assessed in the SGZ and SVZ, it was observed a reduction of ki-67 and neurogenesis in both areas, proposing that the reduced proliferation was secondary to an initial inflammatory response in hand with an activation of the microglia (Coburn *et al.*, 2018). Our present results show that sustained exposure to DEP (3 days) still affects the SVZ-RMS cells under proliferation, unfortunately, we could not correlate it with increased microglia. However, the RMS is limited dorsally by the CX and ventrally by the ST, where lower levels of MMPs were identified and thus the proliferation and migration processes could be negatively influenced (since MMPs participate in neurogenesis).

Furthermore, this thesis proves that if the DEP exposure lasted up to **3 weeks** the number of neural progenitor cells of the RMS was reduced compared to the PBS-instilled animals. Which could be a consequence of the reduced proliferation in the short-time exposure, as explained above. Not only the neural progenitor cells were reduced at 3 weeks post-DEP exposure, since we also observed reduced

amounts of cortical neurons, a region that also displayed higher MMP-8 and -9 in chronic exposures.

Moreover, the present ***in vitro*** experiments in NSC derived from the SVZ exposed to DEP, further demonstrated that high concentrations of particles could reduce their viability which could explain the reduced proliferation observed in the RMS *in vivo*. The hypothesis is that DEP exposure would compromise the mitochondrial activity of NSC of the SVZ niche which in turn would affect their proliferation capacity observed in the reduced viable cells *in vitro* and the reduced proliferative progenitors *in vivo*, finally leading to reduced numbers of migrating neural progenitors, observed in the *in vivo* results after the chronic DEP exposure.

Other *in vitro* experiments exposing different types of stem/progenitor cells to diesel particles showed similar effects on cell viability: in human EPC cultures, DEP reduced their migratory capacity, increased the ROS and increased apoptosis (Pöss *et al.*, 2013). In mouse gastric stem cells exposed to DEP, their metabolic activity was reduced as well, but no significant effects were detected on cell migration, oxidative stress markers or cell death proteins (Al-Sadik *et al.*, 2020). All of which implies that the progenitor cells are highly sensitive to the presence of DEP and that they could experience alterations in their viability resulting in cell death or impaired function.

The processes taking place in the brains of naïve mice are represented in **Figure 47**. Acute exposure to DEP reduced the number of proliferative cells in the RMS and MMPs in OB, HC, ST and CX. This reduction in stem cells could lead to reduced neural progenitor cells at the end of 3 weeks. Furthermore, the chronic exposure did increase MMPs in HC and CX which relates to the cytokine inflammatory response widely studied by others (Bos *et al.*, 2012; Win-Shwe *et al.*, 2006). This increase could partially have an impact on the cortical neurons' population since the cortex is the brain area where MMPs were consistently increased.

At this point, a limitation of our design is that we did not identify the cells producing the MMPs and thus we cannot state the directionality of these mechanisms.

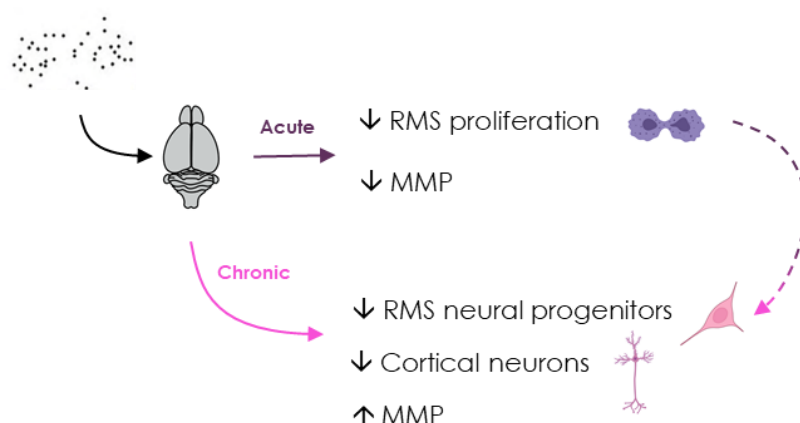


Figure 47: Summary of the observed molecular and cellular alterations in the brain of naïve mice. Acute exposure could compromise the viability of RMS proliferating cells and reduce the MMP content in OB, HC, ST and CX. While after chronic exposure, the neural progenitor cells were reduced in the RMS as well as the cortical neurons. Both processes appeared with an elevation in MMPs in HC and CX.

5.5. Pre-exposure to DEP does not modify the **infarct** lesion and has no impact on the ischemia-induced MMP increase in the ischemic hemisphere.

Mice subjected to cerebral ischemia presented a robust MMP increase in the ipsilateral tissues (except for the OB) as described by several authors both in rodent and human tissues (Cuadrado *et al.*, 2009; Rosell *et al.*, 2006; Zinnhardt *et al.*, 2015). Our results indicate that there is a fast (24h) and consistent inflammatory response to ischemia in both infarct (CX) and peri-infarct (HC, ST) areas. Unexpectedly, there was no further increase in brain MMPs after DEP intranasal instillation pre-ischemia regardless of the exposure time, and infarct lesion exacerbation was not observed either. The explanation here could be that the massive damaging increase in ischemia-induced MMPs is much superior to the increases observed after the chronic DEP exposure. For example, MMP-8

presented a 2-fold increase after DEP exposure in the CX vs. PBS-vehicle, whereas the ischemic insult increases this MMP-8 by 76-fold in the same brain area.

To date, only one article has described the effect of particulate matter in an *in vivo* model of ischemic stroke where mice received 343 µg/m³ nanoPM obtained from Los Angeles ambient for 5 hours/day, 3 days/week for 3 consecutive weeks. Twenty-four hours after the last exposure mice underwent transient proximal MCAo and 24 hours later brains presented increased infarct volume, higher granulocyte cell counts and more complement C5 in the ischemic core compared to the animals exposed to filtered air (Liu *et al.*, 2016). The authors suggested that the inhalation of PM had an impact on the size and magnitude of the induced stroke.

However, our results show that infarct extension was not influenced by the DEP exposure after studying two types of SRM-DEP pollutants and at two different timepoints post-ischemia (24h and 48h). However, we make use of a different ischemia model: permanent vs. transient and distal vs. proximal occlusion, respectively. Moreover, the observed increase in cortical brain MMPs, after 3 weeks DEP exposure in naïve mice, has not been a key factor to worsen the outcome in the short term after cortical cerebral ischemia.

The reasons for these findings could be in part because the inflammatory MMP response to DEP exposure was too mild to finally influence brain ischemia compared to the massive MMP increase acutely produced by the ischemic event. Another possible explanation could be the different models used to induce cerebral ischemia, Liu and colleagues used the transient MCAo where there is secondary damage after the arterial reperfusion with increased ROS and inflammatory cytokines (Candelario-Jalil, 2009; Liu *et al.*, 2016), which perhaps the effect of the previous DEP exposure has an additive effect on, that we did not observe with the permanent MCAo model. Or it could be a matter of the different DEP concentrations or type of PM used in both studies.

5.6. Chronic exposure to diesel exhaust particles can have detrimental consequences in lung inflammatory response after cerebral ischemia.

The lungs are constantly exposed to ambient toxic molecules and pathogens, being considered one of the main entrances of exogenous substances into the organism, which is why pulmonary mechanisms to identify these molecules/organisms and defend against them are essential for survival. The defense mechanisms involve coordination from multiple cell types.

Briefly, **alveolar macrophages** and **epithelial cells** (type I and II pneumocytes) that are in the alveolar epithelium are the first cells encountered by the exogenous substances. Second in line are the cells residing within the parenchyma, these are inflammatory cells like: **dendritic cells** which process antigens and present them to T cells in lymph nodes inducing then an immune response. **Interstitial macrophages** which phagocyte substances reaching the interstitium, and a small proportion of **resident monocytes**. Both types of macrophages secrete chemokines and cytokines promoting local inflammation (Fig. 48)

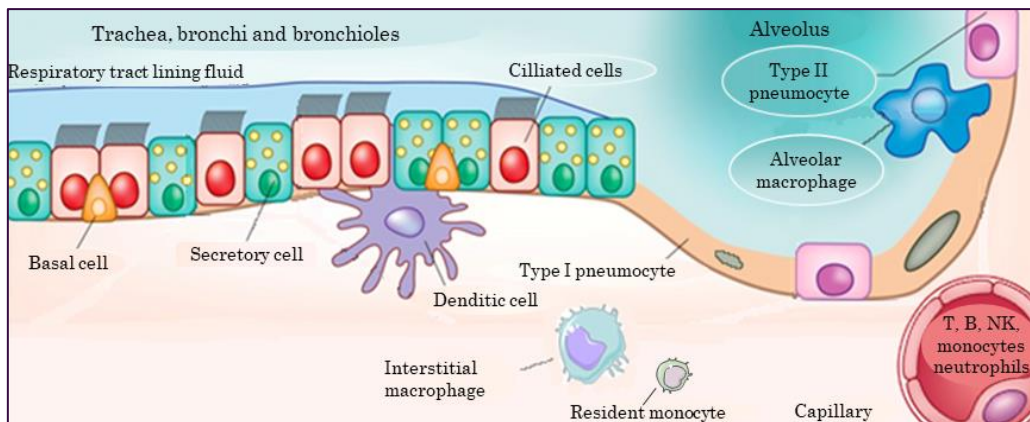


Figure 48: Representation of lung citoarchitecture. Adapted from Leiva-Juárez et al. 2018.

Neutrophils are the first circulatory cells to be recruited to the site of injury where they can kill phagocytosed pathogens with degradative enzymes. **Eosinophils**, on

the other hand, are associated with parasite infections or allergic diseases. **B** and **T Lymphocytes** that reside in the lymph nodes throughout the airways and lung parenchyma, can be activated by dendritic cells and through the circulatory system arrive at the injured site. **B cells** synthesize immunoglobulins and are focused on developing a humoral response while **T cells** and **NK cells** (a subtype of T cell with no specific antigen receptors) promote a cellular immune response (Gangwar *et al.*, 2020; Moldoveanu *et al.*, 2009).

If the lungs are injured, the microdamage activates alveolar macrophages and epithelial cells to secrete a wide variety of inflammatory molecules, including MMPs which are essential in responses to any acute lung injury as well as in lung organogenesis (Hendrix and Kheradmand, 2017). In this line, we hypothesized that 3-days or 3-weeks exposure to DEP would increase the amount of MMPs in **naïve** mice's lungs. However, our results indicate that MMPs were similar in DEP exposed compared to vehicle-exposed animals at both time points.

These findings could be the result of a fast inflammatory response right after the first dose with a posterior adaptation to the stimulus. In this regard, similar studies that found increases in lung inflammatory markers, analyzed the effect of diesel particles after a single administration: Oberdörster and colleagues, exposed rats to ultrafine particles (20 nm) or vehicle and observed greater amounts of Polymorphonuclear Cells (PMN) in BALF of particle-exposed animals 24 hours after the exposure. In the same article, they observed that higher doses of particles did not correlate with the inflammatory cell influx, since from 65 to 650 µg they observed increasing amounts of PMN in BALF, however, the highest administered dose (1000 µg) led to an opposite and significant reduction of the PMN response (Oberdörster *et al.*, 1992). Another group observed an increase in MMP-1 in lungs of mice exposed once to 50 µg of DEP (Amara *et al.*, 2007), but another study that instilled mice with 100 µg of DEP, did not observe modifications of mRNA expression of MMP-2, -9 or -12, neither at 8 or 24 hours after instillation although particles obtained from a different source (RER-train stations of Paris) did show this increase only after 8 hours post-exposure (Bachoual *et al.*, 2007).

However, another study where the DEP exposure period was longer, increases in lung MMPs were found; in C57BL/6 male mice that received intratracheal instillations for 3 consecutive days (6.25 mg/kg/day = 140 µg/day) or saline, MMP-9 activity was increased 2 days after last exposure but normalized after 5 days (Lin *et al.*, 2018). Additionally, Wistar rats exposed to 750 µg/m³ of PM_{2.5} (4h/day, 5d/week) for 2 weeks displayed higher immunolabeling of MMP-9 in the lungs than control rats (Yang *et al.*, 2018). Therefore, in our study, either the chronic intranasal instillation of particles did not develop an inflammatory MMP response in the lungs, which has been observed with intratracheal instillation by others (Lin *et al.*, 2018), or the particles used to reproduce diesel exhaust PM pollution did not stimulate the MMP production in lungs, similar to what others have observed with the different types of administered particles, being the ones extracted from polluted ambient air more damaging (Bachoual *et al.*, 2007; Yang *et al.*, 2018).

Following **stroke**, an acute inflammatory response occurs both locally and systemically (Audebert *et al.*, 2004). In rodent models of stroke, lung changes have been reported such as damaged endothelial cells, enlarged basement membrane thickness, reduced alveolar macrophage phagocytosis as well as increased IL-6, TNFα and IL-1β mRNA expression (Austin *et al.*, 2019; Samary *et al.*, 2018).

In our model of acute/chronic exposure followed by ischemia, in the lungs the MMP levels of 3 weeks-SRM1650b-exposed animals did not increase as did the control group. Supporting the hypothesis that the SRM1650b particles are generating lung damage that we could not demonstrate in naïve animals through MMP content. But after ischemia, it was evidenced by lower MMP production and lower alveolar macrophages.

Based on the bibliography and our results, it is possible that during the instillation period, the MMP response got adapted (Lin *et al.*, 2018), but the particles continued to reach the alveoli, leading to an “overload” condition of the alveolar macrophages which would not phagocytose more PM (Oberdörster *et al.*, 1992; Zhou and Kobzik, 2007). At this point, their phagocytic activity would be compromised (Becker *et al.*, 2003) and the diesel particles would interact with

the scavenger receptor A which is an unspecific receptor in macrophages and its activation could lead to a reduction of pro-inflammatory cytokine production (Miyata and van Eeden, 2011) and even promote macrophage apoptosis (Chao *et al.*, 2001; Gangwar *et al.*, 2020). In this situation, a larger amount of particles would reach the interstitium having access to parenchymal cells and being able to reach the systemic circulation easier (Oberdörster *et al.*, 2002, 1992).

Under homeostatic conditions, alveolar macrophages are self-renewed whereas interstitial macrophages are maintained by circulating monocytes. Moreover, in a study where mice were exposed for 4-weeks to PM_{2.5}, it induced an influx of bone marrow-derived monocytes into lungs with no contribution to the lung alveolar-macrophages pool (Gangwar *et al.*, 2020; Schyns *et al.*, 2018). In the present thesis, during the 3-weeks exposure, the alveolar macrophages might collapse and die, which stimulates the influx of peripheral monocytes increasing the pools of interstitial macrophages. At this point, the MCA occlusion takes place and the systemic inflammation stimulates the alveolar macrophages (Hoyer *et al.*, 2019) which, among others, would liberate inflammatory MMPs in the lungs (Gibbs *et al.*, 1999), being the ischemic event responsible for the MMP release in lungs, but the chronically exposed mice would not be able to meet the PBS-ischemic response.

As a conclusion, based on our experimental results, 3 days or 3 weeks exposure to DEP did not cause an inflammatory MMP response in the lungs of naïve mice, perhaps because the MMPs are not the best molecular marker for lung inflammation at the studied time point for this type of air pollutant. However, the systemic inflammatory response caused by the cerebral ischemia cannot be achieved after 3-weeks instillation with DEP, which was accompanied by a reduction of alveolar macrophages and an increase of total monocytes and interstitial macrophages that aimed to replenish the shortage of alveolar macrophages caused by the previous DEP chronic instillation.

5.7. Acute and chronic particulate matter exposure alters the pro-thrombogenic plasma characteristics developed after ischemia, whereas chronic exposure could accelerate tPA-mediated thrombolysis.

Following stroke, dynamic changes to a pro-thrombotic stage take place in the patients' plasma. It has been described that plasma from acute ischemic stroke patients presented longer clot lysis times, they were more compact, showed increased fiber thickness and shorter lag time for fibrin formation compared to those of control individuals (Undas *et al.*, 2010). Also, TAFI (Thrombin Activatable Fibrinolysis Inhibitor) levels were significantly elevated in ischemic stroke patients (Santamaría *et al.*, 2003). Others have reported that tPA plasma activity is increased in the acute, convalescent and chronic stage while PAI activity was reduced in the acute stage and increased at the chronic stage of stroke compared to matched controls (Zhuang *et al.*, 2015).

In these studies, it is demonstrated that pro-coagulant and anti-fibrinolytic features are developed in the plasma of ischemic patients compared to the plasma from control subjects.

Other studies have focused on the effect of diesel particles in relation to hemostasia. For example, in men with previous myocardial infarction that were exposed to diesel and subjected to moderate exercise, they observed that DEP did not aggravate preexisting vasomotor dysfunction but did reduce the acute release of tPA, studied by intra-arterial agonist infusions (Mills *et al.*, 2007). The same group observed the suppression of the tPA activation, with the same methodology, in healthy volunteers exposed to diesel exhaust for 1 hour during intermittent exercise (Mills *et al.*, 2005).

Additionally, in healthy young adults whose plasma components were analyzed before, during and after the 2008 Olympics in Beijing (when the air pollution was restrained) soluble P-selectin (sP-selectin, a signaling molecule to leukocytes contributing to thrombosis) and Von-Willebrand Factor (vWF, a glycoprotein participating in platelets' aggregation) levels were normalized when compared

to pre-existing low-quality air pollution levels. Also, increases in air pollutant concentrations were significantly associated with increases in fibrinogen, vWF, sP-selectin and sCD40L concentrations (Rich *et al.*, 2012). However, others have reported that fibrinogen in healthy subjects, was not associated with air pollution increases (Thompson *et al.*, 2010).

The pro-thrombotic activity of the air pollutant particles in humans has been also suggested by exposures in *in vitro* and *in vivo* models: *in vitro*, blood clots significantly increased polymerization rates in the presence of PM (Metassan *et al.*, 2010). Another group added 0.5 µg/ml of DEP to hamsters' blood and saw platelet activation within 5 minutes, while *in vivo* instillation with DEP enhanced experimental arterial and venous platelet rich-thrombus formation, as early as 1 hour later (Nemmar *et al.*, 2003). In instilled mice with different types of particles, urban particulate matter enhanced arterial thrombosis but not venous thrombosis (DEP did not alter any). Both types of particles modestly increased factor VII, FVIII and fibrinogen, important elements of the coagulation cascade (Emmrechts *et al.*, 2010).

Our study aimed to identify possible interactions of DEP with the formation and lysis characteristics in a turbidimetric thrombus formation and lysis assay in the context of ischemic stroke. In subacute **ischemic patients** whose plasma was mixed with DEP, the clots were formed faster and were denser than in plasma from control subjects, exacerbating the pro-thrombotic characteristics observed for the stroke plasmas without DEP. In the same line, this thesis presents results with plasma from naïve and ischemic **mice** instilled with DEP or vehicle where both acute and chronic DEP exposures enhanced the thrombogenic condition of ischemic plasmas compared to naïve mice exposed to PBS (mimicking healthy control subjects non exposed to PM pollution). As found in ischemic patients, the plasma from ischemic mice exposed to DEP formed clots faster and denser than those formed by plasma from PBS-naïve mice. However, we did not observe differences within naïve animals that received the particles.

Interestingly, mice that received PBS-instillations for 3 weeks also presented longer lysis times after ischemia; their plasmas were more pro-thrombotic and less

fibrinolytic. One hypothesis is that this additional characteristic may be attributed to the different ages of the animals: 7 weeks (acutely-exposed) vs. 10 weeks (chronically-exposed).

In this regard, a study examining the effects of urban roadside PM exposure in young (10 weeks) and old mice (20 weeks), saw that the older mice presented higher baseline levels of Factor VIII, sP-selectin and vWF (pro-thrombogenic factors). After exposure, young mice presented an sP-selectin increase while the older animals increased their platelet numbers, vWF and sP-selectin to the highest values, sustaining an elevated thrombogenicity after the exposure to PM larger in the older group (Emmerechts *et al.*, 2012). Certainly, the age difference between the animals in this study is greater than the ones in our study (7 weeks vs. 10 weeks), but it could be a reason why the coagulation is enhanced and the lysis is delayed in the long exposure period, because aged animals present higher baseline pro-thrombotic parameters than younger ones.

In a last cohort of subjects, this thesis shows how plasmas from **hypertense individuals** living in high- polluted areas (above the European mean annual limit for PM_{2.5}: 25µg/m³), a significant acceleration in the clot lysis parameters is observed, pointing out that, individuals living in highly polluted areas could lyse the thrombus faster in the presence of tPA, considering that both cohorts were highly matched regarding demographic characteristics, vascular risk factors, or medication. This could explain differences in tPA thrombolysis responses among subjects and could be a factor to consider to adapt drug dosing.

Results from clot formation and lysis are all summarized in **Figure 49** showing that acute or chronic exposures to PM in naïve mice did not alter the hemostatic system which was imbalanced towards a more pro-thrombogenic condition after ischemia in both cases and further exacerbated with the DEP exposure. Also, fibrinolysis was additionally altered in ischemic mice chronically exposed to DEP. Similar pro-coagulant characteristics were observed in plasma from ischemic

patients which were also increased by the addition of DEP. And finally, the fibrinolysis profile was boosted in hypertense subjects living in high-polluted areas.

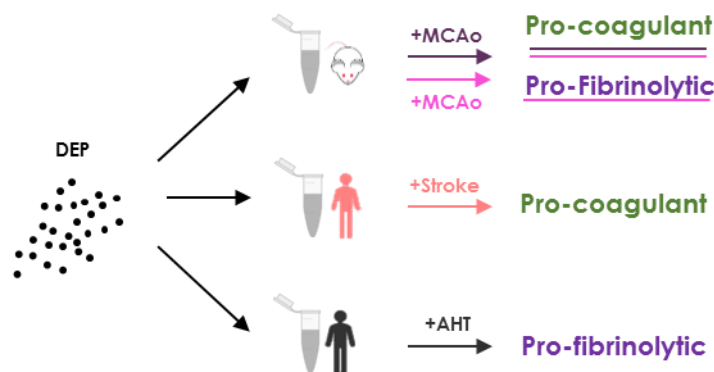


Figure 49: Summary of the observed alterations in the coagulation pathways of the plasma fraction. In mice acute and chronic exposure to particulate matter did not alter the coagulation pathways, however, ischemia preceded by DEP exposure did enhance the pro-coagulant and altered the fibrinolytic systems in mice. In humans DEP exacerbated the pro-coagulant characteristics displayed by the ischemia. Finally, hypertense individuals living in highly polluted areas displayed increased fibrinolytic characteristics. MCAo, Middle Cerebral Artery occlusion, AHT, Arterial Hypertension.

Importantly, after ischemia a procoagulant situation overrules and can be maintained until chronic stages (Santamaría *et al.*, 2003; Undas *et al.*, 2010; Zhuang *et al.*, 2015). Our results evidence that in plasmas of acute (mice) and subacute (patients) stroke subjects prothrombotic changes take place and that in healthy hypertensive subjects exposed to high PM_{2.5} levels (accumulating two risk factors) the fibrinolysis can be altered by accelerating the clot lysis.

Finally, it would be interesting to study the effect of living in high-polluted areas in the clot formation and lysis characteristics in plasmas from ischemic patients attending the emergency room, and to investigate the consequences of DEP enhanced thrombolysis in the context of stroke.

5.8. Limitations of the study and future perspectives

The presented MMP study is limited by the absence of two control groups which could add important information: sham-naïve mice following the same manipulation of the exposed animals but without instillation which could help to confirm the effect of the PBS instillations in the brain; and sham-ischemic mice following the same MCAo surgery procedures except for the arterial electrocoagulation which could help to better identify responses of the ischemic event and differentiate them from those induced by the surgical procedure (such as the changes in MMP levels in the OB). Also, this thesis presents findings associating MMPs dysregulation with changes in neuronal cell numbers or cell proliferation, but causality cannot be established. For this reason, it would be interesting to open new lines of research to identify the cells producing the MMPs to set the directionality of the proposed mechanisms in brain and lungs. Another open question is the impact of DEP exposure on the endogenous or induced-neurorepair mechanisms after cerebral ischemia. We have observed that before the ischemic event the NSC pools are diminished as well as cell proliferation in neurogenic areas due to the chronic DEP exposure, but the final impact on neurovascular remodeling needs to be further investigated.

Finally, the present work also warrants further studies aiming at investigating the effects of DEP/PM exposure in the polluted cities or in green areas related to stroke incidence and to tPA thrombolysis or endovascular thrombectomy treatments, related to recanalization/reperfusion success or the presence of hemorrhagic complications.

Conclusions

1. In **naïve** mice, acute exposure to diesel exhaust particles reduces MMP-3, -8 and -9 levels in all the studied **brain** areas (olfactory bulb, striatum, hippocampus and cortex). Whereas chronic instillation selectively increases them in the hippocampus (MMP-3) and cortex (MMP-8 and -9).
2. MMP levels in **lungs** are not altered by the instillation of diesel exhaust particles in naïve mice. However, the lung inflammatory response related to cerebral **ischemia** is altered by previous chronic instillation with DEP with decreased MMPs and alveolar macrophages but increased interstitial macrophages and monocytes.
3. **Neural populations** are affected by DEP exposures in **naïve** mice since both acute and chronic exposures reduce the progenitors in the rostral migratory stream of naïve mice and chronic exposure reduces the number of cortical neurons too.
4. **Brain** injury after cerebral **ischemia**, as well as motor function, are not aggravated by previous DEP exposure. In this regard, the massive increase in brain MMPs after ischemia is not exacerbated by the previous DEP exposure.
5. DEP exposure enhances **plasma** pro-coagulant characteristics developed by ischemic subjects whereas the tPA-induced clot lysis is accelerated in chronically-exposed ischemic mice and in hypertense subjects living in highly polluted areas.

Bibliography

- Abilleira, S., Montaner, J., Molina, C., Monasterio, J., Castillo, J., Alvarez-Sabín, J., 2003. Matrix metalloproteinase-9 concentration after spontaneous intracerebral hemorrhage. *J. Neurosurg.* 99, 65–70. <https://doi.org/10.3171/JNS.2003.99.1.0065>
- Adams, H., Bendixen, B., Kappelle, L., Biller, J., Love, B., Gordon, D., Marsh, E., 1993. Classification of subtype of acute ischemic stroke. Definitions for use in a multicenter clinical trial. *Stroke* 24, 35–41. <https://doi.org/10.1161/01.STR.24.1.35>
- Al-Sadik, H., Sugathan, S., Saseedharan, P., Sulaiman, S., Beegam, S., Nemmar, A., Attoub, S., Karam, S.M., 2020. Effects of Diesel Exhaust Particles on Mouse Gastric Stem Cells. *Life* 10, 1–17. <https://doi.org/10.3390/life10080149>
- Altman, J., Das, G.D., 1965. Autoradiographic and histological evidence of postnatal hippocampal neurogenesis in rats. *J. Comp. Neurol.* 124, 319–335. <https://doi.org/10.1002/cne.901240303>
- Amara, N., Bachoual, R., Desmard, M., Golda, S., Guichard, C., Lanone, S., Aubier, M., Ogier-Denis, E., Boczkowski, J., 2007. Diesel exhaust particles induce matrix metalloproteinase-1 in human lung epithelial cells via a NADP(H) oxidase/NOX4 redox-dependent mechanism. *Am J Physiol Lung Cell Mol Physiol* 293, 170–181. <https://doi.org/10.1152/ajplung.00445.2006>-Chronic
- Anderson, J.O., Thundiyil, J.G., Stolbach, A., 2012. Clearing the Air: A Review of the Effects of Particulate Matter Air Pollution on Human Health. *J. Med. Toxicol.* 8, 166–175. <https://doi.org/10.1007/s13181-011-0203-1>
- Angels Font, M., Arboix, A., Krupinski, J., 2010. Angiogenesis, Neurogenesis and Neuroplasticity in Ischemic Stroke. *Curr. Cardiol. Rev.* 6, 238–244. <https://doi.org/10.2174/157340310791658802>
- Anrather, J., Iadecola, C., 2016. Inflammation and Stroke: An Overview. *Neurotherapeutics* 13, 661–670. <https://doi.org/10.1007/s13311-016-0483-x>
- Arvidsson, A., Collin, T., Kirik, D., Kokaia, Z., Lindvall, O., 2002. Neuronal replacement from endogenous precursors in the adult brain after stroke.

- Nat. Med. 8, 963–970. <https://doi.org/10.1038/nm747>
- Astrup, J., Siesjö, B.K., Symon, L., 1981. Thresholds in Cerebral Ischemia-The Ischemic penumbra. *Stroke* 12, 723–72. <https://doi.org/10.1161/01.str.8.3.299>
- Audebert, H.J., Rott, M.M., Eck, T., Haberl, R.L., 2004. Systemic inflammatory response depends on initial stroke severity but is attenuated by successful thrombolysis. *Stroke* 35, 2128–2133. <https://doi.org/10.1161/01.STR.0000137607.61697.77>
- Austin, V., Ku, J.M., Miller, A.A., Vlahos, R., 2019. Ischaemic stroke in mice induces lung inflammation but not acute lung injury. *Sci. Rep.* 9, 1–10. <https://doi.org/10.1038/s41598-019-40392-1>
- Aver, J., Goyal, M., Bonafe, A., Diener, H., Levy, E., Pereira, V., Albers, G., Cognard, C., Cohen, D., W, H., O, J., TG, J., HP, M., RG, N., AH, S., DR, Y., BW, B., TG, D., DK, L., VK, R., R, du M. de R., OC, S., R, J., 2015. Stent-retriever thrombectomy after intravenous t-PA vs. t-PA alone in stroke. *N. Engl. J. Med.* 372, 2285–2295. <https://doi.org/10.1056/NEJMOA1415061>
- Bachoual, R., Boczkowski, J., Goven, D., Amara, N., Tabet, L., On, D., Leçon-Malas, V., Aubier, M., Lanone, S., 2007. Biological Effects of Particles from the Paris Subway System. *Chem. Res. Toxicol.* 20, 1426–1433. <https://doi.org/10.1021/tx700093j>
- Badimon, L., Vilahur, G., 2014. Thrombosis formation on atherosclerotic lesions and plaque rupture. *J. Intern. Med.* 276, 618–632. <https://doi.org/10.1111/JOIM.12296>
- Ballesteros, I., Cuartero, M.I., Moraga, A., Parra, J. de la, Lizasoain, I., Moro, M.Á., 2014. Stereological and Flow Cytometry Characterization of Leukocyte Subpopulations in Models of Transient or Permanent Cerebral Ischemia. *J. Vis. Exp.* 52031. <https://doi.org/10.3791/52031>
- Bañeras, J., Ferreira-González, I., Marsal, J.R., Barrabés, J.A., Ribera, A., Lidón, R.M., Domingo, E., Martí, G., García-Dorado, D., 2018. Short-term exposure to air pollutants increases the risk of ST elevation myocardial infarction and

- of infarct-related ventricular arrhythmias and mortality. *Int. J. Cardiol.* 250, 35–42. <https://doi.org/10.1016/j.ijcard.2017.10.004>
- Becker, S., Soukup, J.M., Sioutas, C., Cassee, F.R., 2003. Response of human alveolar macrophages to ultrafine, fine, and coarse urban air pollution particles. *Exp. Lung Res.* 29, 29–44. <https://doi.org/10.1080/01902140303762>
- Berkhemer, O.A., Fransen, P.S.S., Beumer, D., van den Berg, L.A., Lingsma, H.F., Yoo, A.J., Schonewille, W.J., Vos, J.A., Nederkoorn, P.J., Wermer, M.J.H., van Walderveen, M.A.A., Staals, J., Hofmeijer, J., van Oostayen, J.A., Lycklama à Nijeholt, G.J., Boiten, J., Brouwer, P.A., Emmer, B.J., de Bruijn, S.F., van Dijk, L.C., Kappelle, L.J., Lo, R.H., van Dijk, E.J., de Vries, J., de Kort, P.L.M., van Rooij, W.J.J., van den Berg, J.S.P., van Hasselt, B.A.A.M., Aerden, L.A.M., Dallinga, R.J., Visser, M.C., Bot, J.C.J., Vroomen, P.C., Eshghi, O., Schreuder, T.H.C.M.L., Heijboer, R.J.J., Keizer, K., Tielbeek, A. V., den Hertog, H.M., Gerrits, D.G., van den Berg-Vos, R.M., Karas, G.B., Steyerberg, E.W., Flach, H.Z., Marquering, H.A., Sprengers, M.E.S., Jenniskens, S.F.M., Beenen, L.F.M., van den Berg, R., Koudstaal, P.J., van Zwam, W.H., Roos, Y.B.W.E.M., van der Lugt, A., van Oostenbrugge, R.J., Majoie, C.B.L.M., Dippel, D.W.J., 2014. A Randomized Trial of Intraarterial Treatment for Acute Ischemic Stroke. *N. Engl. J. Med.* 372, 11–20. <https://doi.org/10.1056/NEJMOA1411587>
- Block, M.L., Calderon-Garcidueñas, L., 2009. Air pollution: mechanisms of neuroinflammation and CNS disease. *Trends Neurosci.* 32, 506–516. <https://doi.org/10.1016/j.tins.2009.05.009>.Air
- Boehme, A.K., Esenwa, C., Elkind, M.S.V., 2017. Stroke Risk Factors, Genetics, and Prevention. *Circ. Res.* 120, 472–495. <https://doi.org/10.1161/CIRCRESAHA.116.308398>
- Borsi, S.H., Khanjani, N., Nejad, H.Y., Riahi, A., Sekhavatpour, Z., Raji, H., Dastoorpoor, M., 2020. Air pollution and hospital admissions due to deep vein thrombosis (DVT) in Ahvaz, Iran. *Heliyon* 6, 1–8. <https://doi.org/10.1016/j.heliyon.2020.e04814>
- Bos, I., De Boever, P., Emmerechts, J., Buekers, J., Vanoirbeek, J., Meeusen, R., Van

- Poppel, M., Nemery, B., Nawrot, T., Panis, L.I., 2012. Changed gene expression in brains of mice exposed to traffic in a highway tunnel. *Inhal. Toxicol.* 24, 676–686. <https://doi.org/10.3109/08958378.2012.714004>
- Bosch, A., J.T., Rohm, T. V., Alasfoor, S., Dervos, T., Cavelti-Weder, C., 2018. Air Pollution–Induced Diabetes Is Mediated via the Gastrointestinal Tract. *Diabetes* 67, 2416–PUB. <https://doi.org/10.2337/DB18-2416-PUB>
- Brook, R.D., Rajagopalan, S., Pope, C.A., Brook, J.R., Bhatnagar, A., Diez-Roux, A. V., Holguin, F., Hong, Y., Luepker, R. V., Mittleman, M.A., Peters, A., Siscovick, D., Smith, S.C., Whitsel, L., Kaufman, J.D., 2010. Particulate matter air pollution and cardiovascular disease: An update to the scientific statement from the american heart association. *Circulation* 121, 2331–2378. <https://doi.org/10.1161/CIR.0b013e3181dbee1>
- Brouns, R., De Deyn, P.P., 2009. The complexity of neurobiological processes in acute ischemic stroke. *Clin. Neurol. Neurosurg.* 111, 483–495. <https://doi.org/10.1016/j.clineuro.2009.04.001>
- Budinger, G.R.S., McKell, J.L., Urich, D., Foiles, N., Weiss, I., Chiarella, S.E., Gonzalez, A., Soberanes, S., Ghio, A.J., Nigdelioglu, R., Mutlu, E.A., Radigan, K.A., Green, D., Kwaan, H.C., Mutlu, G.M., 2011. Particulate matter-induced lung inflammation increases systemic levels of PAI-1 and activates coagulation through distinct mechanisms. *PLoS One* 6, 1–9. <https://doi.org/10.1371/journal.pone.0018525>
- Buford, M.C., Hamilton, R.F., Jr, Holian, A., 2007. A comparison of dispersing media for various engineered carbon nanoparticles. *Part. Fibre Toxicol.* 4, 1–9. <https://doi.org/10.1186/1743-8977-4-6>
- Burnett, R.T., Arden Pope, C., Ezzati, M., Olives, C., Lim, S.S., Mehta, S., Shin, H.H., Singh, G., Hubbell, B., Brauer, M., Ross Anderson, H., Smith, K.R., Balme, J.R., Bruce, N.G., Kan, H., Laden, F., Prüss-Ustün, A., Turner, M.C., Gapstur, S.M., Diver, W.R., Cohen, A., 2014. An integrated risk function for estimating the global burden of disease attributable to ambient fine particulate matter exposure. *Environ. Health Perspect.* 122, 397–403.

<https://doi.org/10.1289/ehp.1307049>

- Buscemi, L., Price, M., Bezzi, P., Hirt, L., 2019. Spatio-temporal overview of neuroinflammation in an experimental mouse stroke model. *Sci. Rep.* 1–13. <https://doi.org/10.1038/s41598-018-36598-4>
- Cai, W., Liu, S., Hu, M., Huang, F., Zhu, Q., Qiu, W., Hu, X., Colello, J., Zheng, S.G., Lu, Z., 2020. Functional dynamics of neutrophils after ischemic stroke. *Transl. Stroke Res.* 11, 108–121. <https://doi.org/10.1007/S12975-019-00694-Y>
- Calderón-Garcidueñas, L., Azzarelli, B., Acuna, H., Garcia, R., Gambling, T., Osnaya, N., Monroy, S., Tizapantzi, M., Carson, J., Villarreal-Calderon, A., Rewcastle, B., 2002. Air Pollution and Brain Damage. *Toxicol. Pathol.* 30, 373–389.
- Calderón-Garcidueñas, L., Calderón-Garcidueñas, A., Torres-Jardón, R., Avila-Ramírez, J., Kulesza, R.J., Angiulli, A.D., 2014. Air pollution and your brain: what do you need to know right now. *Prim. Health Care Res. Dev.* 16, 329–345. <https://doi.org/10.1017/S146342361400036X>
- Calderón-garcidueñas, L., Franco-Lira, M., Henríquez-, C., Osnaya, N., González-maciel, A., Villarreal-calderon, R., Herritt, L., Brooks, D., Keefe, S., Palacios-moreno, J., Villarreal-calderon, R., Medina-cortina, H., Delgado-chávez, R., Maronpot, R.R., Doty, R.L., 2010. Olfactory dysfunction, olfactory bulb pathology and urban air pollution. *Exp. Toxicol. Pathol.* 62, 91–102. <https://doi.org/10.1016/j.etp.2009.02.117>.Olfactory
- Calderón-Garcidueñas, L., Mora-Tiscareño, A., Ontiveros, E., Gómez-Garza, G., Barragán-Mejía, G., Broadway, J., Chapman, S., Valencia-Salazar, G., Jewells, V., Maronpot, R., Henríquez-Roldán, C., Pérez-Guillé, B., Torres-Jardón, R., Herriř, L., Brooks, D., Osnaya-Brizuela, N., Monroy, M., González-Maciel, A., Reynoso-Robles, R., Villarreal-Calderon, R., Solt, A., Engle, R., 2008a. Air pollution, cognitive deficits and brain abnormalities: A pilot study with children and dogs. *Brain Cogn.* 68, 117–127. <https://doi.org/10.1016/j.bandc.2008.04.008>

- Calderón-Garcidueñas, L., Solt, A., Henríquez-Roldán, C., Torres-Jardón, R., Nuse, B., Herritt, L., Villarreal-Calderón, R., Osnaya, N., Stone, I., García, R., Brooks, D., González-Maciel, A., Reynoso-Robles, R., Delgado-Chávez, R., Reed, W., 2008b. Long-term air pollution exposure is associated with neuroinflammation, an altered innate immune response, disruption of the blood-brain barrier, ultrafine particulate deposition, and accumulation of amyloid β -42 and α -synuclein in children and young adult. *Toxicol. Pathol.* 36, 289–310. <https://doi.org/10.1177/0192623307313011>
- Campbell, A., Oldham, M., Becaria, A., Bondy, S.C., Meacher, D., Sioutas, C., Misra, C., Mendez, L.B., Kleinman, M., 2005. Particulate matter in polluted air may increase biomarkers of inflammation in mouse brain. *Neurotoxicology* 26, 133–140. <https://doi.org/10.1016/j.neuro.2004.08.003>
- Campbell, B., Mitchell, P., Dewey, H., Churilov, L., Yassi, N., Yan, B., Dowling, R., Oxley, T., TY, W., M, B., MA, S., F, M., CR, L., M, K., TJ, H., KC, F., BS, S., M, P., T, A., R, S., PA, B., B, M., T, W., TG, P., W, C., RV, C., CF, B., M, B., H, R., L, de V., H, M., PM, D., GA, D., SM, D., 2015. Endovascular therapy for ischemic stroke with perfusion-imaging selection. *N. Engl. J. Med.* 372, 1009–1018. <https://doi.org/10.1056/NEJMOA1414792>
- Candelario-Jalil, E., 2009. Injury and repair mechanisms in ischemic stroke: Considerations for the development of novel neurotherapeutics. *Curr. Opin. Investig. drugs* 10, 644–654.
- Cárcel-Márquez, J., Cullell, N., Muiño, E., Gallego-Fabrega, C., Lledós, M., Ibañez, L., Krupinski, J., Montaner, J., Cruchaga, C., Lee, J.-M., Gill, D., Paré, G., Mola-Caminal, M., Roquer, J., Jimenez-Conde, J., Martí-Fàbregas, J., Fernandez-Cadenas, I., 2021. Causal Effect of MMP-1 (Matrix Metalloproteinase-1), MMP-8, and MMP-12 Levels on Ischemic Stroke. *Stroke* 52, 316–320. <https://doi.org/10.1161/STROKEAHA.120.033041>
- Carmichael, S.T., 2016. The 3 Rs of Stroke Biology: Radial , Relayed , and Regenerative. *Neurotherapeutics* 13, 348–359. <https://doi.org/10.1007/s13311-015-0408-0>

- Carmichael, S.T., 2005. Rodent Models of Focal Stroke: Size , Mechanism , and Purpose. *Am. Soc. Exp. Neurother.* 2, 396–409.
- Carmichael, S.T., Archibeque, I., Luke, L., Nolan, T., Momiy, J., Li, S., 2005. Growth-associated gene expression after stroke: Evidence for a growth-promoting region in peri-infarct cortex. *Exp. Neurol.* 193, 291–311. <https://doi.org/10.1016/j.expneurol.2005.01.004>
- Carter, A.M., Cymbalista, C.M., Spector, T.D., Grant, P.J., 2007. Heritability of clot formation, morphology, and lysis: The EuroCLOT study. *Arterioscler. Thromb. Vasc. Biol.* 27, 2783–2789. <https://doi.org/10.1161/ATVBAHA.107.153221>
- Chao, S.K., Hamilton, R.F., Pfau, J.C., Holian, A., 2001. Cell surface regulation of silica-induced apoptosis by the SR-A scavenger receptor in a murine lung macrophage cell line (MH-S). *Toxicol. Appl. Pharmacol.* 174, 10–16. <https://doi.org/10.1006/TAAP.2001.9190>
- Cheng, L., Lau, W.K.W., Fung, T.K.H., Lau, B.W.M., Chau, B.K.H., Liang, Y., Wang, Z., So, K.F., Wang, T., Chan, C.C.H., Lee, T.M.C., 2017. PM2.5 Exposure Suppresses Dendritic Maturation in Subgranular Zone in Aged Rats. *Neurotox. Res.* 32, 50–57. <https://doi.org/10.1007/s12640-017-9710-4>
- Chung, E.P., Cotter, J.D., Prakapenka, A. V, Cook, R.L., Diperna, D.M., Sirianni, R.W., 2020. Targeting Small Molecule Delivery to the Brain and Spinal Cord via Intranasal Administration of Rabies Virus Glycoprotein (RVG29) - Modified PLGA Nanoparticles. *Pharmaceutics* 12, 1–16.
- Coburn, J.L., Cole, T.B., Dao, K.T., Costa, L.G., 2018. Acute exposure to diesel exhaust impairs adult neurogenesis in mice: prominence in males and protective effect of pioglitazone. *Arch. Toxicol.* 92, 1815–1829. <https://doi.org/10.1007/s00204-018-2180-5>
- Cuadrado, E., Rosell, A., Borrell-Pagès, M., García-Bonilla, L., Hernández-Guillamon, M., Ortega-Aznar, A., Montaner, J., 2009. Matrix Metalloproteinase-13 is Activated and is found in the Nucleus of Neural Cells after Cerebral Ischemia. *J. Cereb. Blood Flow Metab.* 29, 398–410.

- <https://doi.org/10.1038/JCBFM.2008.130>
- Dabrowska, S., Andrzejewska, A., Lukomska, B., Janowski, M., 2019. Neuroinflammation as a target for treatment of stroke using mesenchymal stem cells and extracellular vesicles. *J. Neuroinflammation* 16. <https://doi.org/10.1186/s12974-019-1571-8>
- de Bont, J., Casas, M., Barrera-Gómez, J., Cirach, M., Rivas, I., Valvi, D., Álvarez, M., Dadvand, P., Sunyer, J., Vrijheid, M., 2019. Ambient air pollution and overweight and obesity in school-aged children in Barcelona, Spain. *Environ. Int.* 125, 58–64. <https://doi.org/10.1016/j.envint.2019.01.048>
- de Homdedeu, M., Cruz, M.J., Sánchez-Díez, S., Gómez-Ollés, S., Ojanguren, I., Ma, D., Muñoz, X., 2020. Role of diesel exhaust particles in the induction of allergic asthma to low doses of soybean. *Environ. Res.* 1–9. <https://doi.org/10.1016/j.envres.2020.110337>
- Dirnagl, U., Iadecola, C., Moskowitz, M.A., 1999. Pathobiology of ischaemic stroke: An integrated view. *Trends Neurosci.* 22, 391–397. [https://doi.org/10.1016/S0166-2236\(99\)01401-0](https://doi.org/10.1016/S0166-2236(99)01401-0)
- Dockery, D., Arden Pope III, C., Xu, X., Spengler, J., Ware, J., Fay, M., Ferris, B., Speizer, F., 1993. An association between air pollution and mortality in six US cities. *N. Engl. J. Med.* 329, 1753–1759.
- Donnan, G.A., Baron, J.C., Ma, H., Davis, S.M., 2009. Penumbral selection of patients for trials of acute stroke therapy. *Lancet Neurol.* 8, 261–269. [https://doi.org/10.1016/S1474-4422\(09\)70041-9](https://doi.org/10.1016/S1474-4422(09)70041-9)
- Dorr, A., Sled, J.G., Kabani, N., 2007. Three-dimensional cerebral vasculature of the CBA mouse brain: A magnetic resonance imaging and micro computed tomography study. *Neuroimage* 35, 1409–1423. <https://doi.org/10.1016/j.neuroimage.2006.12.040>
- Dusenbury, W., Alexandrov, A.W., 2020. Clinical Localization of Stroke. *Crit. Care Nurs. Clin. North Am.* 32, 1–19. <https://doi.org/10.1016/j.cnc.2019.10.001>

- Emmerechts, J., Alfaro-Moreno, E., Vanaudenaerde, B.M., Nemery, B., Hoylaerts, M.F., 2010. Short-term exposure to particulate matter induces arterial but not venous thrombosis in healthy mice. *J. Thromb. Haemost.* 8, 2651–2661. <https://doi.org/10.1111/j.1538-7836.2010.04081.x>
- Emmerechts, J., De Vooght, V., Haenen, S., Loyen, S., van Kerckhoven, S., Hemmeryckx, B., Vanoirbeek, J.A.J., Hoet, P.H., Nemery, B., Hoylaerts, M.F., 2012. Thrombogenic changes in young and old mice upon subchronic exposure to air pollution in an urban roadside tunnel. *Thromb. Haemost.* 108, 756–768. <https://doi.org/10.1160/TH12-03-0161>
- Engineer, N., Kimberley, T., Prudente, C., Dawson, J., Tarver, W., Hays, S., 2019. Targeted Vagus Nerve Stimulation for Rehabilitation After Stroke. *Front. Neurosci.* 13, 1–18. <https://doi.org/10.3389/FNINS.2019.00280>
- Erdő, F., Bors, L.A., Farkas, D., Bajza, Á., Gizurarson, S., 2018. Evaluation of intranasal delivery route of drug administration for brain targeting. *Brain Res. Bull.* 143, 155–170. <https://doi.org/10.1016/j.brainresbull.2018.10.009>
- Farris, B.Y., Monaghan, K.L., Zheng, W., Amend, C.D., Hu, H., Ammer, A.G., Coad, J.E., Ren, X., Wan, E.C.K., 2019. Ischemic stroke alters immune cell niche and chemokine profile in mice independent of spontaneous bacterial infection. *Immunity, Inflamm. Dis.* 7, 326–341. <https://doi.org/10.1002/iid3.277>
- Faura, J., Bustamante, A., Miró-Mur, F., Montaner, J., 2021. Stroke-induced immunosuppression: implications for the prevention and prediction of post-stroke infections. *J. Neuroinflammation* 18, 1–14. <https://doi.org/10.1186/S12974-021-02177-0>
- Fiorito, S., Mastrofrancesco, A., Cardinali, G., Rosato, E., Salsano, F., Su, D.S., Serafino, A., Picardo, M., 2011. Effects of carbonaceous nanoparticles from low-emission and older diesel engines on human skin cells. *Carbon N. Y.* 49, 5038–5048. <https://doi.org/10.1016/J.CARBON.2011.07.022>
- Fonken, L., Xu, X., Weil, Z., Chen, G., Sun, Q., Rajagopalan, S., Nelson, R., 2011. Air pollution impairs cognition, provokes depressive-like behaviors and alters

- hippocampal cytokine expression and morphology. *Mol. Psychiatry* 16, 987–973. <https://doi.org/10.1038/jid.2014.371>
- Fujimura, M., Morita-Fujimura, Y., Murakami, K., Kawase, M., Chan, P.H., 1998. Cytosolic redistribution of cytochrome c after transient focal cerebral ischemia in rats. *J. Cereb. Blood Flow Metab.* 18, 1239–1247. <https://doi.org/10.1097/00004647-199811000-00010>
- Gabriel-Salazar, M., Lei, T., Grayston, A., Costa, C., Medina-Gutiérrez, E., Comabella, M., Montaner, J., Rosell, A., 2021. Angiogenin in the Neurogenic Subventricular Zone After Stroke. *Front. Neurol.* 12, 1–10. <https://doi.org/10.3389/FNEUR.2021.662235>
- Gangwar, R.S., Vinayachandran, V., Rengasamy, P., Chan, R., Park, B., Diamond-Zaluski, R., Cara, E.A., Cha, A., Das, L., Asase, C., Maiseyeu, A., Deiuliis, J., Zhong, J., Mitzner, W., Biswal, S., Rajagopalan, S., 2020. Differential contribution of bone marrow-derived infiltrating monocytes and resident macrophages to persistent lung inflammation in chronic air pollution exposure. *Nat. Sci. reports* 10, 1–15. <https://doi.org/10.1038/s41598-020-71144-1>
- Geiser, M., Rothen-Rutishauser, B., Kapp, N., Schürch, S., Kreyling, W., Schulz, H., Semmler, M., Im Hof, V., Heyder, J., Gehr, P., 2005. Ultrafine particles cross cellular membranes by nonphagocytic mechanisms in lungs and in cultured cells. *Environ. Health Perspect.* 113, 1555–1560. <https://doi.org/10.1289/ehp.8006>
- Gerlofs-Nijland, M.E., van Berlo, D., Cassee, F.R., Schins, R.P.F., Wang, K., Campbell, A., 2010. Effect of prolonged exposure to diesel engine exhaust on proinflammatory markers in different regions of the rat brain. *Part. Fibre Toxicol.* 7, 1–10. <https://doi.org/10.1186/1743-8977-7-12>
- Gibbs, D., Warner, R., Weiss, S., Johnson, K., Varani, J., 1999. Characterization of matrix metalloproteinases produced by rat alveolar macrophages. *Am. J. Respir. Cell Mol. Biol.* 20, 1136–1144. <https://doi.org/10.1165/AJRCMB.20.6.3483>

- González-Maciel, A., Reynoso-Robles, R., Torres-Jardón, R., Sarathi-Mukherjee, P., Calderón-garcidueñas, L., 2017. Combustion Derived nanoparticles in key brain target cells and organelles in young urbanites: culprit hidden in plain sight in alzheimer's disease development. *J. Alzheimer's Dis.* 1–20. <https://doi.org/10.3233/JAD-170012>
- Gonzalez, R.G., Hirsch, J.A., Koroshetz, W.J., Lev, M.H., Schaefer, P., 2006. Acute ischemic stroke. Imaging and intervention, *Journal of Neuroradiology*. [https://doi.org/10.1016/s0150-9861\(06\)77259-5](https://doi.org/10.1016/s0150-9861(06)77259-5)
- González Ortiz, A., Soares, J., 2020. Air quality in Europe - 2020 report, Air quality in Europe-2020 report. Luxembourg.
- Goyal, M., Demchuk, A., Menon, B., Eesa, M., Rempel, J., Thornton, J., Roy, D., Jovin, T., Willinsky, R., Sapkota, B., Dowlathshahi, D., Frei, D., Kamal, N., Montanera, W., Poppe, A., Ryckborst, K., Silver, F., Shuaib, A., Tampieri, D., Williams, D., Bang, O., Baxter, B., Burns, P., Choe, H., Heo, J., Holmstedt, J., Jankowitz, B., Kelly, M., Linares, G., Mandzia, J., Shankar, J., Sohn, S., Swartz, R., Barber, P., Coutts, S., Smith, E., Morrish, W., Weill, A., Subramaniam, S., Mitha, A., JH, W., Lowerison, M., Sajobi, T., Hill, M., 2015. Randomized assessment of rapid endovascular treatment of ischemic stroke. *N. Engl. J. Med.* 372, 1019–1030. <https://doi.org/10.1056/NEJMOA1414905>
- Hacke, W., Kaste, M., Fieschi, C., Toni, D., Emmanuel, L., von Kummer, R., Boysen, G., Bluhmki, E., Höxter, G., Mahagne, M., Hennerici, M., 1995. Intravenous thrombolysis with recombinant tissue plasminogen activator for acute hemispheric stroke. The European Cooperative Acute Stroke Study (ECASS). *JAMA J. Am. Med. Assoc.* 274, 1017–1025. <https://doi.org/10.1001/jama.274.13.1017>
- Hacke, W., Kaste, M., Fieschi, C., von Kummer, R., Davalos, A., Meier, D., Larrue, V., Bluhmki, E., Davis, S., Donnan, G., Schneider, D., Diez-Tejedor, E., Trouillas, P., 1998. Randomised double-blind placebo-controlled trial of thrombolytic therapy with intravenous alteplase in acute ischaemic stroke (ECASS II). Second European-Australasian Acute Stroke Study Investigators. *Lancet*

- (London, England) 352, 1245–1251. [https://doi.org/10.1016/S0140-6736\(98\)08020-9](https://doi.org/10.1016/S0140-6736(98)08020-9)
- Hendrix, A.Y., Kheradmand, F., 2017. The Role of Matrix Metalloproteinases in Development, Repair, and Destruction of the Lungs, in: *Progress in Molecular Biology and Translational Science*. Elsevier B.V., pp. 1–29. <https://doi.org/10.1016/bs.pmbts.2017.04.004>
- Hossmann, K. -A, 1994. Viability thresholds and the penumbra of focal ischemia. *Ann. Neurol.* 36, 557–565. <https://doi.org/10.1002/ana.410360404>
- Hoyer, F.F., Naxerova, K., Schloss, M.J., Hulsmans, M., Nair, A. V., Dutta, P., Calcagno, D.M., Herisson, F., Anzai, A., Sun, Y., Wojtkiewicz, G., Rohde, D., Frodermann, V., Vandoorne, K., Courties, G., Iwamoto, Y., Garriss, C.S., Williams, D.L., Breton, S., Brown, D., Whalen, M., Libby, P., Pittet, M.J., King, K.R., Weissleder, R., Swirski, F.K., Nahrendorf, M., 2019. Tissue-Specific Macrophage Responses to Remote Injury Impact the Outcome of Subsequent Local Immune Challenge. *Immunity* 51, 899–914. <https://doi.org/10.1016/j.immuni.2019.10.010>
- Hu, Q., Liang, X., Chen, D., Chen, Y., Doycheva, D., Tang, J., Tang, J., Zhang, J.H., 2014. Delayed Hyperbaric Oxygen Therapy Promotes Neurogenesis through ROS/HIF-1 α / β -catenin Pathway in MCAO Rats. *Stroke*. 45, 1807. <https://doi.org/10.1161/STROKEAHA.114.005116>
- Iadecola, C., Anrather, J., 2012. The immunology of stroke: from mechanisms to translation. *Nat Med* 17, 796–808. <https://doi.org/10.1038/nm.2399>
- Johnson, C.O., Nguyen, M., Roth, G.A., Nichols, E., Alam, T., Abate, D., Abd-Allah, F., Abdelalim, A., Abraha, H.N., Abu-Rmeileh, N.M., Adebayo, O.M., Adeoye, A.M., Agarwal, G., Agrawal, S., Aichour, A.N., Aichour, I., Aichour, M.T.E., Alahdab, F., Ali, R., Alvis-Guzman, N., Anber, N.H., Anjomshoa, M., Arabloo, J., Arauz, A., Ärnlov, J., Arora, A., Awasthi, A., Banach, M., Barboza, M.A., Barker-Collo, S.L., Bärnighausen, T.W., Basu, S., Belachew, A.B., Belayneh, Y.M., Bennett, D.A., Bensenor, I.M., Bhattacharyya, K., Biadgo, B., Bijani, A., Bikbov, B., Bin Sayeed, M.S., Butt, Z.A., Cahuana-Hurtado, L., Carrero, J.J.,

Carvalho, F., Castañeda-Orjuela, C.A., Castro, F., Catalá-López, F., Chaiah, Y., Chiang, P.P.C., Choi, J.Y.J., Christensen, H., Chu, D.T., Cortinovis, M., Damasceno, A.A.M., Dandona, L., Dandona, R., Daryani, A., Davletov, K., De Courten, B., De la Cruz-Góngora, V., Degefa, M.G., Dharmaratne, S.D., Diaz, D., Dubey, M., Duken, E.E., Edessa, D., Endres, M., Faraon, E.J.A., Farzadfar, F., Fernandes, E., Fischer, F., Flor, L.S., Ganji, M., Gebre, A.K., Gebremichael, T.G., Geta, B., Gezae, K.E., Gill, P.S., Gnedovskaya, E. V., Gómez-Dantés, H., Goulart, A.C., Grosso, G., Guo, Y., Gupta, R., Haj-Mirzaian, A., Haj-Mirzaian, A., Hamidi, S., Hankey, G.J., Hassen, H.Y., Hay, S.I., Hegazy, M.I., Heidari, B., Herial, N.A., Hosseini, M.A., Hostiuc, S., Irvani, S.S.N., Islam, S.M.S., Jahanmehr, N., Javanbakht, M., Jha, R.P., Jonas, J.B., Józwiak, J.J., Jürisson, M., Kahsay, A., Kalani, R., Kalkonde, Y., Kamil, T.A., Kanchan, T., Karch, A., Karimi, N., Karimi-Sari, H., Kasaeian, A., Kassa, T.D., Kazemeini, H., Kefale, A.T., Khader, Y.S., Khalil, I.A., Khan, E.A., Khang, Y.H., Khubchandani, J., Kim, D., Kim, Y.J., Kisa, A., Kivimäki, M., Koyanagi, A., Krishnamurthi, R.K., Anil Kumar, G., Lafranconi, A., Lewington, S., Li, S., Lo, W.D., Lopez, A.D., Lorkowski, S., Lotufo, P.A., Mackay, M.T., Majdan, M., Majdzadeh, R., Majeed, A., Malekzadeh, R., Manafi, N., Mansournia, M.A., Mehndiratta, M.M., Mehta, V., Mengistu, G., Meretoja, A., Meretoja, T.J., Miazgowski, B., Miazgowski, T., Miller, T.R., Mirakshimov, E.M., Mohajer, B., Mohammad, Y., Mohammadoo-Khorasani, M., Mohammed, S., Mohebi, F., Mokdad, A.H., Mokhayeri, Y., Moradi, G., Morawska, L., Moreno Velásquez, I., Mousavi, S.M., Muhammed, O.S.S., Muruet, W., Naderi, M., Naghavi, M., Naik, G., Nascimento, B.R., Negoi, R.I., Nguyen, C.T., Nguyen, L.H., Nirayo, Y.L., Norrving, B., Noubiap, J.J., Ofori-Asenso, R., Ogbo, F.A., Olagunju, A.T., Olagunju, T.O., Owolabi, M.O., Pandian, J.D., Patel, S., Perico, N., Piradov, M.A., Polinder, S., Postma, M.J., Poustchi, H., Prakash, V., Qorbani, M., Rafiei, A., Rahim, F., Rahimi, K., Rahimi-Movaghar, V., Rahman, M., Rahman, M.A., Reis, C., Remuzzi, G., Renzaho, A.M.N., Ricci, S., Roberts, N.L.S., Robinson, S.R., Roeber, L., Roshandel, G., Sabbagh, P., Safari, H., Safari, S., Safiri, S., Sahebkar, A., Salehi Zahabi, S., Samy, A.M., Santalucia, P., Santos, I.S., Santos, J.V., Santric Milicevic, M.M., Sartorius, B., Sawant, A.R., Schutte, A.E.,

- Sepanlou, S.G., Shafieesabet, A., Shaikh, M.A., Shams-Beyranvand, M., Sheikh, A., Sheth, K.N., Shibuya, K., Shigematsu, M., Shin, M.J., Shiue, I., Siabani, S., Sobaih, B.H., Sposato, L.A., Sutradhar, I., Sylaja, P.A., Szoeki, C.E.I., Te Ao, B.J., Temsah, M.H., Temsah, O., Thrift, A.G., Tonelli, M., Topor-Madry, R., Tran, B.X., Tran, K.B., Truelsen, T.C., Tsadik, A.G., Ullah, I., Uthman, O.A., Vaduganathan, M., Valdez, P.R., Vasankari, T.J., Vasanthan, R., Venketasubramanian, N., Vosoughi, K., Vu, G.T., Waheed, Y., Weiderpass, E., Weldegwergs, K.G., Westerman, R., Wolfe, C.D.A., Wondafrash, D.Z., Xu, G., Yadollahpour, A., Yamada, T., Yatsuya, H., Yimer, E.M., Yonemoto, N., Yousefifard, M., Yu, C., Zaidi, Z., Zamani, M., Zarghi, A., Zhang, Y., Zodpey, S., Feigin, V.L., Vos, T., Murray, C.J.L., 2019. Global, regional, and national burden of stroke, 1990–2016: a systematic analysis for the Global Burden of Disease Study 2016. *Lancet Neurol.* 18, 439–458. [https://doi.org/10.1016/S1474-4422\(19\)30034-1](https://doi.org/10.1016/S1474-4422(19)30034-1)
- Jovin, T.G., Chamorro, A., Cobo, E., de Miquel, M.A., Molina, C.A., Rovira, A., San Román, L., Serena, J., Abilleira, S., Ribó, M., Millán, M., Urra, X., Cardona, P., López-Cancio, E., Tomasello, A., Castaño, C., Blasco, J., Aja, L., Dorado, L., Quesada, H., Rubiera, M., Hernandez-Pérez, M., Goyal, M., Demchuk, A.M., von Kummer, R., Gallofré, M., Dávalos, A., 2015. Thrombectomy within 8 Hours after Symptom Onset in Ischemic Stroke. *N. Engl. J. Med.* 372, 2296–2306. <https://doi.org/10.1056/NEJMOA1503780>
- Katan, M., Luft, A., 2018. Global Burden of stroke. *Semin Neurol* 38, 208–211. <https://doi.org/10.1159/000441085.lifetime>
- Kaufmann, A.M., Firlik, A.D., Fukui, M.B., Wechsler, L.R., Jungries, C.A., Yonas, H., 1999. Ischemic Core and Penumbra in Human Stroke. *Stroke* 30, 93–99. <https://doi.org/10.1161/01.STR.30.1.93>
- Kettunen, J., Lanki, T., Tiittanen, P., Aalto, P.P., Koskentalo, T., Kulmala, M., Salomaa, V., Pekkanen, J., 2007. Associations of fine and ultrafine particulate air pollution with stroke mortality in an area of low air pollution levels. *Stroke* 38, 918–922. <https://doi.org/10.1161/01.STR.0000257999.49706.3b>

- Kim, J., Natarajan, S., Vaickus, L.J., Bouchard, J.C., Beal, D., Cruikshank, W.W., Remick, D.G., 2011. Diesel exhaust particulates exacerbate asthma-like inflammation by increasing CXC chemokines. *Am. J. Pathol.* 179, 2730–2739. <https://doi.org/10.1016/j.ajpath.2011.08.008>
- Kim, J.S., 2019. tPA helpers in the treatment of acute ischemic stroke: Are they ready for clinical use? *J. Stroke* 21, 160–174. <https://doi.org/10.5853/jos.2019.00584>
- Kim, S., Lee, D., Park, S., Kim, B., Jang, A., Oh, S., Lee, J., Suh, M., Park, M., 2019. Neuronal and perineuronal changes of cerebral cortex after exposure to inhaled particulate matter. *Sci. Rep.* 9, 1–9. <https://doi.org/10.1038/S41598-019-55956-4>
- Kim, Y.S., Kim, J.K., Kim, B., 2018. Effects of inhaled particulate matter on the central nervous system in mice. *Neurotoxicology* 1–33. <https://doi.org/10.1016/j.neuro.2018.06.001>
- Krupinski, J., Kaluza, J., Kumar, P., Kumar, S., Wang, J.M., 1994. Role of angiogenesis in patients with cerebral ischemic stroke. *Stroke* 25, 1794–1798. <https://doi.org/10.1161/01.STR.25.9.1794>
- Kyu, H.H., Bachman, V.F., Alexander, L.T., Mumford, J.E., Afshin, A., Estep, K., Veerman, J.L., Delwiche, K., Iannarone, M.L., Moyer, M.L., Cercy, K., Vos, T., Murray, C.J.L., Forouzanfar, M.H., 2016. Physical activity and risk of breast cancer, colon cancer, diabetes, ischemic heart disease, and ischemic stroke events: Systematic review and dose-response meta-analysis for the Global Burden of Disease Study 2013. *BMJ* 354, 1–10. <https://doi.org/10.1136/bmj.i3857>
- Lakhan, S.E., Kirchgessner, A., Tepper, D., Aidan, L., 2013. Matrix Metalloproteinases and Blood-Brain Barrier Disruption in Acute Ischemic Stroke. *Front. Neurol.* <https://doi.org/10.3389/FNEUR.2013.00032>
- Langhorne, P., Bernhardt, J., Kwakkel, G., 2011. Stroke rehabilitation. *Lancet* 377, 1693–1702. [https://doi.org/10.1016/S0140-6736\(11\)60325-5](https://doi.org/10.1016/S0140-6736(11)60325-5)

- Le Tertre, A., Medina, S., Samoli, E., Forsberg, B., Michelozzi, P., Boumghar, A., Vonk, J.M., Bellini, A., Atkinson, R., Ayres, J.G., Sunyer, J., Schwartz, J., Katsouyanni, K., 2002. Short-term effects of particulate air pollution on cardiovascular diseases in eight European cities. *J. Epidemiol. Community Health* 56, 773–779. <https://doi.org/10.1136/jech.56.10.773>
- Lee, C.-H., 2020. Pathophysiology of Cardioembolism 105–111. https://doi.org/10.1007/978-981-10-1430-7_9
- Lee, S., Kim, H., Rogowska, J., Zhao, B., Bhide, P., Parent, J., Lo, E., 2006. Involvement of matrix metalloproteinase in neuroblast cell migration from the subventricular zone after stroke. *J. Neurosci.* 26, 3491–3495. <https://doi.org/10.1523/JNEUROSCI.4085-05.2006>
- Lenglet, S., Montecucco, F., Mach, F., Schaller, K., Gasche, Y., Copin, J.C., 2014. Analysis of the expression of nine secreted matrix metalloproteinases and their endogenous inhibitors in the brain of mice subjected to ischaemic stroke. *Thromb. Haemost.* 112, 363–378. <https://doi.org/10.1160/TH14-01-0007>
- Levesque, S., Surace, M.J., McDonald, J., Block, M.L., 2011a. Air pollution and the brain: Subchronic diesel exhaust exposure causes neuroinflammation and elevates early markers of neurodegenerative disease. *J. Neuroinflammation* 8, 1–10. <https://doi.org/10.1186/1742-2094-8-105>
- Levesque, S., Taetzsch, T., Lull, M.E., Kodavanti, U., Stadler, K., Wagner, A., Johnson, J.A., Duke, L., Kodavanti, P., Surace, M.J., Block, M.L., 2011b. Diesel exhaust activates and primes microglia: Air pollution, neuroinflammation, and regulation of dopaminergic neurotoxicity. *Environ. Health Perspect.* 119, 1149–1155. <https://doi.org/10.1289/ehp.1002986>
- Li, S., Nie, E., Yin, Y., Benowitz, L., Tung, S., Vinters, H., Bahjat, F., Stenzel-Poore, M., Kawaguchi, R., Coppola, G., Carmichael, S., 2015. GDF10 Is a Signal for Axonal Sprouting and Functional Recovery after Stroke. *Nat. Neurosci.* 18, 1737–1745. <https://doi.org/10.1038/nn.4146>
- Li, Y., Ouyang, Q., Li, J., Chen, X., Li, L., Xu, L., Yu, M., 2021. Correlation between

- matrix metalloproteinase-2 polymorphisms and first and recurrent atherosclerotic ischemic stroke events: a case–control study. *J. Int. Med. Res.* 49, 1–11. <https://doi.org/10.1177/03000605211022967>
- Liesz, A., Dalpke, A., Mracsko, E., Antoine, D.J., Roth, S., Zhou, W., Yang, H., Na, S.Y., Akhisaroglu, M., Fleming, T., Eigenbrod, T., Nawroth, P.P., Tracey, K.J., Veltkamp, R., 2015. DAMP signaling is a key pathway inducing immune modulation after brain injury. *J. Neurosci.* 35, 583–598. <https://doi.org/10.1523/JNEUROSCI.2439-14.2015>
- Lin, C.I., Tsai, C.H., Sun, Y.L., Hsieh, W.Y., Lin, Y.C., Chen, C.Y., Lin, C.S., 2018. Instillation of particulate matter 2.5 induced acute lung injury and attenuated the injury recovery in ACE2 knockout mice. *Int. J. Biol. Sci.* 14, 253–265. <https://doi.org/10.7150/ijbs.23489>
- Lin, T.-N., Sun, S.-W., Cheung, W.-M., Li, F., Chang, C., 2002. Dynamic Changes in Cerebral Blood Flow and Angiogenesis After Transient Focal Cerebral Ischemia in Rats. *Stroke* 33, 2985–2991. <https://doi.org/10.1161/01.STR.0000037675.97888.9D>
- Linderholm, A., Franzi, L., Bein, K., Pinkerton, K., Last, J., 2015. A quantitative comparison of intranasal and intratracheal administration of coarse PM in the mouse. *Integr. Pharmacol. Toxicol. Genotoxicol.* 1, 5–10. <https://doi.org/10.15761/IPTG.1000103>
- Liu, F., Mccullough, L.D., 2010. Middle Cerebral Artery Occlusion Model in Rodents: Methods and Potential Pitfalls. *J. Biomed. Biotechnol.* 48, 1–9. <https://doi.org/10.1155/2011/464701>
- Liu, Q., Babadjouni, R., Radwanski, R., Cheng, H., Patel, A., Hodis, D.M., He, S., Baumbacher, P., Russin, J.J., Morgan, T.E., Sioutas, C., Finch, C.E., Mack, W.J., 2016. Stroke Damage Is Exacerbated by Nano-Size Particulate Matter in a Mouse Model. *PLoS One* 11, 1–15. <https://doi.org/10.1371/journal.pone.0153376>
- Liu, Q., Jin, W.N., Liu, Y., Shi, K., Sun, H., Zhang, F., Zhang, C., Gonzales, R.J., Sheth,

- K.N., La Cava, A., Shi, F.D., 2017. Brain Ischemia Suppresses Immunity in the Periphery and Brain via Different Neurogenic Innervations. *Immunity* 46, 474–487. <https://doi.org/10.1016/j.immuni.2017.02.015>
- Llovera, G., Roth, S., Plesnila, N., Veltkamp, R., Liesz, A., 2014. Modeling Stroke in Mice: Permanent Coagulation of the Distal Middle Cerebral Artery. *J. Vis. Exp.* 89, 1–8. <https://doi.org/10.3791/51729>
- Ma, F., Martinez-San Segundo, P., Barceló, V., Morancho, A., Gabriel-salazar, M., Giralt, D., Montaner, J., Rosell, A., 2016a. Matrix metalloproteinase-13 participates in neuroprotection and neurorepair after cerebral ischemia in mice. *Neurobiol. Dis.* 91, 236–246. <https://doi.org/10.1016/j.nbd.2016.03.016>
- Ma, F., Morancho, A., Montaner, J., Rosell, A., 2015. Endothelial progenitor cells and revascularization following stroke. *Brain Res.* 1623, 1–10. <https://doi.org/10.1016/j.brainres.2015.02.010>
- Ma, F., Rodriguez, S., Buxo, X., Morancho, A., Riba-Illena, I., Carrera, A., Bustamante, A., Giralt, D., Montaner, J., Martinez, C., Bori, I., Rosell, A., 2016b. Plasma Matrix Metalloproteinases in Patients With Stroke During Intensive Rehabilitation Therapy. *Arch. Phys. Med. Rehabil.* 1–10. <https://doi.org/10.1016/j.apmr.2016.06.007>
- Maher, B.A., Ahmed, I.A.M., Karloukovski, V., MacLaren, D.A., Foulds, P.G., Allsop, D., Mann, D.M.A., Torres-Jardón, R., Calderon-Garciduenas, L., 2016. Magnetite pollution nanoparticles in the human brain. *Proc. Natl. Acad. Sci.* 113, 10797–10801. <https://doi.org/10.1073/pnas.1605941113>
- Malone, K., Amu, S., Moore, A.C., Waeber, C., 2019. The immune system and stroke: from current targets to future therapy. *Immunol. Cell Biol.* 97, 5–16. <https://doi.org/10.1111/IMCB.12191>
- Manners, S., Alam, R., Schwartz, D.A., Gorska, M.M., 2014. A mouse model links asthma susceptibility to prenatal exposure to diesel exhaust. *J. Allergy Clin. Immunol.* 134, 63–72. <https://doi.org/10.1080/10810730902873927>.Testing
- Mannucci, M., Harari, S., Franchini, M., 2019. pollution on cardiovascular disease.

- Haematologica 104, 1–9. <https://doi.org/10.3324/haematol.2019.225086>
- Manwani, B., McCullough, L.D., 2011. Sexual dimorphism in ischemic stroke: Lessons from the laboratory. *Women's Heal.* <https://doi.org/10.2217/whe.11.22>
- Martins, V., Cruz Minguillón, M., Moreno, T., Querol, X., de Miguel, E., Capdevila, M., Centelles, S., Lazaridis, M., 2015. Deposition of aerosol particles from a subway microenvironment in the human respiratory tract. *J. Aerosol Sci.* 90, 103–113. <https://doi.org/10.1016/J.JAEROSCI.2015.08.008>
- Matsui, Y., Sakai, N., Tsuda, A., Terada, Y., Takaoka, M., 2009. Tracking the pathway of diesel exhaust particles from the nose to the brain by X-ray fluorescence analysis. *Spectrochim. Acta Part B At. Spectrosc.* 64, 796–801. <https://doi.org/10.1016/j.sab.2009.06.017>
- Maynard, R., Krzyanowski, M., Vilahur, N., Héroux, M.-E., 2017. Evolution of WHO air quality guidelines. Copenhagen.
- McBride, D.W., Zhang, J.H., 2017. Precision Stroke Animal Models: the Permanent MCAO Model Should Be the Primary Model, Not Transient MCAO. *Transl. Stroke Res.* 8, 397–404. <https://doi.org/10.1007/s12975-017-0554-2>
- McCulloch, J., 1992. Excitatory amino acid antagonists and their potential for the treatment of ischaemic brain damage in man. *Br. J. Clin. Pharmacol.* 34, 106–114. <https://doi.org/10.1111/j.1365-2125.1992.tb04118.x>
- Metassan, S., Charlton, A.J., Routledge, M.N., Scott, D.J.A., Ariëns, R.A.S., 2010. Alteration of fibrin clot properties by ultrafine particulate matter. *Thromb. Haemost.* 103, 103–113. <https://doi.org/10.1160/TH09-05-0330>
- Miller, M.R., Raffis, J.B., Langrish, J.P., McLean, S.G., Samutrtai, P., Connell, S.P., Wilson, S., Vesey, A.T., Fokkens, P.H.B., Boere, A.J.F., Krystek, P., Campbell, C.J., Hadoke, P.W.F., Donaldson, K., Cassee, F.R., Newby, D.E., Duffin, R., Mills, N.L., 2017. Inhaled Nanoparticles Accumulate at Sites of Vascular Disease. *ACS Nano* 11, 4542–4552. <https://doi.org/10.1021/acsnano.6b08551>

- Mills, N.L., Törnqvist, H., Gonzalez, M.C., Vink, E., Robinson, S.D., Söderberg, S., Boon, N.A., Donaldson, K., Sandström, T., Blomberg, A., Newby, D.E., 2007. Ischemic and Thrombotic Effects of Dilute Diesel-Exhaust Inhalation in Men with Coronary Heart Disease. *N. Engl. J. Med.* 357, 1075–1082. <https://doi.org/10.1056/NEJMoa066314>
- Mills, N.L., Törnqvist, H., Robinson, S.D., Gonzalez, M., Darnley, K., MacNee, W., Boon, N.A., Donaldson, K., Blomberg, A., Sandstrom, T., Newby, D.E., 2005. Diesel exhaust inhalation causes vascular dysfunction and impaired endogenous fibrinolysis. *Circulation* 112, 3930–3936. <https://doi.org/10.1161/CIRCULATIONAHA.105.588962>
- Ming, G.L., Song, H., 2011. Adult Neurogenesis in the Mammalian Brain: Significant Answers and Significant Questions. *Neuron*. 70, 687–702. <https://doi.org/10.1016/j.neuron.2011.05.001>.Adult
- Miyata, R., van Eeden, S.F., 2011. The innate and adaptive immune response induced by alveolar macrophages exposed to ambient particulate matter. *Toxicol. Appl. Pharmacol.* 257, 209–226. <https://doi.org/10.1016/j.taap.2011.09.007>
- Moldoveanu, B., Otmishi, P., Jani, P., Walker, J., Sarmiento, X., Guardiola, J., Saad, M., Yu, J., 2009. Inflammatory mechanisms in the lung, *Journal of Inflammation Research*.
- Montaner, J., Molina, C., Monasterio, J., Abilleira, S., Arenillas, J., Ribó, M., Quintana, M., Alvarez-Sabín, J., 2003. Matrix metalloproteinase-9 pretreatment level predicts intracranial hemorrhagic complications after thrombolysis in human stroke. *Circulation* 107, 598–603. <https://doi.org/10.1161/01.CIR.0000046451.38849.90>
- Morancho, A., García-Bonilla, L., Barceló, V., Giralt, D., Campos-Martorell, M., Garcia, S., Montaner, J., Rosell, A., 2012. A new method for focal transient cerebral ischaemia by distal compression of the middle cerebral artery. *Neuropathol. Appl. Neurobiol.* 38, 617–627. <https://doi.org/10.1111/j.1365-2990.2012.01252.x>

- Morancho, A., Ma, F., Barceló, V., Giralt, D., Montaner, J., Rosell, A., 2015. Impaired vascular remodeling after endothelial progenitor cell transplantation in MMP9-deficient mice suffering cortical cerebral ischemia. *JCBFM* 35, 1547–1551. <https://doi.org/10.1038/jcbfm.2015.180>
- Moskowitz, M.A., Lo, E.H., Iadecola, C., 2010. Review The Science of Stroke : Mechanisms in Search of Treatments. *Neuron* 67, 181–198. <https://doi.org/10.1016/j.neuron.2010.07.002>
- Mostany, R., Chowdhury, T.G., Johnston, D.G., Portonovo, S.A., Carmichael, S.T., Portera-Cailliau, C., 2010. Local Hemodynamics Dictate Long-Term Dendritic Plasticity in Peri-Infarct Cortex. *J. Neurosci.* 30, 14116–14126. <https://doi.org/10.1523/JNEUROSCI.3908-10.2010>
- Murphy, S.J., Werring, D.J., 2020. Stroke: causes and clinical features. *Med. (United Kingdom)* 48, 561–566. <https://doi.org/10.1016/j.mpmed.2020.06.002>
- Nemery, B., Hoet, P.H.M., Nemmar, A., 2001. Department of medical history The Meuse Valley fog of 1930 : an air pollution disaster. *Lancet* 357, 704–708.
- Nemmar, A., Hoet, P.H.M., Dinsdale, D., Vermeylen, J., Hoylaerts, M.F., Nemery, B., 2003. Diesel exhaust particles in lung acutely enhance experimental peripheral thrombosis. *Circulation* 107, 1202–1208. <https://doi.org/10.1161/01.CIR.0000053568.13058.67>
- Nemmar, A., Zia, S., Subramaniyan, D., Al-Amri, I., Al Kindi, M.A., Ali, B.H., 2012. Interaction of Diesel Exhaust Particles with Human , Rat and Mouse Erythrocytes in Vitro. *Cell. Physiol. Biochem.* 29, 163–170. <https://doi.org/10.1159/000337597>
- Newman, L., Rodrigues, A.F., Jasim, D.A., Vacchi, I.A., Ménard-Moyon, C., Bianco, A., Bussy, C., Kostarelos, K., 2020. Nose-to-Brain Translocation and Cerebral Biodegradation of Thin Graphene Oxide Nanosheets. *Cell Reports Phys. Sci.* 1, 1–23. <https://doi.org/10.1016/j.xcrp.2020.100176>
- Ng, Y.S., Stein, J., Ning, M., Black-Schaffer, R.M., 2007. Comparison of Clinical Characteristics and Functional Outcomes of Ischemic Stroke in Different

- Vascular Territories 38, 2309–2314.
<https://doi.org/10.1161/STROKEAHA.106.475483>
- Nih, L.R., Gojgini, S., Thomas Carmichael, S., Segura, T., 2018. Dual-function injectable angiogenic biomaterial for the repair of brain tissue following stroke. *Nat. Mater.* 17, 642–651. <https://doi.org/10.1038/s41563-018-0083-8>
- Numano, T., Morioka, M., Higuchi, H., Uda, K., Sugiyama, T., Hagiwara, T., Doi, Y., Imai, N., Kawabe, M., Mera, Y., Tamano, S., 2020. Effects of administering different vehicles via single intratracheal instillation on responses in the lung and pleural cavity of Crl:CD(SD) rats. *J. Toxicol. Pathol.* 33, 11–19. <https://doi.org/10.1293/TOX.2019-0060>
- O'Donnell, M.J., Chin, S.L., Rangarajan, S., Xavier, D., Liu, L., Zhang, H., Rao-Melacini, P., Zhang, X., Pais, P., Agapay, S., Lopez-Jaramillo, P., Damasceno, A., Langhorne, P., McQueen, M.J., Rosengren, A., Dehghan, M., Hankey, G.J., Dans, A.L., Elsayed, A., Avezum, A., Mondo, C., Diener, H.C., Ryglewicz, D., Czonkowska, A., Pogosova, N., Weimar, C., Iqbal, R., Diaz, R., Yusoff, K., Yusufali, A., Oguz, A., Wang, X., Penaherrera, E., Lanas, F., Ogah, O.S., Ogunniyi, A., Iversen, H.K., Malaga, G., Rumboldt, Z., Oveisgharan, S., Al Hussain, F., Magazi, D., Nilanont, Y., Ferguson, J., Pare, G., Yusuf, S., 2016. Global and regional effects of potentially modifiable risk factors associated with acute stroke in 32 countries (INTERSTROKE): a case-control study. *Lancet* 388, 761–775. [https://doi.org/10.1016/S0140-6736\(16\)30506-2](https://doi.org/10.1016/S0140-6736(16)30506-2)
- Oberdörster, G., Ferin, J., Gelein, R., Soderholm, S., Finkelstein, J., 1992. Role of the alveolar macrophage in lung injury: studies with ultrafine particles. *Environ. Health Perspect.* 97, 193–199. <https://doi.org/10.1289/EHP.97-1519541>
- Oberdörster, G., Sharp, Z., Atudorei, V., Elder, A., Gelein, R., Kreyling, W., Cox, C., 2004. Translocation of inhaled ultrafine particles to the brain. *Inhal. Toxicol.* 16, 437–445. <https://doi.org/10.1080/08958370490439597>
- Oberdörster, G., Sharp, Z., Atudorei, V., Elder, A., Gelein, R., Lunts, A., Kreyling, W., Cox, C., 2002. Extrapulmonary translocation of ultrafine carbon particles following whole-body inhalation exposure of rats. *J. Toxicol. Environ. Health*

- 65, 1531–1543. <https://doi.org/10.1080/00984100290071658>
- Offner, H., Subramanian, S., Parker, S.M., Afentoulis, M.E., Vandenbark, A.A., Hurn, P.D., 2006. Experimental stroke induces massive, rapid activation of the peripheral immune system. *J. Cereb. Blood Flow Metab.* 26, 654–665. <https://doi.org/10.1038/sj.jcbfm.9600217>
- Ohab, J.J., Carmichael, S.T., 2008. Poststroke Neurogenesis: Emerging Principles of Migration and Localization of Immature Neurons. *Neurosci.* 14, 369–380. <https://doi.org/10.1177/1073858407309545>
- Otero-Ortega, L., Laso-García, F., Gómex de-Frutos, M.C., Diekhorst, L., Martínez-Arroyo, A., Alonso-López, E., García-Bermejo, M.L., Rodríguez-Serrano, M., Arrúe-Gonzalo, M., Díez-Tejedor, E., Fuentes, B., Gutiérrez-Fernández, M., 2020. Low dose of extracellular vesicles identified that promote recovery after ischemic stroke. *Stem Cell Res. Ther.* 11, 1–15. <https://doi.org/10.1186/s13287-020-01601-1>
- Ould-Yahoui, A., Sbai, O., Baranger, K., Bernard, A., Gueye, Y., Charrat, E., Clément, B., Gigmes, D., Dive, V., Girard, S.D., Féron, F., Khrestchatisky, M., Rivera, S., 2013. Role of Matrix Metalloproteinases in Migration and Neurotrophic Properties of Nasal Olfactory Stem and Ensheathing Cells. *Cell Transplant.* 22, 993–1010. <https://doi.org/10.3727/096368912X657468>
- Palm, F., Pussinen, P., Safer, A., Tervahartiala, T., Sorsa, T., Urbanek, C., Becher, H., Grau, A., 2018. Serum matrix metalloproteinase-8, tissue inhibitor of metalloproteinase and myeloperoxidase in ischemic stroke. *Atherosclerosis* 271, 9–14. <https://doi.org/10.1016/J.ATHEROSCLEROSIS.2018.02.012>
- Park, K., Rosell, A., Foerch, C., Xing, C., Kim, W., Lee, S., Opdenakker, G., Furie, K., Lo, E., 2009. Plasma and brain matrix metalloproteinase-9 after acute focal cerebral ischemia in rats. *Stroke* 40, 2836–2842. <https://doi.org/10.1161/STROKEAHA.109.554824>
- Pascual-Leone, A., Amedi, A., Fregni, F., Merabet, L.B., 2005. The plastic human brain cortex. *Annu. Rev. Neurosci.* 28, 377–401.

<https://doi.org/10.1146/annurev.neuro.27.070203.144216>

Patel, A.T., Duncan, P.W., Lai, S.-M., Studenski, S., 2000. The Relation Between Impairments and Functional Outcomes Poststroke. *Arch. Phys. Med. Rehabil.* 81, 1357–1363. <https://doi.org/10.1053/apmr.2000.9397>

Percie Du Sert, N., Alfieri, A., Allan, S.M., Vo Carswell, H., Deuchar, G.A., Farr, T.D., Flecknell, P., Gallagher, L., Gibson, C.L., Haley, M.J., Macleod, M.R., Mccoll, B.W., Mccabe, C., Morancho, A., Df Moon, L., O'Neill, M.J., Pé Rez De Puig, I., Planas, A., Ragan, I., Rosell, A., Roy, L.A., Ryder, K.O., Simats, A., Sena, E.S., Sutherland, B.A., Tricklebank, M.D., Trueman, R.C., Whitfield, L., Wong, R., Macrae, I.M., 2017. The IMPROVE Guidelines (Ischaemia Models: Procedural Refinements Of in Vivo Experiments). *J. Cereb. Blood Flow Metab.* 37, 3488–3517. <https://doi.org/10.1177/0271678X17709185>

Peterson JN, Evans JP (1937) The anatomical end results of cerebral artery occlusion: an experimental and clinical correlation. *Trans Am Neurol Assoc* 63:83–88

Pope, C.A., Burnett, R.T., Thurston, G.D., Thun, M.J., Calle, E.E., Krewski, D., Godleski, J.J., 2004. Cardiovascular Mortality and Long-Term Exposure to Particulate Air Pollution: Epidemiological Evidence of General Pathophysiological Pathways of Disease. *Circulation* 109, 71–77. <https://doi.org/10.1161/01.CIR.0000108927.80044.7F>

Pöss, J., Lorenz, D., Werner, C., Pavlikova, V., Gensch, C., Speer, T., Alessandrini, F., Berezowski, V., Kuntz, M., Mempel, M., Endres, M., Böhm, M., Laufs, U., 2013. Diesel exhaust particles impair endothelial progenitor cells, compromise endothelial integrity, reduce neoangiogenesis, and increase atherogenesis in mice. *Cardiovasc. Toxicol.* 13, 290–300. <https://doi.org/10.1007/s12012-013-9208-0>

Qin, A.-P., Zhang, H.-L., Qin, Z.-H., 2008. Mechanisms of lysosomal proteases participating in cerebral ischemia-induced neuronal death. *Neurosci Bull* 24, 117–123. <https://doi.org/10.1007/s12264-008-0117-3>

- Rempe, R.G., Hartz, A.M.S., Bauer, B., 2016. Matrix metalloproteinases in the brain and blood-brain barrier: Versatile breakers and makers. *J. Cereb. Blood Flow Metab.* 36, 1481–1507. <https://doi.org/10.1177/0271678X16655551>
- Riba-Llena, I., Jarca, C.I., Mundet, X., Tovar, J.L., Orfila, F., López-Rueda, A., Nafria, C., Fernández, J.L., Castañé, X., Domingo, M., Álvarez-Sabín, J., Fernández-Cortiñas, I., Maisterra, O., Montaner, J., Delgado, P., 2013. Investigating silent strokes in hypertensives: A magnetic resonance imaging study (ISSYS): Rationale and protocol design. *BMC Neurol.* 13, 1–8. <https://doi.org/10.1186/1471-2377-13-130>
- Rich, D.Q., Kipen, H.M., Huang, W., Wang, G., Wang, Y., Zhu, P., Ohman-Strickland, P., Hu, M., Philipp, C., Diehl, S.R., Lu, S.E., Tong, J., Gong, J., Thomas, D., Zhu, T., Zhang, J., 2012. Association between changes in air pollution levels during the Beijing olympics and biomarkers of inflammation and thrombosis in healthy young adults. *JAMA - J. Am. Med. Assoc.* 307, 2068–2078. <https://doi.org/10.1001/jama.2012.3488>
- Robinson, R.K., Birrell, M.A., Adcock, J.J., Wortley, M.A., Dubuis, E.D., Chen, S., McGilvery, C.M., Hu, S., Shaffer, M.S.P., Bonvini, S.J., Maher, S.A., Mudway, I.S., Porter, A.E., Carlsten, C., Tetley, T.D., Belvisi, M.G., 2018. Mechanistic link between diesel exhaust particles and respiratory reflexes. *J. Allergy Clin. Immunol.* 141, 1074–1084. <https://doi.org/10.1016/J.JACI.2017.04.038>
- Rosell, A., Agin, V., Rahman, M., Morancho, A., Ali, C., Koistinaho, J., Wang, X., Vivien, D., Schwaninger, M., 2013a. Distal Occlusion of the Middle Cerebral Artery in Mice : Are We Ready to Assess Long-Term Functional Outcome ? *Transl. Stroke Res.* 4, 297–307. <https://doi.org/10.1007/s12975-012-0234-1>
- Rosell, A., Alvarez-Sabín, J., Arenillas, J., Rovira, A., Delgado, P., Fernández-Cadenas, I., Penalba, A., Molina, C., Montaner, J., 2005. A matrix metalloproteinase protein array reveals a strong relation between MMP-9 and MMP-13 with diffusion-weighted image lesion increase in human stroke. *Stroke* 36, 1415–1420. <https://doi.org/10.1161/01.STR.0000170641.01047.CC>
- Rosell, A., Morancho, A., Hernandez, M., Navarro-sobrino, M., Martí, E., Borra, F.,

- Lope-piedrafita, S., Montaner, J., 2013b. Factors Secreted by Endothelial Progenitor Cells Enhance Neurorepair Responses after Cerebral Ischemia in Mice. *PLoS One* 8, 1–10. <https://doi.org/10.1371/journal.pone.0073244>
- Rosell, A., Ortega-Aznar, A., Alvarez-Sabín, J., Fernández-Cadenas, J., Ribó, M., Molina, C., Lo, E., Montaner, J., 2006. Increased brain expression of matrix metalloproteinase-9 after ischemic and hemorrhagic human stroke. *Stroke* 37, 1399–1406. <https://doi.org/10.1161/01.STR.0000223001.06264.AF>
- Roth, S., Liesz, A., 2016. Stroke research at the crossroads – where are we heading? *Swiss Med. Wkly.* 1–10. <https://doi.org/10.4414/smw.2016.14329>
- Samary, C.S., Ramos, A.B., Maia, L.A., Rocha, N.N., Santos, C.L., Magalhães, R.F., Clevelario, A.L., Pimentel-Coelho, P.M., Mendez-Otero, R., Cruz, F.F., Capelozzi, V.L., Ferreira, T.P.T., Koch, T., De Abreu, M.G., Dos Santos, C.C., Pelosi, P., Silva, P.L., Rocco, P.R.M., 2018. Focal ischemic stroke leads to lung injury and reduces alveolar macrophage phagocytic capability in rats. *Crit. Care* 22, 1–11. <https://doi.org/10.1186/s13054-018-2164-0>
- Santamaría, A., Oliver, A., Borrell, M., Mateo, J., Belvis, R., Martí-Fàbregas, J., Ortín, R., Tirado, I., Souto, J.C., Fontcuberta, J., 2003. Risk of Ischemic Stroke Associated With Functional Thrombin-Activatable Fibrinolysis Inhibitor Plasma Levels. *Stroke* 34, 2387–2391. <https://doi.org/10.1161/01.STR.0000088642.07691.15>
- Scheers, H., Jacobs, L., Casas, L., Nemery, B., Nawrot, T.S., 2015. Long-Term Exposure to Particulate Matter Air Pollution Is a Risk Factor for Stroke: Meta-Analytical Evidence. *Stroke* 46, 3058–3066. <https://doi.org/10.1161/STROKEAHA.115.009913>
- Schyns, J., Bureau, F., Marichal, T., 2018. Lung Interstitial Macrophages: Past, Present, and Future. *J. Immunol. Res.* 2018. <https://doi.org/10.1155/2018/5160794>
- Shin, H.H., Fann, N., Burnett, R.T., Cohen, A., Hubbell, B.J., 2014. Outdoor fine particles and nonfatal strokes: Systematic review and meta-analysis.

- Epidemiology 25, 835–842. <https://doi.org/10.1097/EDE.0000000000000162>
- Sommer, C.J., 2017. Ischemic stroke: experimental models and reality. *Acta Neuropathol.* 133, 245–261. <https://doi.org/10.1007/s00401-017-1667-0>
- Song, C., He, J., Wu, L., Jin, T., Chen, X., Li, R., Ren, P., Zhang, L., Mao, H., 2017. Health burden attributable to ambient PM_{2.5} in China. *Environ. Pollut.* 1–12. <https://doi.org/10.1016/j.envpol.2017.01.060>
- Stafoggia, M., Cesaroni, G., Peters, A., Andersen, Z., Badaloni, C., Beelen, R., Caracciolo, B., Cyrus, J., de Faire, U., de Hoogh, K., Eriksen, K., Fratiglioni, L., Galassi, C., Gigante, B., Havulinna, A., Hennig, F., Hilding, A., Hoek, G., Hoffmann, B., D, H., M, K., T, L., K, L., PK, M., C, M., E, M., K, O., CG, O., NL, P., J, P., J, P., G, P., N, P., A, P., O, R.-N., A, R., F, R., C, S., WJ, S., AW, T., P, V., C, W., G, W., K, W., B, B., F, F., 2014. Long-term exposure to ambient air pollution and incidence of cerebrovascular events: results from 11 European cohorts within the ESCAPE project. *Environ. Health Perspect.* 122, 919–925. <https://doi.org/10.1289/EHP.1307301>
- Stamenkovic, I., 2003. Extracellular matrix remodelling: the role of matrix metalloproteinases. *J. Pathol.* 200, 448–464. <https://doi.org/10.1002/PATH.1400>
- Strak, M., Weinmayr, G., Rodopoulou, S., Chen, J., Hoogh, K. de, Andersen, Z.J., Atkinson, R., Bauwelinck, M., Bekkevold, T., Bellander, T., Boutron-Ruault, M.-C., Brandt, J., Cesaroni, G., Concin, H., Fecht, D., Forastiere, F., Gulliver, J., Hertel, O., Hoffmann, B., Hvidtfeldt, U.A., Janssen, N.A.H., Jöckel, K.-H., Jørgensen, J.T., Ketzel, M., Klompmaker, J.O., Lager, A., Leander, K., Liu, S., Ljungman, P., Magnusson, P.K.E., Mehta, A.J., Nagel, G., Oftedal, B., Pershagen, G., Peters, A., Raaschou-Nielsen, O., Renzi, M., Rizzuto, D., Schouw, Y.T. van der, Schramm, S., Severi, G., Sigsgaard, T., Sørensen, M., Stafoggia, M., Tjønneland, A., Verschuren, W.M.M., Vienneau, D., Wolf, K., Katsouyanni, K., Brunekreef, B., Hoek, G., Samoli, E., 2021. Long term exposure to low level air pollution and mortality in eight European cohorts within the ELAPSE project: pooled analysis. *BMJ* 374, n1904.

<https://doi.org/10.1136/BMJ.N1904>

Suofu, Y., Clark, J.F., Broderick, J.P., Kurosawa, Y., Wagner, K.R., Lu, A., 2012. Matrix metalloproteinase-2 or -9 deletions protect against hemorrhagic transformation during early stage of cerebral ischemia and reperfusion. *Neuroscience* 212. <https://doi.org/10.1016/J.NEUROSCIENCE.2012.03.036>

Suwannasual, U., Lucero, J.A., McDonald, J.D., Lund, A.K., 2018. Exposure to traffic-generated air pollutants mediates alterations in brain microvascular integrity in wildtype mice on a high-fat diet. *Environ. Res.* 160, 449–461. <https://doi.org/10.1016/j.envres.2017.10.029>

Suzuki, Y., Nagai, N., Umemura, K., Collen, D., Lijnen, H., 2007. Stromelysin-1 (MMP-3) is critical for intracranial bleeding after t-PA treatment of stroke in mice. *J. Thromb. Haemost.* 5, 1732–1739. <https://doi.org/10.1111/J.1538-7836.2007.02628.X>

Sztriha, L.K., O'Gorman, R.L., Mado, M., Barker, G.J., Williams, S.C.R., Kalra, L., 2012. Monitoring brain repair in stroke using advanced magnetic resonance imaging. *Stroke* 43, 3124–3131. <https://doi.org/10.1161/STROKEAHA.111.649244>

Tamura, A., Graham, D.I., McCulloch, J., Teasdale, G.M., 1981. Focal cerebral ischaemia in the rat: I. Description of technique and early neuropathological consequences following middle cerebral artery occlusion. *J. Cereb. Blood Flow Metab.* 1, 53–60. <https://doi.org/10.1038/jcbfm.1981.6>

Teng, H., Zhang, Z.G., Wang, L., Zhang, R.L., Zhang, L., Morris, D., Gregg, S.R., Wu, Z., Jiang, A., Lu, M., Zlokovic, B. V, Chopp, M., 2007. Coupling of Angiogenesis and Neurogenesis in Cultured Endothelial Cells and Neural Progenitor Cells after Stroke: *J. Cereb. Blood Flow Metab.* 28, 764–771. <https://doi.org/10.1038/SJ.JCBFM.9600573>

Thompson, A.M.S., Zanobetti, A., Silverman, F., Schwartz, J., Coull, B., Urch, B., Speck, M., Brook, J.R., Manno, M., Gold, D.R., 2010. Baseline repeated measures from controlled human exposure studies: Associations between

- ambient air pollution exposure and the systemic inflammatory biomarkers IL-6 and fibrinogen. *Environ. Health Perspect.* 118, 120–124. <https://doi.org/10.1289/ehp.0900550>
- Tian, Y., Liu, H., Zhao, Z., Xiang, X., Li, M., Juan, J., Song, J., Cao, Y., Wang, X., Chen, L., Wei, C., Hu, Y., Gao, P., 2018. Association between ambient air pollution and daily hospital admissions for ischemic stroke: A nationwide time-series analysis. *PLoS Med.* 15, 1–16. <https://doi.org/10.1371/journal.pmed.1002668>
- Tobwala, S., Zhang, X., Zheng, Y., Wang, H.J., Banks, W.A., Ercal, N., 2013. Disruption of the integrity and function of brain microvascular endothelial cells in culture by exposure to diesel engine exhaust particles. *Toxicol. Lett.* 220, 1–7. <https://doi.org/10.1016/j.toxlet.2013.03.023>
- Undas, A., Slowik, A., Wolkow, P., Szczudlik, A., Tracz, W., 2010. Fibrin clot properties in acute ischemic stroke: relation to neurological deficit. *Thromb. Res.* 125, 357–361. <https://doi.org/10.1016/j.thromres.2009.11.013>
- United Nations Department of Economic and Social Affairs Population, 2018. World Urbanization Prospects, Demographic Research.
- Virani, S.S., Alonso, A., Aparicio, H.J., Benjamin, E.J., Bittencourt, M.S., Callaway, C.W., Carson, A.P., Chamberlain, A.M., Cheng, S., Delling, F.N., Elkind, M.S. V, Evenson, K.R., Ferguson, J.F., Gupta, D.K., Khan, S.S., Kissela, B.M., Knutson, K.L., Lee, C.D., Lewis, T.T., Liu, J., Loop, M.S., Lutsey, P.L., Ma, J., Mackey, J., Martin, S.S., Matchar, D.B., Mussolino, M.E., Navaneethan, S.D., Perak, A.M., Roth, G.A., Samad, Z., Satou, G.M., Schroeder, E.B., Shah, S.H., Shay, C.M., Stokes, A., Vanwagner, L.B., Wang, N.-Y., Tsao, C.W., Chair, V., 2021. Heart Disease and Stroke Statistics-2021 Update A Report From the American Heart Association. *Circulation* 143, 254–743. <https://doi.org/10.1161/CIR.0000000000000950>
- Vivanco-Hidalgo, R.M., Wellenius, G., Basagaña, X., Cirach, M., González, A.G., Ceballos, P. de, Zabalza, A., Jiménez-Conde, J., Soriano-Tarraga, C., Giralte-Steinhauer, E., Alastuey, A., Querol, X., Sunyer, J., Roquer, J., 2018. Short-term exposure to traffic-related air pollution and ischemic stroke onset in

- Barcelona, Spain. Environ. Res. 162, 160–165.
<https://doi.org/10.1016/j.envres.2017.12.024>
- Vogelgesang, A., Becker, K., Dressel, A., 2014. Immunological consequences of ischemic stroke. Acta Neurol. Scand. 129, 1–12.
<https://doi.org/10.1111/ane.12165>
- Wang, J., Liu, Y., Jiao, F., Lao, F., Li, W., Gu, Y., Li, Y., Ge, C., Zhou, G., Li, B., Zhao, Y., Chai, Z., Chen, C., 2008. Time-dependent translocation and potential impairment on central nervous system by intranasally instilled TiO₂ nanoparticles. Toxicology 254, 82–90.
<https://doi.org/10.1016/j.tox.2008.09.014>
- Wang, Y., Eliot, M.N., Wellenius, G.A., 2014. Short-term changes in ambient particulate matter and risk of stroke: A systematic review and meta-analysis. J. Am. Heart Assoc. 3, 1–22. <https://doi.org/10.1161/JAHA.114.000983>
- Wang, Z., Peng, J., Liu, P., Duan, Y., Huang, S., Wen, Y., Liao, Y., Li, H., Yan, S., Cheng, J., Yin, P., 2020. Association between short-term exposure to air pollution and ischemic stroke onset: a time-stratified case-crossover analysis using a distributed lag nonlinear model in Shenzhen, China. Environ. Heal. 19, 1–12. <https://doi.org/10.1186/S12940-019-0557-4>
- Weber, 2019. EL ATLAS DEL ICTUS EN ESPAÑA.
- Wilker, E., Mostofsky, E., Lue, S.-H., Gold, D., Schwartz, J., 2013. Residential proximity to high traffic roadways and post-stroke mortality. J. stroke Cerebrovasc. diseases 22, 366–372. <https://doi.org/10.1088/0031-9155/55/20/011.DigiWarp>
- Win-Shwe, T.-T., Fujitani, Y., Kyi-Tha-Thu, C., Furuyama, A., Michikawa, T., Tsukahara, S., Nitta, H., Hirano, S., 2014. Effects of Diesel Engine Exhaust Origin Secondary Organic Aerosols on Novel Object Recognition Ability and Maternal Behavior in BALB/C Mice. Int. J. Environ. Res. Public Health 11, 11286–11307. <https://doi.org/10.3390/ijerph111111286>
- Win-Shwe, T.-T., Fujitani, Y., Sone, H., Furuyama, A., Nitta, H., Hirano, S., 2012. Effects of acute single intranasal instillation of secondary organic aerosol on

- neurological and immunological biomarkers in the brain and lung of BALB/c mice. *J. Toxicol. Sci.* 38, 71–82. <https://doi.org/10.2131/jts.38.71>
- Win-Shwe, T.-T., Yamamoto, S., Ahmed, S., Kakeyama, M., Kobayashi, T., Fujimaki, H., 2006. Brain cytokine and chemokine mRNA expression in mice induced by intranasal instillation with ultrafine carbon black. *Toxicol. Lett.* 163, 153–160. <https://doi.org/10.1016/j.toxlet.2005.10.006>
- Winklewski, P.J., Radkowski, M., Demkow, U., 2014. Cross-talk between the inflammatory response, sympathetic activation and pulmonary infection in the ischemic stroke. *J. Neuroinflammation* 11, 1–8. <https://doi.org/10.1186/s12974-014-0213-4>
- Wong, C.H.Y., Jenne, C.N., Lee, W.Y., Léger, C., Kubes, P., 2011. Functional innervation of hepatic iNKT cells is immunosuppressive following stroke. *Science (80-.)*. 334, 101–105. <https://doi.org/10.1126/science.1210301>
- Woodward, N.C., Haghani, A., Johnson, R.G., Hsu, T.M., Saffari, A., Sioutas, C., Kanoski, S.E., Finch, C.E., Morgan, T.E., 2018. Prenatal and early life exposure to air pollution induced hippocampal vascular leakage and impaired neurogenesis in association with behavioral deficits. *Transl. Psychiatry* 8, 1–10. <https://doi.org/10.1038/s41398-018-0317-1>
- World Health Organization, 2021. Global Air Quality Guidelines, particulate matter, ozone, nitrogen dioxide, sulfur dioxide and carbon monoxide.
- World Health Organization, 2005. Global Air Quality Guidelines, particulate matter, ozone, nitrogen dioxide, sulfur dioxide and carbon monoxide. [https://doi.org/10.1016/0004-6981\(88\)90109-6](https://doi.org/10.1016/0004-6981(88)90109-6)
- Wu, L., Rodríguez-Rodríguez, C., Cun, D., Yang, M., Saatchi, K., Häfeli, U.O., 2020. Quantitative comparison of three widely-used pulmonary administration methods in vivo with radiolabeled inhalable nanoparticles. *Eur. J. Pharm. Biopharm.* 152, 108–115. <https://doi.org/10.1016/j.ejpb.2020.05.004>
- Xing, C., Arai, K., Lo, E.H., Hommel, M., 2012. Pathophysiologic cascades in ischemic stroke. *Int. J. Stroke* 7, 378–385. <https://doi.org/10.1111/j.1747->

4949.2012.00839.x

Xu, H., Wang, T., Liu, S., Brook, R.D., Feng, B., Zhao, Q., Song, X., Yi, T., Chen, J., Zhang, Y., Wang, Y., Zheng, L., Rajagopalan, S., Li, J., Huang, W., 2019. Extreme Levels of Air Pollution Associated with Changes in Biomarkers of Atherosclerotic Plaque Vulnerability and Thrombogenicity in Healthy Adults: The Beijing AIRCHD Study. *Circ. Res.* 124, 30–43. <https://doi.org/10.1161/CIRCRESAHA.118.313948>

Yang, B., Guo, J., Xiao, C., 2018. Effect of PM2.5 environmental pollution on rat lung. *Environ. Sci. Pollut. Res.* 25, 36136–36146. <https://doi.org/10.1007/s11356-018-3492-y>

Yang, C., Candelario-Jalil, E., 2017. Role of Matrix Metalloproteinases in Brain Edema, Brain Edema: From Molecular Mechanisms to Clinical Practice. Elsevier Inc. <https://doi.org/10.1016/B978-0-12-803196-4.00011-4>

Yang, Q., Huang, Q., Hu, Z., Tang, X., 2019. Potential neuroprotective treatment of stroke: Targeting excitotoxicity, oxidative stress, and inflammation. *Front. Neurosci.* 13, 1–7. <https://doi.org/10.3389/fnins.2019.01036>

Yang, Y., Estrada, E., Thompson, J., Liu, W., Rosenberg, G., 2007. Matrix metalloproteinase-mediated disruption of tight junction proteins in cerebral vessels is reversed by synthetic matrix metalloproteinase inhibitor in focal ischemia in rat. *J. Cereb. blood flow Metab.* 27, 697–709. <https://doi.org/10.1038/SJ.JCBFM.9600375>

Yang, Y., Rosenberg, G.A., 2015. Matrix metalloproteinases as therapeutic targets for stroke. *Brain Res.* 14, 30–38. <https://doi.org/10.1016/j.cogdev.2010.08.003>. Personal

Yang Li, X., Brown, D., Smit, S., MacNee, W., Donaldson, K., 1999. SHORT-TERM INFLAMMATORY RESPONSES FOLLOWING INTRATRACHEAL INSTILLATION OF FINE AND ULTRAFINE CARBON BLACK IN RATS. *Inhal. Toxicol.* 11, 709–731.

Yu, Y.R.A., O'Koren, E.G., Hotten, D.F., Kan, M.J., Kopin, D., Nelson, E.R., Que, L., Gunn, M.D., 2016. A protocol for the comprehensive flow cytometric analysis

- of immune cells in normal and inflamed murine non-lymphoid tissues. *PLoS One* 11, 1–23. <https://doi.org/10.1371/journal.pone.0150606>
- Zhang, C., Meng, Q., Zhang, X., Wu, S., Wang, S., Chen, R., Li, X., 2016. Role of astrocyte activation in fine particulate matter-enhancement of existing ischemic stroke in Sprague-Dawley male rats. *J. Toxicol. Environ. Heal. - Part A Curr. Issues* 79, 393–401. <https://doi.org/10.1080/15287394.2016.1176615>
- Zhang, Y., Fan, F., Zeng, G., Zhou, L., Zhang, Y., lao, H., Zhang, T., Su, D., Yang, C., Xiao, K., Li, H., Zhong, Z., 2017. Temporal analysis of blood-brain barrier disruption and cerebrospinal fluid matrix metalloproteinases in rhesus monkeys subjected to transient ischemic stroke. *J. Cereb. blood flow Metab.* 37, 2963–2974. <https://doi.org/10.1177/0271678X16680221>
- Zhao, B.Q., Wang, S., Kim, H.Y., Storrie, H., Rosen, B.R., Mooney, D.J., Wang, X., Lo, E.H., 2006. Role of matrix metalloproteinases in delayed cortical responses after stroke. *Nat. Med.* 12, 441–445. <https://doi.org/10.1038/nm1387>
- Zhou, H., Kobzik, L., 2007. Effect of concentrated ambient particles on macrophage phagocytosis and killing of *Streptococcus pneumoniae*. *Am. J. Respir. Cell Mol. Biol.* 36, 460–465. <https://doi.org/10.1165/RCMB.2006-0293OC>
- Zhuang, P., Wo, D., Xu, Z.-G., Wei, W., Mao, H.-M., 2015. Clinical Study Dynamic changes in plasma tissue plasminogen activator, plasminogen activator inhibitor-1 and beta-thromboglobulin content in ischemic stroke. *J. Clin. Neurosci.* 22, 1123–1127. <https://doi.org/10.1016/j.jocn.2014.12.027>
- Zinnhardt, B., Viel, T., Wachsmuth, L., Vrachimis, A., Wagner, S., Breyholz, H.-J., Faust, A., Hermann, S., Kopka, K., Faber, C., Dollé, F., Pappata, S., Planas, A.M., Tavitian, B., Schäfers, M., Sorokin, L.M., Kuhlmann, M.T., Jacobs, A.H., 2015. Multimodal imaging reveals temporal and spatial microglia and matrix metalloproteinase activity after experimental stroke. *J. Cereb. Blood Flow Metab.* 35, 1711. <https://doi.org/10.1038/JCBFM.2015.149>

Annex I

SCIENTIFIC CARREER OF THE DOCTORAL STUDENT

Academic education

- **PhD in Neuroscience** (2018-2021). Universidad Autónoma de Barcelona. "Diesel exhaust particles and blablabla" Neurovascular Research Laboratory, Vall d'Hebron Institut de Recerca (VHIR), Barcelona.
- **Master in Pharmacological Research** (2016-2017). Universidad Autónoma de Madrid. "Treatment with exosomes in a model of ischemic stroke to study neural repair and recovery". Neuroscience and cerebrovascular diseases Laboratory, Instituto de Investigación Universitario La Paz (IdiPAZ), Madrid.
- **Internship** (2013). "Implication of amygdalar release of cholecystokinin in activation of the descending controls of pain in persistent pain model in the rat" Central Mechanisms of pain sensitization Laboratory, IINS, Bordeaux.
- **Biology degree, Neurobiology specialization** (2007-2013). Universidad Complutense de Madrid. "Detección del sistema orexinérgico y su posible interacción con el sistema monoaminérgico en *Polypterus senegallus*" Laboratorio de biología celular, UCM.

Scientific production

- Grayston, A., Zhang, Y., Garcia-Gabilondo, M., **Arrúe, M.**, Martin, A., Kopcansky, P., Timko, M., Kovac, J., Strbak, O., Castellote, L., Belloli, S., Moresco, R. M., Picchio, M., Roig, A., & Rosell, A. (2021). *Endovascular administration of magnetized nanocarriers targeting brain delivery after stroke*. Journal of Cerebral Blood Flow and Metabolism, 1–16. <https://doi.org/10.1177/0271678X211028816>
- Otero-Ortega, L., Laso-García, F., Frutos, M. C. G. De, Diekhorst, L., Martínez-Arroyo, A., Alonso-López, E., García-Bermejo, M. L., Rodríguez-Serrano, M., **Arrúe-Gonzalo, M.**, Díez-Tejedor, E., Fuentes, B., & Gutiérrez-Fernández, M. (2020). *Low dose of extracellular vesicles identified that promote recovery after ischemic stroke*. Stem Cell Research and Therapy, 11(1), 70. <https://doi.org/10.1186/s13287-020-01601-1>
- Pradillo, J. M., Grayston, A., Medina-alonso, V., **Arrúe, M.**, & Rosell, A. (2019). *Effects of aging and comorbidities on endothelial progenitor cells*. Conditioning Medicine, 2(1), 18–29.

Congresses

- Virtual attendance and poster presentation at the **VII European Stroke Organization-Congress** (1st-3rd of September 2021) with the title: *Exposure to air pollutants such as Diesel exhaust particles modifies the thrombogenic properties of plasma in the context of ischemic stroke.*
- Virtual attendance to the **1st International Stroke-Immunology Conference** (1st-3rd of March 2021).
- Virtual attendance to the **IV Annual Congress of the Cerebrovascular diseases network-INVICTUS+** (28th of January 2021).
- Attendance and poster presentation at the **XIII Hospital Vall d'Hebron-Scientific Session** (12th-13th of December 2019, Barcelona, Spain) with the title: *Traffic-related pollution can alter levels of matrix metalloproteinases in brain and lungs after cerebral ischemia in mice.*
- Attendance and oral communication at the **VII Neuroscience Institute-Conference** (1st-3rd of October 2019, Sant Feliu de Guíxols, Spain) with the title: *Traffic-related pollution can alter levels of matrix metalloproteinases in brain and lungs after cerebral ischemia in mice.*
- Attendance and poster presentation at the **V European Stroke Organization-Congress** (22nd-24th of May 2019, Milan, Italy) with the title: *Traffic-related pollution reduces the levels of matrix metalloproteinases in hippocampus and striatum after cerebral ischemia in mice.*
- Attendance and poster presentation at the **VIII session in recent molecular advances in neuropathology** with the title: *Familial Alzheimer model using hiN cells* (27th-31st of May 2013, Madrid, Spain).

Courses

- **Good Clinical Practice in Research** (2021). Vall d'Hebron Hospital.
- **Introduction to International Health** (2019). PROSICS.
- **Scientific English** (2017). La Paz Hospital.
- **Laboratory animal training course (A, B, C, D)** (2017).

Annex II



National Institute of Standards & Technology

Certificate of Analysis

Standard Reference Material[®] 2975

Diesel Particulate Matter (Industrial Forklift)

This Standard Reference Material (SRM) is intended for use in evaluating analytical methods for the determination of selected polycyclic aromatic hydrocarbons (PAHs) and nitro-substituted PAHs (nitro-PAHs) in diesel particulate matter and similar matrices. In addition to certified, reference, and information values for selected PAHs and nitro-PAHs, reference or information values are provided for total extractable mass, particle-size distribution, and specific surface area; supplemental information on mutagenic activity is also provided. All of the chemical constituents for which certified, reference, and information values are provided are naturally present in the diesel particulate material. A unit of SRM 2975 consists of a bottle containing 1 g of the diesel particulate matter collected from an industrial diesel-powered forklift.

SRM 1975 Diesel Particulate Extract [1], which is a dichloromethane extract of the diesel particulate matter, was prepared from the same lot of material as SRM 2975. A second diesel particulate material, SRM 1650b Diesel Particulate Matter [2], which was originally issued in 1985, is representative of heavy-duty diesel engine particulate emissions.

Certified Mass Fraction Values: Certified values are provided for PAHs in Table 1 and nitro-PAHs in Table 2. A NIST certified value is a value for which NIST has the highest confidence in its accuracy, in that all known or suspected sources of bias have been investigated or taken into account [3]. The certified values for the PAHs and nitro-PAHs are based on the agreement of results obtained at NIST from two or more independent analytical methods [3].

Reference Mass Fraction Values: Reference values are provided for additional PAHs in Table 3 and nitro-PAHs in Table 4. Some PAHs and nitro-PAHs are listed more than once in the table depending on the extraction conditions used (see "Preparation and Analysis"). Reference values for total extractable mass and the particle-size distribution are provided in Tables 5 and 6, respectively. Reference values are noncertified values that represent the best estimates of the true value; however, the values do not meet the NIST criteria for certification and are provided with associated uncertainties that may reflect only measurement precision, may not include all sources of uncertainty, or may reflect a lack of sufficient statistical agreement among multiple analytical methods.

Information Values: Information mass fraction values are provided for additional PAHs of relative molecular mass 302 in Table 7 and specific surface area as determined by N₂ gas adsorption is provided in Table 8. An information value is considered to be a value that may be of use to the SRM user, but insufficient information is available to assess the uncertainty associated with the value or only a limited number of analyses were performed.

Expiration of Certification: The certification of **SRM 2975** is valid, within the measurement uncertainty specified, until **31 January 2022**, provided the SRM is handled and stored in accordance with the instructions given in this certificate (see "Instructions for Handling, Storage, and Use"). However, the certification is nullified if the SRM is damaged, contaminated, or otherwise modified.

Maintenance of SRM Certification: NIST will monitor this SRM over the period of its certification. If substantive technical changes occur that affect the certification before the expiration of this certificate, NIST will notify the purchaser. Registration (see attached sheet) will facilitate notification.

Carlos A. Gonzalez, Chief
Chemical Sciences Division

Robert L. Watters, Jr, Director
Office of Reference Materials

Gaithersburg, MD 20899
Certificate Issue Date: 03 December 2013
Certificate Revision History on Last Page

SRM 2975

Page 1 of 11
201

The coordination of the technical measurements leading to the certification of SRM 2975 was under the leadership of M.M. Schantz and S.A. Wise of the NIST Chemical Sciences Division.

Analytical measurements for the certification of SRM 2975 were performed by H.M. Bamford, D. Bezabeh, M. Lopez de Alda, D.L. Poster, L.C. Sander, M.M. Schantz, P. Schubert, and L. Walton of the NIST Chemical Sciences Division. Specific surface area, and porosity data were provided by P. Scheepers of the Department of Epidemiology at Katholieke Universiteit Nijmegen, Nijmegen, The Netherlands. The particle-size distribution data were provided by Honeywell, Inc., Clearwater, FL.

The diesel particulate material was provided by M.E. Wright of the Donaldson Company, Inc., Minneapolis, MN.

Statistical consultation was provided by N.A. Heckert, S.D. Leigh and M.G. Vangel of the NIST Statistical Engineering Division.

Support aspects involved in the issuance of this SRM were coordinated through the NIST Office of Reference Materials.

INSTRUCTIONS FOR HANDLING, STORAGE, AND USE

Handling: This material is a naturally occurring diesel particulate material and contains constituents of known and unknown toxicities and mutagenicities; therefore, extreme caution and care should be exercised during its handling and use.

Storage: Store SRM 2975 in its original bottle at temperatures below 30 °C and keep away from direct sunlight.

Use: Prior to removal of subsamples for analysis, the contents of the bottle should be mixed thoroughly. The recommended minimum sample size is 100 mg.

PREPARATION AND ANALYSIS⁽¹⁾

Sample Collection and Preparation: The diesel particulate material used to prepare SRM 2975 was obtained from M.E. Wright of the Donaldson Company, Inc., Minneapolis, MN. The material was collected from a filtering system designed specifically for diesel-powered forklifts [4]. The diesel particulate material was received at NIST in a 55-gallon drum. The material was removed from the drum and homogenized in a V-blender for 1 h and then stored in polyethylene bags. A total of 13.7 kg of diesel particulate material was homogenized; a total of 5.65 kg of material was extracted for preparation of SRM 2975 [1] and the remaining diesel particulate material was bottled for distribution as SRM 2975.

Polycyclic Aromatic Hydrocarbons (PAHs)

The general approach used for the value assignment of the PAHs in SRM 2975 consisted of combining results from analyses using various combinations of different extraction techniques and solvents, cleanup/isolation procedures, and chromatographic separation and detection techniques. This approach consisted of Soxhlet extraction and pressurized fluid extraction (PFE) using dichloromethane (DCM), toluene, or toluene/methanol mixture, cleanup of the extracts using solid-phase extraction (SPE), followed by analysis using the following techniques: (1) reversed-phase liquid chromatography with fluorescence detection (LC-FL) for analysis of isomeric PAH fractions isolated by normal-phase LC (i.e., multidimensional LC) and (2) gas chromatography/mass spectrometry (GC/MS) for analysis of the PAH fraction on four stationary phases of different selectivity (i.e., a 5 % [mole fraction] phenyl-substituted methylpolysiloxane phase, a 50 % phenyl-substituted methylpolysiloxane phase, a non-polar, extra low bleed proprietary phase, and a smectic liquid crystalline stationary phase).

Multiple sets of GC/MS results, designated as GC/MS (Ia and Ib), GC/MS (II), GC/MS (III), GC/MS (IVa, IVb, and IVc), and GC/MS (Va through Vd), were obtained using three columns with different selectivities for the separation of PAHs.

⁽¹⁾Certain commercial instruments, materials, or processes are identified in this report to adequately specify the experimental procedure. Such identification does not imply recommendation or endorsement by the National Institute of Standards and Technology, nor does it imply that the instruments, materials, or processes identified are necessarily the best available for the purpose.

GC/MS (Ia and Ib): For GC/MS (I) analyses, duplicate subsamples of 100 mg from eight bottles of SRM 2975 were extracted with toluene:methanol (1:1 volume fraction) using PFE as described by Schantz et al. [5]. The excess volume in the PFE cells was filled with clean sodium sulfate. The extracts were concentrated to about 0.5 mL and placed on an aminopropylsilane SPE cartridge from which they were eluted with 20 mL of 2 % DCM in hexane (volume fraction). The eluant was concentrated and then analyzed by GC/MS using a 0.25 mm i.d. \times 60 m fused silica capillary column with a 5 % (mole fraction) phenyl-substituted methylpolysiloxane phase (0.25 μ m film thickness; DB-5MS, Agilent Technologies, Wilmington, DE), and these results are designated as GC/MS (Ia). A subset of 8 of the 16 extracts from GC/MS (Ia) were also analyzed on a 50 % (mole fraction) phenyl-substituted methylpolysiloxane stationary phase (0.25 mm i.d. \times 60 m, 0.25 μ m film thickness; DB-17MS, Agilent Technologies), and these results are designated as GC/MS (Ib).

GC/MS (II through V): For the GC/MS (II) analyses, 100 mg samples of SRM 2975 were extracted with DCM using PFE; the extracts were processed and analyzed as described above for GC/MS (Ia). GC/MS (III) was identical to GC/MS (II) except that Soxhlet extraction with DCM for 18 h was used instead of PFE. For the GC/MS (IV) analyses, subsamples of 40 mg to 100 mg of SRM 2975 were extracted with DCM using PFE and the extracts processed as described above for GC/MS (I). The processed extracts were then analyzed by GC/MS using three different columns: 5 % phenyl methylpolysiloxane [GC/MS (IVa)], 50 % phenyl methylpolysiloxane [GC/MS (IVb)], and a 0.2 mm i.d. \times 25 m (0.15 μ m film thickness) smectic liquid crystalline phase [SB-Smectic, Dionex, Lee Scientific Division, Salt Lake City, UT; GC/MS (IVc)].

In addition, a study investigating the effect of increasing the temperature and pressure used for PFE on the extraction efficiency for PAHs was performed. In this study, the solvent used was toluene although a 9:1 toluene:methanol (volume fraction) was also evaluated. The PFE conditions used included: 100 °C with 13.8 MPa; 100 °C with 20.7 MPa; 200 °C with 13.8 MPa; and 200 °C with 20.7 MPa [methods GC/MS (Va) through GC/MS (Vd), respectively]. Following an SPE step similar to GC/MS (I) above, the processed extracts were analyzed using a non-polar, extra low bleed proprietary phase (0.25 mm i.d. \times 60 m, 0.25 μ m film thickness).

Reversed-Phase Liquid Chromatography with Fluorescence Detection (LC-FL): For the LC-FL analyses, subsamples of approximately 200 mg from each of six bottles of SRM 2975 were Soxhlet-extracted for 20 h using 200 mL of DCM. The extracts were concentrated and processed through aminopropylsilane SPE cartridges as described above for the GC/MS analyses. The processed extract was further fractionated using normal-phase LC on a semi-preparative aminopropylsilane column (μ Bondapak NH₂, 9 mm i.d. \times 30 cm, Waters Associates, Milford, MA) to isolate isomeric PAH fractions as described previously [6–8]. Four fractions were collected containing PAHs of relative molecular mass 178 and 202 (fraction 1), 228 (fraction 2), 252 and 276 (fraction 3), and 278 (fraction 4). All of the PAH fractions were analyzed using a 5 μ m particle-size polymeric octadecylsilane (C₁₈) column (4.6 mm i.d. \times 25 cm, Hypersil-PAH, Keystone Scientific, Inc., Bellefonte, PA) with wavelength-programmed fluorescence detection [7–9]. For all of the GC/MS and LC-FL measurements described above, selected perdeuterated PAHs were added to the diesel particulate samples prior to solvent extraction for use as internal standards for quantification purposes.

PAH Isomers of Relative Molecular Mass (M_r) 302: For the determination of the relative molecular mass (M_r) 302 isomers, samples of approximately 100 mg each were extracted using PFE at 100 °C with DCM as the extraction solvent. The extracts were then concentrated with a solvent change to hexane, passed through an aminopropyl SPE cartridge, and eluted with 40 mL of 10 % DCM in hexane (volume fraction). The processed extract was then analyzed by GC/MS using a 0.25 mm i.d. \times 60 m fused silica capillary column with a 50 % phenyl-substituted methylpolysiloxane phase (0.25 μ m film thickness; DB-17MS). Perdeuterated dibenzo[*a,i*]pyrene was added to the diesel particulate matter prior to extraction for use as an internal standard.

Homogeneity Assessment for PAHs: The homogeneity of SRM 2975 was assessed by analyzing duplicate samples of 100 mg each from eight bottles selected by stratified random sampling. Samples were processed and analyzed as described above for GC/MS (I). Statistically significant differences among bottles were observed for the PAHs at the 100 mg sample size, and this source of uncertainty has been incorporated in the calculation of the uncertainty associated with the assigned values.

Nitro-Substituted Polycyclic Aromatic Hydrocarbons (Nitro-PAHs)

SRM 2975 was analyzed at NIST for the determination of nitro-PAHs. Three sets of three, four, and five samples of SRM 2975 (~100 mg each) were spiked with the following perdeuterated nitro-PAHs for use as internal standards: 9-nitroanthracene-*d*₉, 3-nitrofluoranthene-*d*₉, 1-nitropyrene-*d*₉, and 6-nitrochrysene-*d*₁₁. The samples were extracted using PFE with DCM or toluene as the extraction solvent.

Following concentration, each sample was processed through an aminopropylsilane SPE cartridge using 40 mL of 20 % DCM in hexane (volume fraction). The concentrated eluant was then subjected to normal-phase LC using a semi-preparative amino/cyano-phase column with a mobile phase of 20 % DCM in hexane to isolate the nitro-PAH fraction. The nitro-PAH fraction was analyzed by GC with negative chemical ionization mass spectrometry (GC/NCI-MS) using a 0.25 mm i.d. \times 30 m fused silica capillary column containing a 5 % diphenyl-substituted dimethylsiloxane phase (0.25 μ m film thickness) or a 50 % phenyl-substituted methylpolysiloxane phase (0.25 μ m film thickness). Methane was used as the NCI-MS collision gas. The effect of increasing the temperature and pressure used in PFE was also investigated at NIST for the nitro-PAHs using 100 °C with 13.8 MPa; 100 °C with 20.7 MPa; 200 °C with 13.8 MPa; and 200 °C with 20.7 MPa.

The concentration of 1-nitropyrene was also measured at the Department of Epidemiology at Katholieke Universiteit Nijmegen, Nijmegen, The Netherlands using GC/MS [10].

Value Assignment for PAHs and Nitro-PAHs

The current value assignment of PAHs and nitro-PAHs in SRM 2975 is based on the measurements used when SRM 2975 was issued in 2000 and on recent additional measurements using different extraction conditions. Previous studies on solvent extraction of diesel particulate matter for determination of PAHs indicated that PFE at 100 °C removed higher quantities of higher relative molecular mass PAHs than does Soxhlet extraction [5]. Recent studies on the extraction of PAHs and nitro-PAHs from diesel particulate matter [11–13] have shown that using PFE at 200 °C removes higher quantities of some (not all) PAHs and nitro-PAHs than using PFE at 100 °C. As a result of these studies, value assignment for PAHs and nitro-PAHs in SRM 2975 is based on measurements using PFE at both 100 °C and 200 °C and on limited measurements using Soxhlet extraction. In cases where the quantities of the individual PAHs and nitro-PAHs determined do not change with the extraction method or temperature, the measurements were combined and the resulting values are denoted as certified values. When different results are obtained using PFE at 100 °C or at 200 °C, the values are reported for both temperatures, and they are denoted as reference values. These reference values should be considered as “method dependent” values because they are dependent on the extraction method and temperature.

Total Extractable Mass

For the determination of total extractable mass, six subsamples of approximately 1 g to 2 g of SRM 2975 were Soxhlet-extracted for 18 h with DCM. The extract was concentrated to approximately 20 mL and then filtered to remove particulate matter. Aliquots of 100 μ L to 150 μ L were placed in tared aluminum foil pans; the DCM was evaporated until constant mass was obtained, and then the mass of the remaining residue was determined. The total extractable mass reference value is provided in Table 5.

Particle-Size Information

Dry particle-size distribution measurements for SRM 2975 were obtained as part of a collaborative effort with Honeywell, Inc., Clearwater, FL. A Microtrac particle analyzer, which makes use of light-scattering techniques, was used to measure the particle-size distribution of SRM 2975 [14]. Briefly, a reference beam was used to penetrate a field of particles and the light that scatters in the forward direction from the field is measured. The particle size as a volume distribution is derived via a computer-assisted analysis. From these data, the total volume, average size, and a characteristic width of the particle-size distribution were calculated.

Specific Surface Area and Porosity

The specific surface area and porosity were determined based on nitrogen gas adsorption measurements [15]. The gas adsorption measurements were performed on a NOVA-1200 instrument, Quantachrome Corp., Boynton Beach, FL at 77 K after the samples were outgassed for 24 h at 120 °C under vacuum. The nitrogen isotherms were analyzed using the Brunauer-Emmet-Teller (BET) equation [16] to obtain the surface area (Table 8) and the Barrett-Joyner-Halenda (BJH) method [17] to obtain the porosity. Based on the BJH method, SRM 2975 shows a wide distribution of mesopores, but with substantial outer area. The pore diameter of the particles in SRM 2975 range from 4 nm to 35 nm with the greater number of particles at about 20 nm.

Mutagenicity Activity

The mutagenicity of solvent extracts of SRM 2975 has not been determined; however, the reference values for mutagenicity of SRM 1975 were determined by using the the *Salmonella typhimurium*/mammalian microsome mutagenicity assay and should be applicable to extracts of SRM 2975. SRM 1975 was prepared by Soxhlet extraction using DCM of multiple samples of SRM 2975. Reference values for mutagenic activity for SRM 1975 are reported in the Certificate of Analysis for SRM 1975 [1] and described in detail by Hughes et al. [18].

Table 1. Certified Mass Fraction Values for Selected PAHs in SRM 2975

	Mass Fraction ^(a) (mg/kg)
2-Methylphenanthrene ^(b,c,d,e)	2.22 ± 0.21
1-Methylphenanthrene ^(b,c,d,e,f,g)	0.923 ± 0.057
Triphenylene ^(e,h,i)	5.32 ± 0.24
Benzo[<i>j</i>]fluoranthene ^(g,i,j)	0.819 ± 0.093
Benzo[<i>a</i>]fluoranthene ^(e,g,h)	0.066 ± 0.007
Dibenz[<i>a,h</i> + <i>a,c</i>]anthracene ^(e,f,i)	0.523 ± 0.047
Picene ^(e,f,g,i)	0.902 ± 0.091
Dibenzo[<i>a,e</i>]pyrene ^(e,g)	0.599 ± 0.024
Dibenzo[<i>b,k</i>]fluoranthene ^(e,g)	2.54 ± 0.08

^(a) The certified values are weighted means of the mass fractions from two to six analytical methods [19]. The uncertainty listed with each value is an expanded uncertainty about the mean [19,20], with coverage factor, $k = 2$, calculated by combining within method variances with a between method variance [21] following the ISO/JCGM Guide [22,23].

^(b) GC/MS (Ia) on 5 % phenyl-substituted methylpolysiloxane phase after PFE with toluene:methanol mixture (100 °C with 13.8 MPa)

^(c) GC/MS (II) on 5 % phenyl-substituted methylpolysiloxane phase after PFE with DCM (100 °C with 13.8 MPa)

^(d) GC/MS (III) on 5 % phenyl-substituted methylpolysiloxane phase after Soxhlet extraction with DCM

^(e) GC/MS (V) on non-polar extra low bleed proprietary phase after PFE with toluene at two temperatures and two pressures (100 °C with 13.8 MPa; 100 °C with 20.7 MPa; 200 °C with 13.8 MPa; and 200 °C with 20.7 MPa)

^(f) GC/MS (IVa) on 5 % phenyl-substituted methylpolysiloxane phase after PFE with DCM (100 °C with 13.8 MPa)

^(g) GC/MS (IVb) on 50 % phenyl-substituted methylpolysiloxane phase of same extracts as GC/MS (IVa)

^(h) GC/MS (IVc) on a smectic liquid crystalline phase of same extracts as GC/MS (IVa)

⁽ⁱ⁾ LC FL of isomeric PAH fractions after Soxhlet extraction with DCM

^(j) GC/MS (Ib) on 50 % phenyl-substituted methylpolysiloxane phase of selected extracts from GC/MS (Ia)

Table 2. Certified Mass Fraction Values for Selected Nitro-PAHs in SRM 2975

	Mass Fraction ^(a) (mg/kg)
9-Nitrophenanthrene ^(b)	0.466 ± 0.013
3-Nitrophenanthrene ^(c)	0.190 ± 0.007
2-Nitrofluoranthene ^(c)	0.231 ± 0.032
3-Nitrofluoranthene ^(b)	3.80 ± 0.24
1-Nitropyrene ^(b)	35.2 ± 2.2
7-Nitrobenz[<i>a</i>]anthracene ^(b)	3.57 ± 0.32
6-Nitrochrysene ^(b)	2.45 ± 0.33

^(a) The certified values are weighted means of the mass fractions from two to six analytical methods [19]. The uncertainty listed with each value is an expanded uncertainty about the mean [19,20], with coverage factor, $k = 2$, calculated by combining within method variances with a between method variance [21] following the JCGM Guide [22,23].

^(b) Three methods using GC/NCI-MS on either a 5 % phenyl-substituted or 50 % phenyl-substituted methylpolysiloxane phase after PFE with DCM (100 °C with 13.8 MPa) and four methods using GC/NCI-MS on a 50 % phenyl-substituted methylpolysiloxane phase after PFE with toluene at two temperatures and two pressures (100 °C with 13.8 MPa; 100 °C with 20.7 MPa; 200 °C with 13.8 MPa; and 200 °C with 20.7 MPa)

^(c) Two methods using GC/NCI-MS on a 5 % phenyl-substituted methylpolysiloxane phase after PFE with DCM (100 °C with 13.8 MPa) and four methods using GC/NCI-MS on a 50 % phenyl-substituted methylpolysiloxane phase after PFE with toluene at two temperatures and two pressures (100 °C with 13.8 MPa; 100 °C with 20.7 MPa; 200 °C with 13.8 MPa; and 200 °C with 20.7 MPa)

Table 3. Reference Mass Fraction Values for Selected PAHs in SRM 2975
Based on Extraction Method and Conditions

Extraction Conditions	Mass Fractions ^(a) (mg/kg)		
Soxhlet Extraction or PFE at 100 °C			
Naphthalene ^(b,c,d,e)	1.78	±	0.48
Biphenyl ^(e)	0.323	±	0.014 ^(f)
Fluorene ^(e,g,h,i)	0.440	±	0.071
Phenanthrene ^(b,c,d,e,g,h,i)	17.3	±	1.0
Anthracene ^(b,c,e)	0.039	±	0.003
3-Methylphenanthrene ^(c,d,e,g,h,i)	1.06	±	0.07
9-Methylphenanthrene ^(d,e,j)	0.448	±	0.022
1,2-Dimethylphenanthrene ^(c,d)	0.05	±	0.02
1,6-, 1,7-, 2,5-, and 2,9-Dimethylphenanthrene ^(c,d)	0.57	±	0.08
1,8-Dimethylphenanthrene ^(c,d)	0.06	±	0.02
2,6-Dimethylphenanthrene ^(c,d)	0.25	±	0.05
2,7-Dimethylphenanthrene ^(c,d)	0.23	±	0.05
3,6-Dimethylphenanthrene ^(c,d)	0.18	±	0.02
Fluoranthene ^(b,c,d,e,g,h,i)	26.9	±	1.1
Pyrene ^(b,c,d,e,g,h,i)	0.94	±	0.11
1-, 3-, and 7-Methylfluoranthene ^(c)	0.53	±	0.03
2-Methylpyrene ^(c,d)	0.040	±	0.008
4-Methylpyrene ^(c,d)	0.022	±	0.005
Benzo[<i>c</i>]phenanthrene ^(c,d,e,g,h,i,k)	1.15	±	0.21
Benz[<i>a</i>]anthracene ^(b,c,d,e,g,h,i)	0.330	±	0.037
Chrysene ^(b,e,k)	4.58	±	0.17
Benzo[<i>k</i>]fluoranthene ^(b,c,d,e,h,i,j,k)	0.699	±	0.058
Benzo[<i>e</i>]pyrene ^(c,d,e,g,h,i,k)	1.14	±	0.06
Benzo[<i>a</i>]pyrene ^(b,c,d,e,k)	0.053	±	0.003
Perylene ^(b,e)	0.059	±	0.005
Indeno[1,2,3- <i>cd</i>]pyrene ^(b,c,d,e)	1.37	±	0.16
Benzo[<i>ghi</i>]perylene ^(b,c,d,e,g,h,i)	0.489	±	0.032
Dibenz[<i>a,j</i>]anthracene ^(b,c,e)	0.337	±	0.071
Benzo[<i>b</i>]chrysene ^(c,d,e)	0.094	±	0.018
Coronene ^(c,e)	1.32	±	0.27
PFE at 200 °C			
Naphthalene ^(l)	4.00	±	0.13 ^(f)
Biphenyl ^(l)	2.94	±	0.14 ^(f)
Fluorene ^(l)	2.88	±	0.19
Phenanthrene ^(l)	20.7	±	0.3
Anthracene ^(l)	0.049	±	0.002 ^(f)
3-Methylphenanthrene ^(l)	1.38	±	0.08
9-Methylphenanthrene ^(l)	0.587	±	0.040
Fluoranthene ^(l)	30.9	±	0.5
Pyrene ^(l)	1.52	±	0.20
Benzo[<i>c</i>]phenanthrene ^(l)	1.64	±	0.10 ^(f)
Benz[<i>a</i>]anthracene ^(l)	0.966	±	0.043 ^(f)
Chrysene ^(l)	5.73	±	0.11 ^(f)
Benzo[<i>k</i>]fluoranthene ^(l)	1.75	±	0.09 ^(f)
Benzo[<i>e</i>]pyrene ^(l)	2.28	±	0.18
Benzo[<i>a</i>]pyrene ^(l)	0.766	±	0.039 ^(f)
Perylene ^(l)	0.082	±	0.006
Indeno[1,2,3- <i>cd</i>]pyrene ^(l)	2.13	±	0.12 ^(f)
Benzo[<i>ghi</i>]perylene ^(l)	1.59	±	0.09 ^(f)
Dibenz[<i>a,j</i>]anthracene ^(l)	0.433	±	0.008 ^(f)
Benzo[<i>b</i>]chrysene ^(l)	0.210	±	0.011 ^(f)
Coronene ^(l)	2.12	±	0.08 ^(f)

Table 3. Reference Mass Fraction Values for Selected PAHs in SRM 2975
Based on Extraction Method and Conditions (continued)

Extraction Conditions	Mass Fractions ^(a) (mg/kg)
Soxhlet Extraction or PFE using temperatures between 100 °C and 200 °C	
2-Methylnaphthalene ^(c,d,e,l)	1.91 ± 0.32
1-Methylnaphthalene ^(c,d,e,l)	0.99 ± 0.11
Acenaphthene ^(e,l)	0.548 ± 0.029
Benzo[ghi]fluoranthene ^(e,l)	10.6 ± 0.3
Benzo[b]fluoranthene ^(d,i,k)	11.5 ± 2.8

^(a) The reference values, unless otherwise footnoted, are weighted means of the mass fractions from two to six analytical methods [19]. The uncertainty listed with each value is an expanded uncertainty about the mean [19,20], with coverage factor, $k = 2$, calculated by combining within method variances with a between method variance [21] following the ISO/JCGM Guide [22,23].

^(b) LC-FL of isomeric PAH fractions after Soxhlet extraction with DCM

^(c) GC/MS (IVa) on 5 % phenyl-substituted methylpolysiloxane phase after PFE with DCM (100 °C with 13.8 MPa)

^(d) GC/MS (IVb) on 50 % phenyl-substituted methylpolysiloxane phase of same extracts as GC/MS (IVa)

^(e) GC/MS (V) on non-polar extra low bleed proprietary phase after PFE with toluene at one temperature and two pressures (100 °C with 13.8 MPa and 100 °C with 20.7 MPa)

^(f) The reference value is a weighted mean of average mass fractions, with one average from each of two or more analytical methods [19,20]. The expanded uncertainty is the half width of a symmetric 95 % parametric bootstrap confidence interval [24], which is consistent with the ISO/JCGM Guide [22,23]. The effective coverage factor, $k = 2$.

^(g) GC/MS (Ia) on 5 % phenyl-substituted methylpolysiloxane phase after PFE with toluene:methanol mixture (100 °C with 13.8 MPa)

^(h) GC/MS (II) on 5 % phenyl-substituted methylpolysiloxane phase after PFE with DCM (100 °C with 13.8 MPa)

⁽ⁱ⁾ GC/MS (III) on 5 % phenyl-substituted methylpolysiloxane phase after Soxhlet extraction with DCM

^(j) GC/MS (Ib) on 50 % phenyl-substituted methylpolysiloxane phase of selected extracts from GC/MS (Ia)

^(k) GC/MS (IVc) on a smectic liquid crystalline phase of same extracts as GC/MS (IVa)

^(l) GC/MS (V) on non-polar extra low bleed proprietary phase after PFE with toluene at one temperature and two pressures (200 °C with 13.8 MPa and 200 °C with 20.7 MPa)

Table 4. Reference Mass Fraction Values for Selected Nitro-PAHs in SRM 2975

Extraction Conditions	Mass Fractions ^(a) (mg/kg)
PFE using temperatures between 100 °C and 200 °C	
1-Nitronaphthalene ^(b)	0.044 ± 0.002
2-Nitronaphthalene ^(b)	0.118 ± 0.005
PFE at 100 °C	
9-Nitroanthracene ^(c)	3.07 ± 0.28
8-Nitrofluoranthene ^(d)	0.60 ± 0.13
4-Nitropyrene ^(d)	0.175 ± 0.016 ^(e)
6-Nitrobenzo[<i>a</i>]pyrene ^(f)	1.36 ± 0.40 ^(e)
1,3-Dinitropyrene ^(f)	1.12 ± 0.21
1,6-Dinitropyrene ^(f)	2.35 ± 0.51 ^(e)
1,8-Dinitropyrene ^(f)	3.10 ± 0.95
PFE at 200 °C	
9-Nitroanthracene ^(g)	3.94 ± 0.19 ^(e)

^(a) The reference values, unless otherwise footnoted, are weighted means of the mass fractions from two to six analytical methods [19]. The uncertainty listed with each value is an expanded uncertainty about the mean [19,20], with coverage factor, $k=2$, calculated by combining within method variances with a between method variance [21] following the ISO/JCGM Guide [22,23].

^(b) Two methods using GC/NCI-MS on a 5 % phenyl-substituted methylpolysiloxane phase after PFE with DCM (100 °C with 13.8 MPa) and four methods using GC/NCI-MS on a 50 % phenyl-substituted methylpolysiloxane phase after PFE with toluene at two temperatures and two pressures (100 °C with 13.8 MPa; 100 °C with 20.7 MPa; 200 °C with 13.8 MPa; and 200 °C with 20.7 MPa)

^(c) Three methods using GC/NCI-MS on either a 5 % phenyl-substituted or 50 % phenyl-substituted methylpolysiloxane phase after PFE with DCM (100 °C with 13.8 MPa) and two methods using GC/NCI-MS on a 50 % phenyl-substituted methylpolysiloxane phase after PFE with toluene at one temperatures and two pressures (100 °C with 13.8 MPa and 100 °C with 20.7 MPa)

^(d) Two methods using GC/NCI-MS on a 5 % phenyl-substituted methylpolysiloxane phase after PFE with DCM (100 °C with 13.8 MPa)

^(e) The reference value is a weighted mean of average mass fractions, with one average from each of two or more analytical methods [19,20]. The expanded uncertainty is the half width of a symmetric 95 % parametric bootstrap confidence interval [24], which is consistent with the ISO/JCGM Guide [22,23] and the effective coverage factor, k , equals 2.

^(f) Three methods using GC/NCI-MS on either a 5 % phenyl-substituted or 50 % phenyl-substituted methylpolysiloxane phase after PFE with DCM (100 °C with 13.8 MPa)

^(g) Two methods using GC/NCI-MS on a 50 % phenyl-substituted methylpolysiloxane phase after PFE with toluene at one temperature and two pressures (200 °C with 13.8 MPa and 200 °C with 20.7 MPa)

Table 5. Reference Mass Fraction Value for Total Extractable Mass for SRM 2975

	Mass Fraction ^(a,b) (%)
Total Extractable Mass	2.7 ± 0.2

^(a) Extractable mass as determined from Soxhlet extraction using DCM

^(b) The results are expressed as the reference value ± the expanded uncertainty. The reference value for the total extractable mass is the mean value of six measurements. The uncertainty, computed according to the CIPM approach as described in the NIST and ISO/JCGM Guide [3,22,23], is an expanded uncertainty at the 95 % level of confidence with coverage factor, $k=2$. The expanded uncertainty defines a range that contains the best estimate of the true value at a level of confidence of approximately 95 %.

Table 6. Reference Values for Particle-Size Characteristics for SRM 2975

Particle Measurement	Value ^(a)		
Mean diameter (volume distribution, MV, μm) ^(b)	31.9	±	0.6
Mean diameter (area distribution, μm) ^(c)	11.2	±	0.1
Mean diameter (number distribution, μm) ^(d)	1.62	±	0.01
Surface Area (m^2/cm^3) ^(e)	0.538	±	0.006
Percentile ^(f)	Particle Diameter ^(a) (μm)		
95	110	±	3
90	70	±	2
80	44.9	±	0.8
70	32.4	±	0.6
60	24.8	±	0.4
50 ^(g)	19.4	±	0.3
40	15.2	±	0.2
30	11.7	±	0.2
20	8.5	±	0.1
10	5.3	±	0.1

^(a) Each reference value is the mean value of measurements from the analysis of subsamples from four bottles. Each uncertainty, computed according to the CIPM approach as described in the ISO/JCGM Guide [3,22,23], is an expanded uncertainty at the 95 % level of confidence with coverage factor, $k = 2$. The expanded uncertainty defines a range that contains the best estimate of the true value at a level of confidence of approximately 95 %.

^(b) The mean diameter of the volume distribution represents the center of gravity of the distribution and compensates for scattering efficiency and refractive index. This parameter is strongly influenced by coarse particles.

^(c) The mean diameter of the area distribution, calculated from the volume distribution with less influence from the presence of coarse particles than the MV parameter.

^(d) The mean diameter of the number distribution calculated from the volume distribution.

^(e) Calculated specific surface area assuming solid, spherical particles. This is a computation and should not be interchanged with an adsorption method of surface area determination (see Table 8) as this value does not reflect porosity or topographical characteristics.

^(f) The data shown is the percent of the volume that is smaller than the indicated size.

^(g) Median diameter (50 % of the volume is less than 19.4 μm)

Table 7. Information Mass Fraction Values of Selected PAHs of Relative Molecular Mass 302 in SRM 2975

	Mass Fraction ^(a) (mg/kg)
Dibenzo[<i>b,e</i>]fluoranthene	2.7
Naphtho[1,2- <i>b</i>]fluoranthene	7.3
Naphtho[1,2- <i>k</i>]fluoranthene and Naphtho[2,3- <i>j</i>]fluoranthene	2.6
Naphtho[2,3- <i>b</i>]fluoranthene	0.37
Dibenzo[<i>a,k</i>]fluoranthene	0.71
Dibenzo[<i>j,l</i>]fluoranthene	2.3
Naphtho[2,3- <i>e</i>]pyrene	0.56
Dibenzo[<i>e,l</i>]pyrene	3.4

^(a) These mass fraction values are provided for informational purposes only. The values have not been confirmed by an independent analytical technique as required for certification.

Table 8. Information Value for Specific Surface Area of SRM 2975

Specific Surface Area (S)^(a)91 m²/g^(a) Specific surface area determined by multi-point N₂ gas adsorption BET method.

REFERENCES

- [1] SRM 1975; *Diesel Particulate Extract*; National Institute of Standards and Technology; U.S. Department of Commerce: Gaithersburg, MD (07 November 2000).
- [2] SRM 1650b; *Diesel Particulate Matter*; National Institute of Standards and Technology; U.S. Department of Commerce: Gaithersburg, MD (27 September 2006).
- [3] May, W.; Parris, R.; Beck II, C.; Fassett, J.; Greenberg, R.; Guenther, F.; Kramer, G.; Wise, S.; Gills, T.; Colbert, J.; Gettings, R.; MacDonald, B.; *Definition of Terms and Modes Used at NIST for Value Assignment of Reference Materials for Chemical Measurements*; NIST Special Publication 260-136 (2000); available at <http://www.nist.gov/srm/upload/SP260-136.PDF> (accessed Dec 2013).
- [4] Wright, M.E.; Klein, A.D. Jr.; Stesniak, E.J.; *A Diesel Exhaust Filter System for Industrial Diesel Forklifts*; SAE Technical Paper Series 911852: Warrendale, PA (1991).
- [5] Schantz, M.M.; Nichols, J.J.; Wise, S.A.; *Evaluation of Pressurized Fluid Extraction for the Extraction of Environmental Matrix Reference Materials*; Anal. Chem., Vol. 69, pp. 4210–4219 (1997).
- [6] Wise, S.A.; Chesler, S.N.; Hertz, H.S.; Hilpert, L.R.; May, W.E.; *Chemically-Bonded Aminosilane Stationary Phase for the High Performance Liquid Chromatographic Separation of Polynuclear Aromatic Hydrocarbons*; Anal. Chem., Vol. 49, pp. 2306–2310 (1977).
- [7] May, W.E.; Wise, S.A.; *Liquid Chromatographic Determination of Polycyclic Aromatic Hydrocarbons in Air Particulate Extracts*; Anal. Chem., Vol. 56, pp. 225–232 (1984).
- [8] Wise, S.A.; Benner, B.A. Jr.; Byrd, G.D.; Chesler, S.N.; Rebbert, R.E.; Schantz, M.M.; *Determination of Polycyclic Aromatic Hydrocarbons in a Coal Tar Standard Reference Material*; Anal. Chem., Vol. 60, pp. 887–894 (1988).
- [9] Wise, S.A.; Deissler, A.; Sander, L.C.; *Liquid Chromatographic Determination of Polycyclic Aromatic Hydrocarbon Isomers of Molecular Weight 278 and 302 in Environmental Standard Reference Materials*; Polycyclic Aromat. Compd., Vol. 3, pp. 169–184 (1993).
- [10] Scheepers, P.T.J.; Velders, D.D.; Martens, M.H.J.; Noordhoek, J.; Bos, R.P.; *Gas Chromatographic-Mass Spectrometric determination of Nitro Polycyclic Aromatic Hydrocarbons in Airbourne Particulate Matter from Workplace Atmospheres Contaminated with Diesel Exhaust*; J. Chromatogr., Vol. 677, pp. 107–121 (1994).
- [11] Schantz, M.M.; McGaw, E.; Wise, S.A.; *Pressurized Liquid Extraction of Diesel and Air Particulate Standard Reference Materials: Effects of Extraction Temperature and Pressure*; Anal. Chem., Vol. 84, pp. 8222–8231 (2012).
- [12] Bergvall, C.; Westerholm, R.; *Determination of 252-302 Da and Tentative Identification of 316-376 Da Polycyclic Aromatic Hydrocarbons in Standard Reference Materials 1649a Urban Dust and 1650b and 2975 Diesel Particulate Matter by Accelerated Solvent Extration- HPLC-GC-MS*; Anal. Bioanal. Chem., Vol. 391, pp. 2235–2248 (2008).
- [13] Masala, S.; Ahmed, T.; Bergvall, C.; Westerholm, R.; *Improved Efficiency of Extraction of Polycyclic Aromatic Hydrocarbons (PAHs) from the National Institute of Standards and Technology (NIST) Standard Reference Material Diesel Particulate Matter (SRM 2975) using Accelerated Solvent Extraction*; Anal. Bioanal. Chem., Vol. 401, pp. 3305–3315 (2011).
- [14] Cooper, L.R.; Haverland, R.L.; Vendricks, D.M.; Knisel, W.G.; *Microtrac Particle-Size Analyzer: An Alternative Particle-Size Determination Method for Sediments and Soils*; Soil Sci., Vol. 138, pp. 138–146 (1984).
- [15] Gregg, S.J.; Sing, K.S.W.; *Adsorption, Surface Area and Porosity*; 2nd ed., Academic Press, London (1982).
- [16] Brunauer, S.; Emmett, P.H.; Teller, E.; *Adsorption of Gases in Multimolecular Layers*; J. Amer. Chem. Soc., Vol. 60, pp. 309–319 (1938).
- [17] Barrett, E.P.; Joyner, L.G.; Halenda, P.P.; *The Determination of Pore Volume and Area Distributions in Porous Substances. I. Computations for Nitrogen Isotherms*; J. Amer. Chem. Soc., Vol. 73, pp. 373–380 (1951).
- [18] Hughes, T.J.; Lewtas, J.; Claxton, L.D.; *Development of a Standard Reference Material for Diesel Mutagenicity in the Salmonella Plate Incorporation Assay*; Mutat. Res., Vol. 391, pp. 243–258 (1997).
- [19] Dersimonian, R.; Laird, N.; *Meta-Analysis in Clinical Trials*; Control Clin. Trials, Vol. 7, pp. 177–188 (1986).
- [20] Rukhin, A.L.; *Weighted Means Statistics in Interlaboratory Studies*; Metrologia, Vol. 46, pp. 323–331 (2009).
- [21] Horn, R.A.; Horn, S.A.; Duncan, D.B.; *Estimating Heteroscedastic Variance in Linear Models*; J. Am. Stat. Assoc., Vol. 70, pp. 380–385 (1975).

- [22] JCGM 100:2008; *Evaluation of Measurement Data — Guide to the Expression of Uncertainty in Measurement* (GUM 1995 with Minor Corrections); Joint Committee for Guides in Metrology (2008); available at http://www.bipm.org/utis/common/documents/jcgm/JCGM_100_2008_E.pdf (accessed Dec 2013); see also Taylor, B.N.; Kuyatt, C.E.; *Guidelines for Evaluating and Expressing the Uncertainty of NIST Measurement Results*; NIST Technical Note 1297; U.S. Government Printing Office: Washington, DC (1994); available at <http://www.nist.gov/phylab/pubs/index.cfm> (accessed Dec 2013).
- [23] JCGM 101:2008; *Evaluation of Measurement Data – Supplement 1 to the “Guide to the Expression of Uncertainty in Measurement” – Propagation of Distributions using a Monte Carlo method*; JCGM (2008); available at http://www.bipm.org/utis/common/documents/jcgm/JCGM_101_2008_E.pdf (accessed Dec 2013).
- [24] Efron, B.; Tibshirani, R.J.; *An Introduction to the Bootstrap*; Chapman & Hall (1993).

<p>Certificate Revision History: 03 December 2013 (Update certified and reference values for PAHs and nitro-PAHs to address the effect of temperature used for extraction; extension of certification period; editorial changes); 19 March 2009 (Addition of reference and information values and update of expiration date); 10 April 2008 (Update of expiration date and editorial changes); 07 November 2000 (Original certificate date).</p>

Users of this SRM should ensure that the Certificate of Analysis in their possession is current. This can be accomplished by contacting the SRM Program: telephone (301) 975-2200; fax (301) 948-3730; e-mail srminfo@nist.gov; or via the Internet at <http://www.nist.gov/srm>.

Annex III



National Institute of Standards & Technology

Certificate of Analysis

Standard Reference Material[®] 1650b

Diesel Particulate Matter

This Standard Reference Material (SRM) is intended for use in evaluating analytical methods for the determination of selected polycyclic aromatic hydrocarbons (PAHs) and nitro-substituted PAHs (nitro-PAHs) in diesel particulate matter and similar matrices. In addition to certified and reference values for selected PAHs and nitro-PAHs, reference or information values are provided for percent extractable mass, particle-size distribution, and specific surface area; supplemental information on mutagenic activity is also provided. All of the chemical constituents for which certified, reference, and information values are provided are naturally present in the diesel particulate material. SRM 1650b was prepared from the same bulk diesel particulate material that was issued in 1985 as SRM 1650 [1] and in 2000 as SRM 1650a [2–4]. A unit of SRM 1650b consists of a bottle containing approximately 200 mg of diesel particulate material.

Certified Mass Fraction Values: Certified values are provided for PAHs in Table 1 and nitro-PAHs in Table 2. A NIST certified value is a value for which NIST has the highest confidence in its accuracy, in that all known or suspected sources of bias have been investigated or taken into account [5]. The certified values for the PAHs and nitro-PAHs are based on the agreement of results obtained at NIST from two or more independent analytical methods [5].

Reference Mass Fraction Values: Reference values are provided for additional PAHs in Table 3, for PAHs of molecular mass 302 in Table 4, and for additional nitro-PAHs in Table 5. In Tables 3 and 5, the reference values for some PAHs and nitro-PAHs, respectively, are listed more than once depending on the extraction conditions that are used (see “Preparation and Analysis”). A reference value for percent extractable mass is provided in Table 6. Reference values are noncertified values that are the best estimate of the true value; however, the values do not meet the NIST criteria for certification and are provided with associated uncertainties that may reflect only measurement precision, may not include all sources of uncertainty, or may reflect a lack of sufficient statistical agreement among multiple analytical methods [5].

Information Values: Information values for specific surface area, as determined by N₂ gas adsorption, and particle-size characteristics are provided in Table 7. An information value is considered to be a value that may be of use to the SRM user, but insufficient information is available to assess the uncertainty associated with the value or only a limited number of analyses were performed [5].

Expiration of Certification: The certification of **SRM 1650b** is valid, within the measurement uncertainty specified, until **31 December 2022**, provided the SRM is handled and stored in accordance with the instructions given in this certificate (see “Instructions for Handling, Storage, and Use”). However, the certification is invalid if the SRM is damaged, contaminated, or otherwise modified.

Maintenance of SRM Certification: NIST will monitor this SRM over the period of its certification. If substantive technical changes occur that affect the certification before the expiration of this certificate, NIST will notify the purchaser. Registration (see attached sheet) will facilitate notification.

Coordination of the technical measurements leading to the certification of SRM 1650b was under the leadership of M.M. Schantz and S.A. Wise of the NIST Chemical Sciences Division.

Statistical consultation was provided by N.A. Heckert and S.D. Leigh of the NIST Statistical Engineering Division.

Carlos A. Gonzalez, Chief
Chemical Sciences Division

Gaithersburg, MD 20899
Certificate Issue Date: 17 July 2013
Certificate Revision History on Last Page

Robert L. Watters, Jr, Director
Office of Reference Materials

SRM 1650b

Page 1 of 12
215

Analytical measurements for the certification of SRM 1650b were performed by H.A. Bamford, B.J. Porter, D.L. Poster, M.M. Schantz, P. Schubert, and R. Zeisler of the NIST Chemical Sciences Division. Analytical measurements for PAHs and nitro-PAHs were also provided by C. Chiu of the Environmental Technology Centre, Environment Canada (Ottawa, Canada). Specific surface area and porosity measurements and confirmation measurements for 1-nitropyrene were provided by P. Scheepers of the Department of Epidemiology at Katholieke Universiteit Nijmegen (Nijmegen, The Netherlands).

Support aspects involved in the issuance of this SRM were coordinated through the NIST Office of Reference Materials.

INSTRUCTIONS FOR HANDLING, STORAGE, AND USE

Handling: This material is a naturally occurring diesel particulate material and contains constituents of known and unknown toxicities and mutagenicities; therefore, extreme caution and care should be exercised during its handling and use.

Storage: Store SRM 1650b in its original bottle at temperatures below 30 °C and keep away from direct sunlight.

Use: Prior to removal of subsamples for analysis, the contents of the bottle should be mixed thoroughly. The recommended minimum sample size is 50 mg, although smaller sample sizes have been evaluated. The evaluation of the homogeneity of SRM 1650b, at small sample sizes for PAHs, is described in “Homogeneity Assessment for PAHs” and in further detail in reference 6.

PREPARATION AND ANALYSIS⁽¹⁾

Sample Collection and Preparation: The diesel particulate material used for the preparation of SRM 1650b was the same bulk diesel particulate material used for the preparation of SRM 1650 and SRM 1650a. This material was obtained through the Coordinating Research Council, Inc. (Atlanta, GA). The particulate material was collected from the heat exchangers of a dilution tube facility following 200 engine hours of particulate accumulation. Several direct injection four-cycle diesel engines, operating under a variety of conditions were used to generate this particulate material. Therefore, while the sample is not intended to be representative of any particular diesel engine operating under any specific conditions, it should be representative of heavy-duty diesel engine particulate emissions.

Relationship Among SRM 1650, SRM 1650a, and SRM 1650b: SRM 1650b was prepared from the same bulk diesel particulate matter used for preparation of SRM 1650; the bulk material had been stored at –20 °C since the preparation of SRM 1650 in 1984. SRM 1650b was analyzed as described below to confirm that the bulk diesel particulate matter was the same as the material used for SRM 1650 and SRM 1650a. The analyses of SRM 1650b confirmed that the material was the same and that the mass fractions of PAHs and nitro-PAHs had not significantly changed. The results of these analyses were then used to assign new certified and reference mass fractions and to increase again the number of PAHs and nitro-PAHs with values assigned. However, measurements for some properties (e.g., percent extractable mass and pore size) and some PAHs (selected methyl- and dimethyl-substituted PAHs) were not repeated on SRM 1650b; instead it was determined that the information values from SRM 1650a are applicable to SRM 1650b.

Polycyclic Aromatic Hydrocarbons (PAHs)

The general approach used for the value assignment of the PAHs in SRM 1650b consisted of pressurized fluid extraction (PFE) using dichloromethane (DCM), toluene, or a toluene/methanol mixture at two extraction temperatures (100 °C and 200 °C), cleanup of the extracts using solid phase extraction (SPE), and analysis by using gas chromatography/mass spectrometry (GC/MS) on three stationary phases of different selectivity [i.e., a relatively nonpolar phase, a 50 % (mole fraction) phenyl-substituted methylpolysiloxane phase, and a dimethyl 50 % (mole fraction) polysiloxane liquid crystalline stationary phase]. PFE was the only extraction method used at NIST; previous studies indicated that conventional Soxhlet extraction was not as effective as PFE in the removal of higher relative molecular mass PAHs [7]. Results were also obtained from Environment Canada as described in “GC/MS (Environment Canada)”.

⁽¹⁾Certain commercial equipment, instruments or materials are identified in this certificate to adequately specify the experimental procedure. Such identification does not imply recommendation or endorsement by the National Institute of Standards and Technology, nor does it imply that the materials, or equipment identified are necessarily the best available for the purpose.

Multiple sets of GC/MS results performed by the of the NIST Chemical Sciences Division, designated as GC/MS (Ia and Ib), GC/MS (IIa and IIb), GC/MS (IIIa and IIIb), GC/MS (IVa and IVb), GC/MS (Va and Vb), GC/MS (VIa and VIb), GC/MS (VII), GC/MS (VIII) and GC/MS (Environment Canada), were obtained using three columns with different selectivities for the separation of PAHs. For all PAH analyses, the mass spectrometer was operated using electron impact ionization.

GC/MS (Ia and Ib): For GC/MS (I) analyses, duplicate subsamples of 50 mg from six bottles of SRM 1650b were mixed with Hydromatrix (Isco, Lincoln, NE) and extracted with toluene using PFE at 100 °C and 13.8 MPa as described by Schantz et al. [7]. The extracts were concentrated to about 0.5 mL, solvent exchanged to hexane, placed on an aminopropylsilane SPE cartridge, and eluted with 20 mL of 2 % DCM in hexane (volume fraction). The eluant was concentrated and then analyzed by using GC/MS with a 0.25 mm i.d. × 60 m fused silica capillary column with a relatively nonpolar phase (0.25 µm film thickness; DB-XLB, J&W Scientific, Folsom, CA) and these results are denoted as GC/MS (Ia). Concentrated eluants were also analyzed on a 50 % phenyl-substituted methylpolysiloxane stationary phase (0.25 mm i.d. × 60 m, 0.25 µm film thickness; DB-17MS, J&W Scientific), and these results are designated as GC/MS (Ib).

GC/MS (IIa and IIb): For the GC/MS (IIa and IIb) analyses, 50 mg samples from six bottles of SRM 1650b were extracted with toluene using PFE at 200 °C and 13.8 MPa. The extracts were processed and analyzed as described above for GC/MS (Ia) and GC/MS (Ib) and the results are designated GC/MS (IIa) and GC/MS (IIb), respectively.

GC/MS (IIIa and IIIb): For GC/MS (IIIa and IIIb) analyses, subsamples of 50 mg to 100 mg from six bottles of SRM 1650b were mixed with clean sodium sulfate and extracted with DCM using PFE at 100 °C and 13.8 MPa. The extracts were processed as described above for GC/MS (Ia and Ib) and then analyzed by using GC/MS on fused silica capillary columns with a 50 % phenyl-substituted methylpolysiloxane stationary phase (0.25 mm i.d. × 60 m, 0.25 µm film thickness), designated as GC/MS (IIIa), and on a dimethyl 50 % polysiloxane liquid crystalline stationary phase (0.25 mm i.d. × 15 m, 0.25 µm film thickness; LC-50, J&K Environmental, Milton, Ontario, Canada), designated as GC/MS (IIIb).

GC/MS (IVa and IVb): For GC/MS (IVa and IVb) analyses, subsamples of 50 mg to 100 mg from six bottles of SRM 1650b were extracted with DCM using PFE at 200 °C and 13.8 MPa. The extracts were processed and analyzed by using GC/MS on the two columns as described above for GC/MS (IIIa and IIIb).

GC/MS (Va and Vb) and GC/MS (VIa and VIb): Additional extractions and analyses were performed in the same manner as for GC/MS (IIIa and IIIb) and GC/MS (IVa and IVb) to obtain concentrations for selected methylated PAHs. These data sets are designated as GC/MS (Va and Vb) and GC/MS (VIa and VIb).

GC/MS (VII): For the relative molecular mass (M_r) 276 and higher PAHs, additional extractions and analyses were performed in a similar manner as for GC/MS (Ib) except that the PAHs of interest were eluted from the aminopropylsilane SPE cartridge using 40 mL of 10 % DCM in hexane (volume fraction). These data are designated as GC/MS (VII).

GC/MS (VIIIa through VIIId): The effect of increasing the temperature and pressure used for PFE on the extraction efficiency for PAHs was evaluated. The solvent used was toluene, although a 9:1 toluene:methanol (volume fraction) was also evaluated. The PFE conditions used included: 100 °C with 13.8 MPa; 100 °C with 20.7 MPa; 200 °C with 13.8 MPa; and 200 °C with 20.7 MPa, methods GC/MS (VIIIa) through GC/MS (VIIId), respectively. Following an SPE step similar to that of method I above, the processed extracts were analyzed using a non-polar, extra-low bleed phase (0.25 mm i.d. × 60 m, 0.25 µm film thickness).

GC/MS Internal Standards: For all GC/MS measurements described above, except GC/MS (VIa and VIb), selected perdeuterated PAHs were added to the diesel particulate matter prior to extraction for use as internal standards for quantification purposes. For GC/MS (VIa and VIb), fluorinated PAHs were added to the diesel particulate matter prior to extraction for use as internal standards for quantification purposes.

GC/MS (Environment Canada): For PAH measurements at Environment Canada, subsamples of approximately 10 mg from each of four bottles of SRM 1650b were extracted with DCM or hexane/acetone (1:1 volume fraction) using microwave-assisted extraction at 100 °C for 20 min. The extract was filtered through sodium sulfate and concentrated to a few milliliters by rotary evaporation, solvent exchanged to cyclohexane, and then divided into two portions; one portion was processed for PAH measurements and the other portion was processed for nitro-PAH measurements (see below). The PAH fraction was isolated from the extract by using open-column chromatography on silica, with hexane followed by benzene as the mobile phase. The PAH fraction was then analyzed by using GC/MS on a DB-XLB column (0.25 mm i.d. × 30 m, 0.25 µm film thickness). Selected perdeuterated PAHs were added to the diesel particulate matter prior to extraction for use as internal standards for quantification purposes.

PAH Isomers of Relative Molecular Mass (M_r) 302: For the determination of the relative molecular mass (M_r) 302 isomers, the method used was similar to that described by Schubert et al. [8]. Two sets of samples (one set of three subsamples and one set of six subsamples) of approximately 50 mg each were extracted using PFE at 100 °C and 13.8 MPa with DCM. The extracts were then concentrated, solvent exchanged to hexane, passed through an aminopropylsilane SPE cartridge, and eluted with 40 mL of 10 % DCM in hexane (volume fraction). The processed extract was then analyzed by GC/MS using a 0.25 mm i.d. \times 60 m fused silica capillary column with a 50 % phenyl-substituted methylpolysiloxane phase (0.25 μ m film thickness; DB-17MS). Perdeuterated dibenzo[*a,i*]pyrene was added to the diesel particulate matter, prior to extraction, for use as an internal standard.

Homogeneity Assessment for PAHs: The homogeneity of SRM 1650b was assessed by analyzing duplicate samples of 50 mg from six bottles selected by stratified random sampling. Samples were processed and analyzed as described above for GC/MS (I). No statistically significant differences among bottles were observed for the PAHs at the 50 mg sample size. The relative homogeneity of trace levels of PAHs in SRM 1650b in the milligram sampling range was also evaluated. The subsampling contribution to the overall uncertainty varies with PAH considered. Using pyrene as an example, the subsampling error for a 10 mg sample size of SRM 1650b is 2 %, while the subsampling error for a 50 mg sample of SRM 1650b is 0.9 %. A more extensive evaluation of the homogeneity of SRM 1650b, at small sample sizes for PAHs, is described in reference 6.

Nitro-Substituted Polycyclic Aromatic Hydrocarbons (Nitro-PAHs)

SRM 1650b was analyzed at NIST and Environment Canada for the determination of nitro-PAHs. The general procedure for determination of nitro-PAHs at NIST utilizes GC with negative ion chemical ionization mass spectrometry (GC/NICI-MS) [9,10] and high-resolution mass spectrometry using negative chemical ionization (GC/NCI-HRMS). Mass fraction values for nitro-PAHs are provided in Table 2 and 5.

GC/NICI-MS (I): Subsamples of approximately 50 mg from each of six bottles of SRM 1650b were mixed with Hydromatrix (Isco, Lincoln, NE) and extracted with DCM using PFE at 100 °C and 13.8 MPa. The extracts were concentrated to about 0.5 mL, solvent exchanged to hexane, placed on an aminopropylsilane SPE cartridge, and eluted with 40 mL of 20 % DCM in hexane (volume fraction). To isolate the nitro-PAH fraction, the concentrated eluant was analyzed by normal-phase liquid chromatography (LC) using a semi-preparative amino/cyano phase column with a mobile phase of 20 % DCM in hexane [10]. The nitro-PAH fraction was analyzed by GC with GC/NICI-MS using a 0.25 mm i.d. \times 30 m fused silica capillary column containing a 50 % phenyl-substituted methylpolysiloxane stationary phase (0.25 μ m film thickness), and the results are designated as GC/NICI-MS (I).

GC/NICI-MS (II): A second set of four subsamples of SRM 1650b was processed and analyzed at a different time using the same procedures described above and the results are denoted as GC/NICI-MS (II).

GC/NICI-MS (IIIa through IIId): The effect of increasing the temperature and pressure used for PFE on the extraction efficiency for nitro-PAHs was evaluated. The solvent used was toluene, although a 9:1 toluene:methanol (volume fraction) was also evaluated. The PFE conditions used included: 100 °C with 13.8 MPa; 100 °C with 20.7 MPa; 200 °C with 13.8 MPa; and 200 °C with 20.7 MPa [methods GC/NICI-MS (IIIa) through GC/NICI-MS (IIId), respectively]. Following an SPE step similar to that of method I above, the processed extracts were analyzed using a non-polar, extra-low bleed proprietary phase (0.25 mm i.d. \times 60 m, 0.25 μ m film thickness).

GC/NCI-HRMS: For the Environment Canada measurements of nitro-PAHs, five subsamples of SRM 1650b were extracted as described above for PAH measurements. The second portion of the extract was taken to dryness and then redissolved in 1 mL of dimethyl sulfoxide (DMSO). The nitro-PAH fraction was isolated by using a liquid-liquid partition scheme involving hexane extraction of the DMSO to remove aliphatic hydrocarbons, followed by dilution of the DMSO with water and extraction of the polar fraction into cyclohexane. The nitro-PAHs were then isolated by using normal-phase LC on a silica column with a solvent gradient from 5 % DCM in hexane (volume fraction) to 100 % DCM. The nitro-PAH fraction was collected from 60 % DCM in hexane to 100 % DCM, concentrated, and analyzed by using GC on a 30 m 5 % phenyl-substituted methylpolysiloxane column (0.25 mm i.d., 0.25 μ m film thickness) with detection by high-resolution mass spectrometry using negative chemical ionization (GC/NCI-HRMS).

GC/NICI-MS and GC/NCI-HRMS Internal Standards: For the GC/NICI-MS and GC/NCI-HRMS measurements described above, perdeuterated nitro-PAHs were added to the diesel particulate matter, prior to extraction, for use as internal standards for quantification purposes.

Value Assignment for PAHs and Nitro-PAHs

The value assignment of PAHs and nitro-PAHs in SRM 1650b is based on the measurements used when SRM 1650b was issued in 2006 and on recent additional measurements using different extraction temperatures. Recent studies on the extraction of PAHs and nitro-PAHs from diesel particulate matter [11–13] have shown that using PFE at 200 °C removes higher quantities of some PAHs and nitro-PAHs than using PFE at 100 °C. As a result of these studies, value assignment for specific PAHs and nitro-PAHs in SRM 1650b is based on measurements using PFE at both 100 °C and 200 °C. In cases where the quantities of the individual PAHs and nitro-PAHs do not change with the PFE temperature, the measurements were combined and the resulting values are denoted as certified values in Tables 1 and 2. When different results are obtained at 100 °C and 200 °C, the values are reported for both temperatures, and they are denoted as reference values in Tables 3 and 5. These reference values should be considered “method dependent” values, because they are dependent on the extraction method and temperature.

Percent Extractable Mass

For the determination of percent extractable mass, six subsamples of approximately 200 mg were extracted using Soxhlet extraction for 18 h with DCM. The extract was concentrated to approximately 20 mL and then filtered to remove particulate matter. Aliquots of 100 µL to 150 µL were placed in tared aluminum foil pans; the DCM was evaporated until constant mass was obtained, and then the mass of the residue remaining was determined. The percent extractable mass reference value for SRM 1650a is applicable to SRM 1650b and provided in Table 6.

Particle Size Information, Specific Surface Area, and Porosity

Particle-size distribution measurements for SRM 1650b were carried out using a laser diffraction instrument (Mastersizer 2000, Malvern Instruments, Southborough, MA) set at a refractive index of 1.5 and absorption index of 0.1 and the liquid suspension method with the instrument manufacturer’s small volume sample dispersion unit (Hydro 2000 SM). A suspension of 0.1 % (mass fraction) of SRM 1650b in distilled water with 0.001 % Triton (volume fraction) was prepared by ultra-sonication for 1 h and 24 h. After the recording of the background, a portion of the suspension was added to the measurement cell to achieve an obscuration of 5 %. Three passes of the sample solution were recorded and averaged. Results were calculated using the General Purpose Model provided by the instrument manufacturer; the results obtained for the two sonication periods are shown in Figure 1. The diesel particulate matter, as-received, does not have a stable particle size because of agglomeration which is evident, as the particle-size distribution for SRM 1650b measured after the 1 h sonication period did not show a typical profile for a material from a combustion process. The subsequent 24 h sonication broke up most agglomerates, and the size distribution shows a profile typical for combustion engine emissions (see Table 7).

The specific surface area and porosity were determined based on N₂ gas adsorption measurements [14]. The gas adsorption measurements were performed on a NOVA-1200 instrument (Quantachrome Corp., Boynton Beach, FL) at 77 K after the samples were outgassed for 24 h at 120 °C under vacuum. The N₂ isotherms were analyzed using the Brunauer-Emmet-Teller (BET) equation [15] to obtain the surface area (Table 7) and the Barrett-Joyner-Halenda (BJH) method [16] to obtain the porosity. Based on the BJH method, SRM 1650b shows a wide distribution of mesopores, but with substantial outer area. The pore diameter of the particles in SRM 1650b ranges from 4 nm to 45 nm with a mean at about 25 nm.

Supplemental Information for SRM 1650b

Because SRM 1650, SRM 1650a, and SRM 1650b were all prepared from the same bulk diesel particulate matter, some measurements reported for the previous two materials have not been duplicated for SRM 1650b and the previous results are transferable to the current SRM 1650b. In addition, because SRM 1650 and SRM 1650a have been available since 1985, a considerable amount of information on the characterization of these materials has been published. A summary of some of the studies reporting characterization of this diesel particulate matter SRM is provided in Poster et al [3,4]. A description of the mutagenicity assay is provided below as supplemental information for SRM 1650b.

Mutagenicity Activity: Reference values for the mutagenic activity of a dichloromethane extract of SRM 1650 were determined as part of an international collaborative study in 1989 sponsored by the International Programme on Chemical Safety (IPCS) and supported and technically coordinated by the U.S. Environmental Protection Agency's (EPA) Office of Health Research. Twenty laboratories from North America, Europe, and Japan participated in the study for which a complete summary has been published [17,18]. Mutagenicity data were provided by J. Lewtas and L.D. Claxton of the National Health and Environmental Effects Research Laboratory, U.S. EPA (Research Triangle Park, NC).

Table 1. Certified Mass Fraction Values for PAHs in SRM 1650b

PAH	Mass Fraction ^(a) (mg/kg)		
Phenanthrene ^(b,c,d,e,f,g,h,i,j,k)	65.6	±	3.6
1-Methylphenanthrene ^(b,c,d,e,k,l,m)	32.1	±	1.4
2-Methylphenanthrene ^(b,c,d,e,k,l,m)	72.3	±	1.2
3-Methylphenanthrene ^(b,c,d,e,k,l,m)	56.7	±	1.9
9-Methylphenanthrene ^(b,c,d,e,k,l,m)	36.6	±	1.6
Fluoranthene ^(b,c,d,e,f,g,h,i,j,k)	48.1	±	1.1 ⁽ⁿ⁾
Pyrene ^(b,c,d,e,f,g,h,i,j,k)	44.1	±	1.2
Benzo[ghi]fluoranthene ^(c,e,f,g,h,i,j,k)	11.1	±	0.7
Benzo[c]phenanthrene ^(b,c,d,e,f,g,h,i,k)	2.65	±	0.24
Benz[a]anthracene ^(b,c,d,e,f,g,h,i,j,k)	6.45	±	0.39
Chrysene ^(b,d,g,o)	13.4	±	0.6
Triphenylene ^(b,d,g,o)	9.49	±	0.63
Benzo[a]fluoranthene ^(b,c,d,e,f,h,k)	0.384	±	0.023
Benzo[b]fluoranthene ^(c,e,f,g,h,i)	6.77	±	0.92
Benzo[j]fluoranthene ^(c,e,f,h)	3.24	±	0.50 ⁽ⁿ⁾
Benzo[k]fluoranthene ^(b,c,d,e,f,g,h,i,j,k)	2.30	±	0.18 ⁽ⁿ⁾
Benzo[e]pyrene ^(b,c,d,e,f,g,h,i,j,k)	6.36	±	0.37
Benzo[a]pyrene ^(b,c,d,e,f,g,h,i,j,k)	1.25	±	0.12
Perylene ^(c,d,e,k)	0.167	±	0.019 ⁽ⁿ⁾
Indeno[1,2,3-cd]pyrene ^(b,c,d,e,f,g,h,i,j,k,o)	4.48	±	0.21
Benzo[ghi]perylene ^(b,c,d,e,f,g,h,i,j,k,o)	6.04	±	0.30
Dibenz[a,c]anthracene ^(c,e,f,g,h,i)	0.439	±	0.048
Dibenz[a,h]anthracene ^(c,e,g,i)	0.365	±	0.082
Dibenz[a,j]anthracene ^(c,e,g,i)	0.387	±	0.068 ⁽ⁿ⁾
Benzo[b]chrysene ^(b,c,d,e,f,g,h,i,k)	0.301	±	0.019 ⁽ⁿ⁾
Picene ^(b,c,d,e,f,g,h,i,k)	0.506	±	0.058 ⁽ⁿ⁾

- (a) The certified mass fraction values, unless otherwise footnoted, are weighted means of the mass fractions from multiple analytical methods [19]. The uncertainty listed with each value is an expanded uncertainty about the mean [19,20] with coverage factor, $k = 2$, calculated by combining within method variances with a between method variance [21] following the ISO/JCGM Guide [22,23].
- (b) GC/MS (Ia) on a proprietary relatively nonpolar phase after PFE at 100 °C and 13.8 MPa with toluene.
- (c) GC/MS (Ib) on 50 % phenyl-substituted methylpolysiloxane phase, same extract as GC/MS (Ia).
- (d) GC/MS (IIa) on a proprietary relatively nonpolar phase after PFE at 200 °C and 13.8 MPa with toluene.
- (e) GC/MS (IIb) on 50 % phenyl-substituted methylpolysiloxane phase same extract as GC/MS (IIa).
- (f) GC/MS (IIIa) on 50 % phenyl-substituted methylpolysiloxane phase after PFE at 100 °C and 13.8 MPa with DCM.
- (g) GC/MS (IIIb) on dimethyl 50 % polysiloxane liquid crystalline stationary phase with same extract as GC/MS (IIIa).
- (h) GC/MS (IVa) on 50 % phenyl-substituted methylpolysiloxane phase after PFE at 200 °C and 13.8 MPa with DCM.
- (i) GC/MS (IVb) on dimethyl 50 % polysiloxane liquid crystalline stationary phase with same extract as GC/MS (IVa).
- (j) GC/MS (Environment Canada) on a proprietary relatively nonpolar phase.
- (k) GC/MS (VIII) on non-polar extra low bleed proprietary phase after PFE with toluene at 100 °C with 13.8 MPa; 100 °C with 20.7 MPa; 200 °C with 13.8 MPa; and 200 °C with 20.7 MPa.
- (l) GC/MS (Va) on 50 % phenyl-substituted methylpolysiloxane phase after PFE at 100 °C and 13.8 MPa with DCM.
- (m) GC/MS (VIa) on 50 % phenyl-substituted methylpolysiloxane phase after PFE at 200 °C and 13.8 MPa with DCM.
- (n) The certified value is a weighted mean of average mass fractions, with one average from each of two or more analytical methods [19,20]. The expanded uncertainty is the half width of a symmetric 95 % parametric bootstrap confidence interval [24] which is consistent with the ISO/JCGM Guide [22,23] with an effective coverage factor, k , equals 2.
- (o) GC/MS (VII) on 50 % phenyl-substituted methylpolysiloxane phase after PFE at 100 °C with DCM.

Table 2. Certified Mass Fraction Values for Nitro-PAHs in SRM 1650b

Nitro-PAH	Mass Fraction ^(a) (µg/kg)
9-Nitrophenanthrene ^(b,c,d,e)	539 ± 24
3-Nitrophenanthrene ^(b,c,e)	4250 ± 50 ^(f)
2-Nitrofluoranthene ^(b,c,e)	217 ± 15
3-Nitrofluoranthene ^(b,c,e)	65.1 ± 1.1
1-Nitropyrene ^(b,c,e,g)	18400 ± 300
7-Nitrobenz[<i>a</i>]anthracene ^(b,c,e)	943 ± 22 ^(f)
6-Nitrochrysene ^(b,c,e)	46.6 ± 1.1 ^(f)

^(a) The certified mass fraction values, unless otherwise footnoted, are weighted means of the mass fractions from multiple analytical methods [19]. The uncertainty listed with each value is an expanded uncertainty about the mean [19,20] with coverage factor, $k = 2$, calculated by combining within method variances with a between method variance [21] following the ISO/JCGM Guide [22,23].

^(b) GC/NICI-MS (I) on 50 % phenyl-substituted methylpolysiloxane stationary phase.

^(c) GC/NICI-MS (II) on 50 % phenyl-substituted methylpolysiloxane stationary phase.

^(d) GC/NCI-HRMS on 5 % phenyl-substituted methylpolysiloxane stationary phase.

^(e) GC/NICI-MS (III) on 50 % phenyl-substituted methylpolysiloxane phase after PFE with toluene at two temperatures and two pressures (100 °C with 13.8 MPa; 100 °C with 20.7 MPa; 200 °C with 13.8 MPa; and 200 °C with 20.7 MPa).

^(f) The certified value is a weighted mean of average mass fractions, with one average from each of two or more analytical methods [19,20]. The expanded uncertainty is the half width of a symmetric 95 % parametric bootstrap confidence interval [24], which is consistent with the ISO/JCGM Guide [22,23] with an effective coverage factor, k , equals 2.

^(g) Certified value for 1-nitropyrene confirmed original SRM 1650 certified value, which included measurements by two other independent techniques [2,25].

Table 3. Reference Mass Fraction Values for PAHs in SRM 1650b
Based on Extraction Method and Conditions

Extraction Conditions	Mass Fractions (mg/kg) ^(a)
PFE at temperatures between 100 °C and 200 °C	
1-Methylnaphthalene ^(b,c,d,e,f)	1.71 ± 0.26 ^(g)
2-Methylnaphthalene ^(b,c,d,e,f)	3.71 ± 0.21
Acenaphthene ^(c,e,f,h)	0.233 ± 0.021
1,7-Dimethylphenanthrene ^(e,f,i,j)	17.2 ± 0.7
4H-Cyclopenta[<i>def</i>]phenanthrene ^(e,f)	3.35 ± 0.18
Cyclopenta[<i>def</i>]phenanthrene ^(k,l)	15.6 ± 0.8
Cyclopenta[<i>cd</i>]pyrene ^(b,h)	0.349 ± 0.068
1-Methylfluoranthene ^(e,f,i,j,m)	3.17 ± 0.11
3-Methylfluoranthene ^(e,f,i,j,m)	6.09 ± 0.83
1-Methylpyrene ^(e,f,i,j)	2.05 ± 0.14
3-Methylchrysene ^(e,f,i,j,n,o)	2.17 ± 0.10
6-Methylchrysene ^(e,f,i,j,n,o)	1.57 ± 0.04 ^(g)
Coronene ^(e,f,p)	9.48 ± 0.28

Extraction Conditions

Mass Fractions
(mg/kg)^(a)

PFE at 100 °C

Naphthalene ^(e,h,q)	5.16 ± 0.48 ^(g)
Biphenyl ^(e,h,k,q)	0.965 ± 0.035
Acenaphthylene ^(c,e,q)	0.365 ± 0.019
Fluorene ^(e,h,k,q)	0.762 ± 0.029
Anthracene ^(e,h,k,q,r,s)	1.56 ± 0.20 ^(g)
2-Methylanthracene ^(h,q)	0.60 ± 0.11
Dibenzothiophene ^(e,h,q)	9.54 ± 0.56
1,2-Dimethylphenanthrene ^(t)	6.3 ± 0.5
1,6-, 2,5-, and 2,9-Dimethylphenanthrene ^(t)	38 ± 3
1,8-Dimethylphenanthrene ^(t)	4.5 ± 0.5
2,6-Dimethylphenanthrene ^(t)	29 ± 2
2,7-Dimethylphenanthrene ^(t)	20 ± 2
3,6-Dimethylphenanthrene ^(t)	23 ± 2
8-Methylfluoranthene ^(i,j)	3.60 ± 0.12 ^(g)
2-Methylpyrene ^(i,j,n,o)	5.8 ± 1.4
4-Methylpyrene ^(i,j,n)	5.14 ± 0.63
1-Methylchrysene ^(n,o)	1.46 ± 0.05
2-Methylchrysene ^(i,j,n,o)	2.50 ± 0.26 ^(g)
1-Methylbenz[a]anthracene ^(o)	0.355 ± 0.010
2-Methylbenz[a]anthracene ^(i,j)	0.43 ± 0.19
6-Methylbenz[a]anthracene ^(o)	5.28 ± 0.17
9- and 3-Methylbenz[a]anthracene ^(i,j)	0.61 ± 0.17
11-Methylbenz[a]anthracene ^(i,j)	0.36 ± 0.15

PFE at 200 °C

Naphthalene ^(f)	7.29 ± 0.38
Biphenyl ^(b,c,f,l)	3.47 ± 0.17
Acenaphthylene ^(b,c,d,f)	1.36 ± 0.04
Fluorene ^(b,c,d,f)	1.27 ± 0.04
Anthracene ^(b,c,d,f,m)	7.58 ± 0.35
2-Methylanthracene ^(b,c)	5.88 ± 0.46
Dibenzothiophene ^(f,l,m)	20.9 ± 1.5

^(a) The reference values, unless otherwise footnoted, are weighted means of the mass fractions from multiple analytical methods [19]. The uncertainty listed is an expanded uncertainty about the mean [19,20], with coverage factor, $k = 2$, calculated by combining within method variances with a between method variance [21] following the ISO/JCGM Guide [22,23].

^(b) GC/MS (IIa) on a proprietary relatively nonpolar phase after PFE at 200 °C and 13.8 MPa with toluene.

^(c) GC/MS (IIb) on 50 % phenyl-substituted methylpolysiloxane phase same extract as GC/MS (IIa).

^(d) GC/MS (IVa) on 50 % phenyl-substituted methylpolysiloxane phase after PFE at 200 °C and 13.8 MPa with DCM.

^(e) GC/MS (VIII) on non-polar extra low bleed proprietary phase after PFE with toluene at 100 °C and two pressures (13.8 MPa and 20.7 MPa).

^(f) GC/MS (VIII) on non-polar extra low bleed proprietary phase after PFE with toluene at 200 °C and two pressures (13.8 MPa and 20.7 MPa).

^(g) The reference value is a weighted mean of average mass fractions, with one average from each of two or more analytical methods [19,20]. The expanded uncertainty is the half width of a symmetric 95 % parametric bootstrap confidence interval [24], which is consistent with the ISO/JCGM Guide [22,23]. The effective coverage factor, $k = 2$.

^(h) GC/MS (Ia) on a proprietary relatively nonpolar phase after PFE at 100 °C and 13.8 MPa with toluene.

⁽ⁱ⁾ GC/MS (Va) on 50 % phenyl-substituted methylpolysiloxane phase after PFE at 100 °C with DCM.

^(j) GC/MS (VIa) on 50 % phenyl-substituted methylpolysiloxane phase after PFE at 100 °C with DCM.

^(k) GC/MS (IIIa) on 50 % phenyl-substituted methylpolysiloxane phase after PFE at 100 °C and 13.8 MPa with DCM.

^(l) GC/MS (IVa) on 50 % phenyl-substituted methylpolysiloxane phase after PFE at 200 °C and 13.8 MPa with DCM.

^(m) GC/MS (IVb) on dimethyl 50 % polysiloxane liquid crystalline stationary phase with same extract as GC/MS (IVa)

⁽ⁿ⁾ GC/MS (VIb) on dimethyl 50 % polysiloxane liquid crystalline stationary phase with same extract as GC/MS (VIa).

^(o) GC/MS (Vb) on dimethyl 50 % polysiloxane liquid crystalline stationary phase with same extract as GC/MS (Va).

^(p) GC/MS (VII) on 50 % phenyl-substituted methylpolysiloxane phase after PFE at 100 °C with DCM.

^(q) GC/MS (Ib) on 50 % phenyl-substituted methylpolysiloxane phase same extract as GC/MS (Ia).

^(r) GC/MS (Environment Canada) on a proprietary relatively nonpolar phase.

^(s) GC/MS (IIIb) on dimethyl 50 % polysiloxane liquid crystalline stationary phase with same extract as GC/MS (IIIa).

^(t) Reference values based on GC/MS analyses on 5 % and/or 50 % phenyl-substituted methylpolysiloxane phase after PFE at 100 °C and 13.8 MPa with DCM from SRM 1650a.

Table 4. Reference Mass Fraction Values for PAHs of Relative Molecular Mass 302 in SRM 1650b

PAH	Mass Fractions ^(a,b) (mg/kg)	
Dibenzo[<i>b,e</i>]fluoranthene	0.375	± 0.034
Naphtho[1,2- <i>b</i>]fluoranthene	2.31	± 0.21
Naphtho[1,2- <i>k</i>]fluoranthene and Naphtho[2,3- <i>j</i>]fluoranthene	1.71	± 0.17
Naphtho[2,3- <i>b</i>]fluoranthene	0.427	± 0.048
Dibenzo[<i>b,k</i>]fluoranthene	1.68	± 0.17
Dibenzo[<i>a,k</i>]fluoranthene	0.148	± 0.009
Dibenzo[<i>j,l</i>]fluoranthene	1.31	± 0.09
Dibenzo[<i>a,l</i>]pyrene	0.137	± 0.024
Naphtho[2,3- <i>e</i>]pyrene	0.770	± 0.073
Dibenzo[<i>a,e</i>]pyrene	1.13	± 0.049
Naphtho[2,1- <i>a</i>]pyrene	0.818	± 0.052
Dibenzo[<i>e,l</i>]pyrene	0.770	± 0.095
Benzo[<i>b</i>]perylene	0.125	± 0.013

^(a) The reference values are weighted means of the mass fractions from multiple analytical methods [19]. The uncertainty listed with each value is an expanded uncertainty about the mean [19,20], with coverage factor, $k = 2$, calculated by combining within method variances with a between method variance [21] following the ISO/JCGM Guide [22,23].

^(b) GC/MS on 50 % phenyl-substituted methylpolysiloxane phase after PFE at 100 °C and 13.8 MPa with DCM.

Table 5. Reference Mass Fraction Values for Selected Nitro-PAHs in SRM 1650b
Based on Extraction Method and Conditions

Extraction Conditions	Mass Fractions ^(a) (µg/kg)	
PFE at temperatures between 100 °C and 200 °C		
1-Nitronaphthalene ^(b,c,d,e)	85.6 ±	1.1
2-Nitronaphthalene ^(b,c,d,e)	236 ±	5
2-Nitrobiphenyl ^(b,c,d,e)	16.1 ±	0.7 ^(f)
3-Nitrobiphenyl ^(b,c,d,e)	57.3 ±	1.6
5-Nitroacenaphthene ^(b,c,d,e)	36.8 ±	0.6 ^(f)
2-Nitrofluorene ^(b,c,d,e)	46.0 ±	1.5
PFE at 100 °C		
9-Nitroanthracene ^(b,c,d,g)	5940 ±	90 ^(f)
4-Nitrophenanthrene ^(b,c)	152 ±	3
1-Nitrofluoranthene ^(b,c)	272 ±	4 ^(f)
8-Nitrofluoranthene ^(b,c)	112 ±	6 ^(f)
4-Nitropyrene ^(b,c)	137 ±	4 ^(f)
6-Nitrobenzo[<i>a</i>]pyrene ^(b,c,g)	1420 ±	26 ^(f)
3-Nitrobenzo[<i>e</i>]pyrene ^(b,c)	79.8 ±	6.7 ^(f)
1,3-Dinitropyrene ^(b,c,g)	45.5 ±	1.6 ^(f)
1,6-Dinitropyrene ^(b,c)	83.3 ±	2.3 ^(f)
PFE at 200 °C		
9-Nitroanthracene ^(e)	6930 ±	210 ^(f)

^(a) The reference values, unless otherwise footnoted, are weighted means of the mass fractions from multiple analytical methods [19]. The listed uncertainty is an expanded uncertainty about the mean [19,20], with coverage factor, $k = 2$, calculated by combining within-method variances with a between-method variance [21] following the ISO/JCGM Guide [22,23].

^(b) GC/NICI-MS (I) on 50 % phenyl-substituted methylpolysiloxane stationary phase.

^(c) GC/NICI-MS (II) on 50 % phenyl-substituted methylpolysiloxane stationary phase.

^(d) GC/NICI-MS (III) on 50 % phenyl-substituted methylpolysiloxane phase after PFE with toluene at 100 °C and two pressures (13.8 MPa and 20.7 MPa).

^(e) GC/NICI-MS (III) on 50 % phenyl-substituted methylpolysiloxane phase after PFE with toluene at 200 °C and two pressures (13.8 MPa and 20.7 MPa).

^(f) The reference value is a weighted mean of the average mass fractions, with one average from each of two or more analytical methods [19,20]. The expanded uncertainty is the half width of a symmetric 95 % parametric bootstrap confidence interval [24], which is consistent with the ISO/JCGM Guide [22,23] with an effective coverage factor, k , equals 2.

^(g) GC/NCI-HRMS on 5 % phenyl-substituted methylpolysiloxane stationary phase.

Table 6. Reference Value for Percent Extractable Mass for SRM 1650b^(a)

	Mass Fractions ^(b) (%)
Percent Extractable Mass	20.2 ± 0.4

^(a) Reference value for percent extractable mass reported for SRM 1650a is applicable to SRM 1650b.

^(b) Reference value is the mean of results obtained using one analytical technique. The expanded uncertainty, U , is calculated as $U = ku_c$, where u_c is one standard deviation of the analyte mean, and the coverage factor, $k = 2$, is determined from the Student's t -distribution corresponding to the associated degrees of freedom and 95 % confidence level for each analyte.

Table 7. Information Values for Particle-Size Characteristics and Specific Surface Area for SRM 1650b^(a)

Mean Particle Diameter, $d(0.5)$ ^(b)	0.18 μm
Particle Diameter, $d(0.1)$ ^(c)	0.12 μm
Particle Diameter, $d(0.9)$ ^(d)	0.33 μm
Volume Weighted Mean ^(e)	0.22 μm
Specific Surface Area (S) ^(f)	108 m^2/g

^(a) These values are provided for informational purposes only. The values have not been confirmed by an independent analytical technique as required for certification. See Figure 1 for particle-size distribution for SRM 1650b after 1 h and 24 h sonication.

^(b) $d(0.5)$ is the particle-size distribution parameter indicating the particle size below which 50 % of the volume is present.

^(c) $d(0.1)$ is the particle-size distribution parameter indicating the particle size below which 10 % of the volume is present.

^(d) $d(0.9)$ is the particle-size distribution parameter indicating the particle size below which 90 % of the volume is present.

^(e) The volume weighted mean is the particle size in a uniform distribution.

^(f) Specific surface area determined by multi-point N_2 gas adsorption BET equation [15].

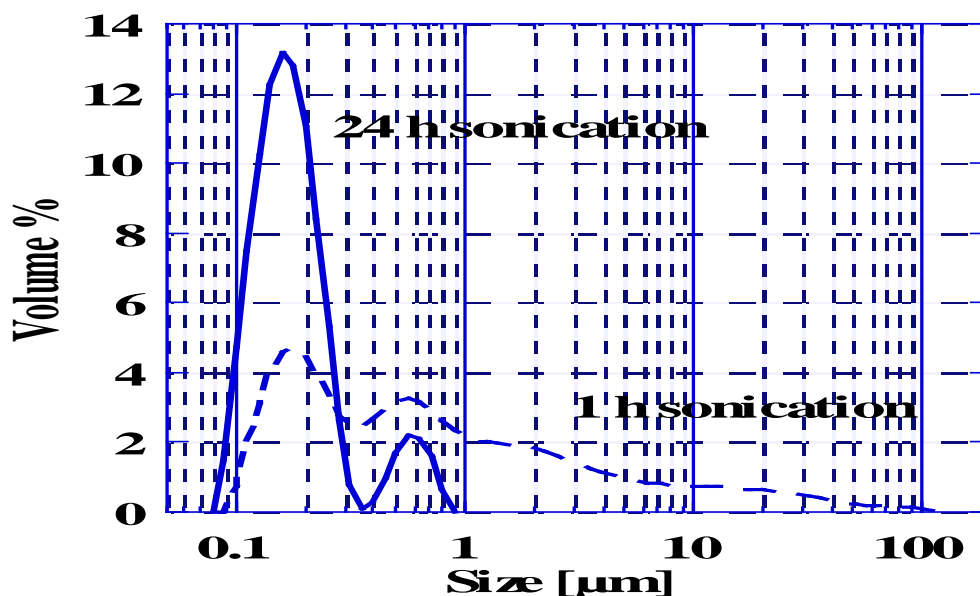


Figure 1. Particle-size distribution for SRM 1650b after 1 h and 24 h sonication. See “Particle Size Information, Specific Surface Area, and Porosity” section for additional information.

REFERENCES

- [1] SRM 1650; *Diesel Particulate Matter*; National Institute of Standards and Technology; U.S. Department of Commerce: Gaithersburg, MD (1985).
- [2] SRM 1650a; *Diesel Particulate Matter*; National Institute of Standards and Technology; Department of Commerce: Gaithersburg, MD (2000).
- [3] Poster, D.L.; Lopez de Alda, M.J.; Schantz, M.M.; Sander, L.C.; Vangel, M.G.; Wise, S.A.; *Development and Analysis of Three Diesel Particulate-Related Standard Reference Materials for the Determination of Chemical, Physical, and Biological Characteristics*; Polycyclic Aromat. Compd., Vol. 23, pp. 141–191 (2003).
- [4] Poster, D.L.; Benner, B.A., Jr.; Schantz, M.M.; Sander, L.C.; Vangel, M.G.; Wise, S.A.; *Determination of Methyl-Substituted Polycyclic Aromatic Hydrocarbons in Diesel Particulate-Related Standard Reference Materials*; Polycyclic Aromat. Compd., Vol. 23, pp. 113–139 (2003).
- [5] May, W.; Parris, R.; Beck II, C.; Fassett, J.; Greenberg, R.; Guenther, F.; Kramer, G.; Wise, S.; Gills, T.; Colbert, J.; Gettings, R.; MacDonald, B.; *Definitions of Terms and Modes Used at NIST for Value-Assignment of Reference Materials for Chemical Measurements*; NIST Special Publication 260-136; U.S. Government Printing Office: Washington, DC (2000); available at: <http://www.nist.gov/srm/publications.cfm> (accessed July 2013).
- [6] Lippa, K.A.; Schantz, M.M.; *Microhomogeneity Evaluation of Polycyclic Aromatic Hydrocarbons in Particulate Standard Reference Materials*; Anal. Bioanal. Chem., Vol. 387, pp. 2389–2399 (2007).
- [7] Schantz, M.M.; Nichols, J.J.; Wise, S.A.; *Evaluation of Pressurized Fluid Extraction for the Extraction of Environmental Matrix Reference Materials*; Anal. Chem., Vol. 69, pp. 4210–4219 (1997).
- [8] Schubert, P.; Schantz, M.M.; Sander, L.C.; Wise, S.A.; *Determination of Polycyclic Aromatic Hydrocarbons with Molecular Mass 300 and 302 in Environmental-Matrix Standard Reference Materials by Gas Chromatography-Mass Spectrometry*; Anal. Chem., Vol. 75, pp. 234–246 (2003).
- [9] Bezabeh, D.Z.; Bamford, H.A.; Schantz, M.M.; Wise, S.A.; *Determination of Nitrated Polycyclic Aromatic Hydrocarbons in Diesel Particulate-Related Standard Reference Materials by Using Gas Chromatography/Mass Spectrometry With Negative Ion Chemical Ionization*; Anal. Bioanal. Chem., Vol. 375, pp. 381–388 (2003).
- [10] Bamford, H.A.; Bezabeh, D.Z.; Schantz, M.M.; Wise, S.A.; Baker, J.E.; *Determination and Comparison of Nitrated-Polycyclic Aromatic Hydrocarbons Measured in Air and Diesel Particulate Reference Materials*; Chemosphere, Vol. 50, pp. 575–587 (2003).
- [11] Schantz, M.M.; McGaw, E.; Wise, S.A.; *Pressurized Liquid Extraction of Diesel and Air Particulate Standard Reference Materials: Effects of Extraction Temperature and Pressure*; Anal. Chem., Vol. 84, pp. 8222–8231 (2012).
- [12] Bergvall, C.; Westerholm, R.; *Determination of 252–302 Da and Tentative Identification of 316–376 Da Polycyclic Aromatic Hydrocarbons in Standard Reference Materials 1649a Urban Dust and 1650b and 2975 Diesel Particulate Matter by Accelerated Solvent Extraction - HPLC-GC-MS*; Anal. Bioanal. Chem., Vol. 391, pp. 2235–2248 (2008).
- [13] Masala, S.; Ahmed, T.; Bergvall, C.; Westerholm, R.; *Improved Efficiency of Extraction of Polycyclic Aromatic Hydrocarbons (PAHs) from the National Institute of Standards and Technology (NIST) Standard Reference Material Diesel Particulate Matter (SRM 2975) using Accelerated Solvent Extraction*; Anal. Bioanal. Chem., Vol. 401, pp. 3305–3315 (2011).
- [14] Gregg, S.J.; Sing, K.S.W.; *Adsorption, Surface Area and Porosity*; 2nd, Academic Press, London (1982).
- [15] Brunauer, S.; Emmett, P.; Teller, E.; *Adsorption of Gases in Multimolecular Layers*; J. Am. Chem. Soc., Vol. 60, pp. 309–319 (1938).
- [16] Barrett, E.P.; Joyner, L.G.; Halenda, P.P.; *The Determination of Pore Volume and Area Distributions in Porous Substances. I. Computations for Nitrogen Isotherms*; J. Am. Chem. Soc., Vol. 73, pp. 373–380 (1951).
- [17] Lewtas, J.; Claxton, L.D.; Rosenkranz, H.S.; Schuetzle, D.; Shelby, M.; Matsushita, H.; Wurgler, F.E.; Zimmermann, F.K.; Lofroth, G.; May, W.E.; Krewski, D.; Matsushima, T.; Ohnishi, Y.; Gopalan, H.N.G.; Sarin, R.; Becking, G.C.; *Design and Implementation of a Collaborative Study of the Mutagenicity of Complex Mixtures in Salmonella Typhimurium*; Mutat. Res., Vol. 276, pp. 3–9 (1992).
- [18] Claxton, L.D.; Douglas, G.; Krewski, D.; Lewtas, J.; Matsushita, H.; Rosenkranz, H.; *Overview, Conclusions, and Recommendations of the IPCS Collaborative Study on Complex Mixtures*; Mutat. Res., Vol. 276, pp. 61–80 (1992).
- [19] Dersimonian, R.; Laird, N.; *Meta-Analysis in Clinical Trials*; Control Clin. Trials, Vol. 7, pp. 177–188 (1986).
- [20] Rukhin, A.L.; *Weighted Means Statistics in Interlaboratory Studies*; Metrologia, Vol. 46, pp. 323–331 (2009).
- [21] Horn, R.A.; Horn, S.A.; Duncan, D.B.; *Estimating Heteroscedastic Variance in Linear Models*; J. Am. Stat. Assoc., Vol. 70, pp. 380–385 (1975).

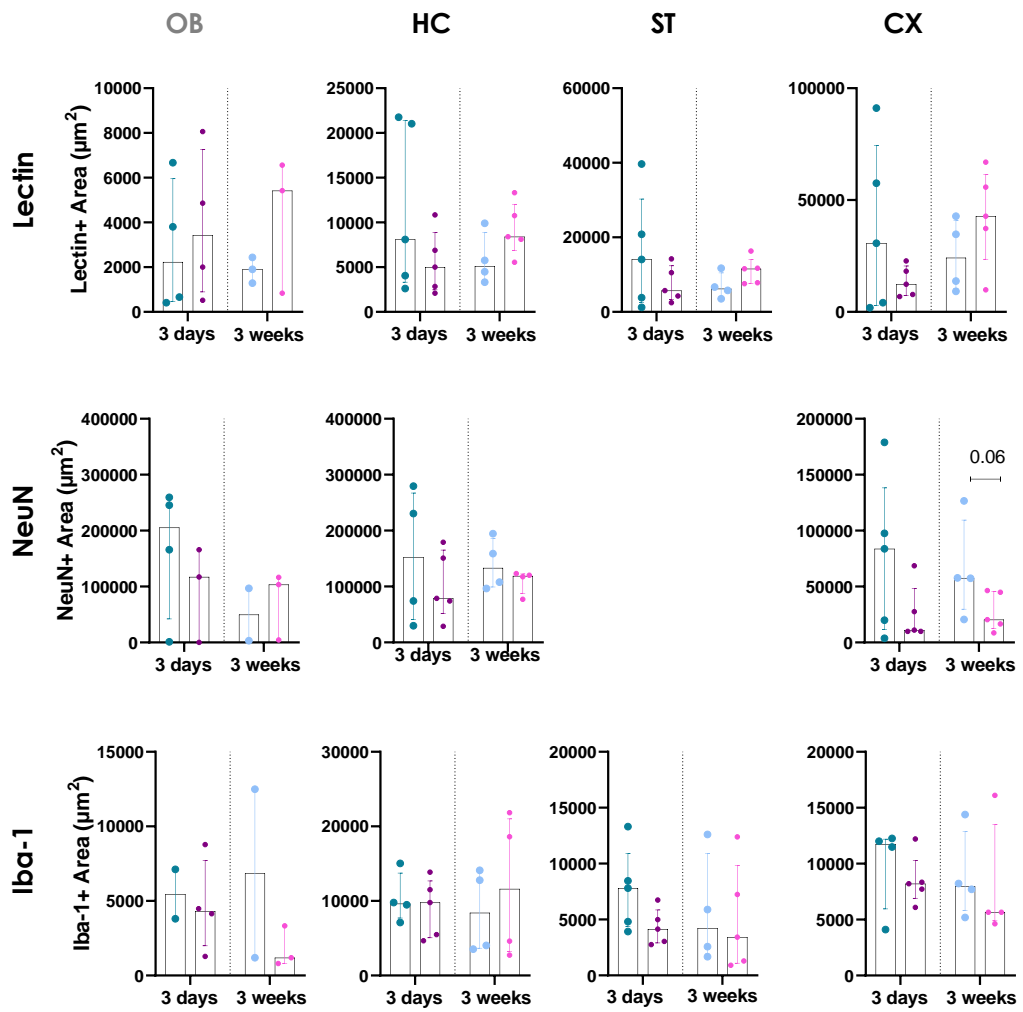
- [22] JCGM 100:2008; *Evaluation of Measurement Data - Guide to the Expression of Uncertainty in Measurement*; (GUM 1995 with Minor Corrections), Joint Committee for Guides in Metrology (JCGM) (2008); available at http://www.bipm.org/utis/common/documents/jcgm/JCGM_100_2008_E.pdf (accessed July 2013); see also Taylor, B.N.; Kuyatt, C.E.; *Guidelines for Evaluating and Expressing the Uncertainty of NIST Measurement Results*; NIST Technical Note 1297, U.S. Government Printing Office: Washington, DC (1994); available at <http://www.nist.gov/pml/pubs/index.cfm> (accessed July 2013).
- [23] JCGM 101:2008; *Evaluation of Measurement Data – Supplement 1 to the “Guide to the Expression of Uncertainty in Measurement” - Propagation of Distributions using a Monte Carlo Method*; JCGM (2008); available at http://www.bipm.org/utis/common/documents/jcgm/JCGM_101_2008_E.pdf (accessed July 2013).
- [24] Efron, B.; Tibshirani, R.J.; *An Introduction to the Bootstrap*; Chapman & Hall (1993).
- [25] MacCrehan, W.A.; May, W.E.; Yang, S.D.; Benner, B.A., Jr.; *Determination of Nitro Polynuclear Aromatic Hydrocarbons in Air and Diesel Particulate Matter Using Liquid Chromatography With Electrochemical and Fluorescence Detection*; *Anal. Chem.*, Vol. 60, pp. 194–199 (1988).

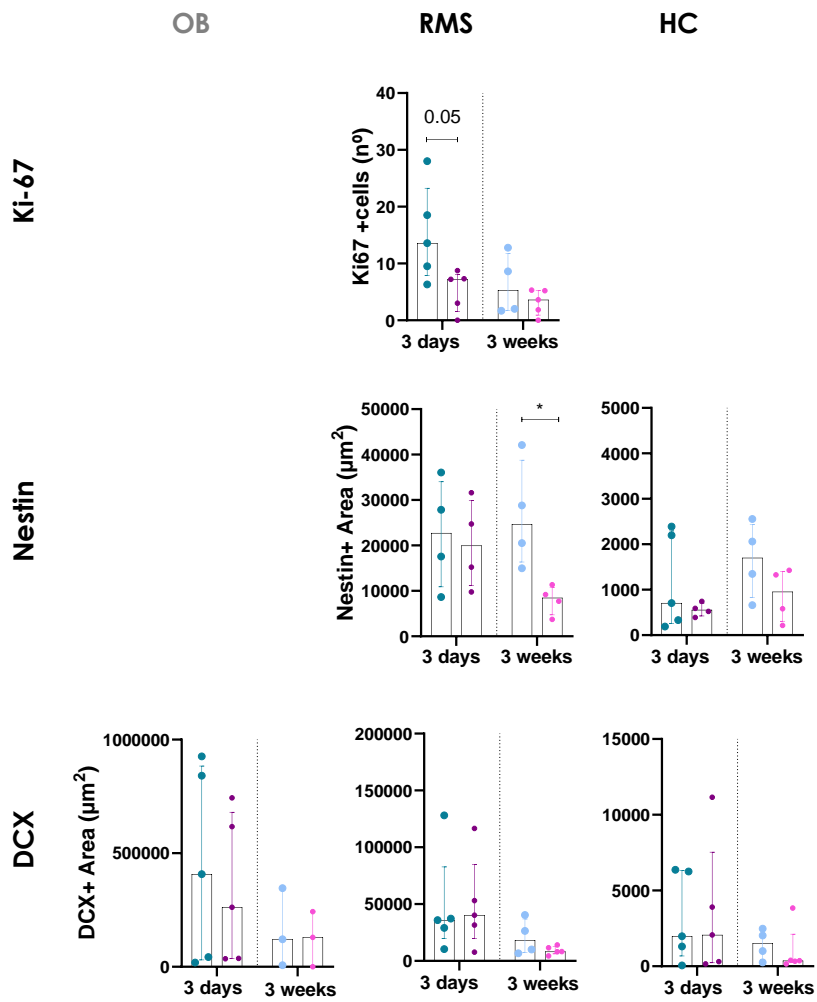
Certificate Revision History: 17 July 2013 (Update certified and reference values for PAHs and nitro-PAHs to address the effect of temperature used for extraction; extension of certification period; editorial changes); 27 September 2003 (Original certificate date).

Users of this SRM should ensure that the Certificate of Analysis in their possession is current. This can be accomplished by contacting the SRM Program: telephone (301) 975-2200; fax (301) 948-3730; e-mail srminfo@nist.gov; or via the Internet at <http://www.nist.gov/srm>.

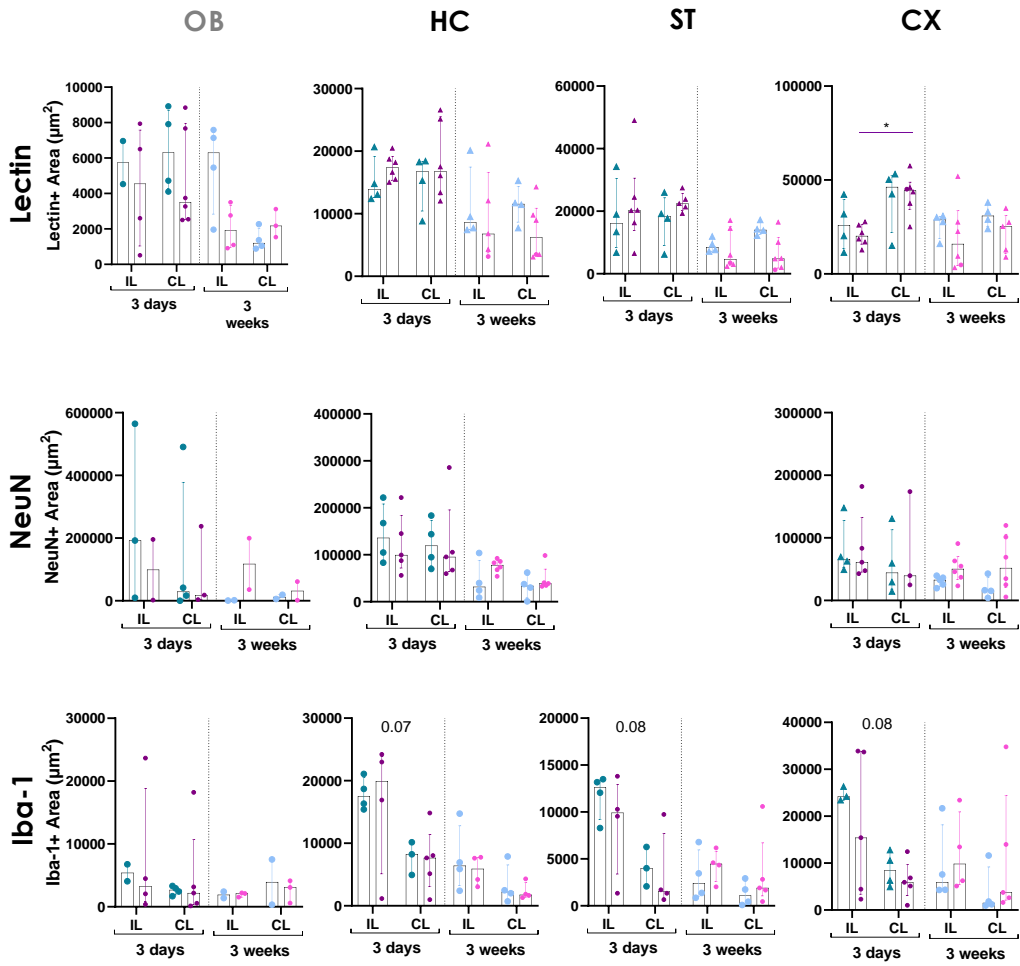
Annex IV

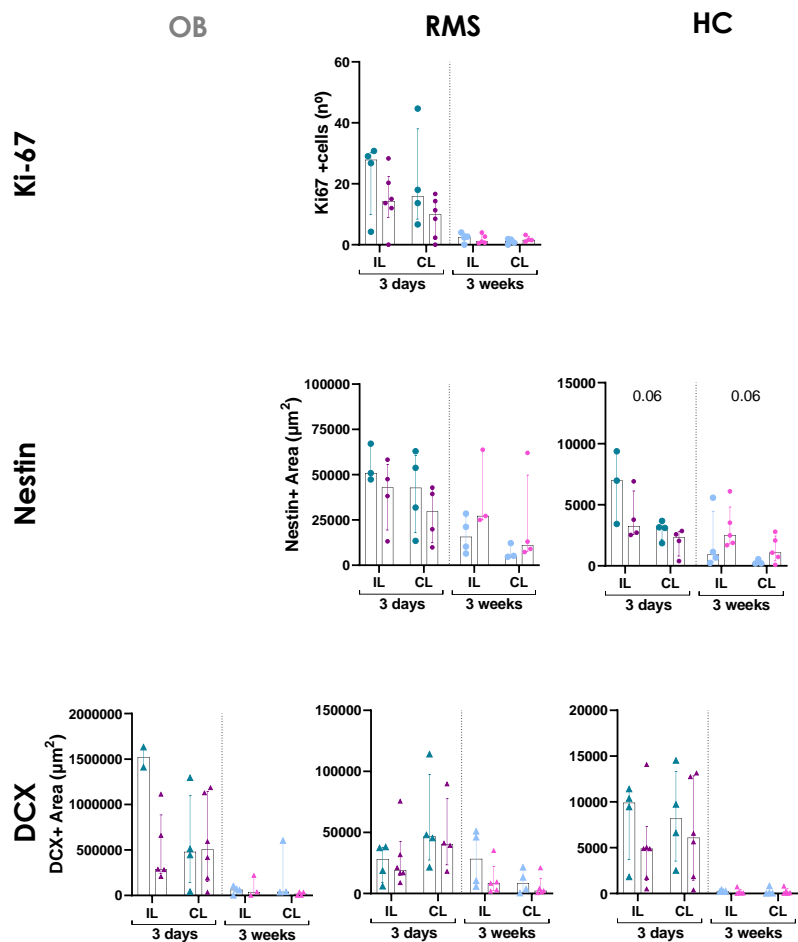
Immunofluorescence in naïve mice





Immunofluorescence in ischemic mice





“La ciencia hace a la gente tratar de luchar desinteresadamente para llegar a la verdad y la objetividad, enseña a la gente a aceptar la realidad con asombro y admiración, por no mencionar el asombro y alegría que el orden natural de las cosas produce en la verdadera mente científica”

Lise Meitner

Notes
